

School of Medicine

**Towards Understanding the Role of Trisomy 21 in Down
Syndrome Leukaemia**

Shannon Lee Carey-Smith

0000-0003-1418-8123

**This thesis is presented for
the degree of Doctor of Philosophy: Biomedical Science
of Curtin University**

February 2024

Declaration

To the best of my knowledge, this thesis does not contain any material previously published by other people, except where appropriate acknowledgment has been given.

This thesis contains no material which has been accepted for the award of any other degree or diploma in any university.

The research presented and reported in this thesis was conducted in compliance with the National Health and Medical Research Council Australian code for the care and use of animals for scientific purposes 8th edition (2013). The proposed research study received animal ethics approval originally by the Telethon Kids Institute Animal Ethics Committee (AEC#341) and received reciprocal animal ethics approval from the Curtin University Animal Ethics Committee, Approval Number ARE2020-4.

Signature:

Date:

29/02/2024

Abstract

Leukaemia is the most common type of childhood cancer, accounting for 35% of cases overall. Outcomes for paediatric leukaemia have significantly improved over the recent decades, with current 5-year overall survival being around 90%. However, many children with high-risk leukaemia continue to have a poor prognosis due to therapy resistance and relapse. These clinical features are exemplified in B cell leukaemia developed by children with Down syndrome (DS, named DS-ALL), a community of children that have a 27-fold increased risk of developing acute lymphoblastic leukaemia (ALL) compared to children without DS. Therefore, improvements must be made to current treatment strategies to improve the overall outcomes for children diagnosed with DS-ALL. Individuals with DS are characterised by the trisomy of chromosome 21 (ch21), and the role of trisomy 21 in leukaemia predisposition, development and maintenance has been reported by several groups. Previous research from our laboratory has identified a minimal region of ch21, the Down syndrome critical region (DSCR), implicated in DS-leukaemia and genes located within this region, such as the Dual-Specificity Tyrosine-Phosphorylation-Regulated Kinase 1A (*DYRK1A*) and High Mobility Group Nucleosome-Binding Domain 1 (*HMGN1*), are critical in DS-ALL development. Here, we hypothesise that targeting the mechanisms altered by trisomy 21 may represent a new avenue to improve outcomes for children with DS that develop DS-ALL.

We propose that the development of novel clinically relevant models of DS-ALL will facilitate the discovery of novel dosage sensitive ch21 genes, and lead to the identification of new molecular weaknesses and actionable therapeutic targets. These models can be established through the reproduction of genetic alterations observed in DS-ALL specimens in a murine background.

In Aim 1 of the PhD project, we set out to generate a triple transgenic mouse model of DS leukaemia by overexpressing the mutated (G12D) Kirsten Rat Sarcoma Viral Oncogene Homologue (*KRAS*^{G12D}) in murine B cell progenitors, with trisomy of the DSCR region (Ts1Rhr model) and loss of the

tumour suppressor Cyclin dependent kinase inhibitor 2a (*Cdkn2a*) and established the Ts1/*Cdkn2a*-*KRAS*^{G12D} cell line. Notably, we showed that without *KRAS*^{G12D}, the donor Ts1Rhr/Mb1-Cre/*Cdkn2a*^{fl/fl} mice did not exhibit a fully penetrant phenotype *in vivo*, indicating that a third mutation is required to develop complete malignancy. Consequently, we assessed the engraftment capacity of the Ts1/*Cdkn2a*-*KRAS*^{G12D} cell line in bone marrow transplant (BMT) experiments and showed that all successfully transplanted recipient mice developed DS-ALL *in vivo*, which can be used for preclinical drug testing.

In aim 2, we extended this approach to a larger trisomy of ch21: Tc1 mouse model; a DS mouse model containing an extra almost entire human ch21 made up of 269 human genes. Notably, the haematopoietic and microenvironment stem cell populations were characterised, confirming trisomy 21 perturbs haematopoiesis, specifically multipotent progenitor (MPP) populations, MPP1 and MPP2. Using Tc1 mice, we overexpressed *KRAS*^{G12D} and Breakpoint Cluster Region-Abelson 1 (*BCR-ABL1*) oncogenes and were able to establish four new cell lines: WT (wild-type)-*KRAS*^{G12D}, Tc1-*KRAS*^{G12D}, WT-*BCR-ABL* and Tc1-*BCR-ABL*. Using these models, as well as unique human DS-ALL cell lines developed in our laboratory, we screened several novel inhibitors of the ch21 kinase DYRK1A *in vitro* and *in vivo*. We showed that DYRK1A inhibition is correlated with decreased growth and survival of both murine and human DS-ALL cell lines, as well as human DS-ALL blasts freshly harvested from patient-derived xenografts (PDX). Leucettinib-21 was the most potent DYRK1A inhibitor tested and thus was selected for *in vivo* efficacy. In DS-ALL PDX, we showed that *in vivo* treatment with Leucettinib-21 significantly decreased leukaemia burden in the peripheral blood of two animal models. In parallel, we showed that it synergises with the standard of care agent vincristine to decrease growth of the human DS-PER961 and DS-PER962 cells *in vitro*. Altogether, our results confirmed that the ch21 kinase DYRK1A is a promising target in DS-ALL.

Identifying new dosage sensitive mechanisms associated with specific ch21 genes may represent new actionable targets in DS-ALL, and potentially other leukaemia subtypes with gain of ch21. In aim 3, we planned to use an

inducible clustered regularly interspaced short palindromic repeats (CRISPR) repression system, ER-dCas9-KRAB, to repress expression of specific ch21 genes in both DS-PER961 and DS-PER962 cells. We set out to optimise the procedure to integrate the ER-dCas9-KRAB system into the genome of our human DS-ALL cell lines and then use single guide RNA (sgRNA) targeting multiple ch21 genes. Initially, we tested procedures for transfection (Lipofectamine Stem reagent) and lentiviral transduction but were unable to successfully recover genetically modified human cells. Alternatively, we tested electroporation and were able to successfully transfect both DS-PER961 and DS-PER962 cell lines, with both single reporter plasmid and co-transfection of the ER-dCas9-KRAB construct. Unfortunately, we were unable to recover the transfected cells in liquid culture post the electroporation procedure, preventing us from establishing stable clones as originally planned. Ultimately, we conclude that our human DS-ALL models could not be genetically modified with our CRISPR repression system, using the procedures we tested, which aligns with observations from other groups regarding the technical challenge of transfecting/transducing human B cell ALL (B-ALL) cell lines. As a follow up, we are now considering modifying the murine trisomy 21 DS-ALL Tc1-KRAS^{G12D} cell line we recently established.

Overall, through our research of DS-ALL, we successfully generated and characterised multiple human and murine *in vitro* and *in vivo* models of DS-ALL. Through the development of these models, we tested several inhibitors of the ch21 kinase DYRK1A, confirming that targeting DYRK1A activity is a viable option as a new therapeutic strategy to improve outcomes for children with DS-ALL. Notably, copy number alterations (CNA) are hallmarks of cancer and gain of ch21 is one of the most frequently acquired chromosomal alterations seen in childhood leukaemia. Thus, targeting ch21 genes like *DYRK1A* will have broad therapeutic impact on multiple subtypes of leukaemia. These newly established DS-ALL models will serve as the basis for future research aiming to understand how ch21 gene expression influences DS-ALL development, progression and response to treatment, and lead to future therapeutic development.

Abbreviations

1.2M: 1.2×10^6
1M: 1×10^6
1R: Primary recipients
200K: 2×10^5
2M: 2×10^6
2R: Secondary recipients
4-OHT: 4-hydroxytamoxifen
600K: 6×10^5
AAVS1: Adeno-associated virus integration site 1
AGRF: Australian Genome Research Facility
ALL: Acute lymphoblastic leukaemia
AMKL: Acute megakaryoblastic leukaemia
AML: Acute myeloid leukaemia
Amplicons: Genomic amplification
B-ALL: B cell acute lymphoblastic leukaemia
BCR-ABL1: Breakpoint Cluster Region-Abelson 1
BFB: Breakage-fusion-bridge
BM: Bone marrow
BMT: Bone marrow transplant
bp: Base pairs
CAR T cell: Chimeric antigen receptor T cell
CAR: CXCL12-abundant reticular cells
Cbr1: Carbonyl reductase 1
CDKN2A: Cyclin Dependent Kinase Inhibitor 2A
CENP-E: Centromere-linked motor protein E
CFU: Colony forming unit
CGH: Comparative genomic hybridisation
ch21: Chromosome 21
CIN: Chromosomal instability
CL: Cell line
CNA: Copy number alteration
CNV: Copy number variation

Cond: Condition
Cre: Cyclisation recombinase
CRISPR: Clustered regularly interspaced short palindromic repeats
CRISPRa: CRISPR activating
CRISPRi: CRISPR interference
CRLF2: Cytokine Receptor Like Factor 2
CTCF: CCCTC-Binding Factor
dCas9: Nuclease-dead Cas9
ddPCR: Digital droplet PCR
DEPC: Diethylpyrocarbonate
DMSO: Dimethyl sulfoxide
Dnmt1: DNA methyltransferase 1
DS: Down syndrome
DS-ALL: Down syndrome acute lymphoblastic leukaemia
DSCR: Down syndrome critical region
DYRK1A: Dual-Specificity Tyrosine-Phosphorylation-Regulated Kinase 1A
E2F: E2F Transcription Factor
ecDNA: Extrachromosomal DNA
ECL: Enhanced chemiluminescence
EDTA: Ethylenediaminetetraacetic acid
EFS: Event free survival
EGFR: Epidermal Growth Factor Receptor
ER: Estrogen receptor
ES: Embryonic stem
ETV6: ETS Variant Transcription Factor 6
EXT: Extension
EZH2: Enhancer of Zeste Homologue 2
FACS: Fluorescence-activated cell sorting
FCS: Foetal calf serum
FeLV: Feline leukaemia virus
FISH: Fluorescence in situ hybridisation
Floxed: Flanked by LoxP
FLT3: Fms-like tyrosine kinase 3
FMO: Full minus one

GaLV: Gibbon ape leukaemia virus
GFP: Green fluorescent protein
GIN: Genomic instability
Gy: Gray
HA: Homology arms
HA-L: Homology arm left
HA-R: Homology arm right
HCL: Hydrochloric acid
HDM2: Human double minute 2
HeH B-ALL: High hyperdiploid B cell acute lymphoblastic leukaemia
HET: Heterozygous
HMGN1: High Mobility Group Nucleosome-Binding Domain 1
HoH: Hypodiploid
HOM: Homozygous
HSC: Hematopoietic stem cell
HSR: Homogeneously staining regions
iAMP21: Intrachromosomal amplification of chromosome 21
IGH: Immunoglobulin Heavy Locus
IKZF1: IKAROS Family Zinc Finger 1
IL-7: Interleukin 7
iPS: Induced pluripotent stem
Iso: Isomer
Itgb2l: Integrin subunit beta 2-like
JAK: Janus Kinase
Kcnj15: Potassium inwardly rectifying channel subfamily j member 15
KD: Knock-down
KRAB: Krüppel-associated box
KRAS: Kirsten Rat Sarcoma Viral Oncogene Homologue
LCTB-21: Leucettinib-21
Lenti: Lentivirus
LOH: Loss of heterozygosity
LoxP: Locus of x-over P1
Lym: Lymphocyte

MACHETE: Molecular alteration of chromosomes with engineered tandem elements

MAPH: Multiplex amplifiable probe hybridisation

Mb: Megabase

Mb1: Cd79a

Mdm2: Murine double minute 2

MEF: Mouse embryonic fibroblasts

MES: 2-(N-morpholino)ethanesulfonic acid

MIC: MSCV-IRES-mCherry

ML-DS: Myeloid leukaemia in Down syndrome

MLPA: Multiplex ligation-dependent probe amplification

MPP: Multipotent progenitor

MSC: Mesenchymal stem cells

MSCV: Murine stem cell virus

N/A: Not applicable

NaCl: Sodium chloride

NAMPT: Nicotinamide phosphoribosyltransferase

NGS: Next generation sequencing

NH₄Cl: Ammonium chloride

NRAS: Neuroblastoma Rat Sarcoma Viral Oncogene Homologue

NSG: NOD.Cg-Prkdc^{scid}||2^{rgtm1Wjl}/SzJ

NT: Non-transduced/non-transfected

OGM: Optical genome mapping

OS: Overall survival

P: Passage

PAR1: Pseudoautosomal Region 1

Pas: PDGFRa(CD140a)+/Sca-1+ cells

PAX5: Paired Box 5

Pb: Polybrene (hexadimethrine bromide)

PBS: Phosphate-buffered saline

PCR: Polymerase chain reaction

PDGFRa: Platelet-derived growth factor receptor alpha

PDGFRb: Platelet-derived growth factor receptor beta

PDX: Patient-derived xenografts

Pos: Positivity
Pre-B-ALL: Precursor B cell acute lymphoblastic leukaemia
PS: Protamine sulphate
PuroR: Puromycin resistance
PVDF: Polyvinylidene difluoride
QMPSF: Quantitative multiplex PCR of short fluorescent fragments
qPCR: Quantitative PCR
Rb: Retinoblastoma protein
RBC: Red blood cell
ReDACT: Restoring disomy in aneuploid cells using CRISPR targeting
RNA-seq: RNA sequencing
RUNX1: RUNX Family Transcription Factor 1
S: Seconds
SCF: Stem cell factor
SCORE: Single-guide CRISPR/Cas targeting of repetitive elements
SDS: Sodium dodecyl sulphate
sgRNA: Single guide RNA
sgRNA-ch21: Single guide RNA directed to ch21 genes
shRNA: Short hairpin RNA
Singlets: Single cells
SNP: Single nucleotide polymorphism
SNV: Single nucleotide variation
SP: Spleen
SRp20: Serine/arginine-rich splicing factor 3
TALEN: Transcription activator-like effector nucleases
TAM: Transient abnormal myelopoiesis
Temp: Temperature
Tris: Tris(hydroxymethyl)aminomethane
TSLPR: Thymic stromal lymphopoietin receptor
WBC: White blood cell
WT: Wild-type
ZFN: Zinc finger nucleases

Acknowledgments

I would firstly like to thank my supervisors, Dr Sébastien Malinge, Dr Laurence Cheung and Dr Rishi Kotecha for all their continuous support, encouragement, and guidance throughout my PhD journey. A special thanks to Dr Sébastien Malinge for your guidance of the projects undertaken and for accommodating for the difficulties faced throughout this PhD. Without this support from my supervisors, this PhD would not have been possible.

I would also like to thank the members of the Translational Genomics in Leukaemia (TGL) team and Leukaemia Translational Research (LTR) team for their wisdom and support over the years, it has been truly appreciated.

Finally, a sincere thank you to my mother Tracey Carey, my grandparents Thomas and Faye Carey, and to my partner Emma Gannon for their constant encouragement and support throughout the PhD. Everything you have done for me is greatly appreciated and this PhD is as much yours as it is mine.

The research conducted throughout this PhD was supported by the Australian Governments Research Training Program (RTP) scholarship.

Acknowledgment to Country

We acknowledge that Curtin University and the Telethon Kids Institute works across hundreds of traditional lands and custodial groups in Australia, and with First Nations people around the globe. We wish to pay our deepest respects to their ancestors and members of their communities, past, present, and to their emerging leaders. Our passion and commitment to work with all Australians and peoples from across the world, including our First Nations peoples are at the core of the work we do, reflective of our institutions' values and commitment to our role as leaders in the Reconciliation space in Australia.

Attribution Statement

For Paper:

Insights into the Clinical, Biological and Therapeutic Impact of Copy Number Alteration in Cancer.

Shannon L. Carey-Smith, Rishi S. Kotecha, Laurence C. Cheung and Sébastien Malinge.

International Journal of Molecular Sciences; accepted 17/06/2024.

	Conception and Design of Paper	Review of Literature	Interpretation/Discussion of Literature
First Author: Shannon L. Carey-Smith	100%	100%	100%
Acknowledgement: I acknowledge that these represent my contribution to the above research output and I have approved the final version.			
Signed:			

For Paper:

Efficacy of DYRK1A inhibitors in novel models of Down syndrome acute lymphoblastic leukemia.

Shannon L. Carey-Smith, Maryam H. Simad, Kunjal Panchal, Carlos Aya-Bonilla, Hannah Smolders, Sang Lin, Jesse D. Armitage, Vivien T. NGuyen, Kathryn Bentley, Jette Ford, Sajla Singh, Joyce Oommen, Anouchka P Laurent, Thomas Mercher, John D. Crispino, Andrew P. Montgomery, Michael Kassiou, Thierry Besson, Emmanuel Deau, Laurent Meijer, Laurence C. Cheung, Rishi S. Kotecha and Sébastien Malinge.

Journal of Haematologica; accepted 19/02/2024.

	Conception and Design	Acquisition of Data and Method	Data Conditioning and Manipulation	Analysis and Statistical Method	Interpretation and Discussion
Co-Author 1: Shannon L. Carey-Smith	50%	50%	50%	50%	60%
<p>Acknowledgement: I acknowledge that these represent my contribution to the above research output and I have approved the final version.</p> <p>Signed:</p>					
Co-Author 2: Maryam H. Simad	50%	50%	50%	50%	40%
<p>Acknowledgement: I acknowledge that these represent my contribution to the above research output and I have approved the final version.</p> <p>Signed:</p>					

Table of Contents

Declaration.....	II
Abstract.....	III
Abbreviations	VI
Acknowledgements.....	XI
Acknowledgement to Country	XII
Attribution Statement	XIII
Table of Contents.....	XV
Chapter 1: Introduction to copy number variation and DS-ALL	1
Introduction to copy number variation.....	1
Introduction to leukaemia.....	25
Introduction to DS-ALL	25
Thesis Overview	28
Chapter 2: Generation of the DS-ALL Ts1Rhr/Mb1-Cre/ <i>Cdkn2a</i> ^{fl/fl} mouse model and Ts1/ <i>Cdkn2a</i> -KRAS ^{G12D} cell line	30
Introduction	30
Methods	32
Results.....	41
Discussion	56
Chapter 3: Therapeutically targeting the chromosome 21 gene <i>DYRK1A</i>	61
Introduction	61
Methods	61
Chapter 3a: Efficacy of DYRK1A inhibitors in novel models of Down syndrome acute lymphoblastic leukemia	75

Chapter 3b: Therapeutically targeting the chromosome 21 gene <i>DYRK1A</i> additional data	90
Results	90
Discussion	101
Chapter 4: Targeting trisomy 21 in the human DS-ALL cell lines.....	104
Introduction	104
Methods	107
Results	115
Discussion	127
Chapter 5: Discussion and future directions	132
Chapter 6: References.....	142

Chapter 1: Introduction to copy number variation and DS-ALL




Introduction to copy number variation:

Genomic copy number variation (CNV, germline), responsible for congenital disorders such as DS (trisomy 21) (1), and CNAs (somatic) are both hallmarks of cancer respectively (2). There are multiple mechanisms that result in these CNVs/CNAs, with the most known consequence being the resulting altered gene dosage imbalances (losses or gains of genetic material) (3, 4). In cancer, CNVs/CNAs have been shown to predispose cancer, contribute to tumorigenesis and impact cellular outcomes by affecting the dosage of oncogenes and tumour suppressors (5-7). We wrote a review paper outlining the impact of CNV/CNA in cancer, as well as discussing the targetability of CNV/CNA. This review was submitted to the International Journal of Molecular Sciences and was accepted on the 17/06/2024.



Review

Insights into the Clinical, Biological and Therapeutic Impact of Copy Number Alteration in Cancer

Shannon L. Carey-Smith ^{1,2}, Rishi S. Kotecha ^{1,2,3,4} , Laurence C. Cheung ^{1,2,5}  and Sébastien Malinge ^{1,2,4,*} 

- ¹ Telethon Kids Cancer Centre, Telethon Kids Institute, Perth, WA 6009, Australia; shannon.carey-smith@telethonkids.org.au (S.L.C.-S.); rishi.kotecha@health.wa.gov.au (R.S.K.); laurence.cheung@telethonkids.org.au (L.C.C.)
² Curtin Medical School, Curtin University, Perth, WA 6102, Australia
³ Department of Clinical Haematology, Oncology, Blood and Marrow Transplantation, Perth Children's Hospital, Perth, WA 6009, Australia
⁴ UWA Medical School, University of Western Australia, Perth, WA 6009, Australia
⁵ Curtin Health Innovation Research Institute, Curtin University, Perth, WA 6102, Australia
* Correspondence: sebastien.malinge@telethonkids.org.au

Abstract: Copy number alterations (CNAs), resulting from the gain or loss of genetic material from as little as 50 base pairs or as big as entire chromosome(s), have been associated with many congenital diseases, de novo syndromes and cancer. It is established that CNAs disturb the dosage of genomic regions including enhancers/promoters, long non-coding RNA and gene(s) among others, ultimately leading to an altered balance of key cellular functions. In cancer, CNAs have been associated with almost all steps of the disease: predisposition, initiation, development, maintenance, response to treatment, resistance, and relapse. Therefore, understanding how specific CNAs contribute to tumorigenesis may provide prognostic insight and ultimately lead to the development of new therapeutic approaches to improve patient outcomes. In this review, we provide a snapshot of what is currently known about CNAs and cancer, incorporating topics regarding their detection, clinical impact, origin, and nature, and discuss the integration of innovative genetic engineering strategies, to highlight the potential for targeting CNAs using novel, dosage-sensitive and less toxic therapies for CNA-driven cancer.



Citation: Carey-Smith, S.L.; Kotecha, R.S.; Cheung, L.C.; Malinge, S. Insights into the Clinical, Biological and Therapeutic Impact of Copy Number Alteration in Cancer. *Int. J. Mol. Sci.* **2024**, *25*, 6815. <https://doi.org/10.3390/ijms25136815>

Academic Editor: Maria Gazouli

Received: 21 May 2024

Revised: 15 June 2024

Accepted: 17 June 2024

Published: 21 June 2024



Copyright: © 2024 by the authors. Licensee MDPI, Basel, Switzerland. This article is an open access article distributed under the terms and conditions of the Creative Commons Attribution (CC BY) license (<https://creativecommons.org/licenses/by/4.0/>).

Keywords: genetic; cancer; prognostic; targeted therapy

1. Introduction

Copy number alterations (CNAs) are a hallmark of cancer, with approximately 25% of the genome of all tumour cells containing either chromosomal amplifications or deletions somatically acquired during cancer development [1–3]. However, while these alterations are clonally selected during tumorigenesis, their role, clinical impact, associations with specific cancers and specific tumour subtypes, and whether they are therapeutically targetable, remains elusive. Further emphasising their influence on cancer development, some congenital and de novo syndromes characterised by specific germline alterations, termed copy number variation (CNV), have a different incidence of cancer compared to the general population, indicating that these gains or losses of genetic material can either protect or promote tumorigenesis. The other chromosomal alterations commonly seen in cancer are inversions and translocations; however, in most cases, they do not modify the gene copy number.

Mechanistically, CNA/CNV arises from a myriad of mechanisms that result in small to large genomic deletions or amplifications, and by definition lead to an altered dosage of genetic material such as regulatory elements (enhancers/promoters, long non-coding RNA, microRNA among others), non-protein-coding and protein-coding genes. Depending on the size (from 50 base pairs (bp) to an entire chromosome), the genomic location altered

(rich or poor in regulatory elements or genes) and the magnitude (number of copy loss or gain of a genomic region), this may affect the expression of several tumour suppressor and tumour promoter genes that will ultimately impact cellular fitness, cell proliferation, differentiation, maturation, survival and response to treatment [4–7]. This becomes even more complex as, in most cases, tumour cells have more than one CNA, and thus together can lead to a precise gene expression profile that has clinical implications [8,9]. Notably, there is also a high level of intra-tumoural heterogeneity in most cancers [10], and CNAs alone may not be sufficient to drive tumorigenesis but rather cooperate with other somatic genetic events. While these cooperating driver mutations have been extensively studied in human and animal models, the true impact of CNAs in cancer initiation, development, response to treatment and outcome remains mostly unknown due to the complex nature of these numerical and structural alterations.

With an incidence varying between 25 and 80% [1,5], a better understanding of the role of CNA/CNV in cancer is key to identifying new vulnerabilities that can lead to the development of novel targeted therapeutic strategies. In this review, we will integrate clinical and fundamental observations of CNA/CNV in cancer, with a particular focus on haematological malignancies to highlight the uprising interest in understanding the impact of CNAs in tumorigenesis to develop innovative therapies.

2. CNA/CNV Detection

From early karyotyping to next-generation sequencing (NGS), the detection of CNA/CNV has vastly evolved in recent decades. Figure 1 shows the main techniques and key steps of this evolution; other approaches and their limitations have been extensively described elsewhere [11,12]. Compared to historical conventional cytogenetics, new detection tools have incrementally refined several features of CNAs such as the size, the specificity (at the gene, transcript or single nucleotide variation (SNV) level) and the depth (to distinguish between cancer and normal cells and assess intra-tumoural heterogeneity). Karyotyping and fluorescence in situ hybridisation (FISH) approaches are still commonly used for the diagnosis of many diseases, whether they are cancer-related or not, but are limited by depth. Towards the turn of the century, the development of array platforms such as comparative genomic hybridisation (CGH) and single nucleotide polymorphism-based microarrays (SNP-arrays) significantly advanced our ability to detect and precisely characterise CNAs, emphasising their incidence and complexity in cancer [13–15]. Polymerase chain reaction (PCR)-based detection methods, such as quantitative multiplex PCR of short fluorescent fragments (QMPSF) [16], multiplex amplifiable probe hybridisation (MAPH) [17], and multiplex ligation-dependent probe amplification (MLPA) [18], were subsequently developed and allowed CNA detection with 150 bp resolution. MLPA is commonly used in the clinic and allows for a cheap, fast, and precise detection of known CNAs. With the advent of NGS, new approaches and bioinformatic pipelines can now be used to detect CNAs and characterise them at the nucleotide level (as bulk or single cell), from DNA and RNA [19,20]. Furthermore, the development of optical genomic mapping (OGM) that uses chromosome band patterns from single DNA strands, assembled bioinformatically to identify genomic alterations at high resolution (de novo assembly: 500 bp), now offers efficient analysis of genetic alterations within a genome without sequencing [21]. Notably, OGM provides an effective tool to detect CNAs in cancer, as shown in haematological malignancies [22], and may represent a cost-effective option for genetic screening in future clinical settings [23]. Implementation of these new detection methods along with a plethora of novel bioinformatic tools has highlighted the role and incidence of CNAs in tumour development, maintenance and response to treatment, and in several cases, associated specific CNA/CNV with clinical outcomes, as further detailed below.

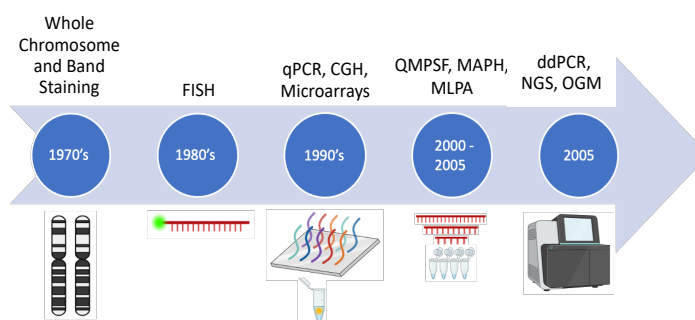


Figure 1. Main methods of detection of copy number alterations/variations. Timeline of the development of methods for detection of CNA/CNV, spanning from the 1970s to the present. Fluorescence in situ hybridisation (FISH), comparative genomic hybridisation (CGH), quantitative polymerase chain reaction (qPCR), quantitative multiplex PCR of short fluorescent fragments (QMPSF), multiplex amplifiable probe hybridisation (MAPH), multiplex ligation-dependent probe amplification (MLPA), digital droplet PCR (ddPCR), next-generation sequencing (NGS) and optical genome mapping (OGM). Created with [BioRender.com](https://www.biorender.com) (accessed on 21 May 2024).

3. Types of CNA/CNV

CNA/CNV is a general term describing a myriad of genomic/chromosomal aberrations that can be inter- and intra-chromosomal; the largest ones such as aneuploidy or chromosomal rearrangements resulting from duplication, deletion or chromothripsis are usually seen by conventional cytogenetic approaches.

Aneuploidy englobes gains and/or losses of whole chromosomes within a single cell, and can affect one single chromosome (as in monosomy and trisomy), several chromosomes (as in hypodiploidy or hyperdiploidy), and even lead to haploid (or ‘nearly’ haploid) or polyploid (as in triploidy or tetraploidy) karyotypes in some cases (Figure 2A,B) [24]. This large variety of aneuploidies, which can vary between tumours, within the same tumour type, or even within the same patient, has hindered our capacity to estimate their true impact on cancer development. Notably, some of these alterations have been associated with specific outcomes and are now integrated into clinical risk stratification, as discussed below. Aneuploidy is often, but not exclusively, the result of chromosomal instability (CIN) [25]. It can occur via various mechanisms including single mutations affecting genes encoding key regulators of chromosomal segregation or mitotic/meiotic process, including improper kinetochore–microtubule attachments (*AURKB* and *AURKC*), defective cohesin complex (*SMC1/3*, *RAD51*, *STAG2*) and defective spindle assembly checkpoint (*BUB1/3*, *MAD1/2*, *BUBR1*, *MPS1*) [26–28]. Importantly, CIN leads to ongoing chromosomal mis-segregation throughout cell progeny, resulting in tumour cell populations with different karyotypes, thus increasing intra-tumoural heterogeneity [29,30]. Notably, aneuploidy can trigger increased genomic instability (GIN) and CIN [31,32], with Passerini et al., showing that aneuploidy increases the frequency of pre-mitotic errors and DNA damage and enhanced sensitivity to replication stress, ultimately leading to genomic rearrangements. The reverse is also true as GIN induced by DNA mutations and epigenetic modifications (DNA methylation and histone modification) has been shown to lead to deletions/duplications [25,33]. In high hyperdiploid B-cell acute lymphoblastic leukaemia (HeH B-ALL, >50 chromosomes), chromosomal gain has been suggested to occur in various ways, including chromosome loss from tetraploid cells, abnormal mitosis linked to impaired condensin and downstream Aurora B kinase function, chromosomal gains resulting from CIN, as well as cell fusion and tripolar division with additional clonal selection over multiple generations [34–36]. To date, the exact mechanism and kinetics of the appearance of the hyperdiploid karyotype in HeH B-ALL are still debated, with some studies indicating that it may be an early event

during tumourigenesis [37,38]. Moreover, emphasising a putative functional advantage of CNAs for tumourigenesis and during clonal selection, there is a lack of randomness of the chromosomes often gained in hyperdiploid B-ALL (gains of chromosome 4, 6, 10, 14, 17, 18, 21, and X) [39], many of which are retained in hypodiploid (HoH) B-ALL (retained chromosome X/Y, 14, 18, and 21) [40].

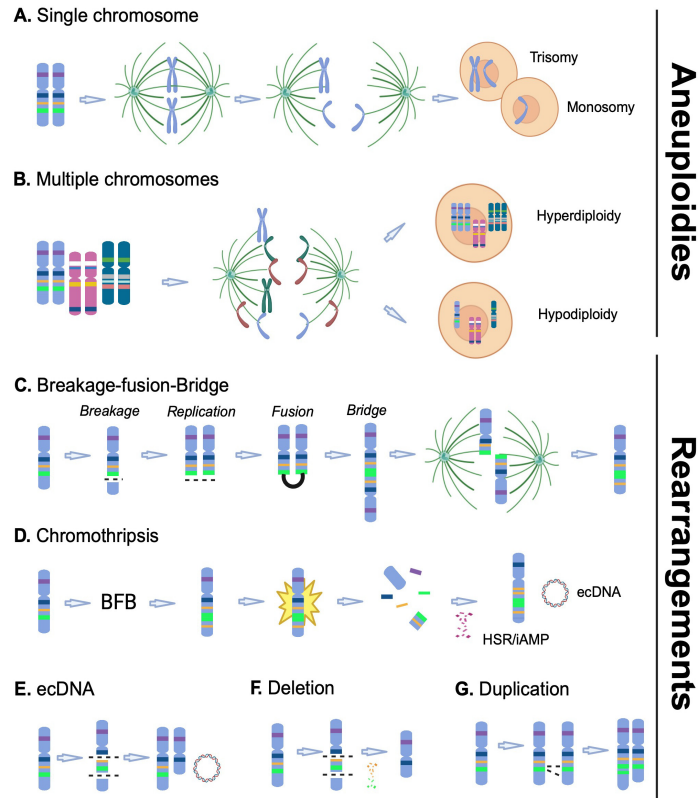


Figure 2. Mechanisms of formation of copy number alterations. Aneuploidies: (A) Chromosomes align during metaphase, followed by mis-segregation at anaphase that may lead to gain (trisomy) or loss (monosomy) of one chromosome. (B) Hypothetical mechanisms leading to hyperdiploidy and hypodiploidy due to mis-segregation of several chromosomes during anaphase. Rearrangements: (C) Amplification of genomic regions by a breakage–fusion bridge (BFB); several sequential BFB cycles can happen. (D) Chromothripsis is a catastrophic event that usually starts with BFB cycle(s), followed by the ‘explosion’ of an unstable rearranged chromosome and reintegration of DNA fragments prior to stabilisation. This process can lead to homogeneously staining regions/intrachromosomal amplification (HSR/iAMP), ring chromosomes and extrachromosomal DNA (ecDNA). (E) Extra-chromosomal circular DNA occurs when a DNA fragment is excised and circularised; or following chromosomal rearrangements such as chromothripsis. (F) In deletions, genomic regions are lost mostly due to DNA double-strand breaks and non-homologous repair. (G) Duplication results from the exchange of homologous genomic segments between sister chromosomes. Dotted line represents DNA-strand breaks. Created with [BioRender.com](https://www.biorender.com) (accessed on 21 May 2024).

For several decades, cytogenetic approaches (karyotyping, FISH or CGH arrays) have also described chromosomal structures and chromosomal rearrangements associated with the amplification of specific DNA segments that can be released from the original chromosome, such as extrachromosomal DNA (ecDNA, also known as double minutes) and ring chromosomes, or remain integrated within the affected chromosome in homogeneously staining regions (HSR) (Figure 2C–G). In most cases, amplification of genomic regions due to these CNAs leads to an elevated expression of oncogenes. Among the best-known examples are the amplifications of *MYCN* and *MYC* oncogenes in neuroblastoma and acute myeloid leukaemia (AML), respectively, in double minutes or HSR structures [41,42]. These chromosomal alterations can result from several mechanisms that are not mutually exclusive, including breakage–fusion bridges (Figure 2C, first reported in 1941) [43] and the more recently described chromothripsis (Figure 2D) [44]. Chromothripsis is described as a one-off ‘catastrophic’ event that initiates with breakage–fusion bridge cycles resulting in a rearranged chromosome characterised by a distinctive pattern of deleted and amplified genomic fragments, in random order and orientation [44,45]. Chromothripsis is part of a larger family of chromosomal rearrangements, which also include chromoplexy and chromoanasythesis. Major breakthroughs into the nature, origin and mechanisms of formation of these massively rearranged structures have been achieved with the implementation of next-generation sequencing approaches (reviewed in [46]). Chromothripsis has been shown to occur in numerous cancer types, including leukaemia, brain tumour and lung carcinoma [47]. A well-known example of chromothripsis in leukaemia is the intrachromosomal amplification of chromosome 21 (iAMP21), a rare subtype of childhood B-ALL associated with a high risk of relapse [48]; this rearrangement can also be found to occur in AML [49]. The mechanism of formation of iAMP21 in B-ALL has been elegantly revealed by Li et al. using a next-generation sequencing approach indicating a rearranged chromosome that alternates gains and losses of key genomic regions/ genes of chromosome 21; in some instances, this whole process can be promoted by a predisposing Robertsonian translocation [50]. Chromothripsis has also been described in paediatric medulloblastoma and is associated with *TP53* mutations [45]; a functional link is also observed in AML [49]. Notably, it is commonly seen in the benign tumour, uterine leiomyoma, but does not seem to be sufficient to drive malignant transformation [51]. Although there is still much more to do to better understand chromothripsis, it is now well established as a significant contributor to cancer development. Additionally, chromothripsis is one of the mechanisms that can lead to the release of extrachromosomal material (Figure 2D). ecDNA usually involves double stranded breaks, replication and circularisation of small fragments that contain one or a few genes and exist separately to chromosomes (Figure 2E) [52]. These ecDNA are commonly found in cancer and a recent observation has shown that oncogene overexpression through ecDNA formation contributes to tumour heterogeneity and genome evolution during cancer progression [53].

Somatic intrachromosomal deletions and duplications ≥ 10 kb are observed in 87.5% of cancer [5]. Interestingly, deletion/duplication of specific genomic regions is commonly found as germline CNV (80–85% deletion, 10–15% duplication) [54]. Classically, deletions are suspected to contain gene or regulatory elements with tumour suppressor function whereas duplications/amplifications contain tumour promoter genes and oncogenes. A well-documented example of this is the amplification of the *MYCN* gene (located in 2p23-24) in approximately 20–30% of neuroblastoma cases [55,56]. *MYCN* amplification can exist either intrachromosomally as well as in ecDNA and can result in over 500-fold amplification in some cases [57]. Other key examples are amplification of *EGFR* (7p11.2) in about 40% of glioblastoma cases [58], *ERBB2/HER2* (17q12) in 15–20% of breast cancer cases [59] and *MET* (7q31) in 1–2% of metastatic colorectal cancer cases [60]. Amplifications of these oncogenes have been shown to have prognostic value, further discussed below. Notably, similar to the concept of oncogene addiction [61], the term ‘aneuploidy addiction’ has also been used to describe the nature of cancers that rely on this specific type of CNA [62]. Indeed, in their

recent study, Girish et al. demonstrated that trisomy of chromosome arm 1q is associated with suppression of TP53 function through overexpression of *MDM4* (1q32.1) [62].

Overall, a large variety of CNAs/CNVs exist that arise through different mechanisms. Notably, similar to what has been described for small indels (insertions/deletions) and single nucleotide mutations [63], Steele et al. described signatures that can explain the CNA pattern of 97% of samples across 33 tumour types, providing a mechanistic explanation of how most of these large chromosomal rearrangements may arise in cancer [3]. These CNAs are clonally selected throughout the tumorigenic process; therefore, the kinetics of appearance (spatial and time-dependent), as well as their interaction with other genetic alterations (including with other CNAs within the same cell), dictates cellular fitness, tumorigenesis, response to treatment and relapse initiation.

4. Incidence and Clinical Impact of CNA/CNV in Cancer

Depending on the subtype of CNA/CNV, the dosage of one to thousands of genes or regulatory elements can be affected, and consequently modify key biological processes. For most of them, the true functional impact of these CNAs/CNVs remains elusive, but it is now well established that they can provide clinical insight. Notably, the type of CNA and the genomic regions implicated may strongly relate to tumour type, and some insights have been unveiled through studying the influence of somatic and germline CNV or genetic disorders on cancer incidence.

4.1. Somatic CNAs in Cancer

Independent of the techniques used to detect somatic CNAs, pan-cancer genomic studies have estimated the incidence of aneuploidy (60–90%), chromothripsis (50%), and other duplication/deletions (25–80%) in primary samples [1–3,5,64]. The amount, type and size of somatic CNAs can be highly variable between cancer [2,5]. An overview of the key CNAs observed in the most common solid tumours and in acute leukaemia is shown in Table 1.

CNA burden (i.e., the ratio of total CNAs on the length of the whole genome) has been identified as a prognostic factor for recurrence and death [4]. Pan-cancer studies have also highlighted the impact of CNAs during tumour development, progression and therapeutic resistance, some of which are commonly deleted/amplified across cancer [11,48,65–67].

Table 1. Overview of the main CNAs affecting autosomes in cancer.

Cancer Type	CNAs (amp/del)	Frequency	Genes of Interest	Refs.
<i>Solid Tumour</i>				
Breast cancer	+1q	>50%	<i>MYC</i> <i>CCND1</i> <i>ERBB2</i>	[68–70]
	+8q	20–40%		
	+11q13	17–51%		
	+17q	9–10%		
	−8p	45–55%		
	−16q	>50%		
Prostate cancer	+8q	30–35%	<i>MYC</i> <i>EGFR</i> <i>NKX3-1</i> <i>RBI</i> <i>CDH1</i>	[71,72]
	+16p	25–50%		
	+7	25%		
	−8p	60–65%		
	−13q	50–55%		
	−16q	50–55%		
Lung cancer	+5p	60–65%	<i>TERT</i> <i>ARNT</i> <i>EGFR</i> <i>CCNE1</i> <i>CDKN2A/B</i>	[73,74]
	+1q	55–60%		
	+7p	40–45%		
	−8p	45%		
	−19p	40–45%		
	−9p	40–45%		

Table 1. Cont.

Cancer Type	CNAs (amp/del)	Frequency	Genes of Interest	Refs.
<i>Solid Tumour</i>				
Colorectal cancer	+7	41–46%	<i>EGFR, MET</i>	[75–77]
	+13q	56%	<i>AURKA, ASXL1, HNF4A</i>	
	+20q	72%		
	−8p	50%	<i>TP53</i>	
	−17p	56%		
−18	61–66%	<i>CADH7</i>		
Skin cancer	+7	50–55%	<i>EGFR</i>	[78–80]
	+6p	20–50%	<i>MYC</i>	
	+8q	5–40%		
	−6q	30–50%	<i>CDKN2A/B</i>	
	−9	20–50%		
−10	5–50%	<i>PTEN</i>		
<i>Acute leukaemia</i>				
Adult AML	+8	10–15%	<i>MYC</i>	[81,82]
	+21	4–6%	<i>ERG</i>	
	+22	4–6%	<i>EZH2</i>	
	−5/5q	10–15%		
	−7/7q	6–7%	<i>TP53</i>	
Paediatric AML	+8	10–14%	<i>MYC</i>	[81,83]
	+21	7–10%	<i>ERG</i>	
	+19	5%	<i>EZH2</i>	
	−5/5q	1.2%		
−7/7q	4–5%			
Adult B-ALL	+21	11%	<i>RUNX1, DYRK1A</i>	[84,85]
	−9p21	25–40%	<i>CDKN2A/B</i>	
	−7p12	30–40%	<i>IKZF1</i>	
	−9p13	20–40%	<i>PAX5</i>	
Paediatric B-ALL	+21	27% (100% HeH)	<i>RUNX1, DYRK1A</i>	[38,86,87]
	+6	90% in HeH	<i>CDKN2A/B</i>	
	+14	90% in HeH		
	−9p21	30–40%	<i>PAX5</i>	
	−9p13	20–30%	<i>IKZF1</i>	
−7p12	15–20%			

Data were extracted from references and using cBioportal [88] and the Mitelman database (available at <https://mitelmandatabase.isb-cgc.org/>) [89,90]. Lists of CNAs are not exhaustive and represent common alterations seen in the selected tumour type.

Somatic CNAs affecting well-known oncogenes and tumour suppressor genes such as *MYC* (located in 8q24), *EGFR* (7p11.2), *TP53* (17q13.1), *RB1* (13q14.2), and *CDKN2A/B* (9p21.3) are commonly seen across cancer. A recent study using computational analysis of 10,884 patients across 33 cancer types reported that the gain of human ch1q has prognostic value across multiple cancers [62]. In solid tumours, genomic amplification (amplicons) of *EGFR*, *MET*, *CCND1*, or *ERBB2* have been associated with inferior survival rates and have correlated with resistance to targeted therapies [91–95]. In prostate cancer, a recent study conducted by Alfahed et al. identified several markers associated with disease stage, Gleason grade group features and progression-free survival, confirming earlier observations [67,71]. They also showed that the combination of seven markers can differentiate patients with localised and advanced stages of prostate cancer. Another important aspect of screening CNAs in cancer patient samples is the potential to identify if CNAs infer sensitivity or cytotoxicity to therapeutic agents, as recently shown in melanoma and neuroblastoma [96,97]. Wong et al. correlated the gain of *PPM1D/GNA13* genes or loss of *CBL/DNMT3A* genes with enhanced cytotoxicity, whilst gains of *PI3K* or *STAT* family

genes sensitise neuroblastoma cells to cell cycle inhibitors [97]. Moreover, using the cancer proteome atlas, a predictive link between CNAs and phosphorylation changes has been discovered, providing a new potential readout to assess sensitivity to kinase inhibition in cancer [98].

At the chromosomal arm level, amplifications of 5p, 8q and 7p are among the most frequent CNAs seen in solid tumours and are often associated with 5q, 8p and 7q deletions through the formation of isochromosomes. This is observed in $\approx 25\%$ of solid tumours and the most frequent are i3q, i5p, i8q and i20q, with i8q being one of the most broadly acquired isochromosomes [99]. i8q or 8p deletions have also been associated with disease progression and poorer prognosis in breast, colorectal and prostate cancer [7,100,101]. In breast cancer, Cai et al. have shown that 8p deletions confer a loss of heterozygosity (LOH) phenotype, which results in alterations to lipid metabolism with an increase in drug resistance and tumour invasiveness [7]. Interestingly, while chromosome 7 is mostly gained in solid tumours, it is frequently lost in haematological malignancies (Table 1). This reflects the tissue specificity of CNAs in cancer and is most likely due to the presence of key oncogenes in solid tumours (*EGFR*, *MET* and *BRAF*), and well-known tumour suppressor genes in blood cancers (*CLIX1* and *IKZF1*).

Paediatric B-ALL is a well-known example of how treatments have been adapted using risk-stratification based on genetic alterations, including CNAs, to successfully improve outcomes. HeH B-ALL is the most common subtype of childhood B-ALL (25–30% of cases) and has a good prognosis overall [102]. The presence of double (+4, +10) or triple (+4, +10, +17) trisomy has also been shown to confer better outcomes [103,104]. Furthermore, with regard to drug sensitivity, ex vivo pharmacotypic profiling performed in a recent study revealed differential sensitivity to asparaginase, cytarabine and thiopurines in paediatric HeH B-ALL. Several chromosome-specific associations were identified, including the gain of chromosomes 7 and 9 with asparaginase resistance, the gain of chromosomes 16 and 17 with asparaginase sensitivity, and the gain of chromosomes 14 and 17 with mercaptopurine sensitivity [105].

At least two other subgroups are strictly defined by CNAs in B-ALL: HoH and iAMP21, both of which have poorer outcomes [102]. Inferior outcomes and drug resistance have also been associated with deletion of the *IKZF1* gene (7p12) in paediatric B-ALL but its impact on the outcome of adult B-ALL remains controversial; *IKZF1* encodes a critical regulator of lymphoid differentiation [85,86,106]. Notably, a recent study has recently refined the prognostic value of *IKZF1* alterations in a large cohort of paediatric B-ALL, demonstrating that MRD-positivity in patients with *IKZF1*^{plus} signature (i.e., *IKZF1* deletion plus other co-occurring deletions such as *CDKN2A*, *PAX5* or *PARI*) are associated with a very-poor prognosis [107]. CNAs also hold significant prognostic value in myeloid leukaemia. Deletions of the long arm of chromosome 7 (–7q) occur in up to 33% of AML cases [108,109]. In paediatric AML, monosomy 7 or 7q deletions are associated with a poor prognosis [108,110]; 5q deletions also result in inferior survival outcomes in AML and are sometimes observed together with 7q deletions [111]. Other common CNAs seen in leukaemia are gain of chromosome X in HeH B-ALL and loss of chromosome Y in AML but their role in leukaemogenesis and prognostic value remains unclear [81,87]. Notably, some CNAs seen in childhood acute leukaemia (+21 in B-ALL) are less frequently acquired in adult malignancies and vice versa (–5/5q in adult AML), emphasising the time and spatial sensitivity to CNAs for cellular transformation.

Altogether, these data illustrate the impact of integrating CNAs as prognostic factors to inform risk stratification and further explore sensitivity to conventional treatments

4.2. Constitutional CNV and Cancer

The impact of CNAs on cancer has also been unveiled by studying the phenotypes associated with inheritable and constitutional CNV-driven syndromes. Interestingly, studies assessing CNAs amongst healthy individuals revealed that 5–12% of the genome is subject to these genomic variations [112,113]. This includes large-scale differences of several kilo-

bases or greater, which for the most part do not result in disease phenotypes [114]. In line with these observations, Zarrei et al. highlighted that about 100 genes commonly implicated in CNV could be deleted without being associated with phenotypic differences [113]. In 2010, Conrad et al. referenced 30 loci with a potential role in the predisposition to specific diseases such as hepatitis B, schizophrenia, Crohn's disease and cancer [115]. Several germline or constitutional CNVs have been shown to increase the risk of cancer and affect development, progression, response to treatment, relapse and outcomes [116] (Table 2).

Among constitutional aneuploidies, individuals with Down syndrome (DS, trisomy 21), Turner syndrome (45,X) or Klinefelter syndrome (47,XXY) face a specific pattern of cancer incidence compared to the general population, with both an increased and decreased risk of developing tumours depending on time and tissue/organ [117–123]. Exemplifying this tumourigenic pattern, children with DS, but not adults, are at a significantly higher risk of developing both myeloid leukaemia (ML-DS, with features of megakaryoblastic leukaemia, 150-fold increased) and ALL (DS-ALL, 20-fold increased) compared to children without DS, while they have a reduced frequency of solid tumours apart from testicular germ cell tumour (reviewed in [117]). ML-DS is preceded by a pre-leukaemic transient abnormal myelopoiesis (TAM) that initiates during foetal life and often regresses spontaneously shortly after birth. Indicative of the impact of trisomy 21 in tumour initiation, Roberts et al. showed that nearly all neonates with DS exhibit perturbed haematopoiesis characterised by higher haematocrit and dyserythropoiesis, lower platelet count and several leukocyte abnormalities. More than 95% of cases had blasts in the peripheral blood and 20–30% of them developed TAM through the acquisition of a mutation in the *GATA1* gene [124]; the progression from TAM to ML-DS requires additional somatic alterations [117,125,126]. While the event-free survival is favourable and is approaching 90% in ML-DS, a recent international retrospective study showed that survival of relapsed/refractory ML-DS remains below 25% [127]. Children with DS are also predisposed to develop ALL with inferior outcomes compared to non-DS children due to increased incidence of relapse, death in induction and death in remission [128–130]. The genomic landscape of DS-ALL has been recently refined, emphasising new potential targetable mechanisms of oncogenic cooperation with trisomy 21 [131]. Of note, the pattern of gain of chromosome 21 as a somatic event in non-DS leukaemia (ranging from 4–34% in blood cancer in general) is further indicative of the pro-tumourigenic role associated with extra copies of this chromosome [132]. Other less frequent constitutional aneuploidies affecting autosomes such as trisomy 13 and trisomy 18 have also been shown to have an increased incidence of cancer; however, their prognostic value is not known due to the rarity of these CNV-driven cancers [133–135]. Constitutional trisomy 8 mosaicism has been shown to predispose to myeloid leukaemia in individual cases [136], which may correlate with somatic +8 being observed in 10–15% of AML cases [81,83].

Constitutional gain or loss of sex chromosome X has also been associated with variable incidence of cancer (Table 2). Several reports have shown that females with Turner syndrome (45,X) have a decreased incidence of breast cancer, although this remains contentious [119–121]. Notably, a gain of chromosome X in Klinefelter syndrome (47,XXY) leads to a higher rate of developing breast cancer, together with an increased incidence of non-Hodgkin lymphoma and leukaemia compared to the general population [123]. To date, there is no clear evidence of an increased incidence of breast cancer in constitutional trisomy/tetrasomy X syndromes; however, it has been speculated that this may be due to the fact that the additional X chromosomes are inactivated [137]. Strikingly, somatic gain of chromosome X, as well as defects in X inactivation, has been associated with more aggressive disease and poorer prognosis in breast cancer [138]. Extra copies of chromosome X have also been reported in pancreatic cancer as well as in specific subtypes of childhood ALL [87,139,140], but to date, its role in tumourigenesis remains unclear. Additionally, a large study of 2561 British patients with constitutional autosomal deletions of chromosomal arms, confirmed the known association between deletion 11p and 13q with Wilms tumour and retinoblastoma, respectively, and identified that deletions of the genomic region 11q24 may predispose to anogenital cancer, in line with the recurrent somatic alterations described

in these solid tumours [141–143]. Notably, several studies have reported cancer cases with other constitutional CNV such as Prader–Willi syndrome (deletion 15q11.2–q13) [144], DiGeorge syndrome (deletion 22q11.2) [145], Cri du Chat syndrome (deletion 5p) [146], and Williams–Beuren syndrome (deletion 7q11.23) [147], but their true incidence and any potential link with clinical outcomes remains unclear.

Altogether, whether they are pro- or anti-tumourigenic, the role of CNA/CNV in tumour development and response to treatment is now well established. This is in line with the increasing amount of pharmacogenomic studies showing that germline alterations not only predispose to cancer but also modify treatment outcomes between patients that have a similar tumour type [148]. However, the exact role of most CNA/CNV remains elusive and is likely to depend on the cellular context, temporal acquisition and cooperation with other genetic alterations (including other CNAs). Due to their high incidence, a better understanding of the intimate link between CNAs and tumourigenesis would provide new opportunities to prevent and improve outcomes for individuals with cancer.

Table 2. Common CNV-related disorders associated with cancer.

CNV-Driven Syndromes (Incidence)	Type of CNV	Higher Incidence of Cancer	Lower Incidence of Cancer	Refs.
Down syndrome (1/700–800)	Trisomy 21	ALL, TAM/ML-DS, testicular germ cell tumour	Solid tumours	[117,118]
Edwards syndrome (1/6000)	Trisomy 18	Hepatoblastoma, Wilms tumour, benign cardiac tumours *	N/A	[134,135]
Patau syndrome (1/10,000–20,000)	Trisomy 13	Embryonic tumours, malignant germ cell tumours, leukaemia, carcinoma, brain cancer and sarcoma	N/A	[133]
Turner syndrome (1/1200–2500, female births)	Monosomy X (45,X)	Benign/malignant skin neoplasm and cancers, brain tumours, bladder and urethral cancer, colorectal cancer	Breast cancer	[119–121]
Klinefelter syndrome (1.72/1000 male births)	Extra X (47,XXY)	Breast cancer, lung cancer, germ cell tumours, non-Hodgkin lymphoma, ALL and myeloid leukaemia	Solid tumours, prostate cancer	[120,122,123]
Warkany syndrome 2 (1/25,000–50,000)	Mosaic Trisomy 8	Myeloid leukaemia *	N/A	[136]
Prader–Willi syndrome (1/15,000–30,000)	Deletion 15q11.2–q13	ALL and myeloid leukaemia, biliary cancer, melanoma, hemangiopericytoma, adenocarcinoma, colon cancer *	N/A	[144,149]
11p deletion/WAGR syndrome (<1/500,000)	Deletion 11p13	Wilms tumour	N/A	[143]
13q deletion syndrome (very rare)	Deletion 13q14	Retinoblastoma	N/A	[143]
11q24 deletion syndrome (very rare)	Deletion 11q24	Anogenital cancer	N/A	[143]

* based on case studies. N/A = not applicable.

5. Overview of the Mechanisms Disturbed by CNA/CNV in Cancer

As CNA/CNV perturb the dosage of genes and regulatory elements (promoters, enhancers, microRNA), it is viewed that they ultimately alter the expression of hundreds or thousands of genes, not only in the chromosomal regions amplified or deleted but also genome-wide, thus impacting key biological functions such as transcription, splicing machinery, DNA methylation, histone modification and cell metabolism, among others. In cancer cells, it has been proposed that CNAs promote tumourigenesis by providing the cellular fitness required for transformation, depending on the balance of tumour-suppressive and oncogenic function of the genes included within the amplified/deleted genomic region.

Whether these alterations are direct oncogenic drivers or passively promote genetic instability to facilitate tumorigenesis remains elusive. Thus, understanding the impact of this CNA/CNV and identifying the dosage-sensitive genes may provide a detailed network of cancer-promoting/targetable pathways. However, this is a complex task as (1) there are a limited amount of clinically relevant models that can be used to assess CNA/CNV function, (2) not all genes/regulatory elements included in the CNA/CNV are dosage sensitive and so may not be targetable, (3) tumour heterogeneity (cohabitation of distinct genetic phenotypic clones) may impede the discovery of dosage-sensitive mechanisms, (4) CNAs may cooperate with other genetic alterations (including other CNAs) that could be tissue-specific and may be modulated by the tumour microenvironment. As an example of the latter, xenograft models have revealed that CNAs can provide cellular fitness and facilitate clonal selection in an exogenous murine environment [150]. In this section, we will present selected examples of models and experimental approaches used to dissect the role of CNAs in cancer, drawing a snapshot of the key mechanisms they alter and exposing the challenges that remain to fully understand their role.

5.1. Identifying Dosage Sensitive Genes

The number of genes/regulatory elements included within the CNAs does not always correlate with tumorigenicity, as not all of them are expressed or active in a specific cell type, at a specific time (ontogenic and/or cellular state, therapeutic response and resistance) or in a specific clinical condition (healthy, chronic disease, cancer progression). It is also tempting to speculate that cellular function affected by dosage sensitivity may be dependent upon the precise 'number of copies' of key genes/regulatory elements. Apart from the CNAs that affect the expression of well-known tumour-associated genes (such as *MYC*, *TP53*, *RBI* and *CDKN2A/B*), the true impact of many genes affected by CNAs and whether these genes are dosage-sensitive remains unknown. Genomic analyses aiming at refining minimal regions that are deleted or amplified between different specimens have facilitated the identification of such genes.

According to the 'two-hit' Knudson hypothesis, the minimal genomic region deleted in 11p13 deletion/WAGR syndrome led to the identification of one of the first tumour suppressor genes *WT1* [151,152], a gene that encodes a zinc finger transcription factor known to control transcription via its direct interaction with DNA, DNA hydroxymethylation and RNA metabolism. Interestingly, *WT1* has been shown to regulate many cellular processes, such as cell proliferation, survival and differentiation, as well as tissue-specific processes such as mesenchymal-epithelial transition in the nephron and epithelial-mesenchymal transition in the developing heart [153]. These contrasting roles are exemplified by the observation that *WT1* is now also considered as an oncogene in several cancers including breast cancer, glioblastoma, pancreatic cancer and AML. In the latter, *WT1* is overexpressed in more than 80% of cases, has been associated with resistance to therapy, increased rate of relapse and inferior overall survival, and can be used as a biomarker for the detection of minimal residual disease [154]. Moreover, amplification of the tyrosine kinase receptors *HER2/ERBB2*, *MET* and *EGFR* has been observed in many solid tumours (breast, lung and brain, among others), driving tumorigenesis through the uncontrolled activation of downstream signalling (such as PI3K/PTEN/mTOR and RAS/MAPK pathways) leading to growth, proliferation and survival; amplifications of these genes are also commonly associated with metastasis and therapy resistance [91,155–157].

One of the best examples of the impact of large CNA/CNV in tumorigenesis lies in understanding the critical balance of tumour suppressor genes and tumour promoter dosage-sensitive genes located on chromosome 21. Figure 3 proposes several *scenarios* that may explain the preventative and predisposing/promoting role of trisomy 21. This small chromosome 21 is gained more often than any other chromosome in haematological malignancies, which is in contrast to solid tumours [2] (Table 1). Strikingly, the incidence of complete or partial gain of chromosome 21 reaches 25–30% in paediatric B-ALL and 30–35% in acute megakaryoblastic leukaemia (AMKL), and the observation that individ-

uals with DS are predisposed to B-ALL and AMKL indicates that both the B-cell and megakaryocytic lineages are strongly sensitive to the increased dosage of chromosome 21 genes during childhood [132]. To investigate this dichotomy, several groups have used murine models of DS harbouring various sizes of trisomy 21 to identify the chromosome 21 genes that are implicated (reviewed in [132]). It has been confirmed that trisomy 21 promotes leukaemia development [158–160], but also prevents solid tumour formation, the latter being linked to the impact of trisomy 21 on neural development, angiogenesis and metabolism [118,161–163]. Interestingly, this confirms that several dosage-sensitive genes can either promote or suppress tumourigenesis and that several dosage-sensitive chromosome 21 genes cooperate to drive these phenotypes. For instance, it has been shown that trisomy of the chromosome 21 genes *DYRK1A* plus *RCAN1* decreases solid tumour growth through the additive inhibition of the Calcineurin/NFAT pathway [161]. Using a similar approach, Reynolds et al. demonstrated that trisomy of *JAM-B*, *PTTG1IP*, *ADAMTS1* and *ERG* (a well-known oncogene in prostate cancer and leukaemia) prevents tumour growth by inhibiting neo-angiogenesis [162]. In line with tissue specificity, several studies have shown that increased dosage and expression of *ERG*, *ETS2*, *HMGNI*, *CHAF1B* and *DYRK1A*, as well as disequilibrium in transcripts of the chromosome 21 gene *RUNX1* induced by trisomy 21, promote leukaemia development [158,159,164–167]. Interestingly, *DYRK1A* has been shown to modulate the activity of many effectors with oncogenic and tumour suppressive functions (STAT3, NOTCH1, FOXO1, Cyclin D1/D3, Rb1, TP53, P21) in a tissue-dependent manner, altering several signalling pathways through distinct mechanisms, regulating the cellular fitness, metabolism, DNA repair, cell division, proliferation/growth and survival in different cancers [168].

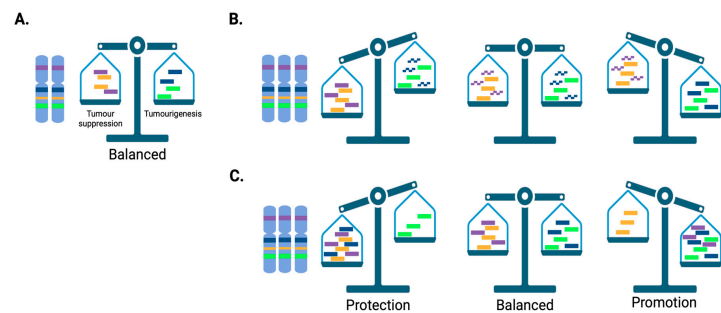


Figure 3. Dosage sensitivity and tumourigenesis. (A) Disomic cells have the right dosage of tumour-suppressing and tumour-promoting genes (or regulatory elements) to maintain cellular homeostasis. (B,C) Two examples of trisomic cells with different scenarios of genes/regulatory elements expressed (solid) versus not expressed (dashed) that may protect, not affect (balanced) or promote tumourigenesis in different tissues. Created with [BioRender.com](https://www.biorender.com) (accessed on 21 May 2024).

5.2. Role of large CNA/CNV and Aneuploidy in Cancer Development

Characterisation of single dosage-sensitive genes has the potential to lead to novel targeted therapies but does not offer the opportunity to understand the role of CNA/CNV as a whole, with potentially hundreds or thousands of genes affected by dosage imbalances. Historically, animal models harbouring aneuploidies have been used to better understand the impact of chromosomal deletion and amplification in specific syndromes such as Prader–Willi syndrome, Williams–Beuren syndrome or DS (reviewed in [169]). While crucial mechanisms have been identified using these models, the location of the chromosomal regions syntenic to the human chromosomes within the murine genome may also be a confounding factor. As an example, syntenic regions of human chromosome 13 (Hsa13) are spread over six murine chromosomes and Hsa21 over three murine chromosomes: Mm10, Mm16 and Mm17. Therefore, trisomy of Mm16 (as in Ts65Dn, the most commonly used

model to study DS) does not completely recapitulate human trisomy 21, as it is disomic for Mm10 and Mm17 and has additional Mm16 trisomic genes that are not syntenic to Hsa21 [170]. To bypass these limitations, new models of DS have been established. This includes transgenic models triplicated for Mm10, Mm16 and Mm17 [171], as well as the Tc1 and TcMAC21 models, which were developed using microcell mediated chromosome transfer [172], that span 70–75% of the protein-coding Hsa21 genes [173,174]. As mentioned above, many of these models have been used to dissect the role of trisomy 21 in promoting leukaemia and preventing solid tumour development.

Whereas understanding the impact of aneuploidy remains challenging in transgenic mice, several key observations have been obtained using cellular models. In mouse embryonic fibroblasts (MEF), it has been shown that single gains of murine chromosome 1, 13, 16 and 19 decrease tumourigenicity, in part by promoting premature growth arrest, while a gain of murine chromosome 2 increased proliferation; reduction in tumourigenicity due to specific trisomies was also reported in the colorectal cell line HCT116 [175]. However, in another study, Vasudevan et al. demonstrated that trisomy of chromosome 5 specifically promotes tumour progression and invasiveness of HCT116 cells [176]. Contrasting results are also observed in MEF cells that have reduced levels of the centromere-linked motor protein E (CENP-E^{+/-}), where aneuploidy can both promote or inhibit transformation in vitro, and tumourigenesis in vivo in a tissue-dependent manner (lymphoma versus liver cancer, respectively) [177]. Other roles known to be affected by CNAs in cancer are linked to cell metabolism (reactive oxygen species levels, glycolysis, mitochondrial activity and endoplasmic reticulum stress) and modulation of the immune environment (reviewed in [178]) [179,180]. This evidence supports the dichotomic role of CNAs in cancer and re-emphasises the complexity of understanding their true impact on cancer development.

With the advent of gene editing technologies such as Transcription Activator-Like Effector Nucleases (TALEN) and Clustered Regularly Interspaced Short Palindromic Repeats (CRISPR), new approaches have been designed to reproduce and dissect the role of CNA/CNV in debilitating diseases and cancer. For example, Tai et al. applied single-guide CRISPR/Cas targeting of repetitive elements (SCORE), a CRISPR-based approach that targets the homologous sites in flanking segmental duplications, to create microdeletion (15q13.3) and microduplication (16q11.2) syndromes [181]. In a model of breast cancer, Cai et al. used TALEN to model chromosome 8p LOH by non-homologous end-joining in MCF10A mammary epithelial cells (33 Mb deletion, downregulation of 81 protein-coding genes) and showed that alterations in lipid metabolism result in increased drug resistance and tumour invasiveness [7]. TALEN and CRISPR technology have also been used to restore gene dosage in trisomic samples. Focusing on DS and leukaemia, Banno et al. deleted a 4 Mb region of chromosome 21 in DS induced pluripotent stem (iPS) cells to show that the transcription factors ERG, RUNX1 and ETS2 play a role in TAM/ML-DS [182]. Alternative applications of CRISPR and TALEN technologies have allowed for the elimination and silencing of the extra chromosome 21 in DS iPS cells by inducing multiple DNA strand breaks or by integrating long non-coding RNA X-inactive specific transcript into the extra copy of chromosome 21, respectively [183,184]. Recently, CRISPR technology has allowed for the development of elegant approaches such as molecular alteration of chromosomes with engineered tandem elements (MACHETE) and restoring disomy in aneuploid cells using CRISPR targeting (ReDACT) to model CNAs in cancer [62,185]. MACHETE provides the opportunity to efficiently delete large chromosomal segments and has been used to show that homozygous deletion of the type I interferon cluster, seen in more than 10% of cancer, promotes metastasis by mediating immune evasion in a syngeneic murine model of pancreatic cancer [185]. Girish et al. showed that a gain of chromosome 1q associated with increased *MDM4* expression and suppression of TP53 signalling is an early event in cancer development and developed ReDACT to demonstrate that loss of trisomy 1q blocked growth and prevented malignant transformation of cancer cell lines in vitro and in vivo [62]. This system has been used for several other CNA/aneuploidy in different cellular contexts to confirm that these chromosomal alterations modulate cellular fitness

and draw on the concept of ‘aneuploidy/CNA addiction’ in cancer. Overall, these selected examples show that TALEN/CRISPR technologies have been instrumental in dissecting the roles and mechanisms induced by CNAs in cancer.

Altogether, this evidence confirms that CNAs are key drivers of tumourigenesis with functions dependent upon multiple factors including the size (number of tumour promotor/suppressor genes/regulatory elements), the chromosome or genomic region affected, the cell type/tissue, tumour stage, clonal heterogeneity and the impact of the microenvironment. Despite increasing knowledge in this area of research, the true role of CNA/CNV remains controversial in some instances, which exemplifies the complexity of dissecting their role in cancer, as opposed to gene mutations or translocations. Further investigations are warranted and will require the development of innovative approaches to unlock new mechanisms of cancer development and identify novel therapeutic targets.

6. Targeting CNA/CNV to Improve Outcomes

Due to their incidence in cancer and dosage dependency, therapeutically targeting CNAs/CNVs to restore disomy represents an attractive opportunity to improve patient outcomes. Whether this can be achieved directly by targeting the key dosage-sensitive genes/regulatory elements or the mechanisms they perturb, or by ‘unbalancing’ the cellular fitness provided by CNAs to disturb tumour homeostasis, is a promising therapeutic avenue.

While alternative strategies are still needed to target the ‘undruggable’ *MYC* oncogene (overexpressed in about 70% of all cancers), targeting tyrosine kinases amplified and overexpressed in specific cancers has shown some success. Perhaps one of the best examples is therapy targeting *HER2/ERBB2* amplifications in breast cancer. In recent decades, new targeted agents have been developed, which are now used in the clinic to treat patients with breast cancer such as monoclonal antibodies (trastuzumab, pertuzumab, margetuximab) and tyrosine kinase inhibitors (afatinib, lapatinib, neratinib, pyrotinib and tucatinib) [186,187]. Other well-known examples of tyrosine kinase inhibitors and monoclonal antibodies proven to be of clinical use are those targeting *c-MET* (in lung cancer), *EGFR* (in breast, lung, gastric and pancreatic cancer), and *FLT3* (acute leukaemia). However, various mechanisms of resistance can develop by the tumour cells themselves (e.g., gene amplification, mutations and clonal selection) or by the stroma (protective effects) to bypass the efficacy of these agents, thus emphasising the need for alternative strategies to improve long-term outcomes.

Through the identification of new dosage-sensitive genes in children with DS and leukaemia, several groups have shown that targeting the product of the chromosome 21 genes *HMGN1* and *DYRK1A* may be broadly applicable to many blood cancers and potentially solid tumours [158,159,165]. Indeed, increased dosage of the high mobility group nucleosome-binding protein N1 (*HMGN1*) has been shown to upregulate B-cell-specific transcriptional signatures in DS-ALL as well as subtypes of B-ALL harbouring gain of chromosome 21, by antagonising the PRC2 complex (reduced H3K27me3 marks) and increasing chromatin accessibility (increased H3K27ac marks) [159]; notably, *HMGN1* has also been shown to cooperate with the transcript fusion *AML1-ETO9a* to promote AML [188]. Restoring chromatin accessibility using inhibitors of histone demethylase (GSK-J4) or histone acetyl transferase (C646) has shown promising in vitro and in vivo results for both B-ALL and AML [159,188,189]. Another attractive target encoded by chromosome 21 is the dual-specificity tyrosine-regulated kinase *DYRK1A*. We and others have shown that trisomy of *DYRK1A* contributes to the development of both ML-DS and DS-ALL, and that inhibition of its kinase activity or of its targets (*STAT3*, *FOXO1*, *Cyclin D3*) decreases growth and survival in vitro and prolongs in vivo survival [165,190]. Results from in vitro drug combination testing are promising, and future directions should consider clinical evaluation in early phase trials for leukaemia, as well as for tumours with poor prognosis, such as glioblastoma or head and neck cancer, where *DYRK1A* has also been implicated [191,192]. Finally, a recent study from Memon et al. demonstrated that CNAs

modulate signalling pathway activity in many cancers and can be used as a predictor of sensitivity to kinase inhibitors, suggesting that disturbing this refined and balanced activity may help to design more adapted and less toxic therapies [98]. This ‘kinase addiction’ phenomenon indicates that the use of biologically informed inhibitors has the potential to improve outcomes for patients with CNA-driven cancer. Interestingly, a recent study also demonstrated that aneuploid cancer cells are sensitive to spindle assembly checkpoint inhibitors due to their intrinsically perturbed activity of the kinesin KIF18A [193].

Further investigations are warranted to assess the functional output and crosstalk between CNA/CNV as well as with other somatic alterations within the individual cancer cell, between several clones, and with the tumour microenvironment. A clearer understanding of these mechanisms will allow the identification of biomarkers to develop new monitoring tools to better follow response to treatments and of an ‘Achilles heel’ to design novel effective combination therapies to decrease treatment toxicity, prevent relapse and improve long-term survival.

7. Future Directions

CNAs/CNVs constitute a considerable genomic phenomenon that not only affects the primary target (i.e., the chromosome) but also creates several imbalances at the genomic, transcriptomic and proteomic levels. Thus, CNAs/CNVs may have huge consequences on cellular biology by affecting intracellular signalling, epigenetic mechanisms, metabolism, immune response, and therapy resistance among others, which ultimately result in providing cellular fitness to tumour cells. While they are one of the most known and frequent alterations seen in cancer cells, we are only just beginning to understand their true function. Clinically, CNAs/CNVs can be informative with regard to cancer predisposition, cancer development and progression, response to treatment and resistance, and long-term outcomes. Recent observations have emphasised that manipulation of CNAs strongly affects tumour homeostasis, suggesting that we have opened Pandora’s box regarding new opportunities to better understand tumorigenesis, identify new actionable targets and integrate dosage-dependent therapies into the clinic.

Author Contributions: S.L.C.-S., R.S.K. and S.M. wrote the manuscript. L.C.C. provided critical insights. All authors have read and agreed to the published version of the manuscript.

Funding: This research was funded by the Child Cancer Research Foundation (CCRF) and the Jérôme Lejeune Foundation. S.L.C.-S. is supported by Australian Government Research Training Program (RTP) Scholarship. R.S.K., L.C.C. and S.M. are supported by project grants from the Child Cancer Research Foundation (CCRF). S.M. is supported by a Fellowship from the Cancer Council Western Australia (CCWA).

Conflicts of Interest: R.S.K. discloses advisory board participation from Jazz Pharmaceuticals, Amgen and Link Healthcare. The remaining authors declare that the research was conducted in the absence of any commercial or financial relationships that could be construed as a potential conflict of interest.

References

1. Beroukhi, R.; Mermel, C.H.; Porter, D.; Wei, G.; Raychaudhuri, S.; Donovan, J.; Barretina, J.; Boehm, J.S.; Dobson, J.; Urashima, M.; et al. The landscape of somatic copy-number alteration across human cancers. *Nature* **2010**, *463*, 899–905. [\[CrossRef\]](#)
2. Duijff, P.H.; Schultz, N.; Benezra, R. Cancer cells preferentially lose small chromosomes. *Int. J. Cancer* **2013**, *132*, 2316–2326. [\[CrossRef\]](#)
3. Steele, C.D.; Abbasi, A.; Islam, S.M.A.; Bowes, A.L.; Khandekar, A.; Haase, K.; Hames-Fathi, S.; Ajayi, D.; Verfaillie, A.; Dhani, P.; et al. Signatures of copy number alterations in human cancer. *Nature* **2022**, *606*, 984–991. [\[CrossRef\]](#)
4. Hieronymus, H.; Murali, R.; Tin, A.; Yadav, K.; Abida, W.; Moller, H.; Berney, D.; Scher, H.; Carver, B.; Scardino, P.; et al. Tumor copy number alteration burden is a pan-cancer prognostic factor associated with recurrence and death. *eLife* **2018**, *7*, e37294. [\[CrossRef\]](#)
5. Harbers, L.; Agostini, F.; Nicos, M.; Poddighe, D.; Bienko, M.; Crosetto, N. Somatic Copy Number Alterations in Human Cancers: An Analysis of Publicly Available Data from the Cancer Genome Atlas. *Front. Oncol.* **2021**, *11*, 700568. [\[CrossRef\]](#)
6. Shao, X.; Lv, N.; Liao, J.; Long, J.; Xue, R.; Ai, N.; Xu, D.; Fan, X. Copy number variation is highly correlated with differential gene expression: A pan-cancer study. *BMC Med. Genet.* **2019**, *20*, 175. [\[CrossRef\]](#)

7. Cai, Y.; Crowther, J.; Pastor, T.; Abbasi Asbagh, L.; Baietti, M.F.; De Troyer, M.; Vazquez, I.; Talebi, A.; Renzi, F.; Dehairs, J.; et al. Loss of Chromosome 8p Governs Tumor Progression and Drug Response by Altering Lipid Metabolism. *Cancer Cell* **2016**, *29*, 751–766. [[CrossRef](#)] [[PubMed](#)]
8. Parris, T.Z.; Danielsson, A.; Nemes, S.; Kovacs, A.; Delle, U.; Fallenius, G.; Mollerstrom, E.; Karlsson, P.; Helou, K. Clinical implications of gene dosage and gene expression patterns in diploid breast carcinoma. *Clin. Cancer Res.* **2010**, *16*, 3860–3874. [[CrossRef](#)]
9. Li, L.; Li, M.; Sun, C.; Francisco, L.; Chakraborty, S.; Sabado, M.; McDonald, T.; Gyorffy, J.; Chang, K.; Wang, S.; et al. Altered hematopoietic cell gene expression precedes development of therapy-related myelodysplasia/acute myeloid leukemia and identifies patients at risk. *Cancer Cell* **2011**, *20*, 591–605. [[CrossRef](#)]
10. Dagogo-Jack, I.; Shaw, A.T. Tumour heterogeneity and resistance to cancer therapies. *Nat. Rev. Clin. Oncol.* **2018**, *15*, 81–94. [[CrossRef](#)]
11. Pos, O.; Radvanszky, J.; Buglyo, G.; Pos, Z.; Rusnakova, D.; Nagy, B.; Szemes, T. DNA copy number variation: Main characteristics, evolutionary significance, and pathological aspects. *Biomed. J.* **2021**, *44*, 548–559. [[CrossRef](#)] [[PubMed](#)]
12. Gordeeva, V.; Sharova, E.; Arapidi, G. Progress in Methods for Copy Number Variation Profiling. *Int. J. Mol. Sci.* **2022**, *23*, 2143. [[CrossRef](#)] [[PubMed](#)]
13. Kallioniemi, A.; Kallioniemi, O.P.; Sudar, D.; Rutovitz, D.; Gray, J.W.; Waldman, F.; Pinkel, D. Comparative genomic hybridization for molecular cytogenetic analysis of solid tumors. *Science* **1992**, *258*, 818–821. [[CrossRef](#)] [[PubMed](#)]
14. Wang, D.G.; Fan, J.B.; Siao, C.J.; Berno, A.; Young, P.; Sapolsky, R.; Ghandour, G.; Perkins, N.; Winchester, E.; Spencer, J.; et al. Large-scale identification, mapping, and genotyping of single-nucleotide polymorphisms in the human genome. *Science* **1998**, *280*, 1077–1082. [[CrossRef](#)] [[PubMed](#)]
15. LaFramboise, T. Single nucleotide polymorphism arrays: A decade of biological, computational and technological advances. *Nucleic Acids Res.* **2009**, *37*, 4181–4193. [[CrossRef](#)] [[PubMed](#)]
16. Charbonnier, F.; Raux, G.; Wang, Q.; Drouot, N.; Cordier, F.; Limacher, J.M.; Saurin, J.C.; Puisieux, A.; Olschwang, S.; Frebourg, T. Detection of exon deletions and duplications of the mismatch repair genes in hereditary nonpolyposis colorectal cancer families using multiplex polymerase chain reaction of short fluorescent fragments. *Cancer Res.* **2000**, *60*, 2760–2763. [[PubMed](#)]
17. Armour, J.A.; Sismani, C.; Patsalis, P.C.; Cross, G. Measurement of locus copy number by hybridisation with amplifiable probes. *Nucleic Acids Res.* **2000**, *28*, 605–609. [[CrossRef](#)] [[PubMed](#)]
18. Schouten, J.P.; McElgunn, C.J.; Waaijer, R.; Zwijnenburg, D.; Diepvens, F.; Pals, G. Relative quantification of 40 nucleic acid sequences by multiplex ligation-dependent probe amplification. *Nucleic Acids Res.* **2002**, *30*, e57. [[CrossRef](#)]
19. Mallory, X.F.; Edrisi, M.; Navin, N.; Nakhleh, L. Methods for copy number aberration detection from single-cell DNA-sequencing data. *Genome Biol.* **2020**, *21*, 208. [[CrossRef](#)] [[PubMed](#)]
20. Zhao, M.; Wang, Q.; Wang, Q.; Jia, P.; Zhao, Z. Computational tools for copy number variation (CNV) detection using next-generation sequencing data: Features and perspectives. *BMC Bioinform.* **2013**, *14* (Suppl. 11), S1. [[CrossRef](#)]
21. Yang, H.; Garcia-Manero, G.; Sasaki, K.; Montalban-Bravo, G.; Tang, Z.; Wei, Y.; Kadia, T.; Chien, K.; Rush, D.; Nguyen, H.; et al. High-resolution structural variant profiling of myelodysplastic syndromes by optical genome mapping uncovers cryptic aberrations of prognostic and therapeutic significance. *Leukemia* **2022**, *36*, 2306–2316. [[CrossRef](#)] [[PubMed](#)]
22. Neveling, K.; Mantere, T.; Vermeulen, S.; Oorsprong, M.; van Beek, R.; Kater-Baats, E.; Pauper, M.; van der Zande, G.; Smeets, D.; Weghuis, D.O.; et al. Next-generation cytogenetics: Comprehensive assessment of 52 hematological malignancy genomes by optical genome mapping. *Am. J. Hum. Genet.* **2021**, *108*, 1423–1435. [[CrossRef](#)] [[PubMed](#)]
23. Levy, B.; Kanagal-Shamanna, R.; Sahajpal, N.S.; Neveling, K.; Rack, K.; Dewaele, B.; Olde Weghuis, D.; Stevens-Kroef, M.; Puiggros, A.; Mallo, M.; et al. A framework for the clinical implementation of optical genome mapping in hematologic malignancies. *Am. J. Hematol.* **2024**, *99*, 642–661. [[CrossRef](#)] [[PubMed](#)]
24. Ben-David, U.; Amon, A. Context is everything: Aneuploidy in cancer. *Nat. Rev. Genet.* **2020**, *21*, 44–62. [[CrossRef](#)] [[PubMed](#)]
25. McGranahan, N.; Burrell, R.A.; Endesfelder, D.; Novelli, M.R.; Swanton, C. Cancer chromosomal instability: Therapeutic and diagnostic challenges. *EMBO Rep.* **2012**, *13*, 528–538. [[CrossRef](#)] [[PubMed](#)]
26. Cairo, G.; Lacefield, S. Establishing correct kinetochore-microtubule attachments in mitosis and meiosis. *Essays Biochem.* **2020**, *64*, 277–287. [[CrossRef](#)]
27. Antony, J.; Chin, C.V.; Horsfield, J.A. Cohesin Mutations in Cancer: Emerging Therapeutic Targets. *Int. J. Mol. Sci.* **2021**, *22*, 6788. [[CrossRef](#)]
28. Sun, S.C.; Kim, N.H. Spindle assembly checkpoint and its regulators in meiosis. *Hum. Reprod. Update* **2012**, *18*, 60–72. [[CrossRef](#)] [[PubMed](#)]
29. Tjihuis, A.E.; Johnson, S.C.; McClelland, S.E. The emerging links between chromosomal instability (CIN), metastasis, inflammation and tumour immunity. *Mol. Cytogenet.* **2019**, *12*, 17. [[CrossRef](#)] [[PubMed](#)]
30. Bolhaqueiro, A.C.F.; Ponsioen, B.; Bakker, B.; Klaasen, S.J.; Kucukkose, E.; van Jaarsveld, R.H.; Vivie, J.; Verlaan-Klink, I.; Hami, N.; Spierings, D.C.J.; et al. Ongoing chromosomal instability and karyotype evolution in human colorectal cancer organoids. *Nat. Genet.* **2019**, *51*, 824–834. [[CrossRef](#)]
31. Passerini, V.; Ozeri-Galai, E.; de Pagter, M.S.; Donnelly, N.; Schmalbrock, S.; Kloosterman, W.P.; Kerem, B.; Storchova, Z. The presence of extra chromosomes leads to genomic instability. *Nat. Commun.* **2016**, *7*, 10754. [[CrossRef](#)]

32. Molina, O.; Ortega-Sabater, C.; Thampi, N.; Fernandez-Fuentes, N.; Guerrero-Murillo, M.; Martinez-Moreno, A.; Vinyoles, M.; Velasco-Hernandez, T.; Bueno, C.; Trincado, J.L.; et al. Chromosomal instability in aneuploid acute lymphoblastic leukemia associates with disease progression. *EMBO Mol. Med.* **2024**, *16*, 64–92. [[CrossRef](#)]
33. Negrini, S.; Gorgoulis, V.G.; Halazonetis, T.D. Genomic instability—An evolving hallmark of cancer. *Nat. Rev. Mol. Cell Biol.* **2010**, *11*, 220–228. [[CrossRef](#)]
34. Onodera, N.; McCabe, N.R.; Rubin, C.M. Formation of a hyperdiploid karyotype in childhood acute lymphoblastic leukemia. *Blood* **1992**, *80*, 203–208. [[CrossRef](#)]
35. Molina, O.; Vinyoles, M.; Granada, I.; Roca-Ho, H.; Gutierrez-Aguera, F.; Valledor, L.; Lopez-Lopez, C.M.; Rodriguez-Gonzalez, P.; Trincado, J.L.; Menendez, S.T.; et al. Impaired condensin complex and Aurora B kinase underlie mitotic and chromosomal defects in hyperdiploid B-cell ALL. *Blood* **2020**, *136*, 313–327. [[CrossRef](#)]
36. Paulsson, K.; Morse, H.; Fioretos, T.; Behrendtz, M.; Strombeck, B.; Johansson, B. Evidence for a single-step mechanism in the origin of hyperdiploid childhood acute lymphoblastic leukemia. *Genes Chromosomes Cancer* **2005**, *44*, 113–122. [[CrossRef](#)]
37. Woodward, E.L.; Yang, M.; Moura-Castro, L.H.; van den Bos, H.; Gunnarsson, R.; Olsson-Arvidsson, L.; Spierings, D.C.J.; Castor, A.; Duployez, N.; Zaliouva, M.; et al. Clonal origin and development of high hyperdiploidy in childhood acute lymphoblastic leukaemia. *Nat. Commun.* **2023**, *14*, 1658. [[CrossRef](#)]
38. Brady, S.W.; Roberts, K.G.; Gu, Z.; Shi, L.; Pounds, S.; Pei, D.; Cheng, C.; Dai, Y.; Devidas, M.; Qu, C.; et al. The genomic landscape of pediatric acute lymphoblastic leukemia. *Nat. Genet.* **2022**, *54*, 1376–1389. [[CrossRef](#)]
39. Paulsson, K.; Johansson, B. High hyperdiploid childhood acute lymphoblastic leukemia. *Genes Chromosomes Cancer* **2009**, *48*, 637–660. [[CrossRef](#)]
40. Molina, O.; Bataller, A.; Thampi, N.; Ribera, J.; Granada, I.; Velasco, P.; Fuster, J.L.; Menendez, P. Near-Haploidy and Low-Hypodiploidy in B-Cell Acute Lymphoblastic Leukemia: When Less Is Too Much. *Cancers* **2021**, *14*, 32. [[CrossRef](#)]
41. Storlazzi, C.T.; Fioretos, T.; Surace, C.; Lonoce, A.; Mastrorilli, A.; Strombeck, B.; D’Addabbo, P.; Iacovelli, F.; Minervini, C.; Aventin, A.; et al. MYC-containing double minutes in hematologic malignancies: Evidence in favor of the episome model and exclusion of MYC as the target gene. *Hum. Mol. Genet.* **2006**, *15*, 933–942. [[CrossRef](#)] [[PubMed](#)]
42. Liu, R.; Shi, P.; Wang, Z.; Yuan, C.; Cui, H. Molecular Mechanisms of MYCN Dysregulation in Cancers. *Front. Oncol.* **2020**, *10*, 625332. [[CrossRef](#)]
43. McClintock, B. The Stability of Broken Ends of Chromosomes in Zea Mays. *Genetics* **1941**, *26*, 234–282. [[CrossRef](#)]
44. Stephens, P.J.; Greenman, C.D.; Fu, B.; Yang, F.; Bignell, G.R.; Mudie, L.J.; Pleasance, E.D.; Lau, K.W.; Beare, D.; Stebbings, L.A.; et al. Massive genomic rearrangement acquired in a single catastrophic event during cancer development. *Cell* **2011**, *144*, 27–40. [[CrossRef](#)]
45. Rausch, T.; Jones, D.T.; Zapotka, M.; Stutz, A.M.; Zichner, T.; Weischenfeldt, J.; Jager, N.; Remke, M.; Shih, D.; Northcott, P.A.; et al. Genome sequencing of pediatric medulloblastoma links catastrophic DNA rearrangements with TP53 mutations. *Cell* **2012**, *148*, 59–71. [[CrossRef](#)]
46. Ostapinska, K.; Styka, B.; Lejman, M. Insight into the Molecular Basis Underlying Chromothripsis. *Int. J. Mol. Sci.* **2022**, *23*, 3318. [[CrossRef](#)] [[PubMed](#)]
47. Cortes-Ciriano, I.; Lee, J.J.; Xi, R.; Jain, D.; Jung, Y.L.; Yang, L.; Gordenin, D.; Klimczak, L.J.; Zhang, C.Z.; Pellman, D.S.; et al. Comprehensive analysis of chromothripsis in 2,658 human cancers using whole-genome sequencing. *Nat. Genet.* **2020**, *52*, 331–341. [[CrossRef](#)]
48. Moorman, A.V.; Ensor, H.M.; Richards, S.M.; Chilton, L.; Schwab, C.; Kinsey, S.E.; Vora, A.; Mitchell, C.D.; Harrison, C.J. Prognostic effect of chromosomal abnormalities in childhood B-cell precursor acute lymphoblastic leukaemia: Results from the UK Medical Research Council ALL97/99 randomised trial. *Lancet Oncol.* **2010**, *11*, 429–438. [[CrossRef](#)]
49. Xie, W.; Xu, J.; Hu, S.; Li, S.; Wang, W.; Cameron Yin, C.; Toruner, G.; Tang, Z.; Medeiros, L.J.; Tang, G. iAMP21 in acute myeloid leukemia is associated with complex karyotype, TP53 mutation and dismal outcome. *Mod. Pathol.* **2020**, *33*, 1389–1397. [[CrossRef](#)] [[PubMed](#)]
50. Li, Y.; Schwab, C.; Ryan, S.; Papaemmanuil, E.; Robinson, H.M.; Jacobs, P.; Moorman, A.V.; Dyer, S.; Borrow, J.; Griffiths, M.; et al. Constitutional and somatic rearrangement of chromosome 21 in acute lymphoblastic leukaemia. *Nature* **2014**, *508*, 98–102. [[CrossRef](#)]
51. Mehine, M.; Makinen, N.; Heinonen, H.R.; Aaltonen, L.A.; Vahteristo, P. Genomics of uterine leiomyomas: Insights from high-throughput sequencing. *Fertil. Steril.* **2014**, *102*, 621–629. [[CrossRef](#)] [[PubMed](#)]
52. Ilic, M.; Zaalberg, I.C.; Raaijmakers, J.A.; Medema, R.H. Life of double minutes: Generation, maintenance, and elimination. *Chromosoma* **2022**, *131*, 107–125. [[CrossRef](#)] [[PubMed](#)]
53. Turner, K.M.; Deshpande, V.; Beyter, D.; Koga, T.; Rusert, J.; Lee, C.; Li, B.; Arden, K.; Ren, B.; Nathanson, D.A.; et al. Extrachromosomal oncogene amplification drives tumour evolution and genetic heterogeneity. *Nature* **2017**, *543*, 122–125. [[CrossRef](#)] [[PubMed](#)]
54. Mancini-DiNardo, D.; Judkins, T.; Kidd, J.; Bernhisel, R.; Daniels, C.; Brown, K.; Mee, K.; Craft, J.; Holladay, J.; Morris, B.; et al. Detection of large rearrangements in a hereditary pan-cancer panel using next-generation sequencing. *BMC Med. Genom.* **2019**, *12*, 138. [[CrossRef](#)] [[PubMed](#)]
55. Corvi, R.; Amler, L.C.; Savelyeva, L.; Gehring, M.; Schwab, M. MYCN is retained in single copy at chromosome 2 band p23-24 during amplification in human neuroblastoma cells. *Proc. Natl. Acad. Sci. USA* **1994**, *91*, 5523–5527. [[CrossRef](#)] [[PubMed](#)]

56. Otte, J.; Dyberg, C.; Pepich, A.; Johnsen, J.I. MYCN Function in Neuroblastoma Development. *Front. Oncol.* **2020**, *10*, 624079. [\[CrossRef\]](#)
57. Savelyeva, L.; Schwab, M. Amplification of oncogenes revisited: From expression profiling to clinical application. *Cancer Lett.* **2001**, *167*, 115–123. [\[CrossRef\]](#) [\[PubMed\]](#)
58. Verhaak, R.G.; Hoadley, K.A.; Purdom, E.; Wang, V.; Qi, Y.; Wilkerson, M.D.; Miller, C.R.; Ding, L.; Golub, T.; Mesirov, J.P.; et al. Integrated genomic analysis identifies clinically relevant subtypes of glioblastoma characterized by abnormalities in PDGFRA, IDH1, EGFR, and NF1. *Cancer Cell* **2010**, *17*, 98–110. [\[CrossRef\]](#)
59. Bertucci, F.; Borie, N.; Ginestier, C.; Groulet, A.; Charafe-Jauffret, E.; Adelaide, J.; Geneix, J.; Bachelart, L.; Finetti, P.; Koki, A.; et al. Identification and validation of an ERBB2 gene expression signature in breast cancers. *Oncogene* **2004**, *23*, 2564–2575. [\[CrossRef\]](#)
60. Raghav, K.; Morris, V.; Tang, C.; Morelli, P.; Amin, H.M.; Chen, K.; Manyam, G.C.; Broom, B.; Overman, M.J.; Shaw, K.; et al. MET amplification in metastatic colorectal cancer: An acquired response to EGFR inhibition, not a de novo phenomenon. *Oncotarget* **2016**, *7*, 54627–54631. [\[CrossRef\]](#)
61. Weinstein, I.B.; Joe, A. Oncogene addiction. *Cancer Res.* **2008**, *68*, 3077–3080; discussion 3080. [\[CrossRef\]](#) [\[PubMed\]](#)
62. Girish, V.; Lakhani, A.A.; Thompson, S.L.; Scaduto, C.M.; Brown, L.M.; Hagenson, R.A.; Sausville, E.L.; Mendelson, B.E.; Kandikuppa, P.K.; Lukow, D.A.; et al. Oncogene-like addiction to aneuploidy in human cancers. *Science* **2023**, *381*, eadg4521. [\[CrossRef\]](#) [\[PubMed\]](#)
63. Alexandrov, L.B.; Nik-Zainal, S.; Wedge, D.C.; Aparicio, S.A.; Behjati, S.; Biankin, A.V.; Bignell, G.R.; Bolli, N.; Borg, A.; Borresen-Dale, A.L.; et al. Signatures of mutational processes in human cancer. *Nature* **2013**, *500*, 415–421. [\[CrossRef\]](#)
64. Zack, T.I.; Schumacher, S.E.; Carter, S.L.; Cherniack, A.D.; Saksena, G.; Tabak, B.; Lawrence, M.S.; Zhsng, C.Z.; Wala, J.; Mermel, C.H.; et al. Pan-cancer patterns of somatic copy number alteration. *Nat. Genet.* **2013**, *45*, 1134–1140. [\[CrossRef\]](#) [\[PubMed\]](#)
65. Niu, C.; Wu, D.; Li, A.J.; Qin, K.H.; Hu, D.A.; Wang, E.J.; Tucker, A.B.; He, F.; Huang, L.; Wang, H.; et al. Identification of a prognostic signature based on copy number variations (CNVs) and CNV-modulated gene expression in acute myeloid leukemia. *Am. J. Transl. Res.* **2021**, *13*, 13683–13696.
66. Satgunaseelan, L.; Porazinski, S.; Strbenac, D.; Istadi, A.; Willet, C.; Chew, T.; Sadsad, R.; Palme, C.E.; Lee, J.H.; Boyer, M.; et al. Oral Squamous Cell Carcinoma in Young Patients Show Higher Rates of EGFR Amplification: Implications for Novel Personalized Therapy. *Front. Oncol.* **2021**, *11*, 750852. [\[CrossRef\]](#) [\[PubMed\]](#)
67. Alafahed, A.; Ebili, H.O.; Almoammar, N.E.; Alasiri, G.; AlKhamees, O.A.; Aldali, J.A.; Al Othaim, A.; Hakami, Z.H.; Abdulwahed, A.M.; Waggiallah, H.A. Prognostic Values of Gene Copy Number Alterations in Prostate Cancer. *Genes* **2023**, *14*, 956. [\[CrossRef\]](#) [\[PubMed\]](#)
68. Horlings, H.M.; Lai, C.; Nuyten, D.S.; Halfwerk, H.; Kristel, P.; van Beers, E.; Joosse, S.A.; Klijn, C.; Nederlof, P.M.; Reinders, M.J.; et al. Integration of DNA copy number alterations and prognostic gene expression signatures in breast cancer patients. *Clin. Cancer Res.* **2010**, *16*, 651–663. [\[CrossRef\]](#) [\[PubMed\]](#)
69. Cancer Genome Atlas, N. Comprehensive molecular portraits of human breast tumours. *Nature* **2012**, *490*, 61–70. [\[CrossRef\]](#)
70. Curtis, C.; Shah, S.P.; Chin, S.F.; Turashvili, G.; Rueda, O.M.; Dunning, M.J.; Speed, D.; Lynch, A.G.; Samarajiwa, S.; Yuan, Y.; et al. The genomic and transcriptomic architecture of 2000 breast tumours reveals novel subgroups. *Nature* **2012**, *486*, 346–352. [\[CrossRef\]](#)
71. Taylor, B.S.; Schultz, N.; Hieronymus, H.; Gopalan, A.; Xiao, Y.; Carver, B.S.; Arora, V.K.; Kaushik, P.; Cerami, E.; Reva, B.; et al. Integrative genomic profiling of human prostate cancer. *Cancer Cell* **2010**, *18*, 11–22. [\[CrossRef\]](#) [\[PubMed\]](#)
72. Williams, J.L.; Greer, P.A.; Squire, J.A. Recurrent copy number alterations in prostate cancer: An in silico meta-analysis of publicly available genomic data. *Cancer Genet.* **2014**, *207*, 474–488. [\[CrossRef\]](#) [\[PubMed\]](#)
73. Weir, B.A.; Woo, M.S.; Getz, G.; Perner, S.; Ding, L.; Beroukhi, R.; Lin, W.M.; Province, M.A.; Kraja, A.; Johnson, L.A.; et al. Characterizing the cancer genome in lung adenocarcinoma. *Nature* **2007**, *450*, 893–898. [\[CrossRef\]](#) [\[PubMed\]](#)
74. Cancer Genome Atlas Research, N. Comprehensive molecular profiling of lung adenocarcinoma. *Nature* **2014**, *511*, 543–550. [\[CrossRef\]](#) [\[PubMed\]](#)
75. Cancer Genome Atlas, N. Comprehensive molecular characterization of human colon and rectal cancer. *Nature* **2012**, *487*, 330–337. [\[CrossRef\]](#) [\[PubMed\]](#)
76. Oliveira, D.M.; Santamaria, G.; Laudanna, C.; Migliozi, S.; Zoppoli, P.; Quist, M.; Grasso, C.; Mignogna, C.; Elia, L.; Faniello, M.C.; et al. Identification of copy number alterations in colon cancer from analysis of amplicon-based next generation sequencing data. *Oncotarget* **2018**, *9*, 20409–20425. [\[CrossRef\]](#) [\[PubMed\]](#)
77. Xie, T.; d'Ario, G.; Lamb, J.R.; Martin, E.; Wang, K.; Tejpar, S.; Delorenzi, M.; Bosman, F.T.; Roth, A.D.; Yan, P.; et al. A comprehensive characterization of genome-wide copy number aberrations in colorectal cancer reveals novel oncogenes and patterns of alterations. *PLoS ONE* **2012**, *7*, e42001. [\[CrossRef\]](#) [\[PubMed\]](#)
78. Shoushtari, A.N.; Chatila, W.K.; Arora, A.; Sanchez-Vega, F.; Kantheti, H.S.; Rojas Zamalloa, J.A.; Krieger, P.; Callahan, M.K.; Betof Warner, A.; Postow, M.A.; et al. Therapeutic Implications of Detecting MAPK-Activating Alterations in Cutaneous and Unknown Primary Melanomas. *Clin. Cancer Res.* **2021**, *27*, 2226–2235. [\[CrossRef\]](#) [\[PubMed\]](#)
79. Cancer Genome Atlas, N. Genomic Classification of Cutaneous Melanoma. *Cell* **2015**, *161*, 1681–1696. [\[CrossRef\]](#)
80. Curtin, J.A.; Fridlyand, J.; Kageshita, T.; Patel, H.N.; Busam, K.J.; Kutzner, H.; Cho, K.H.; Aiba, S.; Brocker, E.B.; LeBoit, P.E.; et al. Distinct sets of genetic alterations in melanoma. *N. Engl. J. Med.* **2005**, *353*, 2135–2147. [\[CrossRef\]](#)

81. Bolouri, H.; Farrar, J.E.; Triche, T., Jr.; Ries, R.E.; Lim, E.L.; Alonzo, T.A.; Ma, Y.; Moore, R.; Mungall, A.J.; Marra, M.A.; et al. The molecular landscape of pediatric acute myeloid leukemia reveals recurrent structural alterations and age-specific mutational interactions. *Nat. Med.* **2018**, *24*, 103–112. [CrossRef] [PubMed]
82. Walter, M.J.; Payton, J.E.; Ries, R.E.; Shannon, W.D.; Deshmukh, H.; Zhao, Y.; Baty, J.; Heath, S.; Westervelt, P.; Watson, M.A.; et al. Acquired copy number alterations in adult acute myeloid leukemia genomes. *Proc. Natl. Acad. Sci. USA* **2009**, *106*, 12950–12955. [CrossRef] [PubMed]
83. Cheng, C.K.; Yung, Y.L.; Chan, H.Y.; Leung, K.T.; Chan, K.Y.Y.; Leung, A.W.K.; Cheng, F.W.T.; Li, C.K.; Wan, T.S.K.; Luo, X.; et al. Deep genomic characterization highlights complexities and prognostic markers of pediatric acute myeloid leukemia. *Commun. Biol.* **2023**, *6*, 356. [CrossRef] [PubMed]
84. Liu, Y.F.; Wang, B.Y.; Zhang, W.N.; Huang, J.Y.; Li, B.S.; Zhang, M.; Jiang, L.; Li, J.F.; Wang, M.J.; Dai, Y.J.; et al. Genomic Profiling of Adult and Pediatric B-cell Acute Lymphoblastic Leukemia. *EBioMedicine* **2016**, *8*, 173–183. [CrossRef] [PubMed]
85. Moorman, A.V.; Barretta, E.; Butler, E.R.; Ward, E.J.; Twentyman, K.; Kirkwood, A.A.; Enshaei, A.; Schwab, C.; Creasey, T.; Leongamornlert, D.; et al. Prognostic impact of chromosomal abnormalities and copy number alterations in adult B-cell precursor acute lymphoblastic leukaemia: A UKALL14 study. *Leukemia* **2022**, *36*, 625–636. [CrossRef] [PubMed]
86. Steeghs, E.M.P.; Boer, J.M.; Hoogkamer, A.Q.; Boeree, A.; de Haas, V.; de Groot-Kruseman, H.A.; Horstmann, M.A.; Escherich, G.; Pieters, R.; den Boer, M.L. Copy number alterations in B-cell development genes, drug resistance, and clinical outcome in pediatric B-cell precursor acute lymphoblastic leukemia. *Sci. Rep.* **2019**, *9*, 4634. [CrossRef] [PubMed]
87. Paulsson, K.; Lilljebjorn, H.; Biloglav, A.; Olsson, L.; Rissler, M.; Castor, A.; Barbany, G.; Fogelstrand, L.; Nordgren, A.; Sjogren, H.; et al. The genomic landscape of high hyperdiploid childhood acute lymphoblastic leukemia. *Nat. Genet.* **2015**, *47*, 672–676. [CrossRef] [PubMed]
88. Cerami, E.; Gao, J.; Dogrusoz, U.; Gross, B.E.; Sumer, S.O.; Aksoy, B.A.; Jacobsen, A.; Byrne, C.J.; Heuer, M.L.; Larsson, E.; et al. The cBio cancer genomics portal: An open platform for exploring multidimensional cancer genomics data. *Cancer Discov.* **2012**, *2*, 401–404. [CrossRef] [PubMed]
89. Mitelman, F. Mitelman Database of Chromosome Aberrations and Gene Fusions in Cancer. 2024. Available online: <https://mitelmandatabase.isb-cgc.org/> (accessed on 15 June 2024).
90. Wang, J.; LaFramboise, T. CytoConverter: A web-based tool to convert karyotypes to genomic coordinates. *BMC Bioinform.* **2019**, *20*, 467. [CrossRef]
91. Uribe, M.L.; Marrocco, I.; Yarden, Y. EGFR in Cancer: Signaling Mechanisms, Drugs, and Acquired Resistance. *Cancers* **2021**, *13*, 2748. [CrossRef]
92. Guo, R.; Luo, J.; Chang, J.; Rekhtman, N.; Arcila, M.; Drilon, A. MET-dependent solid tumours—Molecular diagnosis and targeted therapy. *Nat. Rev. Clin. Oncol.* **2020**, *17*, 569–587. [CrossRef] [PubMed]
93. Chen, Y.; Huang, Y.; Gao, X.; Li, Y.; Lin, J.; Chen, L.; Chang, L.; Chen, G.; Guan, Y.; Pan, L.K.; et al. CCND1 Amplification Contributes to Immunosuppression and Is Associated with a Poor Prognosis to Immune Checkpoint Inhibitors in Solid Tumors. *Front. Immunol.* **2020**, *11*, 1620. [CrossRef] [PubMed]
94. Zhu, K.; Yang, X.; Tai, H.; Zhong, X.; Luo, T.; Zheng, H. HER2-targeted therapies in cancer: A systematic review. *Biomark. Res.* **2024**, *12*, 16. [CrossRef]
95. Gillis, N.K.; Rotroff, D.M.; Mesa, T.E.; Yao, J.; Chen, Z.; Carulli, M.A.; Yoder, S.J.; Walko, C.M.; Teer, J.K.; McLeod, H.L. Tumor exome sequencing and copy number alterations reveal potential predictors of intrinsic resistance to multi-targeted tyrosine kinase inhibitors. *Oncotarget* **2017**, *8*, 115114–115127. [CrossRef] [PubMed]
96. Wilson, M.A.; Zhao, F.; Khare, S.; Roszik, J.; Woodman, S.E.; D'Andrea, K.; Wubbenhorst, B.; Rimm, D.L.; Kirkwood, J.M.; Kluger, H.M.; et al. Copy Number Changes Are Associated with Response to Treatment with Carboplatin, Paclitaxel, and Sorafenib in Melanoma. *Clin. Cancer Res.* **2016**, *22*, 374–382. [CrossRef] [PubMed]
97. Wong, R.L.Y.; Wong, M.R.E.; Kuick, C.H.; Saffari, S.E.; Wong, M.K.; Tan, S.H.; Merchant, K.; Chang, K.T.E.; Thangavelu, M.; Periyasamy, G.; et al. Integrated Genomic Profiling and Drug Screening of Patient-Derived Cultures Identifies Individualized Copy Number-Dependent Susceptibilities Involving PI3K Pathway and 17q Genes in Neuroblastoma. *Front. Oncol.* **2021**, *11*, 709525. [CrossRef] [PubMed]
98. Memon, D.; Gill, M.B.; Papachristou, E.K.; Ochoa, D.; D'Santos, C.S.; Miller, M.L.; Beltrao, P. Copy number aberrations drive kinase rewiring, leading to genetic vulnerabilities in cancer. *Cell Rep.* **2021**, *35*, 109155. [CrossRef] [PubMed]
99. Tuna, M.; Amos, C.I.; Mills, G.B. Whole-chromosome arm acquired uniparental disomy in cancer development is a consequence of isochromosome formation. *Neoplasia* **2022**, *25*, 9–17. [CrossRef] [PubMed]
100. Sheffer, M.; Bacolod, M.D.; Zuk, O.; Giardina, S.F.; Pincas, H.; Barany, F.; Paty, P.B.; Gerald, W.L.; Notterman, D.A.; Domany, E. Association of survival and disease progression with chromosomal instability: A genomic exploration of colorectal cancer. *Proc. Natl. Acad. Sci. USA* **2009**, *106*, 7131–7136. [CrossRef]
101. Kluth, M.; Amschler, N.N.; Galal, R.; Moller-Koop, C.; Barrow, P.; Tsourlakis, M.C.; Jacobsen, F.; Hinsch, A.; Wittmer, C.; Steurer, S.; et al. Deletion of 8p is an independent prognostic parameter in prostate cancer. *Oncotarget* **2017**, *8*, 379–392. [CrossRef]
102. Iacobucci, I.; Kimura, S.; Mullighan, C.G. Biologic and Therapeutic Implications of Genomic Alterations in Acute Lymphoblastic Leukemia. *J. Clin. Med.* **2021**, *10*, 3792. [CrossRef] [PubMed]

103. Moorman, A.V.; Richards, S.M.; Martineau, M.; Cheung, K.L.; Robinson, H.M.; Jalali, G.R.; Broadfield, Z.J.; Harris, R.L.; Taylor, K.E.; Gibson, B.E.; et al. Outcome heterogeneity in childhood high-hyperdiploid acute lymphoblastic leukemia. *Blood* **2003**, *102*, 2756–2762. [[CrossRef](#)] [[PubMed](#)]
104. Enshaei, A.; Vora, A.; Harrison, C.J.; Moppett, J.; Moorman, A.V. Defining low-risk high hyperdiploidy in patients with paediatric acute lymphoblastic leukaemia: A retrospective analysis of data from the UKALL97/99 and UKALL2003 clinical trials. *Lancet Haematol.* **2021**, *8*, e828–e839. [[CrossRef](#)] [[PubMed](#)]
105. Lee, S.H.R.; Ashcraft, E.; Yang, W.; Roberts, K.G.; Gocho, Y.; Rowland, L.; Inaba, H.; Karol, S.E.; Jeha, S.; Crews, K.R.; et al. Prognostic and Pharmacotypic Heterogeneity of Hyperdiploidy in Childhood ALL. *J. Clin. Oncol.* **2023**, *41*, 5422–5432. [[CrossRef](#)] [[PubMed](#)]
106. Mullighan, C.G.; Su, X.; Zhang, J.; Radtke, I.; Phillips, L.A.; Miller, C.B.; Ma, J.; Liu, W.; Cheng, C.; Schulman, B.A.; et al. Deletion of IKZF1 and prognosis in acute lymphoblastic leukemia. *N. Engl. J. Med.* **2009**, *360*, 470–480. [[CrossRef](#)]
107. Stanulla, M.; Dagdan, E.; Zaliova, M.; Moricke, A.; Palmi, C.; Cazzaniga, G.; Eckert, C.; Te Kronnie, G.; Bourquin, J.P.; Bornhauser, B.; et al. IKZF1(plus) Defines a New Minimal Residual Disease-Dependent Very-Poor Prognostic Profile in Pediatric B-Cell Precursor Acute Lymphoblastic Leukemia. *J. Clin. Oncol.* **2018**, *36*, 1240–1249. [[CrossRef](#)] [[PubMed](#)]
108. Hasle, H.; Alonzo, T.A.; Auvrignon, A.; Behar, C.; Chang, M.; Creutzig, U.; Fischer, A.; Forestier, E.; Fynn, A.; Haas, O.A.; et al. Monosomy 7 and deletion 7q in children and adolescents with acute myeloid leukemia: An international retrospective study. *Blood* **2007**, *109*, 4641–4647. [[CrossRef](#)] [[PubMed](#)]
109. Greenberg, P.L.; Tuechler, H.; Schanz, J.; Sanz, G.; Garcia-Manero, G.; Sole, F.; Bennett, J.M.; Bowen, D.; Fenaux, P.; Dreyfus, F.; et al. Revised international prognostic scoring system for myelodysplastic syndromes. *Blood* **2012**, *120*, 2454–2465. [[CrossRef](#)] [[PubMed](#)]
110. Eisfeld, A.K.; Kohlschmidt, J.; Mrozek, K.; Volinia, S.; Blachly, J.S.; Nicolet, D.; Oakes, C.; Kroll, K.; Orwick, S.; Carroll, A.J.; et al. Mutational Landscape and Gene Expression Patterns in Adult Acute Myeloid Leukemias with Monosomy 7 as a Sole Abnormality. *Cancer Res.* **2017**, *77*, 207–218. [[CrossRef](#)]
111. Pitel, B.A.; Sharma, N.; Zepeda-Mendoza, C.; Smadbeck, J.B.; Pearce, K.E.; Cook, J.M.; Vasmatzis, G.; Sachs, Z.; Kanagal-Shamanna, R.; Viswanatha, D.; et al. Myeloid malignancies with 5q and 7q deletions are associated with extreme genomic complexity, biallelic TP53 variants, and very poor prognosis. *Blood Cancer J.* **2021**, *11*, 18. [[CrossRef](#)]
112. Redon, R.; Ishikawa, S.; Fitch, K.R.; Feuk, L.; Perry, G.H.; Andrews, T.D.; Fiegler, H.; Shapero, M.H.; Carson, A.R.; Chen, W.; et al. Global variation in copy number in the human genome. *Nature* **2006**, *444*, 444–454. [[CrossRef](#)] [[PubMed](#)]
113. Zarrei, M.; MacDonald, J.R.; Merico, D.; Scherer, S.W. A copy number variation map of the human genome. *Nat. Rev. Genet.* **2015**, *16*, 172–183. [[CrossRef](#)] [[PubMed](#)]
114. Sebat, J.; Lakshmi, B.; Troge, J.; Alexander, J.; Young, J.; Lundin, P.; Maner, S.; Massa, H.; Walker, M.; Chi, M.; et al. Large-scale copy number polymorphism in the human genome. *Science* **2004**, *305*, 525–528. [[CrossRef](#)] [[PubMed](#)]
115. Conrad, D.F.; Pinto, D.; Redon, R.; Feuk, L.; Gokcumen, O.; Zhang, Y.; Aerts, J.; Andrews, T.D.; Barnes, C.; Campbell, P.; et al. Origins and functional impact of copy number variation in the human genome. *Nature* **2010**, *464*, 704–712. [[CrossRef](#)] [[PubMed](#)]
116. Park, R.W.; Kim, T.M.; Kasif, S.; Park, P.J. Identification of rare germline copy number variations over-represented in five human cancer types. *Mol. Cancer* **2015**, *14*, 25. [[CrossRef](#)] [[PubMed](#)]
117. Baruchel, A.; Bourquin, J.P.; Crispino, J.; Cuartero, S.; Hasle, H.; Hitzler, J.; Klusmann, J.H.; Izraeli, S.; Lane, A.A.; Malinge, S.; et al. Down syndrome and leukemia: From basic mechanisms to clinical advances. *Haematologica* **2023**, *108*, 2570–2581. [[CrossRef](#)] [[PubMed](#)]
118. Hasle, H.; Friedman, J.M.; Olsen, J.H.; Rasmussen, S.A. Low risk of solid tumors in persons with Down syndrome. *Genet. Med.* **2016**, *18*, 1151–1157. [[CrossRef](#)] [[PubMed](#)]
119. Viuff, M.H.; Stochholm, K.; Lin, A.; Berglund, A.; Juul, S.; Gravholt, C.H. Cancer occurrence in Turner syndrome and the effect of sex hormone substitution therapy. *Eur. J. Endocrinol.* **2021**, *184*, 79–88. [[CrossRef](#)] [[PubMed](#)]
120. Ji, J.; Zoller, B.; Sundquist, J.; Sundquist, K. Risk of solid tumors and hematological malignancy in persons with Turner and Klinefelter syndromes: A national cohort study. *Int. J. Cancer* **2016**, *139*, 754–758. [[CrossRef](#)]
121. Schoemaker, M.J.; Swerdlow, A.J.; Higgins, C.D.; Wright, A.F.; Jacobs, P.A.; Group, U.K.C.C. Cancer incidence in women with Turner syndrome in Great Britain: A national cohort study. *Lancet Oncol.* **2008**, *9*, 239–246. [[CrossRef](#)]
122. Bonouvrie, K.; van der Werff Ten Bosch, J.; van den Akker, M. Klinefelter syndrome and germ cell tumors: Review of the literature. *Int. J. Pediatr. Endocrinol.* **2020**, *2020*, 18. [[CrossRef](#)]
123. Swerdlow, A.J.; Schoemaker, M.J.; Higgins, C.D.; Wright, A.F.; Jacobs, P.A.; Group, U.K.C.C. Cancer incidence and mortality in men with Klinefelter syndrome: A cohort study. *J. Natl. Cancer Inst.* **2005**, *97*, 1204–1210. [[CrossRef](#)]
124. Roberts, I.; Alford, K.; Hall, G.; Juban, G.; Richmond, H.; Norton, A.; Vallance, G.; Perkins, K.; Marchi, E.; McGowan, S.; et al. GATA1-mutant clones are frequent and often unsuspected in babies with Down syndrome: Identification of a population at risk of leukemia. *Blood* **2013**, *122*, 3908–3917. [[CrossRef](#)]
125. Yoshida, K.; Toki, T.; Okuno, Y.; Kanezaki, R.; Shiraishi, Y.; Sato-Otsubo, A.; Sanada, M.; Park, M.J.; Terui, K.; Suzuki, H.; et al. The landscape of somatic mutations in Down syndrome-related myeloid disorders. *Nat. Genet.* **2013**, *45*, 1293–1299. [[CrossRef](#)]
126. Labuhn, M.; Perkins, K.; Matzk, S.; Varghese, L.; Garnett, C.; Papaemmanuil, E.; Metzner, M.; Kennedy, A.; Amstislavskiy, V.; Risch, T.; et al. Mechanisms of Progression of Myeloid Preleukemia to Transformed Myeloid Leukemia in Children with Down Syndrome. *Cancer Cell* **2019**, *36*, 123–138.e10. [[CrossRef](#)]

127. Raghuram, N.; Hasegawa, D.; Nakashima, K.; Rahman, S.; Antoniou, E.; Skajaa, T.; Merli, P.; Verma, A.; Rabin, K.R.; Aftandilian, C.; et al. Survival outcomes of children with relapsed or refractory myeloid leukemia associated with Down syndrome. *Blood Adv.* **2023**, *7*, 6532–6539. [\[CrossRef\]](#)
128. Buitenkamp, T.D.; Izraeli, S.; Zimmermann, M.; Forestier, E.; Heerema, N.A.; van den Heuvel-Eibrink, M.M.; Pieters, R.; Korbijn, C.M.; Silverman, L.B.; Schmiegelow, K.; et al. Acute lymphoblastic leukemia in children with Down syndrome: A retrospective analysis from the Ponte di Legno study group. *Blood* **2014**, *123*, 70–77. [\[CrossRef\]](#)
129. Rabin, K.R.; Devidas, M.; Chen, Z.; Ji, L.; Kairalla, J.; Hitzler, J.K.; Yang, J.J.; Carroll, A.J.; Heerema, N.A.; Borowitz, M.J.; et al. Outcomes in Children, Adolescents, and Young Adults with Down Syndrome and ALL: A Report from the Children's Oncology Group. *J. Clin. Oncol.* **2024**, *42*, 218–227. [\[CrossRef\]](#)
130. Ceppi, F.; Duval, M.; Leclerc, J.M.; Laverdiere, C.; Delva, Y.L.; Cellot, S.; Teira, P.; Bittencourt, H. Improvement of the Outcome of Relapsed or Refractory Acute Lymphoblastic Leukemia in Children Using a Risk-Based Treatment Strategy. *PLoS ONE* **2016**, *11*, e0160310. [\[CrossRef\]](#)
131. Li, Z.; Chang, T.C.; Junco, J.J.; Devidas, M.; Li, Y.; Yang, W.; Huang, X.; Hedges, D.J.; Cheng, Z.; Shago, M.; et al. Genomic landscape of Down syndrome-associated acute lymphoblastic leukemia. *Blood* **2023**, *142*, 172–184. [\[CrossRef\]](#)
132. Laurent, A.P.; Kotecha, R.S.; Malinge, S. Gain of chromosome 21 in hematological malignancies: Lessons from studying leukemia in children with Down syndrome. *Leukemia* **2020**, *34*, 1984–1999. [\[CrossRef\]](#) [\[PubMed\]](#)
133. Satge, D.; Nishi, M.; Sirvent, N.; Vekemans, M.; Chenard, M.P.; Barnes, A. A tumor profile in Patau syndrome (trisomy 13). *Am. J. Med. Genet. A* **2017**, *173*, 2088–2096. [\[CrossRef\]](#)
134. Cereda, A.; Carey, J.C. The trisomy 18 syndrome. *Orphanet J. Rare Dis.* **2012**, *7*, 81. [\[CrossRef\]](#) [\[PubMed\]](#)
135. Satge, D.; Nishi, M.; Sirvent, N.; Vekemans, M. A tumor profile in Edwards syndrome (trisomy 18). *Am. J. Med. Genet. C Semin. Med. Genet.* **2016**, *172*, 296–306. [\[CrossRef\]](#) [\[PubMed\]](#)
136. Narendran, A.; Hawkins, L.M.; Ganjavi, H.; Vanek, W.; Gee, M.F.; Barlow, J.W.; Johnson, G.; Malkin, D.; Freedman, M.H. Characterization of bone marrow stromal abnormalities in a patient with constitutional trisomy 8 mosaicism and myelodysplastic syndrome. *Pediatr. Hematol. Oncol.* **2004**, *21*, 209–221. [\[CrossRef\]](#)
137. Tartaglia, N.R.; Howell, S.; Sutherland, A.; Wilson, R.; Wilson, L. A review of trisomy X (47,XXX). *Orphanet J. Rare Dis.* **2010**, *5*, 8. [\[CrossRef\]](#) [\[PubMed\]](#)
138. Richardson, A.L.; Wang, Z.C.; De Nicolo, A.; Lu, X.; Brown, M.; Miron, A.; Liao, X.; Iglehart, J.D.; Livingston, D.M.; Ganesan, S. X chromosomal abnormalities in basal-like human breast cancer. *Cancer Cell* **2006**, *9*, 121–132. [\[CrossRef\]](#) [\[PubMed\]](#)
139. Waddell, N.; Pajic, M.; Patch, A.M.; Chang, D.K.; Kassahn, K.S.; Bailey, P.; Johns, A.L.; Miller, D.; Nones, K.; Quek, K.; et al. Whole genomes redefine the mutational landscape of pancreatic cancer. *Nature* **2015**, *518*, 495–501. [\[CrossRef\]](#) [\[PubMed\]](#)
140. Harrison, C.J.; Moorman, A.V.; Schwab, C.; Carroll, A.J.; Raetz, E.A.; Devidas, M.; Strehl, S.; Nebral, K.; Harbott, J.; Teigler-Schlegel, A.; et al. An international study of intrachromosomal amplification of chromosome 21 (iAMP21): Cytogenetic characterization and outcome. *Leukemia* **2014**, *28*, 1015–1021. [\[CrossRef\]](#) [\[PubMed\]](#)
141. Miller, R.W.; Fraumeni, J.F., Jr.; Manning, M.D. Association of Wilms' Tumor with Aniridia, Hemihypertrophy and Other Congenital Malformations. *N. Engl. J. Med.* **1964**, *270*, 922–927. [\[CrossRef\]](#)
142. Knudson, A.G., Jr. Mutation and cancer: Statistical study of retinoblastoma. *Proc. Natl. Acad. Sci. USA* **1971**, *68*, 820–823. [\[CrossRef\]](#)
143. Swerdlow, A.J.; Schoemaker, M.J.; Higgins, C.D.; Wright, A.F.; Jacobs, P.A. Cancer risk in patients with constitutional chromosome deletions: A nationwide British cohort study. *Br. J. Cancer* **2008**, *98*, 1929–1933. [\[CrossRef\]](#)
144. Pellikaan, K.; Nguyen, N.Q.C.; Rosenberg, A.G.W.; Coupaye, M.; Goldstone, A.P.; Hoybye, C.; Markovic, T.; Grugni, G.; Crino, A.; Caixas, A.; et al. Malignancies in Prader-Willi Syndrome: Results from a Large International Cohort and Literature Review. *J. Clin. Endocrinol. Metab.* **2023**, *108*, e1720–e1730. [\[CrossRef\]](#) [\[PubMed\]](#)
145. McDonald-McGinn, D.M.; Reilly, A.; Wallgren-Pettersson, C.; Hoyme, H.E.; Yang, S.P.; Adam, M.P.; Zackai, E.H.; Sullivan, K.E. Malignancy in chromosome 22q11.2 deletion syndrome (DiGeorge syndrome/velocardiofacial syndrome). *Am. J. Med. Genet. A* **2006**, *140*, 906–909. [\[CrossRef\]](#)
146. Guala, A.; Spunton, M.; Kalantari, S.; Kennerknecht, I.; Danesino, C. Neoplasia in Cri du Chat Syndrome from Italian and German Databases. *Case Rep. Genet.* **2017**, *2017*, 5181624. [\[CrossRef\]](#)
147. Kimura, R.; Ishii, Y.; Tomiwa, K.; Awaya, T.; Nakata, M.; Kato, T.; Okazaki, S.; Heike, T.; Hagiwara, M. Williams-Beuren Syndrome as a Potential Risk Factor for Burkitt Lymphoma. *Front. Genet.* **2018**, *9*, 368. [\[CrossRef\]](#) [\[PubMed\]](#)
148. Shah, S.M.; Demidova, E.V.; Lesh, R.W.; Hall, M.J.; Daly, M.B.; Meyer, J.E.; Edelman, M.J.; Arora, S. Therapeutic implications of germline vulnerabilities in DNA repair for precision oncology. *Cancer Treat. Rev.* **2022**, *104*, 102337. [\[CrossRef\]](#) [\[PubMed\]](#)
149. Davies, H.D.; Leusink, G.L.; McConnell, A.; Deyell, M.; Cassidy, S.B.; Fick, G.H.; Coppes, M.J. Myeloid leukemia in Prader-Willi syndrome. *J. Pediatr.* **2003**, *142*, 174–178. [\[CrossRef\]](#)
150. Ben-David, U.; Ha, G.; Tseng, Y.Y.; Greenwald, N.F.; Oh, C.; Shih, J.; McFarland, J.M.; Wong, B.; Boehm, J.S.; Beroukhim, R.; et al. Patient-derived xenografts undergo mouse-specific tumor evolution. *Nat. Genet.* **2017**, *49*, 1567–1575. [\[CrossRef\]](#)
151. Call, K.M.; Glaser, T.; Ito, C.Y.; Buckler, A.J.; Pelletier, J.; Haber, D.A.; Rose, E.A.; Kral, A.; Yeager, H.; Lewis, W.H.; et al. Isolation and characterization of a zinc finger polypeptide gene at the human chromosome 11 Wilms' tumor locus. *Cell* **1990**, *60*, 509–520. [\[CrossRef\]](#)

152. Gessler, M.; Poustka, A.; Cavenee, W.; Neve, R.L.; Orkin, S.H.; Bruns, G.A. Homozygous deletion in Wilms tumours of a zinc-finger gene identified by chromosome jumping. *Nature* **1990**, *343*, 774–778. [[CrossRef](#)]
153. Hastie, N.D. Wilms' tumour 1 (WT1) in development, homeostasis and disease. *Development* **2017**, *144*, 2862–2872. [[CrossRef](#)]
154. Rampal, R.; Figueroa, M.E. Wilms tumor 1 mutations in the pathogenesis of acute myeloid leukemia. *Haematologica* **2016**, *101*, 672–679. [[CrossRef](#)]
155. Hsu, J.L.; Hung, M.C. The role of HER2, EGFR, and other receptor tyrosine kinases in breast cancer. *Cancer Metastasis Rev.* **2016**, *35*, 575–588. [[CrossRef](#)] [[PubMed](#)]
156. Rexer, B.N.; Arteaga, C.L. Intrinsic and acquired resistance to HER2-targeted therapies in HER2 gene-amplified breast cancer: Mechanisms and clinical implications. *Crit. Rev. Oncog.* **2012**, *17*, 1–16. [[CrossRef](#)]
157. Qin, K.; Hong, L.; Zhang, J.; Le, X. MET Amplification as a Resistance Driver to TKI Therapies in Lung Cancer: Clinical Challenges and Opportunities. *Cancers* **2023**, *15*, 612. [[CrossRef](#)]
158. Malinge, S.; Bliss-Moreau, M.; Kirsammer, G.; Diebold, L.; Chlon, T.; Gurbuxani, S.; Crispino, J.D. Increased dosage of the chromosome 21 ortholog Dyrk1a promotes megakaryoblastic leukemia in a murine model of Down syndrome. *J. Clin. Investig.* **2012**, *122*, 948–962. [[CrossRef](#)]
159. Lane, A.A.; Chapuy, B.; Lin, C.Y.; Tivey, T.; Li, H.; Townsend, E.C.; van Bodegom, D.; Day, T.A.; Wu, S.C.; Liu, H.; et al. Triplication of a 21q22 region contributes to B cell transformation through HMGN1 overexpression and loss of histone H3 Lys27 trimethylation. *Nat. Genet.* **2014**, *46*, 618–623. [[CrossRef](#)] [[PubMed](#)]
160. Laurent, A.P.; Siret, A.; Ignacimoutou, C.; Panchal, K.; Diop, M.; Jenni, S.; Tsai, Y.C.; Roos-Weil, D.; Aid, Z.; Prade, N.; et al. Constitutive Activation of RAS/MAPK Pathway Cooperates with Trisomy 21 and Is Therapeutically Exploitable in Down Syndrome B-cell Leukemia. *Clin. Cancer Res.* **2020**, *26*, 3307–3318. [[CrossRef](#)]
161. Baek, K.H.; Zaslavsky, A.; Lynch, R.C.; Britt, C.; Okada, Y.; Siarey, R.J.; Lensch, M.W.; Park, I.H.; Yoon, S.S.; Minami, T.; et al. Down's syndrome suppression of tumour growth and the role of the calcineurin inhibitor DSCR1. *Nature* **2009**, *459*, 1126–1130. [[CrossRef](#)]
162. Reynolds, L.E.; Watson, A.R.; Baker, M.; Jones, T.A.; D'Amico, G.; Robinson, S.D.; Joffre, C.; Garrido-Urbani, S.; Rodriguez-Manzaneque, J.C.; Martino-Echarri, E.; et al. Tumour angiogenesis is reduced in the Tc1 mouse model of Down's syndrome. *Nature* **2010**, *465*, 813–817. [[CrossRef](#)]
163. Osuna-Marco, M.P.; Lopez-Barahona, M.; Lopez-Ibor, B.; Tejera, A.M. Ten Reasons Why People with Down Syndrome are Protected from the Development of Most Solid Tumors—A Review. *Front. Genet.* **2021**, *12*, 749480. [[CrossRef](#)]
164. Stankiewicz, M.J.; Crispino, J.D. ETS2 and ERG promote megakaryopoiesis and synergize with alterations in GATA-1 to immortalize hematopoietic progenitor cells. *Blood* **2009**, *113*, 3337–3347. [[CrossRef](#)]
165. Bhansali, R.S.; Rammohan, M.; Lee, P.; Laurent, A.P.; Wen, Q.; Suraneni, P.; Yip, B.H.; Tsai, Y.C.; Jenni, S.; Bornhauser, B.; et al. DYRK1A regulates B cell acute lymphoblastic leukemia through phosphorylation of FOXO1 and STAT3. *J. Clin. Investig.* **2021**, *131*, e135937. [[CrossRef](#)]
166. Volk, A.; Liang, K.; Suraneni, P.; Li, X.; Zhao, J.; Bulic, M.; Marshall, S.; Pulakanti, K.; Malinge, S.; Taub, J.; et al. A CHAF1B-Dependent Molecular Switch in Hematopoiesis and Leukemia Pathogenesis. *Cancer Cell* **2018**, *34*, 707–723.e7. [[CrossRef](#)] [[PubMed](#)]
167. Gialesaki, S.; Brauer-Hartmann, D.; Issa, H.; Bhayadia, R.; Alejo-Valle, O.; Verboon, L.; Schmell, A.L.; Laszig, S.; Regenyi, E.; Schuschel, K.; et al. RUNX1 isoform disequilibrium promotes the development of trisomy 21-associated myeloid leukemia. *Blood* **2023**, *141*, 1105–1118. [[CrossRef](#)] [[PubMed](#)]
168. Rammohan, M.; Harris, E.; Bhansali, R.S.; Zhao, E.; Li, L.S.; Crispino, J.D. The chromosome 21 kinase DYRK1A: Emerging roles in cancer biology and potential as a therapeutic target. *Oncogene* **2022**, *41*, 2003–2011. [[CrossRef](#)]
169. Sheppard, O.; Wiseman, F.K.; Ruparella, A.; Tybulewicz, V.L.; Fisher, E.M. Mouse models of aneuploidy. *Sci. World J.* **2012**, *2012*, 214078. [[CrossRef](#)] [[PubMed](#)]
170. Reeves, R.H.; Irving, N.G.; Moran, T.H.; Wohn, A.; Kitt, C.; Sisodia, S.S.; Schmidt, C.; Bronson, R.T.; Davisson, M.T. A mouse model for Down syndrome exhibits learning and behaviour deficits. *Nat. Genet.* **1995**, *11*, 177–184. [[CrossRef](#)]
171. Yu, T.; Li, Z.; Jia, Z.; Clapcote, S.J.; Liu, C.; Li, S.; Asrar, S.; Pao, A.; Chen, R.; Fan, N.; et al. A mouse model of Down syndrome trisomic for all human chromosome 21 syntenic regions. *Hum. Mol. Genet.* **2010**, *19*, 2780–2791. [[CrossRef](#)]
172. Ege, T.; Ringertz, N.R. Preparation of microcells by enucleation of micronucleate cells. *Exp. Cell Res.* **1974**, *87*, 378–382. [[CrossRef](#)] [[PubMed](#)]
173. O'Doherty, A.; Ruf, S.; Mulligan, C.; Hildreth, V.; Errington, M.L.; Cooke, S.; Sesay, A.; Modino, S.; Vanes, L.; Hernandez, D.; et al. An aneuploid mouse strain carrying human chromosome 21 with Down syndrome phenotypes. *Science* **2005**, *309*, 2033–2037. [[CrossRef](#)] [[PubMed](#)]
174. Kazuki, Y.; Gao, F.J.; Li, Y.; Moyer, A.J.; Devenney, B.; Hiramatsu, K.; Miyagawa-Tomita, S.; Abe, S.; Kazuki, K.; Kajitani, N.; et al. A non-mosaic transchromosomal mouse model of down syndrome carrying the long arm of human chromosome 21. *elife* **2020**, *9*, e56223. [[CrossRef](#)] [[PubMed](#)]
175. Sheltzer, J.M.; Ko, J.H.; Replogle, J.M.; Habibe Burgos, N.C.; Chung, E.S.; Meehl, C.M.; Sayles, N.M.; Passerini, V.; Storchova, Z.; Amon, A. Single-chromosome Gains Commonly Function as Tumor Suppressors. *Cancer Cell* **2017**, *31*, 240–255. [[CrossRef](#)] [[PubMed](#)]

176. Vasudevan, A.; Baruah, P.S.; Smith, J.C.; Wang, Z.; Sayles, N.M.; Andrews, P.; Kendall, J.; Leu, J.; Chunduri, N.K.; Levy, D.; et al. Single-Chromosomal Gains Can Function as Metastasis Suppressors and Promoters in Colon Cancer. *Dev. Cell* **2020**, *52*, 413–428.e6. [[CrossRef](#)] [[PubMed](#)]
177. Weaver, B.A.; Silk, A.D.; Montagna, C.; Verdier-Pinard, P.; Cleveland, D.W. Aneuploidy acts both oncogenically and as a tumor suppressor. *Cancer Cell* **2007**, *11*, 25–36. [[CrossRef](#)] [[PubMed](#)]
178. Newman, D.L.; Gregory, S.L. Co-Operation between Aneuploidy and Metabolic Changes in Driving Tumorigenesis. *Int. J. Mol. Sci.* **2019**, *20*, 4611. [[CrossRef](#)] [[PubMed](#)]
179. Davoli, T.; Uno, H.; Wooten, E.C.; Elledge, S.J. Tumor aneuploidy correlates with markers of immune evasion and with reduced response to immunotherapy. *Science* **2017**, *355*, eaaf8399. [[CrossRef](#)] [[PubMed](#)]
180. Kuang, X.; Li, J. Chromosome instability and aneuploidy as context-dependent activators or inhibitors of antitumor immunity. *Front. Immunol.* **2022**, *13*, 895961. [[CrossRef](#)]
181. Tai, D.J.; Ragavendran, A.; Manavalan, P.; Stortchevoi, A.; Seabra, C.M.; Erdin, S.; Collins, R.L.; Blumenthal, I.; Chen, X.; Shen, Y.; et al. Engineering microdeletions and microduplications by targeting segmental duplications with CRISPR. *Nat. Neurosci.* **2016**, *19*, 517–522. [[CrossRef](#)]
182. Banno, K.; Omori, S.; Hirata, K.; Nawa, N.; Nakagawa, N.; Nishimura, K.; Ohtaka, M.; Nakanishi, M.; Sakuma, T.; Yamamoto, T.; et al. Systematic Cellular Disease Models Reveal Synergistic Interaction of Trisomy 21 and GATA1 Mutations in Hematopoietic Abnormalities. *Cell Rep.* **2016**, *15*, 1228–1241. [[CrossRef](#)] [[PubMed](#)]
183. Zuo, E.; Huo, X.; Yao, X.; Hu, X.; Sun, Y.; Yin, J.; He, B.; Wang, X.; Shi, L.; Ping, J.; et al. CRISPR/Cas9-mediated targeted chromosome elimination. *Genome Biol.* **2017**, *18*, 224. [[CrossRef](#)] [[PubMed](#)]
184. Chiang, J.C.; Jiang, J.; Newburger, P.E.; Lawrence, J.B. Trisomy silencing by XIST normalizes Down syndrome cell pathogenesis demonstrated for hematopoietic defects in vitro. *Nat. Commun.* **2018**, *9*, 5180. [[CrossRef](#)] [[PubMed](#)]
185. Barriga, F.M.; Tsanov, K.M.; Ho, Y.J.; Sohail, N.; Zhang, A.; Baslan, T.; Wuest, A.N.; Del Priore, I.; Meskauskaite, B.; Livshits, G.; et al. MACHETE identifies interferon-encompassing chromosome 9p21.3 deletions as mediators of immune evasion and metastasis. *Nat. Cancer* **2022**, *3*, 1367–1385. [[CrossRef](#)]
186. Schlam, I.; Swain, S.M. HER2-positive breast cancer and tyrosine kinase inhibitors: The time is now. *NPJ Breast Cancer* **2021**, *7*, 56. [[CrossRef](#)] [[PubMed](#)]
187. Behl, A.; Wani, Z.A.; Das, N.N.; Parmar, V.S.; Len, C.; Malhotra, S.; Chhillar, A.K. Monoclonal antibodies in breast cancer: A critical appraisal. *Crit. Rev. Oncol. Hematol.* **2023**, *183*, 103915. [[CrossRef](#)]
188. Cabal-Hierro, L.; van Galen, P.; Prado, M.A.; Higby, K.J.; Togami, K.; Mowery, C.T.; Paulo, J.A.; Xie, Y.; Cejas, P.; Furusawa, T.; et al. Chromatin accessibility promotes hematopoietic and leukemia stem cell activity. *Nat. Commun.* **2020**, *11*, 1406. [[CrossRef](#)]
189. Page, E.C.; Heatley, S.L.; Eadie, L.N.; McClure, B.J.; de Bock, C.E.; Omari, S.; Yeung, D.T.; Hughes, T.P.; Thomas, P.Q.; White, D.L. HMGN1 plays a significant role in CRLF2 driven Down Syndrome leukemia and provides a potential therapeutic target in this high-risk cohort. *Oncogene* **2022**, *41*, 797–808. [[CrossRef](#)]
190. Carey-Smith, S.L.; Simad, M.H.; Panchal, K.; Aya-Bonilla, C.; Smolders, H.; Lin, S.; Armitage, J.D.; Nguyen, V.T.; Bentley, K.; Ford, J.; et al. Efficacy of DYRK1A inhibitors in novel models of Down syndrome acute lymphoblastic leukemia. *Haematologica* **2024**, ahead of print. [[CrossRef](#)]
191. Pozo, N.; Zahonero, C.; Fernandez, P.; Linares, J.M.; Ayuso, A.; Hagiwara, M.; Perez, A.; Ricoy, J.R.; Hernandez-Lain, A.; Sepulveda, J.M.; et al. Inhibition of DYRK1A destabilizes EGFR and reduces EGFR-dependent glioblastoma growth. *J. Clin. Investig.* **2013**, *123*, 2475–2487. [[CrossRef](#)]
192. Radhakrishnan, A.; Nanjappa, V.; Raja, R.; Sathe, G.; Puttamalles, V.N.; Jain, A.P.; Pinto, S.M.; Balaji, S.A.; Chavan, S.; Sahasrabudde, N.A.; et al. A dual specificity kinase, DYRK1A, as a potential therapeutic target for head and neck squamous cell carcinoma. *Sci. Rep.* **2016**, *6*, 36132. [[CrossRef](#)] [[PubMed](#)]
193. Cohen-Sharir, Y.; McFarland, J.M.; Abdusamad, M.; Marquis, C.; Bernhard, S.V.; Kazachkova, M.; Tang, H.; Ippolito, M.R.; Laue, K.; Zerbib, J.; et al. Aneuploidy renders cancer cells vulnerable to mitotic checkpoint inhibition. *Nature* **2021**, *590*, 486–491. [[CrossRef](#)] [[PubMed](#)]

Disclaimer/Publisher's Note: The statements, opinions and data contained in all publications are solely those of the individual author(s) and contributor(s) and not of MDPI and/or the editor(s). MDPI and/or the editor(s) disclaim responsibility for any injury to people or property resulting from any ideas, methods, instructions or products referred to in the content.

Introduction to leukaemia:

In Australia, approximately 700 new paediatric cancer cases were diagnosed each year between 2011-2015, with leukaemia accounting for 35% of these cancer cases (myeloid and lymphoid), with lymphoid leukaemia specifically accounting for 27% (8). With advancements in treatment strategies, Australian children with lymphoid leukaemia's, as of 2015, achieved an overall survival of 92%. Unfortunately, due to its high incidence in children, ALL remains the second highest cause of "deaths" by cancer in children at 13% overall (59% of all deaths caused by leukaemia's) (8). Additionally, current therapeutic strategies are toxic, leaving patients with negative secondary effects (9, 10). This indicates that there is still a need for further research into ALL, to identify novel therapeutic strategies that are less toxic and further improve survival of children with ALL.

Leukaemia is caused by disruption of haematopoiesis, which is the hierarchical system whereby haematopoietic stem cells (HSCs) differentiate into lineage specific mature cells in a highly regulated manner (11-13). Homeostasis of the entire system results from the HSCs self-renewal capacities in which daughter HSCs will maintain the HSC pool, while the other daughter cells will differentiate to allow for the continuous production of mature blood cells (14). This process is highly regulated by intrinsic and extrinsic factors including cytokines and growth factors, transcription factors, epigenetic regulators, and bone marrow stromal cells (15-18). Disruption of the haematopoietic process and ultimately the deregulation cell proliferation, self-renewal, differentiation, and survival capacities result from mutations in critical oncogenes and tumour suppressors which leads to uncontrolled proliferation of progenitor cells and a blockage in differentiation (19).

Introduction to DS-ALL:

Down syndrome children are specifically susceptible to leukaemia and are predisposed to two types: myeloid leukaemia in DS (ML-DS; also known as DS acute megakaryoblastic leukaemia) and DS-ALL (7, 20, 21). Down syndrome was first described in 1959, where the extra copy of ch21 (trisomy 21) was reported (1), and has since been associated with numerous

phenotypes, including haematopoietic abnormalities (7, 11, 22). Research into the leukaemia developed by children with DS has identified specific somatic mutations that functionally cooperate with the overexpressed genes of the extra copy of ch21, in both ML-DS and DS-ALL. It is known that 20-30% of DS children develop transient abnormal myelopoiesis (TAM), of which 30% will go onto develop ML-DS, because of *GATA1* mutations and others in genes *RAD21*, Neuroblastoma (*N*)/*KRAS*, Janus Kinase (*JAK*) 2/3, CCCTC-Binding Factor (*CTCF*) and Enhancer of Zeste Homologue 2 (*EZH2*), indicating cooperation between these mutations and trisomy of ch21 (23-26). In DS-ALL, there is a proportionally distinct mutational landscape, in comparison to non-DS-ALL, that includes genomic alterations such as Cytokine Receptor Like Factor 2 (*CRLF2*) rearrangements (most common in DS-ALL - 54%), ETS Variant Transcription Factor 6 (*ETV6*)-RUNX Family Transcription Factor 1 (*RUNX1*) fusions and Paired Box 5 (*PAX5*) alterations, mutations in *N/KRAS* and *JAK2*, as well as deletions of *CDKN2A* (7, 27, 28). These somatic mutations leading to disruption of critical cellular pathways that facilitates DS-ALL progression (7, 27, 28). Additionally, studies have shown that specific ch21 genes are implicated in DS-ALL and includes the ch21 genes *DYRK1A* (29, 30) and *HMGN1* (31). These genes were identified as critical for DS-ALL since *DYRK1A* was shown to regulate B cell quiescence and B-ALL proliferation/survival, whilst *HMGN1* overexpression suppresses the repressive histone methylation marker H3K27me3 promoting B cell proliferation (29-31). Together, this data highlights the importance of trisomy 21 in leukaemogenesis, which leads us to hypothesise that there are unidentified ch21 genes implicated in DS-ALL that may provide insight for novel therapeutic targets.

To understand the oncogenic cooperation between trisomy 21 and the acquired somatic mutations, trisomy 21 mouse models have been used to successfully model ML-DS (21) and DS-ALL (31, 32), since they share a similar haematopoietic stem and progenitor cell compartment to humans (33). Specifically the Ts1Rhr mouse model, which harbours trisomy of the DSCR murine homologous genes (33 genes associated to the phenotypes of DS (34-36)), was used to investigate DS-ALL *in vitro* through

transduction/transformation of Ts1Rhr bone marrow progenitor cells with the addition of the *KRAS*^{G12D} mutation (32). This allowed the discovery of oncogenic cooperation between the trisomy of the ch21 DSCR and the activation of RAS/MAPK pathway, as well as therapeutic vulnerability to RAS/MAPK targeted inhibition (32). Notably, the Ts1Rhr model only contains trisomy of the DSCR, therefore has some limitation as it excludes any potential cooperation from genes outside of this region.

To overcome this, other models such as the Tc1 mouse model may prove more useful since it harbours an additional copy of the entire human ch21, consisting of 269 human genes (37). Thus, genes outside the DSCR can be investigated for implication in DS-ALL development. Importantly, gene editing technology advancements have increased the capacity we have to analyse gene function in cancer. CRISPR technology has allowed for specific gene targeting, through its unique sequence specific RNA binding (38). This technology has been successfully used to perform genomic screens to uncover drug targets, drug resistance genes and identifying cancer dependent genes (39). Applying this technology to DS-ALL models with robust experimental design has potential to uncover novel leukaemogenesis pathways and aid in identifying new therapeutic targets.

Overall, significant advances to therapeutic strategies are required to improve the lives of children with DS who develop DS-ALL. Using trisomy 21 models and PDX models, we investigated the development of DS-ALL, ch21 gene directed therapeutics and applied gene editing technology to our models. Ultimately, we aimed to identify advanced therapeutics that have high potential to be translated into the clinic.

Thesis Overview

Children with DS are predisposed to leukaemia and face an unfair disadvantage regarding treatment options with poorer outcomes due to therapeutic toxicity and other complications, such as relapse and treatment failure. Therefore, we designed this project to unravel the impact of trisomy 21 in DS-ALL, with hope that this work will lead to the improvement of current treatment strategies. This thesis aimed to identify novel ch21 genes implicated in DS-ALL and ultimately identify novel oncogenic pathways that have the potential to be therapeutically exploited. To achieve this, the aims of the project outlined below were followed to develop relevant models of DS-ALL, test novel therapeutic agents, and screen for novel ch21 genes implicated in ALL.

Aim 1: Generation of the DS-ALL Ts1Rhr/Mb1-Cre/*Cdkn2a*^{fl/fl} mouse model and Ts1/*Cdkn2a*-KRAS^{G12D} cell line

In Aim 1 of this project, we set out to develop new *in vitro* and *in vivo* models of DS-ALL, which is presented in Chapter 2 of this thesis. The contents of this chapter contain the development of a triple transgenic *in vivo* model of DS-ALL from a multigenerational breeding strategy that incorporated the Ts1Rhr, Mb1-Cre and *Cdkn2a* knock-out mice into one model. From this model, we successfully generated the cell line model Ts1/*Cdkn2a*-KRAS^{G12D}, that was used in following BMT assays to re-create DS-ALL in recipient mice.

Aim 2: Therapeutically targeting the chromosome 21 gene *DYRK1A*

In Aim 2, we set out to establish new human and murine *in vivo* and *in vitro* models of DS-ALL, which we used to test several *DYRK1A* kinase inhibitors. This data is presented across Chapters 3a and 3b. Chapter 3a consists of the published data from this aim, in the journal of Haematologica, and titled “**Efficacy of *DYRK1A* inhibitors in novel models of Down syndrome acute lymphoblastic leukemia**”. This chapter details the successful development of murine DS-ALL *in vitro* and *in vivo* models derived from the Tc1 mouse model, and development of the PDX human cell line models DS-PER961 and DS-PER962, which were targeted therapeutically. Our data showed that *DYRK1A* can successfully be targeted in DS-ALL with specific

kinase inhibitors. Chapter 3b consists of the unpublished additional data that corresponds to Chapter 3a and the published work.

Aim 3: Targeting trisomy 21 in the human DS-ALL cell lines

In the final Aim 3 of this project, we pursued the goal of screening the human ch21 in our human DS-ALL cell line models DS-PER961 and DS-PER962, with the ER-dCas9-KRAB repression system. This data is included in Chapter 4 of this thesis, which covers the optimisation of transfection and transduction protocols within both cell lines and the final co-transfection of the DS-PER961 cell line with ER-dCas9-KRAB. As reported by others, transfecting/transducing human B-ALL cells is very challenging, and consequently we had difficulty genetically modifying our human DS-ALL models. However, this chapter warrants further optimisation in these human cellular models, or in the murine DS-ALL cell lines we developed (see Chapter 3); our ultimate goal being to screen and identify novel dosage sensitive ch21 genes in DS-ALL.

Chapter 2: Generation of the DS-ALL Ts1Rhr/Mb1-Cre/*Cdkn2a*^{fl/fl} mouse model and Ts1/*Cdkn2a*-KRAS^{G12D} cell line

Introduction:

Since children with DS that develop ALL suffer from inferior outcomes (10, 40), improved treatment strategies are urgently required. To this end, clinically relevant models of leukaemia that accurately model disease development are needed to uncover novel molecular weaknesses and to identify and test therapeutic targets. To date, only few DS-ALL models have been established (7, 31, 32), especially for *in vivo* use, thus preventing us from screening trisomy 21 targeted therapies. Therefore, new clinically relevant models are required to investigate mechanisms of disease development, therapeutic susceptibility, and resistance.

In this chapter, we set out to generate new *in vitro/in vivo* models of DS-ALL that could be used to assess the mechanistic development of leukaemia and test new therapeutic agents. To achieve this outcome, we designed a breeding strategy that would incorporate homogenous expression of trisomy 21 (DSCR) with deletion of the tumour suppressor *Cdkn2a*, since alterations of *CDKN2A* occurs in between 15-24% of DS-ALL cases (27, 41, 42). Previously, *in vivo* analysis performed by Sewastianik *et al.*, utilising a CD19-Cre induced conditional knock-out of *Cdkn2a* model, revealed that loss of one allele led to a precursor B-ALL (murine Pre-B-ALL) (43). Additionally, upon of the incorporation of the *Kras*^{G12D} mutation and complete loss of *Cdkn2a*, mice succumbed to a rapidly progressive form of Pre-B-ALL (43). These results highlighting the impact of *Cdkn2a* deletion on B-ALL development, as well as its potential for oncogenic cooperation with other genetic abnormalities, as was observed with the *Kras*^{G12D} mutation (43). Notably, our strategy would allow us to observe oncogenic cooperation between trisomy 21 and *Cdkn2a* knock-out *in vivo* and observe the impact of *Cdkn2a* deletion alone and in a trisomy 21 background. This strategy included cross breeding the Ts1Rhr mouse model (44) with the Mb1-Cre mouse model (45) and the *Cdkn2a*^{fl/fl} mouse model (46) to develop the triple

transgenic mouse model we called the Ts1Rhr/Mb1-Cre/*Cdkn2a*^{fl/fl} mouse model.

The Ts1Rhr mouse model was originally generated by duplication of 3.9 megabases of the murine genome, homologous to the 33 DSCR genes located on human ch21, firstly in embryonic stem (ES) cells (44). This was achieved via Cre-mediated recombination of LoxP (Locus of x-over P1) sites located on different murine chromosomes that facilitated the duplication of the DSCR (44). These modified ES cells were then injected into blastocysts, from which chimeras were bred with C57BL/6J mice to create the Ts1Rhr model (44). Interestingly, this model was used to determine the DSCR was insufficient to cause craniofacial dysmorphology (44) and brain hippocampal impairment (35) that is associated with DS. However, the Ts1Rhr model was used to generate a model of DS-ALL by Lane *et al.*, which they demonstrated that five genetic alterations were required to develop B-ALL, with addition of trisomy of DSCR (Ts1Rhr) resulting in higher penetrance and reduced latency (31).

The second transgenic model used was the Mb1-Cre mouse model (45). This model was developed by inserting a humanised Cyclisation recombinase (*Cre*) gene into the *Mb1* (Cd79a) locus in ES cells, which were injected into blastocysts to create an *in vivo* model (45). This specific insertion of *Cre* in the *Mb1* locus allowed for B cell specific deletion of floxed (flanked by LoxP) genes Serine/arginine-rich splicing factor 3 (*SRp20*) and DNA methyltransferase 1 (*Dnmt1*), within B cell progenitors of the bone marrow and spleen (45). Expression of *Cre* results in cleaved DNA at sites specified by flanking LoxP sites which the *Cre* recombinase recognises, binds and excises the DNA (47). Notably, this system is commonly used to create knock-in and knock-out models by allowing *Cre* expression that can effectively disrupt gene function through recombination (46).

The third mouse model used for cross breeding was the *Cdkn2a*^{fl/fl} mouse model (46). The *Cdkn2a* gene is located on murine ch4 and encodes two proteins required for cell cycle regulation: p16^{Ink4a} is a negative regulator of D-type cyclin Cdk4/6 complex, thus blocking phosphorylation of

Retinoblastoma protein (Rb) and in an alternative reading frame p19^{Arf} (human p14) blocks Murine double minute 2 (Mdm2) (human HDM2) to inhibit the tumour suppressor p53 (48, 49). In the *Cdkn2a^{fl/fl}* mouse model, the exons 2 and 3 are deleted upon Cre excision of the LoxP flanked region of *Cdkn2a*, resulting in a knock-out of *Cdkn2a* upon Cre expression (46). This ultimately disrupts the gene and protein function, as well as its ability to inhibit tumour development, which was highlighted by the increased tumourigenesis observed in these mice (46).

In this aim, incorporating all three transgenes into one murine model allows for B cell specific deletion of *Cdkn2a* in a trisomy 21 background (Ts1Rhr). Generating such a model which incorporates multiple transgenes and with the homozygous loss of *Cdkn2a* is challenging as it requires multiple generations. In this chapter, the Ts1Rhr/Mb1-Cre/*Cdkn2a^{fl/fl}* model allowed us to observe potential oncogenic cooperation between trisomy of 33 ch21 genes with *Cdkn2a* loss *in vivo*, that warrants further investigation. We also used this model to develop a new murine DS-ALL cell line (Ts1/Cdkn2a-KRAS^{G12D}) and performed BMT assays showing that it successfully resulted in the development of an *in vivo* model of DS-ALL.

Some of this data was used in the manuscript recently published in the journal of Haematologica: “Efficacy of DYRK1A inhibitors in novel models of Down syndrome acute lymphoblastic leukemia”.

Methods:

Triple transgenic mouse model breeding strategy:

The Ts1Rhr/Mb1-Cre/*Cdkn2a^{fl/fl}* mouse model was generated by cross breeding the Ts1Rhr (B6.129S6-Dp(16Cbr1-Fam3b)1Rhr/J, JAX stock #:005383) (Background of origin: 129S6/SvEv x C57BL/6J x C3H) mouse model (44) with the Mb1-Cre (B6.C(Cg)-Cd79a^{tm1(cre)Reth}/EhobJ, JAX stock #:020505) (Background of origin: BALB/c x C57BL/6) mouse model (45) and *Cdkn2a^{fl/fl}* (Background of origin: IB10 x C57BL/6J x FVB/N) knock-out mouse model (46), and back-crossed for multiple generations, in-house at the Bio-Resource’s facility (Telethon Kids Institute, Perth WA) (Fig. 1). This was achieved via selective breeding of parents and offspring, which were

back-crossed for C57BL/6J genetic background selection. All animals were validated via genotyping, to incorporate all three desired genotypes into one mouse.

DNA extraction for genotyping Ts1Rhr/Mb1-Cre/Cdkn2a^{fl/fl} mouse model:

DNA was extracted from mouse ear tags for genotype polymerase chain reaction (PCR) validation (extracted with Ethanol precipitation). Firstly, ear tags were placed into 1.5 mL Eppendorf tubes and were resuspended in 200 μ L of lysis buffer (tris(hydroxymethyl)aminomethane (Tris)-hydrochloric acid (HCL) 100 mM, sodium chloride (NaCl) 200 mM, sodium dodecyl sulphate (SDS) 0.2%, ethylenediaminetetraacetic acid 5 mM (EDTA), in double-distilled H₂O - containing 10 μ g/mL of proteinase K). Samples were then incubated overnight on a shaker set to 350 rpm at 55°C. The next day, ear tag samples were heated to 95°C for 20 minutes to inactivate the proteinase K. Samples were then centrifuged at 14000 rpm for 5-10 minutes and supernatant was collected into a new 1.5 mL Eppendorf tube. Next, 160 μ L of 100% isopropanol was added to each sample and the tubes were gently inverted 2-3 times. The samples were then centrifuged at 14000 rpm for 10 minutes at 4°C, discarding supernatant. The DNA pellet was then washed with 500 μ L of 70% ethanol, then centrifuged at 14000 rpm for 5 minutes at 4°C, discarding supernatant. DNA pellets were then air dried for 1 hour and then resuspended in 50 μ L of diethylpyrocarbonate (DEPC) treated water. DNA concentration/purity was then determined with the NanoDrop 2000, following standard protocol (Thermo Fisher Scientific).

PCR for genetic validation of the Ts1Rhr/Mb1-Cre/Cdkn2a^{fl/fl} mouse model:

Genomic DNA from ear tags was used as template DNA to amplify a section of the Ts1Rhr ch21, the Mb1-Cre integration, and the LoxP sites of *Cdkn2a* according to the recommended Taq Recombinant Polymerase protocol (Thermo Fisher Scientific), using specific primers, annealing temperature, and extension time (Table 1). PCR products were analysed via agarose gel electrophoresis (1% agarose (Fisher Biotec Australia) gel, prepared with 1x Tris-acetate EDTA buffer (Thermo Fisher Scientific)) with 0.1 μ L/mL SYBR Safe (Thermo Fisher Scientific) to validate the presence of the desired

transgenes according to product size (Table 1). The gel was run at 100V for approximately 35 minutes and imaged on the BioRad GelDoc XR+ to visualise the bands and assess PCR product amplification.

Primer Name	Primer Sequence (5'-3')	Annealing Temp (°C)	Ext Time (S)	Product Size (bp)
Mb1.Cre WT For	CTC TTT ACC TTC CAA GCA CTG A	59	45	WT: 197 Cre: 230
Mb1.Cre Mut For	CAT TTT CGA GGG AGC TTC A			
Mb1.Cre Com Rev	ACT GAG GCA GGA GGA TTG G			
Ts1Rhr Dup F	GCC AGA GGC CAC TTG TGT AG	62-57	30	Ts1Rhr: 200-300
Ts1Rhr Dup R	TGT TGA CCT CGA GGG ACC TA			
CDKN2A F	ACG TGT ATG CCA CCC TGA CC	60	40	WT: 160 LoxP: 260
CDKN2A R	GAC TGC TCG GGA ATC TTG CC			

Table 1. Genotyping PCR reactions. Primer name, sequence, annealing temperature (Temp), extension (Ext) time in seconds (S) used, and product size in base pairs (bp).

Monthly blood analysis with flow cytometry of Ts1Rhr/Mb1-Cre/Cdkn2a^{fl/fl} mouse model cohort:

Mice were bled at age matched monthly timepoints for more than a year (383 days), via tail vein bleed for flow cytometry analysis. 25-50 μ L of blood was collected in 1.5 mL Eppendorf tubes containing 10 μ L of 10% EDTA. Samples underwent red blood cell (RBC) lysis in 500 μ L of 1x ammonium chloride (NH₄Cl) (STEMCELL Technologies) for 7 minutes at room temperature, which were then transferred to flow cytometry tubes and washed with 1 mL of 2% Cell Sera Australia foetal calf serum (FCS)/1x phosphate-buffered saline (PBS) solution (Thermo Fisher Scientific). Samples were then centrifuged at 1500 rpm for 5 minutes at room temperature, discarding supernatant. Single stains for antibodies and the viability stain were made according to Table 2, with cell pellets resuspended in 100 μ L of 2% FCS/PBS containing the fluorochrome conjugated antibody mixture (Table 2). Cells were incubated for \geq 20 minutes in the dark at 4°C. Cells were then washed with 1 mL of 2% FCS/PBS solution and centrifuged at 1500 rpm for 5 minutes at room

temperature, discarding supernatant and then resuspending in Sytox Blue viability stain solution. Samples were then analysed via flow cytometry using the BD LSRFortessa™ X-20 and analysed using FlowJo software (Version 10.9.0, BD Biosciences).

Murine Antibody	Fluorochrome Detection Channel	Antibody Dilution	Supplier	Product Reference
B220	APC	1/100	Invitrogen	17-0452-82
CD19	APC-Cy7	1/100	BD Biosciences	557655
Gr1	PE-Cy7	1/100	Invitrogen	25-5931-82
CD11b	PE	1/100	BD Biosciences	557397
Sytox Blue	BV421	1/4000	Invitrogen	S11348

Table 2. Monthly blood analysis flow cytometry antibody panel.

Monthly blood analysis of Ts1Rhr/Mb1-Cre/Cdkn2a^{fl/fl} mouse model cohort cell population counts:

Initially, 10 µL of mouse blood collected from tail vein bleed was mixed with 10 µL of Diluent V-52D (Mindray) in a 1.5 mL Eppendorf tube and then underwent analysis with the BC-5000 Vet Auto Hematology Analyzer (Mindray) post quality control with BC-5D haematology controls (Mindray). Analysis followed standard protocol in whole blood mode.

Murine bone marrow and spleen sample collection:

Samples were collected from time point culled or symptomatic mice. The hip, femur and tibia bones were collected, as well as the spleen. Bone marrow was collected from the hip, femur, and tibia into 50 mL Falcon tubes, containing 10 mL of 2% FCS/PBS solution, via flushing with a 3 mL syringe and a 21-gauge needle. Spleen was processed using a 100 µm cell strainer placed in a 50 mL Falcon tube, containing 10 mL of 2% FCS/PBS solution. The spleen was firstly placed into the cell strainer and broken down with a 3 mL syringe plunger and washed through the 100 µm cell strainer with the 10 mL of 2% FCS/PBS solution with a pipette. Bone marrow and spleen cells were then lysed with 2 mL of 1x NH₄Cl RBC lysis buffer for 7 minutes at room temperature, which were then washed with 8 mL 2% FCS/PBS solution. Samples were then centrifuged at 1500 rpm for 5 minutes at room temperature, discarding supernatant. Samples were then resuspended in 10

mL of 2% FCS/PBS solution and cell density was determined using Trypan Blue (Thermo Fisher Scientific) exclusion. If samples were not analysed by flow cytometry on the same day, cell vials were made with densities from 10-30 million cells per vial, using 10% dimethyl sulfoxide (DMSO)/FCS solution, with samples stored at -80°C or in liquid nitrogen.

Flow cytometry analysis of Ts1Rhr/Mb1-Cre/Cdkn2a^{fl/fl} mouse model cohort:

Freshly harvested cells or vials collected from the triple transgenic Ts1Rhr/Mb1-Cre/Cdkn2a^{fl/fl} mouse model cohort (which were thawed in a water bath at 37°C, then washed in 9 mL of 2% FCS/PBS within a 15 mL Falcon tube) were used for analysis. Cells were centrifuged at 1500 rpm for 5 minutes at room temperature, discarding supernatant. Cells were then resuspended in 50 µL of 2% FCS/PBS and transferred to a 96 well plate for antibody staining, including single stain and isotype controls. The 96 well plate was then centrifuged at 1500 rpm for 5 minutes at room temperature, discarding supernatant. Cells were then stained with two fluorochrome conjugated antibody panels (Table 3) via resuspension in 50 µL of the antibody solution consisting of 2% FCS/PBS and antibody dilutions as in Table 3. Cells were stained for ≥20 minutes in the dark at 4°C, then centrifuged at 1500 rpm for 5 minutes at room temperature, discarding supernatant. Cells were then washed with 1 mL of 2% FCS/PBS solution as they were transferred to flow cytometry tubes. Cells were then centrifuged at 1500 rpm for 5 minutes at room temperature, discarding supernatant, and resuspended in 200 µL of 2% FCS/PBS containing Sytox Blue viability stain (Table 3). The cell samples were then analysed via flow cytometry using the BD LSRFortessa™ X-20 and analysed using FlowJo software (Version 10.9.0).

Murine Antibody	Fluorochrome Detection Channel	Antibody Dilution	Supplier	Product Reference
Panel 1				
B220	APC	1/200	Invitrogen	17-0452-82
CD43	PE	1/200	Invitrogen	12-0431-82
CD117	APC-H7	1/100	BD Biosciences	560185
IgM	PerCP-Cy5.5	1/100	BD Biosciences	550881
IgD	FITC	1/100	Invitrogen	11-5993-82
Sytox Blue	BV421	1/4000	Invitrogen	S11348
Panel 2				
B220	APC	1/200	Invitrogen	17-0452-82
CD19	APC-H7	1/200	BD Biosciences	560245
Ter119	FITC	1/100	Invitrogen	11-5921-82
CD11b	BV510	1/500	BD Biosciences	562950
Gr1	PE-Cy7	1/500	Invitrogen	25-5931-82
CD4	PerCP-Cy5.5	1/200	Invitrogen	45-0042-82
CD8a	PE	1/200	BD Biosciences	553033
Sytox Blue	BV421	1/4000	Invitrogen	S11348
Controls				
Isotype	APC	1/200	BD Biosciences	550854
Isotype	APC-Cy7	1/200	BD Biosciences	557873
Isotype	BV510	1/500	BD Biosciences	562951
Isotype	PE-Cy7	1/500	BD Biosciences	557872
Isotype	PerCP-Cy5.5	1/200	BD Biosciences	552834
Isotype	PE	1/200	Invitrogen	12-4714-82
Isotype	FITC	1/100	Invitrogen	11-4714-81

Table 3. Ts1Rhr/Mb1-Cre/*Cdkn2a*^{fl/fl} model cohort flow cytometry analysis antibody panels.

CFU Pre-B cell assay:

Colony forming unit (CFU) Pre-B cell assays were performed by obtaining bone marrow cells from the 10-week-old Ts1Rhr/Mb1-Cre/*Cdkn2a*^{fl/fl} mice, which were transduced with an mCherry expressing murine stem cell virus (MSCV) containing the oncogene *KRAS*^{G12D} (MSCV-*KRAS*^{G12D}) (32) or the empty vector control MIC (MSCV-IRES-mCherry). Cells then underwent fluorescence-activated cell sorting (FACS) with the FACS Aria™ III (BD Biosciences) based upon positive mCherry expression. mCherry positive cells were counted using Trypan Blue exclusion, from which 1x10⁴ cells were obtained and washed with 10 mL of 2% FCS/PBS in a 15 mL Falcon tube, centrifuged at 24°C for 5 minutes at 1500 rpm, discarding supernatant. Cell pellets were resuspended in 300 µL of RPMI1640 (Gibco) media and dispensed into the 2.7 mL of pre-aliquoted MethoCult™ M3630 medium

using a sterile 3 mL luer lock syringe and sterile 16-gauge blunt-end needle. This cell mixture was dispensed into a 35 mm petri dish, which were then incubated at 37°C, in 5% CO₂ with 95% relative humidity for 7 days (Heracell VIOS 160i incubator). On day 7, cell colonies were counted. Once colony number was determined, the culture was resuspended with 2% FCS/PBS and cell number determined with Trypan Blue exclusion. Then 2x10⁴ cells were replated as described and cultured for another 7 days. This process was serially repeated every 7 days over 4 passages.

Cell line generation from methylcellulose culture:

Cells were extracted from the methylcellulose (MethoCult™ M3630) by dispensing 5 mL of 2% FCS/PBS solution into the culture dish and mixed with the methylcellulose by repetitive pipetting. The medium was then transferred to a 50 mL falcon tube (process repeated twice), which were then centrifuged at 1500 rpm for 5 minutes at room temperature, discarding supernatant. The cell pellet was then resuspended with 2% FCS/PBS solution and cell number determined using Trypan Blue exclusion. Once the cell number and viability was determined, cells were cultured in media consisting of IMDM (Gibco), 20% heat inactivated FCS, 1% non-essential amino acids (MP Biomedicals), 1 mM of sodium pyruvate (MP Biomedicals), 50 µM of 2-mercaptoethanol (Sigma-Aldrich), penicillin (100 U/mL)-streptomycin (100 µg/mL) (Thermo Fisher Scientific), and supplemented with recombinant murine interleukin 7 (IL-7) (10 ng/mL), stem cell factor (SCF) (10 ng/mL) and Fms-like tyrosine kinase 3 (Flt3)-ligand (10 ng/mL) (PeproTech and STEMCELL Technologies). The cell culture was then incubated at 37°C, in 5% CO₂ with 95% relative humidity.

Ts1/Cdkn2a-KRAS^{G12D} cell line phenotyping:

The Ts1/Cdkn2a-KRAS^{G12D} cell line was incubated with the fluorochrome conjugated antibody panel and dilutions listed in Table 4, along with single stain and isotype controls. The antibody/cell mixtures were incubated at 4°C for ≥20 minutes in the dark, then washed with 1 mL of 2% FCS/PBS and centrifuged at 1500 rpm for 5 minutes, discarding supernatant. Cell pellets were resuspended in 200 µL of 2% FCS/PBS with Sytox Blue to determine

cell viability. Samples were then then analysed via flow cytometry using the BD LSRFortessa™ X-20 and analysed using FlowJo software (Version 10.9.0).

Murine Antibody	Fluorochrome Detection Channel	Antibody Dilution	Supplier	Product Reference
BP1	FITC	1/200	Invitrogen	11-5891-82
CD24	PE-Cy7	1/300	BD Biosciences	560536
CD19	BV510	1/100	BD Biosciences	562956
B220	APC	1/200	Invitrogen	17-0452-82
CD117	APC-H7	1/100	BD Biosciences	560185
IgM	PerCP-Cy5.5	1/100	BD Biosciences	550881
Sytox Blue	BV421	1/4000	Invitrogen	S11348
mCherry	PE-Texas-Red	N/A	N/A	N/A
Isotype	FITC	1/200	Invitrogen	11-4714-81
Isotype	PE-Cy7	1/300	BD Biosciences	557872
Isotype	BV510	1/100	BD Biosciences	562951
Isotype	APC	1/200	BD Biosciences	550854
Isotype	APC-Cy7	1/100	BD Biosciences	557873
Isotype	PerCP-Cy5.5	1/100	BD Biosciences	552834

Table 4. Ts1/Cdkn2a-KRAS^{G12D} cell line phenotyping antibody panel.

Bone marrow transplant:

Age matched 8-week-old recipient C57BL/6J (JAX stock #:000664) mice were sub-lethally irradiated (550 Gray (Gy)) and injected via tail vein injection with 2×10^6 Ts1/Cdkn2a-KRAS^{G12D} cells. Mice were monitored weekly via tail vein bleed and assessed by flow cytometry (BD LSRFortessa™ X-20), using Sytox Blue viability stain (1/4000) and single stain controls, to analyse mCherry expression. Transplanted mice upon expression of mCherry in peripheral blood or if symptomatic were culled and samples of bone marrow and spleen were collected for analysis via flow cytometry. All mice were maintained at the Telethon Kids Institute preclinical facility (Bio-Resources).

Bone marrow transplant vial analysis:

Bone marrow and spleen vials collected from the Ts1/Cdkn2a-KRAS^{G12D} cell line BMT were thawed in a water bath at 37°C and then washed in 9 mL of 2% FCS/PBS within a 15 mL Falcon Tube. Cells were then centrifuged at 1500 rpm for 5 minutes at room temperature, discarding supernatant. Cells were then resuspended in 50 µL of 2% FCS/PBS and transferred to a 96 well

plate for antibody staining, including single stain controls. The 96 well plate was then centrifuged at 1500 rpm for 5 minutes at room temperature, discarding supernatant. Cells were then stained with two fluorochrome conjugated antibody panels (Table 5) via resuspension in 50 μ L of the antibody solution consisting of 2% FCS/PBS and antibody dilutions as in Table 5. Cells were stained for \geq 20 minutes in the dark at 4°C, then centrifuged at 1500 rpm for 5 minutes at room temperature, discarding supernatant. Cells were then washed with 1 mL of 2% FCS/PBS solution as samples were transferred to flow cytometry tubes. Cells were then centrifuged at 1500 rpm for 5 minutes at room temperature, discarding supernatant, and resuspended in 200 μ L of 2% FCS/PBS containing Sytox Blue viability stain (Table 5). The cell samples were then analysed via flow cytometry using the BD LSRFortessa™ X-20 and analysed using FlowJo software (Version 10.9.0).

Murine Antibody	Fluorochrome Detection Channel	Antibody Dilution	Supplier	Product Reference
Panel 1				
B220	APC	1/200	Invitrogen	17-0452-82
CD19	BV510	1/100	BD Biosciences	562956
CD117	APC-H7	1/100	BD Biosciences	560185
IgM	PerCP-Cy5.5	1/100	BD Biosciences	550881
IgD	FITC	1/100	Invitrogen	11-5993-82
Sytox Blue	BV421	1/4000	Invitrogen	S11348
mCherry	PE-Texas-Red	N/A	N/A	N/A
Panel 2				
CD19	APC-H7	1/100	BD Biosciences	560245
Ter119	FITC	1/200	Invitrogen	11-5921-82
CD11b	BV510	1/500	BD Biosciences	562950
Gr1	PE-Cy7	1/500	Invitrogen	25-5931-82
Sytox Blue	BV421	1/4000	Invitrogen	S11348
mCherry	PE-Texas-Red	N/A	N/A	N/A

Table 5. Ts1/Cdkn2a-KRAS^{G12D} cell line bone marrow transplant sample phenotyping antibody panels.

Statistical analysis:

All statistical analysis was performed in GraphPad Prism (Version 8.4.3), with statistical significance determined by unpaired two-tailed *t*-test and a significance P-value <0.05. Data is presented as mean with standard deviation.

Results:

Development of the Ts1Rhr/Mb1-Cre/Cdkn2a^{fl/fl} mouse model.

Through the breeding strategy outlined in Figure 1, we were able to breed and generate the Ts1Rhr/Mb1-Cre/Cdkn2a^{fl/fl} (Ts1Rhr/Mb1-Cre/Cdkn2aHOM) (n= 3) triple transgenic mouse model, as well as several controls: WT (n= 3), Ts1Rhr (n= 4), Mb1-Cre/Cdkn2aHET (n= 2), Mb1-Cre/Cdkn2aHOM (n= 1) and Ts1Rhr/Mb1-Cre/Cdkn2aHET (n= 1) controls. Notably, we did not observe a difference in the proportion of males and females for any specific genotype, thus only males were selected for analysis. All genotypes containing Mb1-Cre expressed a heterozygous genotype (to not completely lose *Mb1* expression), while Cdkn2aHET and Cdkn2aHOM genotype mice were heterozygous (HET) and homozygous (HOM) for *Cdkn2a* floxed sites respectively. Therefore, Cdkn2aHET genotype resulted in heterozygous loss of *Cdkn2a* and Cdkn2aHOM genotype resulted in homozygous loss of *Cdkn2a*.



Figure 1. Breeding strategy to develop the triple transgenic mouse model Ts1Rhr/Mb1-Cre/Cdkn2a^{fl/fl}. The two breeding strategies A and B performed in parallel to generate the Ts1Rhr/Mb1-Cre/Cdkn2a^{fl/fl} mouse model, through back-crossing the Ts1Rhr mouse model with the Mb1-Cre mouse model and Cdkn2a^{fl/fl} mouse model. Created with BioRender.com.

The cohort of Ts1Rhr/Mb1-Cre/Cdkn2a^{fl/fl} mice and controls were followed with monthly aged-matched blood samples from 16-weeks to 52-weeks of age (Fig. 2).

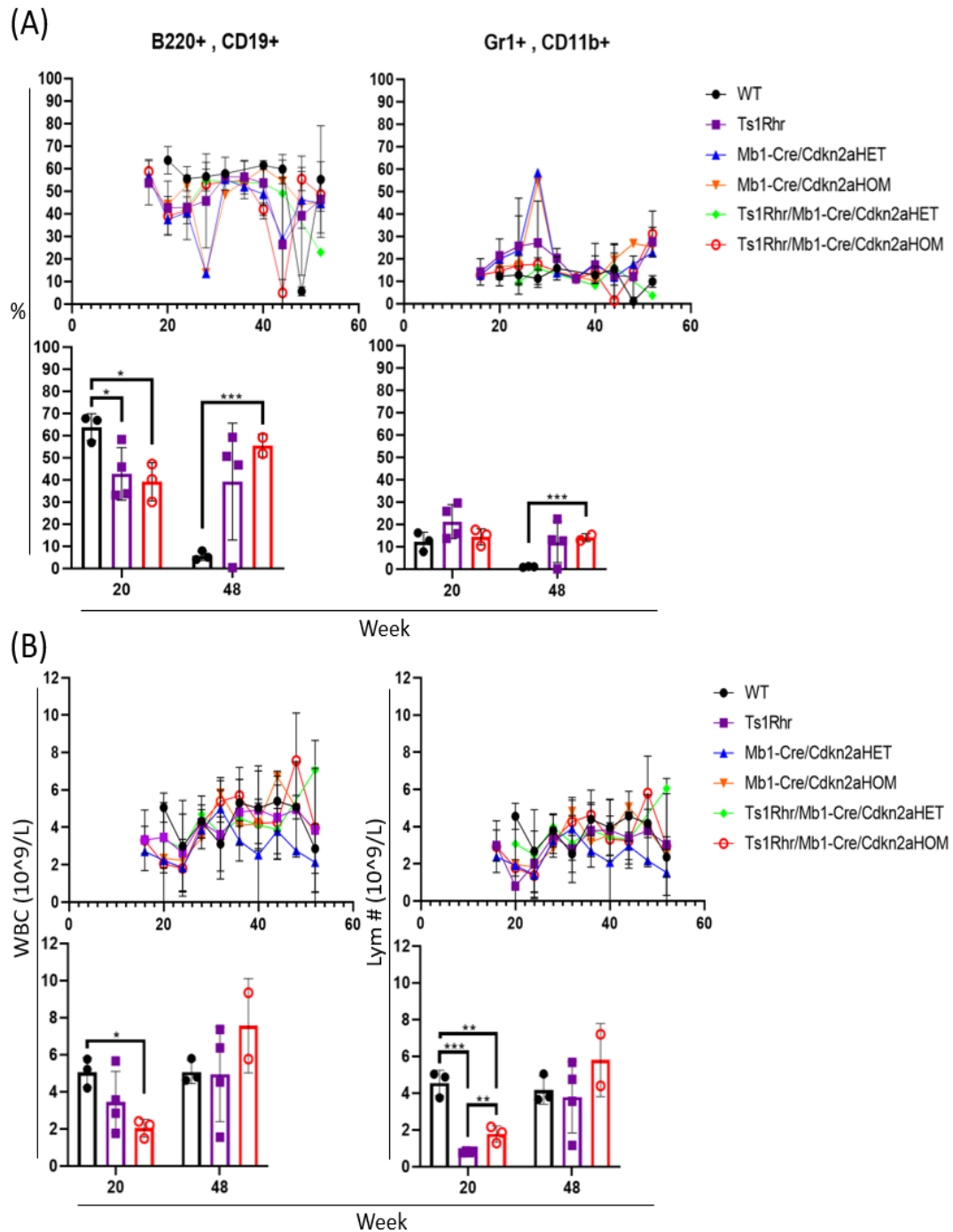


Figure 2. Ts1Rhr/Mb1-Cre/Cdkn2a^{fl/fl} mouse model cohort analysis. (A) Monthly blood sample flow cytometry analysis of Ts1Rhr/Mb1-Cre/Cdkn2aHOM (Ts1Rhr/Mb1-Cre/Cdkn2a^{fl/fl}) mouse model (n= 3) and WT (n= 3), Ts1Rhr (n= 4), Mb1-Cre/Cdkn2aHET (n= 2), Mb1-Cre/Cdkn2aHOM (n= 1), Ts1Rhr/Mb1-Cre/Cdkn2aHET (n= 1) controls with B220/CD19 and Gr1/CD11b antibodies. (B) Monthly blood sample analysis of Ts1Rhr/Mb1-Cre/Cdkn2a^{fl/fl} mouse model cohort total white blood cell (WBC) count (WBC (10⁹/L)) and lymphocyte count (Lym # (10⁹/L)) with the BC-5000 Vet Auto Hematology Analyzer. Corresponding P-value for week 20 and 48 (* P <0.05, ** P <0.01, *** P <0.001).

The cohort of Ts1Rhr/Mb1-Cre/*Cdkn2a*^{fl/fl} mice and controls were analysed by flow cytometry to assess expression of B220, CD19, Gr1 and CD11b surface markers (Fig. 2A). B220/CD19 markers were used to detect potential amplification of B cell leukaemia in the peripheral blood, while myeloid Gr1/CD11b positive cells were used as controls. As shown in Figure 2A, a high degree of variability between monthly blood samples and replicates was observed across B220/CD19 positive cells and Gr1/CD11b positive cells independently of the genotype. We therefore did not observe any phenotype changes that would indicate leukaemia development. In parallel, WBC and lymphocyte counts were analysed with the BC-5000 Vet Auto Hematology Analyzer (Mindray) (Fig. 2B). Similarly, we observed high variability between monthly blood samples and replicates, making it difficult to distinguish any disease development based on WBC and lymphocyte counts. Overall, we were unable to draw definitive conclusions on any potential leukaemia development from the peripheral blood data alone, especially since it was highly variable. Therefore, we needed to inspect the Ts1Rhr/Mb1-Cre/*Cdkn2a*^{fl/fl} model and control mice tissues for any disease burden.

To examine the potential development of leukaemia internally, we euthanised the Ts1Rhr/Mb1-Cre/*Cdkn2a*^{fl/fl} mouse model cohort at 383 days of age. Spleens were harvested from the triple transgenic and control mice and were weighed to identify if there was any enlargement in size associated with a particular genotype, indicative of potential disease development (Fig. 3).

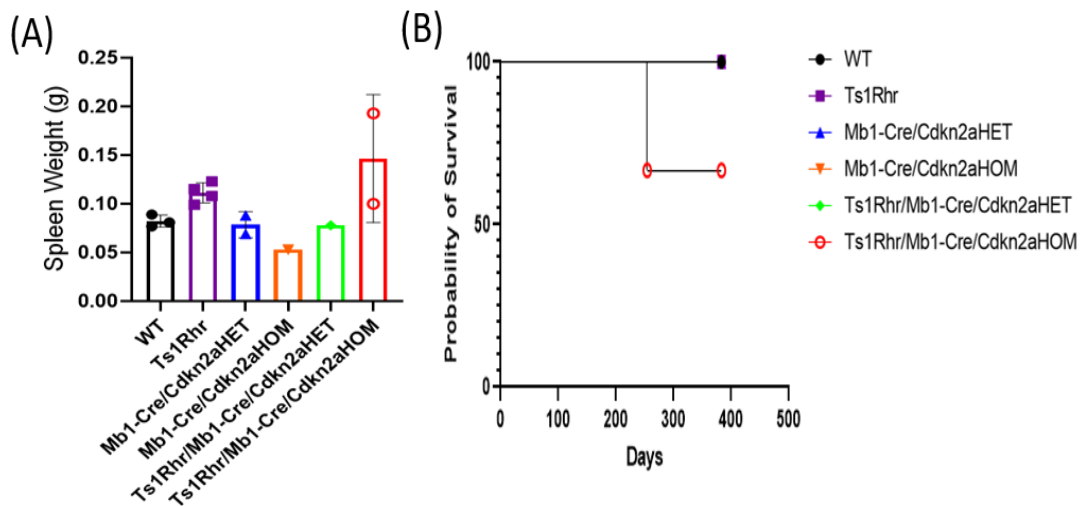


Figure 3. Ts1Rhr/Mb1-Cre/*Cdkn2a*^{fl/fl} mouse model cohort spleen weight and survival. (A) Spleen weight of the Ts1Rhr/Mb1-Cre/*Cdkn2a*^{fl/fl} mouse model (n= 2) and WT (n= 3), Ts1Rhr (n= 4), Mb1-Cre/*Cdkn2a*HET (n= 2), Mb1-Cre/*Cdkn2a*HOM (n= 1), Ts1Rhr/Mb1-Cre/*Cdkn2a*HET (n= 1) controls at cull. (B) Survival curve of Ts1Rhr/Mb1-Cre/*Cdkn2a*^{fl/fl} (n= 3) model and controls (n= as above), remaining cohort culled day 383.

Probably due to the limited number of mice per group, we did not see a striking difference in spleen weight observed between the Ts1Rhr/Mb1-Cre/*Cdkn2a*^{fl/fl} mouse model and controls (Fig. 3A). We also tracked survival of the cohort for over a year (383 days, Fig. 3B). Only one triple transgenic Ts1Rhr/Mb1-Cre/*Cdkn2a*^{fl/fl} mouse model was found dead at day 254, however disease burden could not be determined due to sample loss. The remaining Ts1Rhr/Mb1-Cre/*Cdkn2a*^{fl/fl} mice were culled at day 383 asymptomatic compared to controls, from which bone marrow and spleen samples were collected for further phenotype analysis by flow cytometry.

*Phenotyping the Ts1Rhr/Mb1-Cre/*Cdkn2a*^{fl/fl} mouse model.*

Bone marrow and spleen samples were collected from mice at end of experiment (timepoint cull 383 days), which were analysed phenotypically by flow cytometry to observe any identification of B-ALL development, following B cell differentiation (Fig. 4) and the flow cytometry gating strategy in Figure 5.

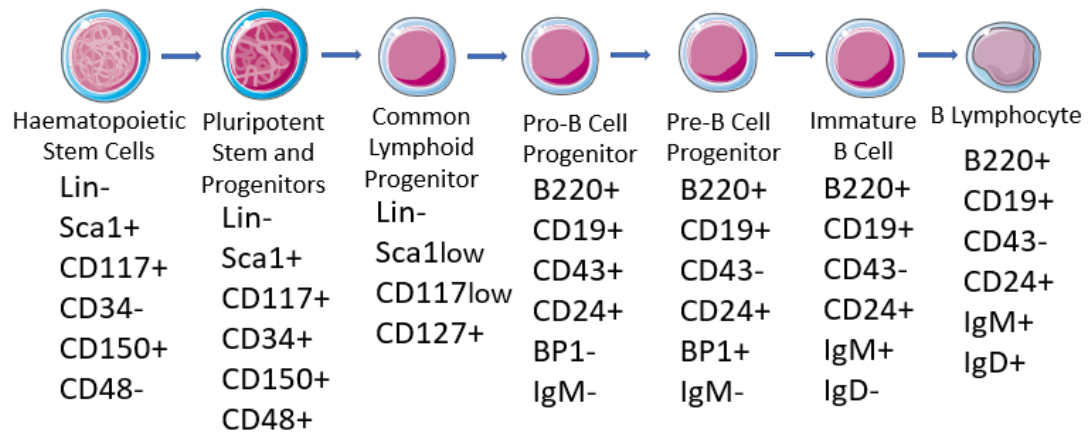


Figure 4. B cell lineage flow cytometry cell surface markers. The flow cytometry cell surface antibody markers used to identify and differentiate the haematopoietic stem cells, pluripotent stem and progenitor cells, common lymphoid progenitors, Pro-B cell progenitors, Pre-B cell progenitors, immature B cells and B lymphocytes (mature B cell). This marker definition was used to differentiate and assess the cell populations analysed by flow cytometry within this study. Created partly with Servier Medical Art (smart.servier.com).

Phenotype analysis was carried out by flow cytometry to examine the myeloid, T cell and B cell lineages. We assessed the B cell populations with markers B220 and CD19 to identify the B cell lineage, as well as with markers used to recognise B cell progenitors including CD117 for common lymphoid progenitors and CD43, IgD and IgM to analyse the Pro/Pre-B cell progenitors and immature/mature B cell populations (Fig. 4). The myeloid markers Gr1 and CD11b were used to observe any potential impact on the myeloid population, Ter119 for the erythroid population, whilst CD8a and CD4 were used to observe the T cell lineage (Fig. 5).

We did not see differences in the myeloid nor the T cell lineages. These analysis also revealed no significant differences in expression of the cell surface markers analysed in the B cell differentiation, with marker expression confirming no disease development occurred within the Ts1Rhr/Mb1-Cre/*Cdkn2a*^{fl/fl} mouse model (Fig. 6).

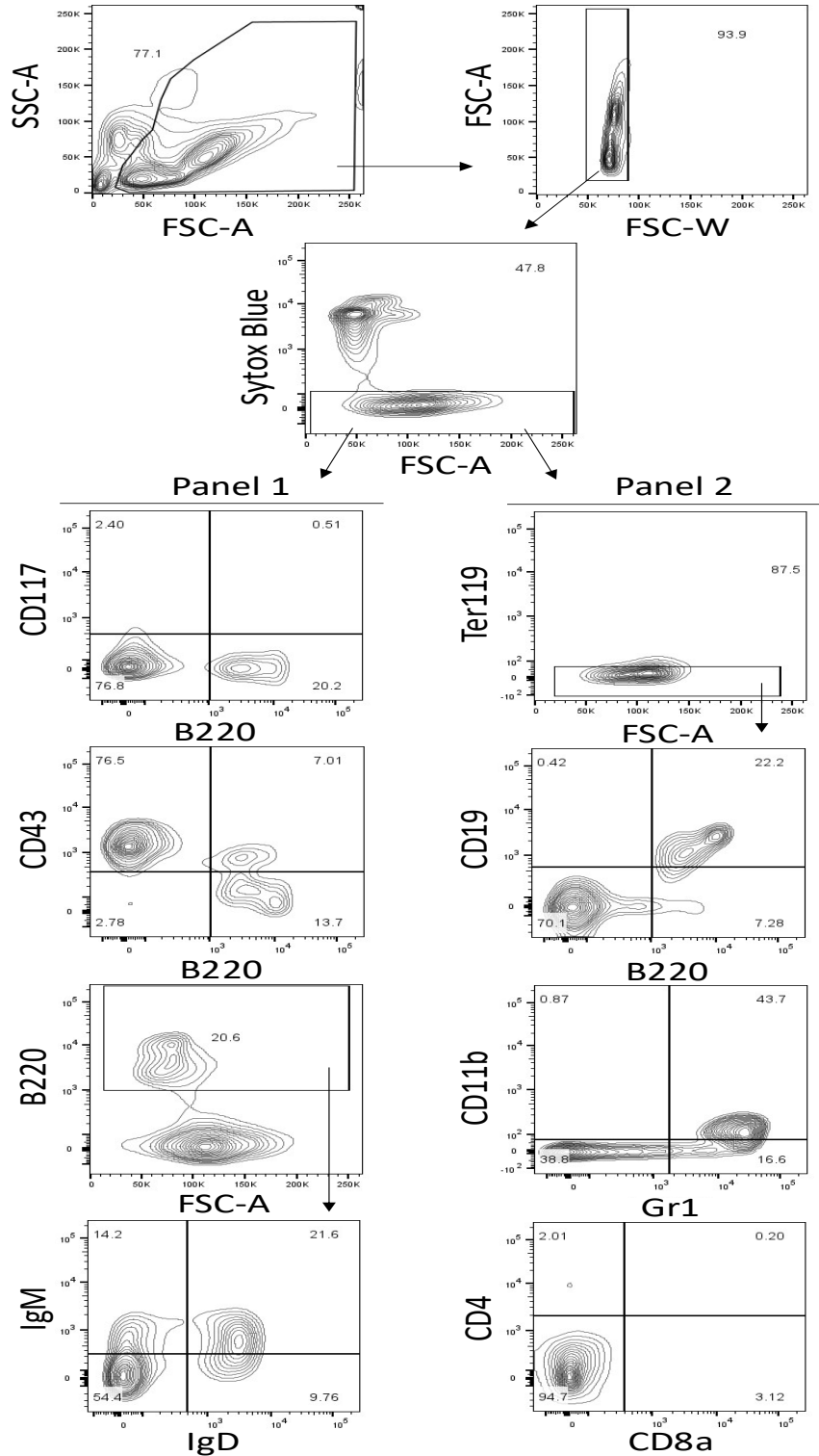


Figure 5. Ts1Rhr/Mb1-Cre/Cdkn2a^{fl/fl} mouse model cohort bone marrow and spleen sample flow cytometry phenotyping strategy. Bone marrow and spleen samples collected from the Ts1Rhr/Mb1-Cre/Cdkn2a^{fl/fl} mouse models and controls were phenotypically analysed with this gating strategy, including antibody panel 1 and panel 2.

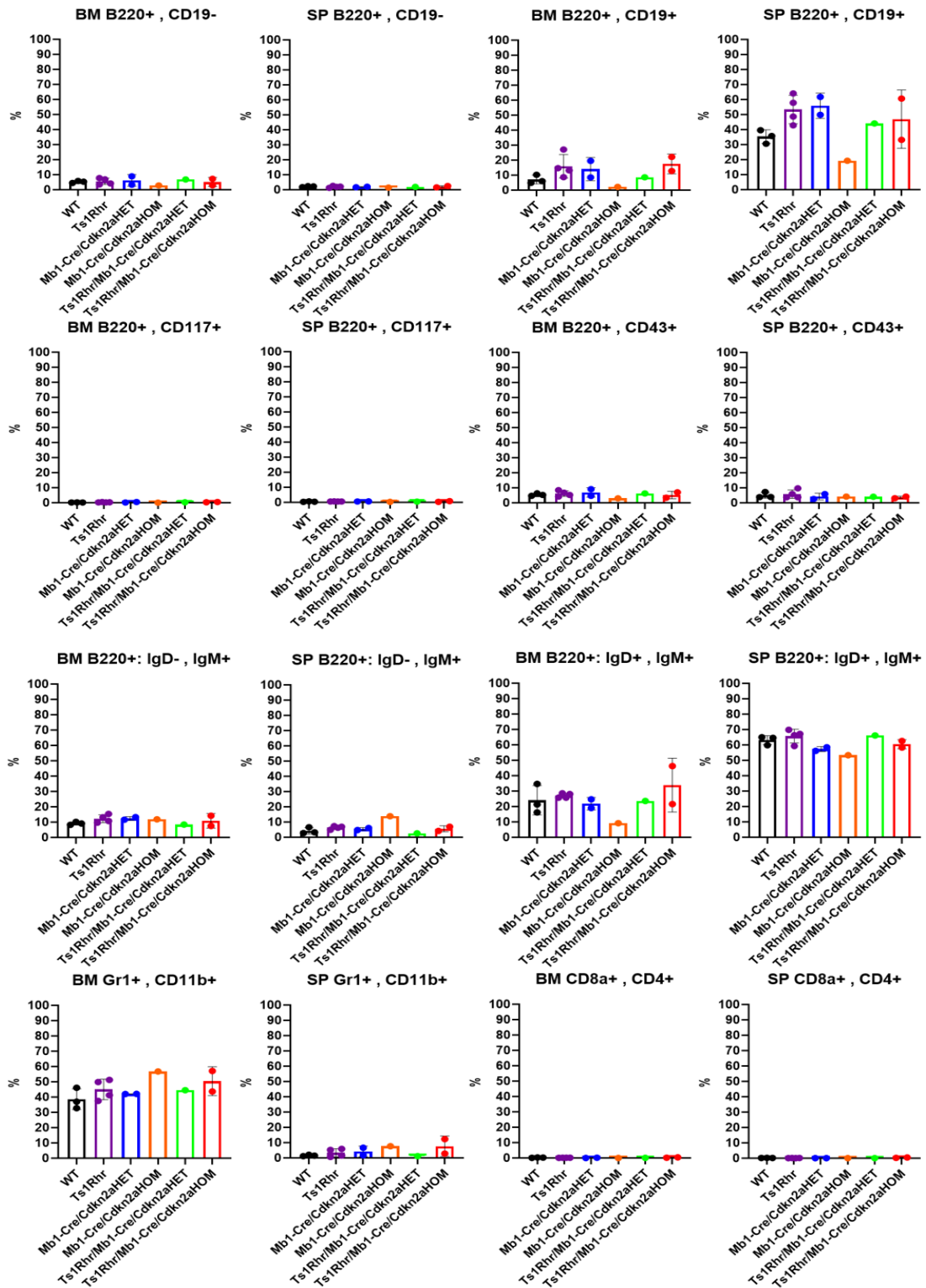


Figure 6. *Ts1Rhr/Mb1-Cre/Cdkn2a^{fl/fl}* mouse model cohort phenotype analysis. Bone marrow (BM) and spleen (SP) sample flow cytometry analysis of the *Ts1Rhr/Mb1-Cre/Cdkn2a^{fl/fl}* mouse model (n= 2) and WT (n= 3), *Ts1Rhr* (n= 4), *Mb1-Cre/Cdkn2aHET* (n= 2), *Mb1-Cre/Cdkn2aHOM* (n= 1), *Ts1Rhr/Mb1-Cre/Cdkn2aHET* (n= 1) controls with panel 1 and panel 2.

Variability between genotype replicates and monthly blood samples analysed was likely due to small sample sizes (strongly delayed by the COVID-19

pandemic). Further increased sample size and optimisation of tracking disease development would improve our monitoring of B cell alterations if any (currently ongoing). However, obtaining a larger sample size remains challenging as several generations are needed to obtain the correct genotype, therefore we are now aiming to finish this study by increasing the number of samples. Overall, these results reveal that trisomy of the DSCR (Ts1Rhr) and knock-out of both *Cdkn2a* alleles is insufficient to cause B-ALL *in vivo*.

Development of the Ts1/Cdkn2a-KRAS^{G12D} DS-ALL cell line.

As additional alterations are required, we sought to increase the oncogenic potential of the Ts1Rhr/Mb1-Cre/*Cdkn2a^{fl/fl}* model through the incorporation of the *KRAS^{G12D}* mutation. Previous work by our laboratory identified oncogenic cooperation between the Ts1Rhr trisomy of the DSCR and the *KRAS^{G12D}* mutation (32), thus we hypothesised it would allow for the transformation of B cell progenitors from the Ts1Rhr/Mb1-Cre/*Cdkn2a^{fl/fl}* mouse model. Therefore, we set out to incorporate the *KRAS^{G12D}* mutation ectopically into bone marrow cells extracted from the Ts1Rhr/Mb1-Cre/*Cdkn2a^{fl/fl}* mouse model via transduction with MSCV-*KRAS^{G12D}*. The MSCV vector used to transduce the Ts1Rhr/Mb1-Cre/*Cdkn2a^{fl/fl}* mouse model bone marrow cells expressed mCherry in successfully transduced cells, thus cells sorted for mCherry positive expression were used for the CFU Pre-B cell assay. Using this strategy, we compared ectopic expression of *KRAS^{G12D}* in the Ts1Rhr/Mb1-Cre/*Cdkn2a^{fl/fl}* mouse model and WT, Ts1Rhr and Mb1-Cre/*Cdkn2a^{HOM}* control mice bone marrow cells. This was conducted alongside the empty vector MSCV control (MIC) for Mb1-Cre/*Cdkn2a^{HOM}* and Ts1Rhr/Mb1-Cre/*Cdkn2a^{fl/fl}* mice (Fig. 7A); 1×10^4 sorted cells from each condition were dispensed into B cell lineage specific methylcellulose, from which, colony numbers were counted every 7 days and serially replated over 4 passages.

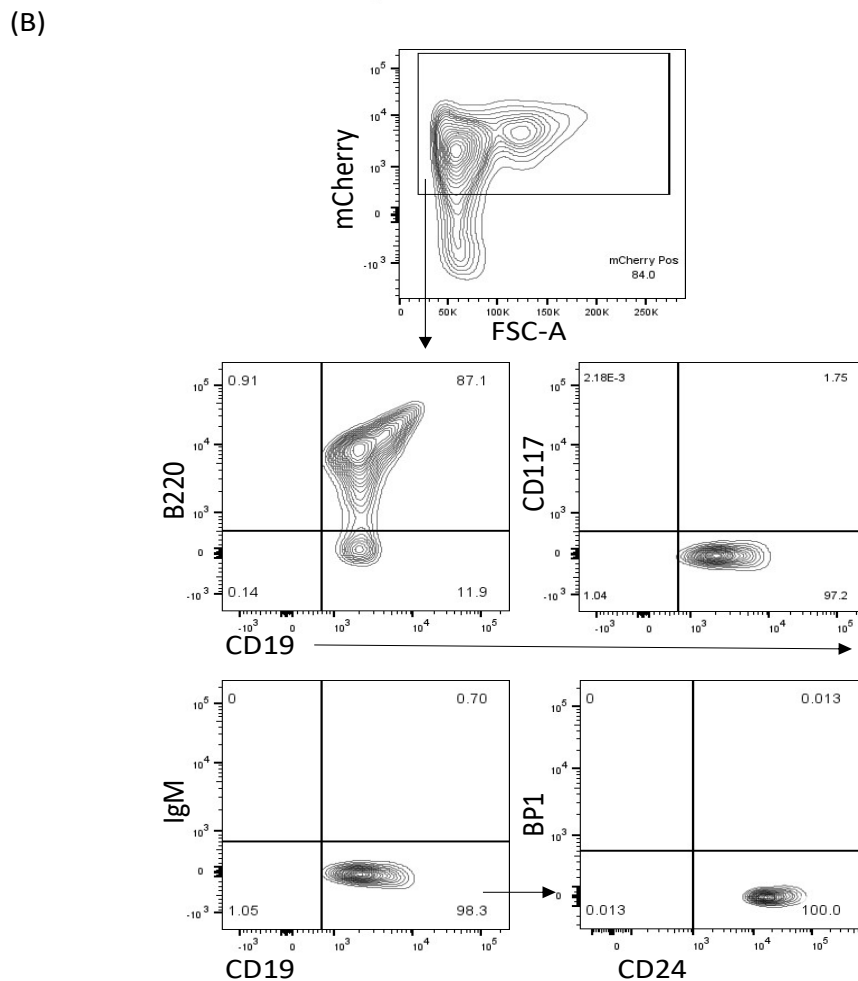
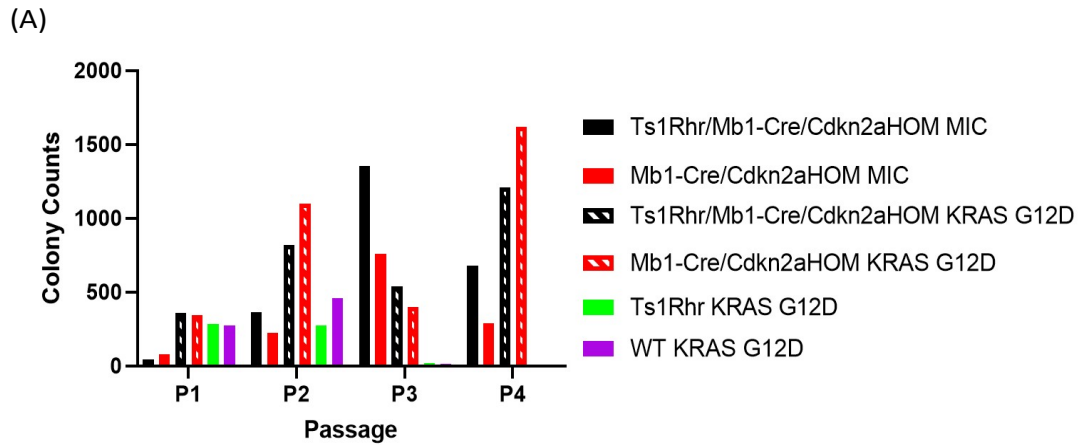


Figure 7. Development of the Ts1/Cdkn2a-KRAS^{G12D} cell line model. (A) CFU Pre-B cell assay of the Ts1Rhr/Mb1-Cre/Cdkn2aHOM (Ts1Rhr/Mb1-Cre/Cdkn2a^{fl/fl}) mouse model and WT, Ts1Rhr, Mb1-Cre/Cdkn2aHOM control bone marrow cells transduced with empty vector control MIC or MSCV-KRAS^{G12D} (harbouring oncogene KRAS^{G12D}), followed over 4 passages (P1-4). (B) Ts1/Cdkn2a-KRAS^{G12D} cell line flow cytometry phenotype analysis, gated on the total cell population, size (single cells - FSC-W), Sytox Blue negativity (live cells) and mCherry positivity (Pos).

Due to the small sample size statistical significance could not be determined, however as previously published (32), we observed that KRAS^{G12D}

overexpression is associated with an increased number of CFU Pre-B cell colonies, cooperating with the trisomy of the DSCR over serially replated passages. Interestingly, we also observed that complete knock-out of *Cdkn2a* did cooperate with trisomy of the DSCR, as the Ts1Rhr/Mb1-Cre/*Cdkn2a*^{fl/fl} MIC transduced cells had the highest colony number at P3 overall (Fig. 7A). Together, with the Ts1Rhr/Mb1-Cre/*Cdkn2a*^{fl/fl} mouse model cohort analysis, our data indicates that homozygous loss of *Cdkn2a* does cooperate with the DSCR but is insufficient to cause leukaemia *in vivo* alone. Additional experiments are needed to validate this interesting observation.

In parallel, *KRAS*^{G12D} transduced Ts1Rhr/Mb1-Cre/*Cdkn2a*^{fl/fl} donor bone marrow cells (Ts1Rhr/Mb1-Cre/*Cdkn2a*^{HOM} *KRAS* G12D) were collected from methylcellulose culture at P1 and placed into liquid culture to establish the Ts1/*Cdkn2a*-*KRAS*^{G12D} cell line. This cell line was phenotypically characterised based upon B220, CD19, CD117, IgM, BP1 and CD24 cell surface expression, revealing the cells were B220, CD19 and CD24 positive Pro-B cells (Fig. 4, 7B).

Ts1/Cdkn2a-KRAS^{G12D} cell line bone marrow transplant.

Donor C57BL/6J mice were sub-lethally irradiated (550 Gy) and injected with 2×10^6 Ts1/*Cdkn2a*-*KRAS*^{G12D} cells. Recipient mice were monitored weekly via peripheral blood analysis for mCherry expression (from tail vein bleed) to determine disease engraftment (Fig. 8A). Survival of C57BL/6J recipient mice post injection was also determined, with mice surviving between 15 and 42 days overall (Fig. 8B).

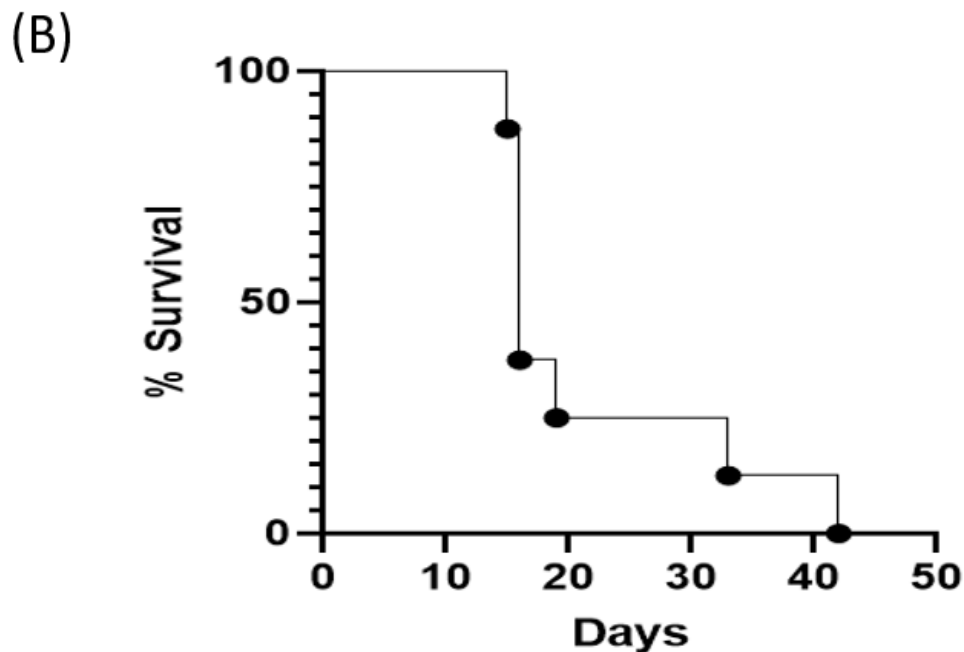
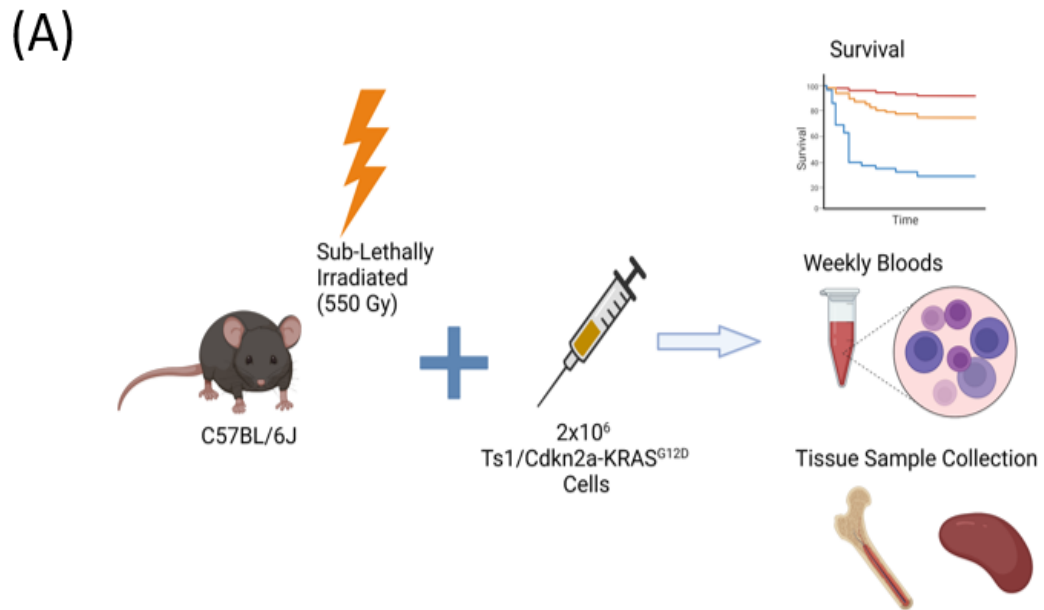


Figure 8. Ts1/Cdkn2a-KRAS^{G12D} cell line bone marrow transplant strategy and survival. (A) Bone marrow transplant strategy whereby sub-lethally irradiated 8-week-old C57BL/6J mice were injected with 2×10^6 Ts1/Cdkn2a-KRAS^{G12D} cells to assess survival and disease engraftment (created with BioRender.com). (B) Survival curve (days since irradiated and injected) of C57BL/6J recipients ($n = 8$) injected with Ts1/Cdkn2a-KRAS^{G12D} cells.

Bone marrow and spleen cells were collected from mice transplanted with the Ts1/Cdkn2a-KRAS^{G12D} cell line at euthanasia and subsequently analysed by flow cytometry to characterise disease burden (mCherry positive cells) and phenotype, as outlined in the gating strategy shown in Figure 9A. This was done to confirm if the Ts1/Cdkn2a-KRAS^{G12D} cells had successfully engrafted

into recipient mice and if the mice succumbed to leukaemia. Based upon mCherry expression in both the bone marrow (around 80%) and spleen (around 60%) (Fig. 9B), the Ts1/Cdkn2a-KRAS^{G12D} cell line successfully engrafted into the recipient mice.

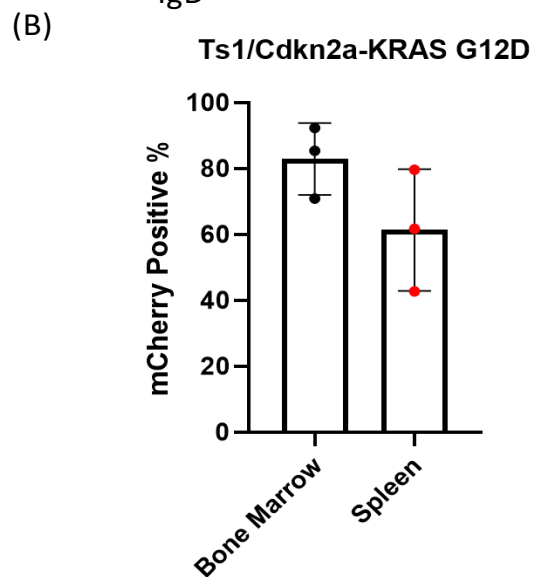
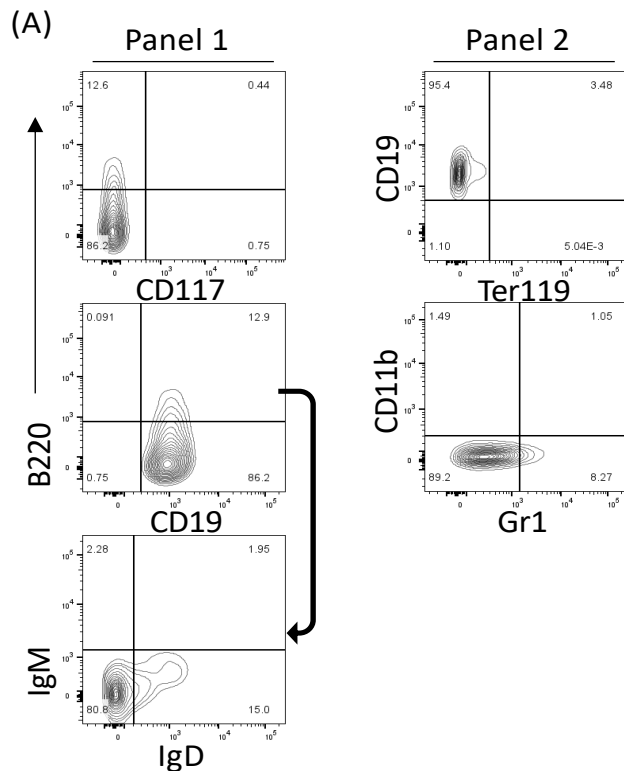


Figure 9. Representative flow cytometry gating strategy and mCherry expression from the Ts1/Cdkn2a-KRAS^{G12D} cell line bone marrow transplant analysis. (A) Bone marrow and spleen samples collected from C57BL/6J recipient mice phenotypically analysed by flow cytometry, whereby mCherry positive cells were analysed with antibody panel 1 and panel 2, following the flow cytometry gating strategy outlined. The mCherry positive live single cells analysed by this strategy were gated upon the total cell population, size (single cells - FSC-W), Sytox Blue negativity (live cells) and mCherry positivity. (B) Bone marrow and spleen samples from Ts1/Cdkn2a-KRAS^{G12D} cell line C57BL/6J recipient mice (n= 3) mCherry positivity.

Flow cytometry phenotype analysis revealed that mCherry positive bone marrow and spleen samples had mostly retained B220/CD19 positivity, which

was observed in the initial phenotype characterisation of the Ts1/Cdkn2a-KRAS^{G12D} cell line (Fig. 10A).

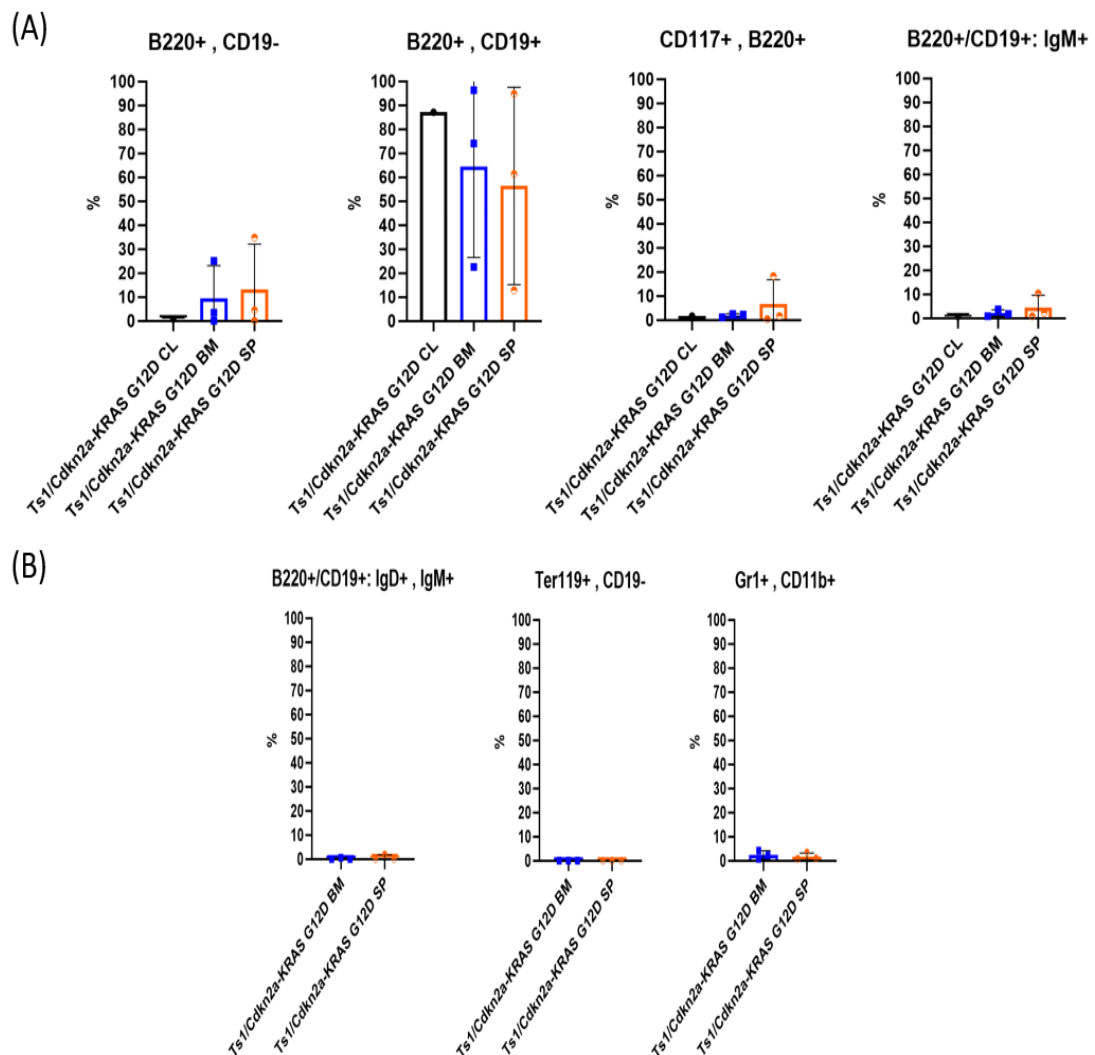


Figure 10. Ts1/Cdkn2a-KRAS^{G12D} cell line bone marrow transplant phenotype. (A) The mCherry positive bone marrow (BM) and spleen (SP) samples collected from Ts1/Cdkn2a-KRAS^{G12D} cell line transplanted C57BL/6J recipient mice (n= 3) phenotype flow cytometry analysis compared to the initial Ts1/Cdkn2a-KRAS^{G12D} cell line (CL) phenotype. (B) Extended BMT phenotype analysis with IgD, IgM, Ter119, Gr1 and CD11b.

The variability in expression of B220/CD19 between replicates and from the original positivity in the Ts1/Cdkn2a-KRAS^{G12D} cell line suggests that external environmental factors influenced the phenotype changes between replicates, driving clonal selection. CD117 and IgM expression was also like the original cell line phenotype, however one replicate had slightly higher expression in the spleen, supporting the hypothesis of clonal selection *in vivo*. Additionally, there was no IgD/IgM and Ter119 positive expression, as well as very little to no myeloid marker expression (Gr1/CD11b) (Fig. 10B). Further investigation

of the bone marrow microenvironment and HSC compartment post engraftment would likely provide insight into reasons for phenotype evolution. Overall, based upon the high mCherry expression observed in both bone marrow and spleen samples, coincided by their B220/CD19 phenotype, the Ts1/Cdkn2a-KRAS^{G12D} cell line successfully engrafted the bone marrow and spleen of irradiated C57BL/6J recipient mice, recapitulating DS-ALL *in vivo*. Thus, development of this DS-ALL model provides a strategy and basis for future model development and therapeutic drug testing.

Discussion:

Children with DS who develop leukaemia have an inferior prognosis compared to non-DS children, which is mostly due to higher rate of treatment related toxicity and relapse (9, 10, 40, 50). Recently however, targeted therapy and immunotherapy have demonstrated promising results in leukaemia (51). Therefore, further investigation into novel therapeutic strategies is urgently required to adapt these novel therapies into the clinic to improve patient outcomes. To advance current therapeutic strategies in DS-ALL requires the use of clinically relevant *in vitro* and *in vivo* models that enable investigation into the mechanisms of DS-ALL development and the testing of potential therapeutic targets. Existing alongside other established patient derived leukaemia models (52-55), PDX models of DS-ALL established by our laboratory have previously been used to identify sensitivity to DYRK1A inhibition by EHT1610 (30), and the inhibition of the RAS/MAPK pathway with trametinib (32). The generation of these murine models followed patient sample collection and subsequent PDX model development (30, 32, 52-55). This method limits the development of novel DS-ALL models as it relies on patients to develop ALL and the collection of these samples with successful engraftment into recipient mice. Therefore, we set out to generate novel DS-ALL models that accurately replicated leukaemia development and that did not rely on PDX.

In this chapter, we were able to successfully incorporate three transgenes into one mouse model, generating the Ts1Rhr/Mb1-Cre/*Cdkn2a*^{fl/fl} triple transgenic mouse model, which included trisomy of the DSCR (Ts1Rhr),

heterozygous expression of Mb1-Cre and homozygous expression of *Cdkn2a* knock-out alleles. Overall, this transgenic combination allowed for homozygous loss of *Cdkn2a* in the presence of trisomy of the DSCR. This model did not display any disease burden or leukaemia phenotype that was expected and did not impact overall survival. Variability in flow cytometry analysis from age-matched monthly blood samples was likely due to variability in blood volume collection, impacting the detection of our interest population (B220/CD19 positive). Variability was also observed in WBC and lymphocyte count analysis with the BC-5000 Vet Auto Hematology Analyzer and was likely impacted by the same variability as flow cytometry analysis, as the same blood samples were used for both flow cytometry and WBC/lymphocyte analysis. Methodologically, dilution of the sample with Diluent V-52D could have been avoided with separate blood collection dates, which would have provided a larger blood volume for WBC and lymphocyte count analysis and eliminate the need for dilution. Since no disease phenotype was detected upon bone marrow and spleen sample analysis with flow cytometry, any disease burden would not have been detected, however less variability would have significantly improved our blood analysis and be clearly represented in Figure 2. Notably, small sample size was a limitation of this study, which was mostly due to difficulty in generating desired genotypes with our breeding strategy (and due to delays caused by the COVID-19 pandemic), as we would have ideally included 5-6 replicates per genotype group. Moving forward however, the laboratory is continuing to generate more transgenic models to complete this study.

Deletion of *CDKN2A/B* is common in paediatric ALL (approximately 20% of cases) (56), with deletion of *CDKN2A* found in between 15-24% of DS-ALL cases (27, 41, 42) and is a known significant secondary event in leukaemia (57). Additionally, previous work has demonstrated that loss of *Cdkn2a* alone is sufficient to drive Pre-B-ALL (43). Thus, we hypothesised homozygous deletion of *Cdkn2a*, in the presence of trisomy 21, would be sufficient to cause ALL. Since our model did not spontaneously develop leukaemia, it suggests that although *Cdkn2a* deletion is a significant event in leukaemia development, homozygous deletion of *Cdkn2a* is not capable of driving

leukaemia development in the presence of 33 extra ch21 genes. Although this did not replicate previous findings where *Cdkn2a* deletion alone resulted in a pre-B-ALL that was not fully-penetrant, *Cdkn2a* deletion was driven by an alternative Cre strategy utilising CD19-Cre, and utilised a different *Cdkn2a* knock-out model (43). Due to these technical differences, there are many possibilities as to why we did not observe leukaemia development in our model. This includes the requirement for additional mutations, such as *KRAS*^{G12D} and *Pax5* deletion, to result in a fully penetrant B-ALL, as supported by the previous literature where a combination of multiple mutations was required (31, 58). This was especially highlighted by Lane *et al.*, who required five genetic alterations within their DS-ALL model to re-create leukaemia (31). Alternatively, our restrictions in sample size did not allow us to observe an incomplete leukaemia phenotype. Moreover, perhaps trisomy of more than 33 genes is required to re-create DS-ALL in combination with *Cdkn2a* deletion. Therefore we attempted to incorporate a larger trisomy 21 (Tc1 (37)) with the Mb1-Cre and *Cdkn2a*^{fl/fl} models, however the trisomy 21 could not be maintained within the offspring of the second generation. Additionally, we also attempted to generate a model incorporating trisomy of the DSCR (Ts1Rhr) with homogenous *KRAS*^{G12D} expression and *Cdkn2a* knock-out alleles, however due to the COVID-19 pandemic delays and the time limit of the project, we could not continue to develop this model. Overall, we concluded that trisomy of the DSCR and deletion of both *Cdkn2a* alleles was insufficient to cause DS-ALL *in vivo*.

To overcome this challenge and improve the model's ability to re-create DS-ALL, we sought to increase the oncogenic potential of the model. To do so, we incorporated activation of the RAS/MAPK pathway, by introducing the *KRAS*^{G12D} mutation via retroviral transduction of Ts1Rhr/Mb1-Cre/*Cdkn2a*^{fl/fl} bone marrow cells. This approach was successfully used by Laurent *et al.*, to transform Ts1Rhr mouse progenitor B cells, thus we predicted it would confer the appropriate cellular fitness for transformation (32). Utilising the B cell specific methylcellulose MethoCult™ M3630, we were able to selectively culture B cell progenitor colonies that were then extracted post colony formation in methylcellulose and placed into liquid culture. Phenotype

analysis confirmed the cells were B220/CD19/CD24 positive Pro-B cell progenitors (Fig. 7B). Thus, we successfully created an *in vitro* model of DS-ALL, the Ts1/Cdkn2a-KRAS^{G12D} cell line. RAS/MAPK pathway activation alone cooperates with trisomy of the DSCR and leads transformation of Ts1Rhr progenitor B cells (32), and was also shown to cooperate with *Cdkn2a* deletion (43). Since we were not able to establish WT-KRAS^{G12D} or *Cdkn2a*-KRAS^{G12D} cell models in the Ts1Rhr background, we could not exclusively conclude that *Cdkn2a* knock-out was necessary for transformation in our model. Notably, generating these cell line models is ongoing within the laboratory, however we were able to develop a model incorporating some of the most common alterations seen in DS-ALL (7, 27, 28). Overall, we hypothesised loss of *Cdkn2a* added to the aggressiveness of the cell line. Therefore, we wanted to assess its ability to re-create DS-ALL *in vivo* by investigating its engraftment capacity.

Since we successfully created the DS-ALL Ts1/Cdkn2a-KRAS^{G12D} cell line, we next assessed its capacity to re-create leukaemia *in vivo*, via BMT in sub-lethally irradiated C57BL/6J recipient mice. The Ts1/Cdkn2a-KRAS^{G12D} cell line successfully engrafted into the bone marrow and spleen of recipient mice with complete penetrance (Fig. 8-10). This model displayed an aggressive engraftment phenotype with recipient mice reaching a minimum survival of 15 days and maximum survival of at 42 days. This is a very interesting phenotype as it allows for an efficient development of DS-ALL in a timely manner, compared to >100 days, with incomplete penetrance published by Lane *et al.*, (31). To our knowledge, this is the first description of a trisomy 21 DS-ALL model with complete penetrance in a C57BL/6J background. Thus, our model would be suitable for future rigorous mechanistic analysis and therapeutic testing, both *in vitro* and *in vivo*. Overall, successful engraftment of the Ts1/Cdkn2a-KRAS^{G12D} cell line into recipient mice indicated that trisomy 21 (DSCR), knock-out of *Cdkn2a* and activation of the RAS/MAPK pathway is sufficient to cause DS-ALL *in vivo*.

Development of the *in vitro* Ts1/Cdkn2a-KRAS^{G12D} cell line and its ability to re-create DS-ALL *in vivo*, provides us with both a strategy to develop new leukaemia models, as well as providing clinically relevant models that

represent human disease for novel therapeutic testing. Notably, generation of other murine models that contain common alterations, such as *CRLF2* rearrangement (54% of DS-ALL) with *JAK2* alterations (50% of *CRLF2* rearranged DS-ALL), or with IKAROS Family Zinc Finger 1 (*IKZF1*) alteration (31% of *CRLF2* rearranged DS-ALL) (27), will continue add to the repertoire of tools for testing novel therapies, which the laboratory will aim to address in the future. Additionally, our model also provides an ideal setting for future mechanistic studies of oncogenic cooperation between trisomy 21 and additional somatic mutations. Notably, the ch21 genes *DYRK1A* and *HMGN1* contribute to the development of DS-ALL (30, 31), however the roles of other ch21 genes remain elusive. Moving forward, the roles of these unknown genes can be tested in our new model to ultimately identify novel ch21 genes with gene dosage effects located in the DSCR region, that have an impact on leukaemogenesis *in vitro* and *in vivo*.

Chapter 3: Therapeutically targeting the chromosome 21 gene *DYRK1A*

Introduction:

Therapeutic advancements have drastically improved the overall survival of children diagnosed with ALL, however treatment of children with DS-ALL has proved difficult due to the toxicity related side effects of current chemotherapy agents, as well as a higher relapse rate (9, 10, 59, 60). Therefore, we need to improve our current understanding of the molecular pathways involved in leukaemia development to identify therapeutically targetable weaknesses that enable implementation of treatment strategies. To aid in the development of these novel improved therapeutics for DS children with ALL, we focused on the role of the ch21 kinase DYRK1A, which has been shown to be a key player in leukaemogenesis DS-related or not (30), and tested the efficacy of novel DYRK1A inhibitors. To this end, we extended our panel of DS-ALL models by establishing new *in vitro/in vivo* human and murine models of DS-ALL. These cell models were characterised at the genetic, phenotypic, and transcriptomic level to ensure clinical relevance and were then used to test novel DYRK1A inhibitors. The ch21 gene *DYRK1A* has been identified as a therapeutic target of interest in DS-ALL, as it regulates B cell development by controlling the B cells ability to enter quiescence via cyclin D3 phosphorylation and repression of E2F Transcription Factor (*E2F*) genes (29, 30). Notably, subsequent research revealed that DS-ALL is sensitive to inhibition of DYRK1A (30). Therefore, we analysed the efficacy of multiple DYRK1A inhibitors, including in combination with current chemotherapeutic agents. This research was published in the journal of Haematologica and is presented in Chapter 3a.

Methods:

Cell culture and cell lines:

The human DS-PER961 and DS-PER962 cell lines were established from PDX models previously described (32). Human DS-ALL cells harvested from PDX models were cultured in “complete” RPMI1640 media (Gibco)

supplemented with 2 mM L-glutamine (Gibco), 50 μ M 2-mercaptoethanol (Sigma-Aldrich), penicillin (100 U/mL)-streptomycin (100 μ g/mL) (Thermo Fisher Scientific), 1% non-essential amino acids (MP Biomedicals), 1 mM sodium pyruvate (MP Biomedicals) and 20% of heat inactivated FCS (Cell Sera Australia). The DS-PER961 cell line was cultured with recombinant human IL-7 (10 ng/mL, PeproTech and STEMCELL Technologies), and the DS-PER962 cell line with recombinant human FLT3-ligand (10 ng/mL, PeproTech and STEMCELL Technologies). MHH-CALL4 cells were cultured in complete RPMI1640 media containing 20% heat inactivated FCS. Murine cell models were extracted from the methylcellulose (MethoCult™ M3630) in their generation, by dispensing 5 mL of 2% FCS/PBS solution into the culture dish and mixed with the methylcellulose by repetitive pipetting. The medium was then transferred to a 50 mL falcon tube (process repeated twice), which were then centrifuged at 1500 rpm for 5 minutes at room temperature, discarding supernatant. The cell pellet was then resuspended with 2% FCS/PBS solution and cell number determined using Trypan Blue (Thermo Fisher Scientific) exclusion. Once the cell number and viability was determined, cells were cultured in media consisting of IMDM (Gibco) containing 20% heat inactivated FCS, 1% non-essential amino acids, sodium pyruvate (1 mM), 2-mercaptoethanol (50 μ M), penicillin (100 U/mL)-streptomycin (100 μ g/mL) and supplemented with recombinant murine IL-7 (10 ng/mL), SCF (10 ng/mL) and Flt3-ligand (10 ng/mL) (PeproTech and STEMCELL Technologies). For growth curve experiments (with or without cytokines), 5×10^5 murine cells were plated and counted every second day with Trypan Blue exclusion. The short hairpin RNA (shRNA) DYRK1A used in this study to transduce murine cells were previously described (21). All cell lines were cultured at 37°C, in 5% CO₂ with 95% relative humidity (Heracell VIOS 160i incubator).

Flow cytometry:

For all flow cytometry experiments, cells were stained in 1x PBS supplemented with 2% FCS for ≥ 20 minutes at 4°C, then washed with 2% FCS/PBS via centrifugation. Cells were then incubated with 1/4000 dilution Sytox Blue reagent (Invitrogen) in 2% FCS/PBS to determine cell viability.

Analyses were performed with LSRFortessa™ X-20 or LSRFortessa™ instruments (BD Biosciences), transduced cells were sorted on the FACSAria™ III or Fusion (BD Biosciences), and data was analysed using FlowJo software (Version 10.9.0, BD Biosciences).

Murine cell line phenotyping:

The murine cell lines were stained with the fluorochrome conjugated antibody panel and dilutions listed in Table 1, along with single stain and isotype controls. The antibody/cell mixtures were incubated at 4°C for ≥20 minutes in the dark, then washed with 1 mL of 2% FCS/PBS and centrifuged at 1500 rpm for 5 minutes at room temperature. Cell pellets were resuspended in 200 µL of 2% FCS/PBS with 1/4000 Sytox Blue to determine cell viability. Samples were then analysed via flow cytometry.

Murine Antibody	Fluorochrome Detection Channel	Antibody Dilution	Supplier	Product Reference
BP1	FITC	1/200	Invitrogen	11-5891-82
CD24	PE-Cy7	1/300	BD Biosciences	560536
CD19	BV510	1/100	BD Biosciences	562956
B220	APC	1/200	Invitrogen	17-0452-82
CD117	APC-H7	1/100	BD Biosciences	560185
IgM	PerCP-Cy5.5	1/100	BD Biosciences	550881
Sytox Blue	BV421	1/4000	Invitrogen	S11348
mCherry	PE-Texas-Red	N/A	N/A	N/A
Isotype	FITC	1/200	Invitrogen	11-4714-81
Isotype	PE-Cy7	1/300	BD Biosciences	557872
Isotype	BV510	1/100	BD Biosciences	562951
Isotype	APC	1/200	BD Biosciences	550854
Isotype	APC-Cy7	1/100	BD Biosciences	557873
Isotype	PerCP-Cy5.5	1/100	BD Biosciences	552834

Table 1. Murine cell line phenotyping antibody panel.

Human cell line phenotyping:

A total of 2×10^6 DS-PER961 and DS-PER962 cells were prepared for flow cytometry analysis and resuspended in 2% FCS/PBS, stained with fluorochrome conjugated antibodies (Table 2) and incubated in the dark at 4°C for ≥20 minutes. Stained cells were then washed with 1 mL of 2% FCS/PBS and resuspended in 200 µL of 2% FCS/PBS containing Sytox Blue at a 1/4000 dilution. Single stain controls were used to ensure correct gating

and compensation. All samples were analysed on the BD LSRFortessa™ X-20 flow cytometer and data analysed using FlowJo software (Version 10.9.0).

Human Antibody	Fluorochrome Detection Channel	Antibody Dilution	Supplier	Product Reference
CD19	PE-Cy7	1/100	BD Biosciences	560728
CD34	PerCP-Cy5.5/eFluor 710	0.5/100	Invitrogen	46-0349-42
CD38	APC	1/100	BD Biosciences	555462
CD10	FITC	1/100	BD Biosciences	340925
CD45	APC-Cy7/eFluor 780	1/100	Invitrogen	47-0459-42
CD135	BV510	1/100	BD Biosciences	743338
TSLPR	PE	1/100	BD Biosciences	563149
Sytox Blue	BV421	1/4000	Invitrogen	S11348

Table 2. Human cell line phenotype antibody panel.

Sanger sequencing:

DNA was extracted from DS-PER961 and DS-PER962 cells using the QIAGEN AllPrep DNA/RNA Mini kit. A PCR was carried out to amplify exon 2 of the *KRAS* gene and exon 16 of the *JAK2* gene using primers outlined below (Table 3). PCR products were separated on a 1.8% agarose gel (Fisher Biotec Australia) (prepared with 1x Tris-acetate EDTA buffer) with 0.1 µL/mL of SYBR Safe (Thermo Fisher Scientific). The gel was then run at 120V for 35 minutes and imaged on the BioRad GelDoc XR+ to visualise the bands and assess PCR product amplification. To prepare for Sanger sequencing, PCR products were purified using the QIAGEN QIAquick PCR Purification Kit and prepared according to the standards outlined in the Australian Genome Research Facility (AGRF) Sanger sequence preparation guide, with primers listed in Table 3. Purified products were sequenced by the AGRF, and sequencing results were analysed using SnapGene Version 5.0.4.

Gene	Primer Name	Primer Sequence (5'-3')	Annealing Temp (°C)	Ext Time (S)	Product Size (bp)
<i>KRAS</i>	Hs-KRAS-F	TGA GTT TGT ATT AAA AGG TAC TGG	60	30	382
	Hs-KRAS-R	ATG GTT ACA TAT AAC TTG AAA CCC			
<i>JAK2</i>	Hs-JAK2-F	CCA TGT CAG CCT TAG AAC TCA T	58	30	616
	Hs-JAK2-R	AAA ATC ACC TCA CAG TCC ATG G			

Table 3. Human cell line PCR and Sanger sequencing primers. Primer name, sequence, annealing temperature (Temp), extension (Ext) time in seconds (S) used, and product size in base pairs (bp) per gene.

Human cell line bioinformatic validation:

Bi-allelic frequencies were obtained from single nucleotide polymorphism (SNP) arrays using the HumanCytoSNP-12v2.1 BeadChip (Illumina) and analysed by AGRF. Spearman correlation of the transcriptional profiles obtained from the DS-PER961 and DS-PER962 cell lines was performed. Correlation analysis began with Raw FASTQ files which were processed using Trim Galore and FASTQC/MultiQC for quality control, followed by alignment using Kallisto (GENCODE v34 reference). Kallisto count tables were read into DESeq2 via TxImport. Genes with an average of 0 counts across all 5 samples were excluded from downstream analysis. Spearman correlation was then used to correlate normalised transcripts per million (Log2TPM) between cell lines and corresponding PDX models.

Genomic DNA extraction for genetic validation of models by PCR:

DNA was extracted from mouse ear tags for genotype PCR validation. Firstly, ear tags were placed into 1.5 mL Eppendorf tubes and were resuspended in 200 µL of lysis buffer (Tris-HCL 100 mM, NaCl 200 mM, SDS 0.2%, EDTA 5 mM, in double-distilled H₂O - containing 10 µg/mL of proteinase K). Samples were then incubated overnight on a shaker set to 350 rpm at 55°C. The next day, ear tag samples were heated to 95°C for 20 minutes to inactivate the

proteinase K. Samples were then centrifuged at 14000 rpm for 5-10 minutes and supernatant was collected into a new 1.5 mL Eppendorf tube. Next, 160 μ L of 100% isopropanol was added to each sample and the tubes were gently inverted 2-3 times. The samples were then centrifuged at 14000 rpm for 10 minutes at 4°C, discarding supernatant. The DNA pellet was then washed with 500 μ L of 70% ethanol, then centrifuged at 14000 rpm for 5 minutes at 4°C, discarding supernatant. DNA pellets were then air dried for 1 hour and then resuspended in 50 μ L of DEPC water. DNA concentration/purity was then determined with the NanoDrop 2000, following standard protocol (Thermo Fisher Scientific).

Genetic validation of models by PCR:

Genomic DNA extracted from murine ear tags and was used as template DNA to amplify a section of the Tc1 ch21, Ts1Rhr ch21, the Mb1-Cre integration, and the LoxP sites of *Cdkn2a* according to the recommended Taq Recombinant Polymerase protocol (Thermo Fisher Scientific), using specific primers, annealing temperature, and extension time presented in Table 4. For the *P2RY8-CRLF2* gene fusion validation, RNA was extracted from cells using the QIAGEN AllPrep DNA/RNA Mini kit. Purified RNA underwent reverse transcription using the SuperScript III Reverse Transcriptase Kit (Invitrogen) with 50 μ M of random hexamers (Invitrogen) to obtain cDNA. The cDNA was then used as a template to amplify the *P2RY8-CRLF2* fusion transcript with the P2RY8-F and CRLF2-R primers (Table 4), using the recommended Taq Recombinant Polymerase protocol. PCR products were analysed via agarose gel electrophoresis (1% agarose gel, prepared with 1x Tris-acetate EDTA buffer) with 0.1 μ L/mL of SYBR Safe. The gel was then run at 100V for approximately 35 minutes and imaged on the BioRad GelDoc XR+ to visualise the bands and assess PCR product amplification (Table 4).

Primer Name	Primer Sequence (5'-3')	Annealing Temp (°C)	Ext Time (S)	Product Size (bp)
Mb1.Cre WT For	CTC TTT ACC TTC CAA GCA CTG A	59	45	WT: 197 Cre: 230
Mb1.Cre Mut For	CAT TTT CGA GGG AGC TTC A			
Mb1.Cre Com Rev	ACT GAG GCA GGA GGA TTG G			
Ts1Rhr Dup F	GCC AGA GGC CAC TTG TGT AG	62-57	30	Ts1Rhr: 200-300
Ts1Rhr Dup R	TGT TGA CCT CGA GGG ACC TA			
CDKN2A F	ACG TGT ATG CCA CCC TGA CC	60	40	WT: 160 LoxP: 260
CDKN2A R	GAC TGC TCG GGAATC TTG CC			
Tc1-For	CAG AGC TAC AGC CTC TGA CAC T	60	45	Int-control: 324 Tc1: 205
Tc1-Rev	TTT GAG GGA ACA CAA AGC TTA AC			
Tc1-int For	CTA GGC CAC AGA ATT GAA AGA TCT			
Tc1-int Rev	GTA GGT GGA AAT TCT AGC ATC ATC C			
P2RY8-F	TTG CAA GGT TGC TGG ACA GAT GGA A	64-60	30	P2RY8- CRLF2: 500
CRLF2-R	GTC TAG GAG GCA CCC CGA AGT GTG A			

Table 4. PCR primers and conditions. Primer name, sequence, annealing temperature (Temp), extension (Ext) time in seconds (S) used, and product size in base pairs (bp).

Animal models:

PDX models DS01, DS02, DS03 and DS06 have been previously described (32). Briefly, 1×10^6 DS-ALL cells (from earlier generation of PDX or DS-ALL cell lines) were injected into (7-9 weeks old) NOD.Cg-Prkdc^{scid}Il2rgtm1Wjl/SzJ (NSG) (JAX stock #:005557) mice by tail vein injection. Leukaemia engraftment was assessed weekly from week 3 after injection by tail vein bleed and flow cytometry analysis using antibodies listed in Table 5. *In vivo* treatments (4 weeks) started when 0.5-1% of human blasts were detected in the peripheral blood. NSG mice were then treated with two doses of

Leucettinib-21 (0.5 mg/kg and 5 mg/kg, by oral gavage 5 times per week) compared to the vehicle treated mice (0.5% carboxymethylcellulose). The Tc1 mice used in this study were validated by genotyping as described above using the primers referenced in Table 4.

For the BMT experiments, 2×10^6 WT-*KRAS*^{G12D}, Tc1-*KRAS*^{G12D} or Ts1/*Cdkn2a*-*KRAS*^{G12D} cells were injected in 8-week-old primary recipient (1R) C57BL/6J sub-lethally irradiated (550 Gy) mice. Regarding secondary recipients (2R), 1×10^6 spleen cells from 1R were used for injection. Blast percentage was monitored via tail vein bleed and flow cytometry to follow mCherry expression in the peripheral blood, utilising Sytox Blue viability stain at 1/4000 dilution. Histological examination was performed on paraffin embedded spleen and stained with hematoxylin and eosin. All mice were maintained at the Telethon Kids Institute preclinical facility (Bio-Resources).

Antibody	Fluorochrome Detection Channel	Antibody Dilution	Supplier	Product Reference
Human-CD19	PE-Cy7	1/100	BD Biosciences	560728
Human-CD45	APC-Cy7/eFluor 780	1/100	Invitrogen	47-0459-42
Murine-CD45.1	FITC	1/100	BD Biosciences	553775
Sytox Blue	BV421	1/4000	Invitrogen	S11348

Table 5. Human cell line transplant weekly flow cytometry analysis antibody panel.

Murine bone marrow and spleen sample collection:

Samples were collected from time point culled or symptomatic mice. The hip, femur and tibia bones were collected, as well as the spleen (weighed at harvest). Bone marrow was collected from the hip, femur, and tibia into 50 mL Falcon tubes, containing 10 mL of 2% FCS/PBS solution, via flushing with a 3 mL syringe and a 21-gauge needle. Spleen was processed using a 100 µm cell strainer placed in a 50 mL Falcon tube, containing 10 mL of 2% FCS/PBS solution. The spleen was firstly placed into the cell strainer and broken down with a 3 mL syringe plunger and washed through the 100 µm cell strainer with the 10 mL of 2% FCS/PBS solution with a pipette. Bone

marrow and spleen cells were then lysed with 2 mL of 1x NH₄Cl RBC lysis buffer (STEMCELL Technologies) for 7 minutes at room temperature, which were then washed with 8 mL 2% FCS/PBS solution. Samples were then centrifuged at 1500 rpm for 5 minutes at room temperature, discarding supernatant. Samples were then resuspended in 10 mL of 2% FCS/PBS solution and cell density was determined using Trypan Blue exclusion. If samples were not analysed by flow cytometry on the same day, cell vials were made with densities from 10-30 million cells per vial, using 10% DMSO/FCS solution, with samples stored at -80°C or in liquid nitrogen.

Mouse model bone marrow B cell characterisation:

Bone marrow samples from Tc1 mice and WT littermates were analysed with flow cytometry as described above, using the antibody panel in Table 6. The B cell lineage fractions were determined following previously established protocol (61).

Murine Antibody	Fluorochrome Detection Channel	Antibody Dilution	Supplier	Product Reference
B220	APC	1/200	Invitrogen	17-0452-82
CD43	PE	1/200	Invitrogen	12-0431-82
BP1	FITC	1/200	Invitrogen	11-5891-82
CD24	PE-Cy7	1/300	BD Biosciences	560536
Sytox Blue	BV421	1/4000	Invitrogen	S11348

Table 6. Mouse model bone marrow B cell characterisation antibody panel.

Bone marrow transplant vial analysis:

Bone marrow and spleen vials collected from the BMT assays were thawed in a water bath at 37°C and then washed in 9 mL of 2% FCS/PBS within a 15 mL Falcon Tube. Cells were then centrifuged at 1500 rpm for 5 minutes at room temperature, discarding supernatant. Cells were then resuspended in 50 µL of 2% FCS/PBS and transferred to a 96 well plate for antibody staining, including single stain controls. The 96 well plate was then centrifuged at 1500 rpm for 5 minutes at room temperature, discarding supernatant. Cells were then stained with two fluorochrome conjugated antibody panels via resuspension in 50 µL of the antibody solution consisting of 2% FCS/PBS and antibody dilutions as presented in Table 7. Cells were incubated for ≥20

minutes in the dark at 4°C, then centrifuged at 1500 rpm for 5 minutes at room temperature, discarding supernatant. Cells were then washed with 1 mL of 2% FCS/PBS solution as samples were transferred to flow cytometry tubes. Cells were then centrifuged at 1500 rpm for 5 minutes at room temperature, discarding supernatant, and resuspended in 200 µL of 2% FCS/PBS containing Sytox Blue viability stain. The cell samples were then analysed via flow cytometry.

Murine Antibody	Fluorochrome Detection Channel	Antibody Dilution	Supplier	Product Reference
Panel 1				
B220	APC	1/200	Invitrogen	17-0452-82
CD19	BV510	1/100	BD Biosciences	562956
CD117	APC-H7	1/100	BD Biosciences	560185
IgM	PerCP-Cy5.5	1/100	BD Biosciences	550881
IgD	FITC	1/100	Invitrogen	11-5993-82
Sytox Blue	BV421	1/4000	Invitrogen	S11348
mCherry	PE-Texas-Red	N/A	N/A	N/A
Panel 2				
CD19	APC-H7	1/100	BD Biosciences	560245
Ter119	FITC	1/200	Invitrogen	11-5921-82
CD11b	BV510	1/500	BD Biosciences	562950
Gr1	PE-Cy7	1/500	Invitrogen	25-5931-82
Sytox Blue	BV421	1/4000	Invitrogen	S11348
mCherry	PE-Texas-Red	N/A	N/A	N/A

Table 7. Bone marrow transplant sample phenotyping antibody panels.

Lineage depletion and HSC/MPP population analysis:

Bone marrow cells were harvested as described above and then underwent lineage depletion, which was performed using the EasySep Mouse Hematopoietic Progenitor Cell Isolation Kit (STEMCELL Technologies). Briefly, 80×10^6 - 100×10^6 total bone marrow cells were collected in a 50 mL Falcon tube, without rat serum. Next, cells were incubated with the biotinylated-antibody cocktail (50 µL/mL), washed with 40 mL of 2% FCS/PBS, and incubated with Rapid Sphere (streptavidin beads) for 20 minutes. Cell-antibody-bead complexes were placed in the magnet for 5 minutes. The beads were washed, and the supernatants were pooled. Cells were then placed on the magnet for an additional 5 minutes, for further isolation. The final supernatant was collected in a 15 mL falcon tube and cells

were counted by Trypan Blue exclusion. Lineage depleted cells were then stained with fluorochrome conjugated antibody at optimised dilutions (Table 8) and incubated for ≥ 20 minutes in the dark at 4°C, to determine the populations of HSCs and MPP cells via flow cytometry. To ensure correct gating, full minus one (FMO) staining excluding the markers CD34-FITC, CD48-BV421, CD150-APC and CD135-PE and single stain controls were made. The previously described (62) gating strategy was used to identify HSCs, MPP1, MPP2, MPP3 and MPP4 populations.

Murine Antibody	Fluorochrome Detection Channel	Antibody Dilution	Supplier	Product Reference
CD135	PE	1/50	BD Biosciences	553842
Sca-1	PE-Cy7	1/50	BD Biosciences	558162
CD150	APC/Alexa Fluor 647	1/50	BD Biosciences	562647
Streptavidin	APC-Cy7	1/100	BD Biosciences	554063
CD117	PerCP-Cy5.5	1/50	BD Biosciences	560557
CD34	FITC	1/50	Invitrogen	11-0341-82
CD48	BV421/eFluor 450	1/50	Invitrogen	48-0481-82

Table 8. Antibody table for analysing murine HSC/MPP compartment.

Bone marrow microenvironment analysis:

To analyse the bone marrow microenvironment of 6-week-old, 8-10-week-old and 18-19-week-old WT and Tc1 mice, initially femurs were harvested, from which the bone marrow was flushed from the medullary cavity. The bones were then processed and analysed following the strategy previously established (63). The harvested bone marrow microenvironment cell populations were incubated with the antibody panel presented in Table 9, and analysed by flow cytometry.

Murine Antibody	Fluorochrome Detection Channel	Antibody Dilution	Supplier	Product Reference
CD51-Biotin	-	1/200	BD Bioscience	551380
Sca-1	BV510	1/100	BD Bioscience	565507
CD31	FITC	1/200	BD Bioscience	553372
Ter119	PerCP-Cy5.5	1/400	BD Bioscience	560512
CD45	PerCP-Cy5.5	1/400	BD Bioscience	550994
CD140a	APC	1/50	Invitrogen	17-1401-81
CD140b	PE	1/50	BioLegend	136006
CD24	PE-Cy7	1/100	BD Bioscience	560536
Streptavidin	BV421	1/400	BD Bioscience	563259
Horizon Fixable Viability Stain 700	APC/Alexa Fluor 700	1/20000	BD Bioscience	564997

Table 9. Bone marrow microenvironment analysis antibody panel.

CFU Pre-B cell assays:

Initially, 0.5×10^6 bone marrow cells harvested from 8-10-week-old WT and Tc1 mice were plated on semi-solid MethoCult™ M3630 (STEMCELL Technologies) media to assess clonogenicity of B cell precursors. On day 7, CFU pre-B cell colonies were counted and replated with 2×10^4 cells weekly over the 4 passages to assess their proliferation and self-renewal capacities.

To assess oncogenic cooperation, freshly harvested bone marrow cells from 6-week and 8-10-week-old WT and Tc1 mice were spinoculated with retroviral particles allowing for the expression of *KRAS*^{G12D} (MSCV-*KRAS*^{G12D}) or *BCR-ABL1* (MSCV-*BCR-ABL1*) oncogenes as described previously (32, 64), and compared to the empty vector control MIC (MSCV-IRES-mCherry). On day 2, transduced cells underwent FACS with initially 1×10^4 transduced mCherry positive bone marrow cells plated on the M3630 methylcellulose media. These CFU pre-B cell colonies were also counted on day 7 and replated with 2×10^4 cells weekly, over 4 passages.

Western blots:

Western blots were performed using NuPage 4-12% Bis-Tris gels with 2-(N-morpholino)ethanesulfonic acid (MES)-SDS running buffer. Protein transfer was achieved using the polyvinylidene difluoride (PVDF) membrane and Bio-Rad Trans-Blot Turbo Transfer System. Following blocking and primary

antibody incubation (Table 10), desired protein was revealed using secondary antibodies (Anti-Mouse or Anti-Rabbit IgG), membranes incubated with enhanced chemiluminescence (ECL) reagent (Bio-Rad) and viewed with the ChemiDoc MP system (Bio-Rad). To assess constitutive phosphorylation of the JAK2/STAT5 and RAS/MAPK pathways, human and murine cell lines were serum starved for 5-6 hours prior to protein extraction as described previously (32). For Phospho-cyclin D3 and Phospho-FOXO1 validation, cell lines were treated for 6 hours with increasing doses (0.001, 0.01, 0.1, 1, 2.5, 5 and 10 μ M) of DYRK1A inhibitors EHT1610, Leucettinib-21 and AM30 before protein extraction. Antibodies used are indicated in Table 10.

Western Blot Antibody	Dilution	Supplier	Product Reference
Primary Antibody			
Phospho-STAT5	1/1000	Cell Signalling Technology	9351S
STAT5	1/1000	Cell Signalling Technology	94205S
Phospho-ERK1/2	1/1000	Cell Signalling Technology	9101S
ERK1/2	1/1000	Cell Signalling Technology	9102S
Phospho-FOXO1	1/1000	Aviva Biosciences	OAAF07382
FOXO1	1/1000	Cell Signalling Technology	2880S
DYRK1A	1/500	Abnova	H00001859-M01
Phospho-JAK2	1/1000	Cell Signalling Technology	3771S
JAK2	1/1000	Cell Signalling Technology	3230S
Phospho-Cyclin D3	1/1000	Cell Signalling Technology	53966S
Cyclin D3	1/1000	Cell Signalling Technology	2936S
KRAS	1/500	Santa Cruz	sc-30
Anti-HSC70	1/2000	Sigma-Aldrich	SAB3701436
Secondary Antibody			
Anti-Mouse IgG	1/10000	Sigma-Aldrich	A9917
Anti-Rabbit IgG	1/10000	Cell Signalling Technology	7074S

Table 10. Western blot antibodies.

Drug treatment:

Human and murine cell lines were dispensed into a 384 well cell culture plate (PerkinElmer) using the automated Multidrop Combi Reagent Dispenser (Thermo Fisher Scientific). These cells were then treated with varying concentrations (0.001-10 μM) of DYRK1A inhibitors EHT1610, AM28, AM30, AM45, Leucettinib-21 and inactive isomer (Iso) Leucettinib-21. Synergistic analysis was performed utilising various doses of Leucettinib-21 (0.01 to 10 μM) with standard of care agents and targeted inhibitors trametinib (from 0.0001 to 20 μM), ruxolitinib (from 0.0001 to 20 μM), vincristine (from 0.0025 to 20 μM), dexamethasone (from 0.0025 to 20 μM) and L-asparaginase (from 0.0025 to 20 μM) in the human DS-ALL cell lines. The drugs were delivered using the Tecan D300e Digital Dispenser. Cells were then incubated at 37°C in 5% CO₂ with 95% relative humidity. After 72 hours, the cells were incubated with AlamarBlue reagent (Thermo Fisher Scientific) to determine cell viability. The BioTek SynergyMx plate reader was then used to measure absorbance values. Data was analysed on Microsoft Excel and GraphPad Prism to determine cell viability and relative IC₅₀ values. Synergistic analysis was performed with SynergyFinder 3.0 (65). For survival assays, cells were incubated for 48 hours with increasing doses (1, 2.5, 5 and 10 μM) of EHT1610, AM30, Leucettinib-21 and Iso Leucettinib-21, before washed and stained with Annexin V-APC and propidium iodide, following standard protocol (BD Biosciences); data was analysed by flow cytometry and FlowJo software (Version 10.9.0).

Statistical analysis:

Statistical analysis was performed using GraphPad Prism (Version 8/9), unless otherwise mentioned. The log-rank test was used for survival analysis. For other experiments, statistical significance was evaluated using the Mann-Whitney U test or the two-tailed unpaired *t*-test, unless otherwise specified.

Chapter 3a: Efficacy of DYRK1A inhibitors in novel models of Down syndrome acute lymphoblastic leukemia

Below is the publication titled Efficacy of DYRK1A inhibitors in novel models of Down syndrome acute lymphoblastic leukemia. This paper was submitted to the Journal of Haematologica and accepted on the 19/02/2024.

Efficacy of DYRK1A inhibitors in novel models of Down syndrome acute lymphoblastic leukemia

Despite significant advances, outcomes for children with Down syndrome (DS, trisomy 21) who develop acute lymphoblastic leukemia (ALL) remain poor. Reports of large DS-ALL cohorts have shown that children with DS have inferior event-free survival (EFS) and overall survival (OS) compared to children without DS.¹⁻³

Children with DS also exhibit increased treatment-related mortality due to infections and toxicities following chemotherapy, higher cumulative risk of relapse and inferior outcomes following relapse.⁴ This situation highlights the dire need for the development of more potent and targeted therapies to improve the survival and quality of care for these vulnerable children, who often have additional co-morbidities linked to trisomy 21 that complicates their clinical management. Targeted approaches and immunotherapies have shown promising results for pediatric leukemia.⁵ Hence, the development of new models of DS-ALL are needed to rapidly advance drug discovery and refine existing treatment strategies. We recently established DS-ALL patient-derived xenografts (PDX) and demonstrated that targeting somatic alterations found in DS-ALL using MEK inhibitors combined with conventional treatment has the potential to improve outcomes for these children.⁶ Targeting the dosage-sensitive mechanisms resulting from the extra copy of chromosome 21 is also an area of intense investigation.⁷⁻⁹ As such, inhibition of the chromosome 21 kinase DYRK1A using EHT1610 or of its direct targets FOXO1 and STAT3, has shown promising cytotoxic effects both *in vitro* and *in vivo*.⁸

In this study, we developed novel clinically relevant models of DS-ALL to facilitate the assessment of new therapeutic agents. First, we modeled oncogenic cooperation seen in DS-ALL *in vitro*.¹⁰ To this end, we transduced wild-type (WT) and trisomic (Tc1) 8-10-week-old bone marrow cells with retroviruses encoding the frequently observed mutant KRAS^{G12D} or the more rarely seen BCR-ABL fusion¹¹ (animal experiments were approved by institutional ethics committee and followed Australian guidelines for the care and use of animals). Of note, the bone marrow stroma and hematopoietic stem cell and progenitor compartment composition did not significantly differ between disomic and trisomic mice, except from an increased proportion of multipotent progenitors MPP2 at the expense of the less committed MPP1 (Online Supplementary Figure S1A-C). Trisomic Tc1 progenitors exhibited increased capacity to form colony-forming unit (CFU) pre-B colonies *in vitro* compared to WT (Online Supplementary Figure S1D), as seen previously in the partially trisomic Ts1Rhr (Ts1) model.⁷ Ectopic expression of KRAS^{G12D} or BCR-ABL enhanced the number and replating capacity of both WT and Tc1 CFU pre-B colonies compared to the

empty vector MIC (MSCV-IRES-mCherry) (Online Supplementary Figure S1E, F). Next, we established two murine DS-ALL cell lines (Tc1-KRAS^{G12D} and Tc1-BCR-ABL), disomic controls (WT-KRAS^{G12D} and WT-BCR-ABL), as well as an independent Ts1/Cdkn2a-KRAS^{G12D} cell line (established from triple transgenic Ts1Rhr, Mb1-Cre, Cdkn2a^{fl/fl} donor mice); attempts to develop CRLF2-rearranged/JAK2 mutant murine DS-ALL cell lines were unsuccessful. Interestingly, although KRAS^{G12D} led to a constitutive phosphorylation of Erk1/2, the highest levels of Erk1/2 phosphorylation and cytokine independence for cell proliferation were only observed in WT-KRAS^{G12D} cells (Figure 1A, B). All KRAS^{G12D}-expressing murine cell lines engrafted in sub-lethally irradiated C57BL/6J mice in primary and secondary recipients and ultimately succumbed to leukemia with complete penetrance, with recipients displaying mCherry-positive cells in the peripheral blood, bone marrow, and in the spleen (*data not shown*). Engrafted recipient mice exhibited splenomegaly associated with a leukemia-driven disorganized architecture (Online Supplementary Figure S1G, H). We also confirmed that the engrafted cell lines exhibit a phenotype similar to the cell lines cultured *in vitro*; although we noted clonal selection of a CD24⁺/BP1⁻ pro-B population from the WT-KRAS^{G12D} cells *in vivo*, which was retained in secondary recipients (Figure 1C, D; and *data not shown*). Altogether, we developed novel murine models of DS-ALL, providing a unique platform suitable for testing targeted therapies.

In order to validate the clinical relevance of these murine cells, we focused on the therapeutically targetable chromosome 21 kinase DYRK1A, as recent reports have emphasized its role in childhood leukemia, regardless of Down syndrome.⁸ First, we used short hairpin RNA (shRNA) interference to show that all five cell lines, disomic (N=2) or trisomic (N=3) and expressing either KRAS^{G12D} or BCR-ABL oncogenes, were sensitive to *Dyrk1a* knock-down (KD) (Figure 2A, B; Online Supplementary Figure S1I). We next assessed the efficacy of new potent DYRK1A inhibitors using a DYRK1A-focused library which included EHT1610 used as control, Leucettinib-21 and its inactive isomer (compounds inspired by Leucettines and Leucettamine B, a natural substance produced by the marine sponge *Leucetta microraphis*),^{12,13} and three additional DYRK1A inhibitors whose chemical structure is based on the 7-azaindole scaffold, AM28, AM30 and AM45.¹⁴ In dose-response experiments, we showed that AM30 and Leucettinib-21 were cytotoxic in both WT-KRAS^{G12D} and Tc1-KRAS^{G12D} cell lines (Figure 2C). We also observed that Leucettinib-21, AM30 and AM45 were more potent than EHT1610 in decreasing cellular growth in all cell lines tested, and that Tc1-KRAS^{G12D} cells always exhibited lower half-maximal inhibitory concentra-

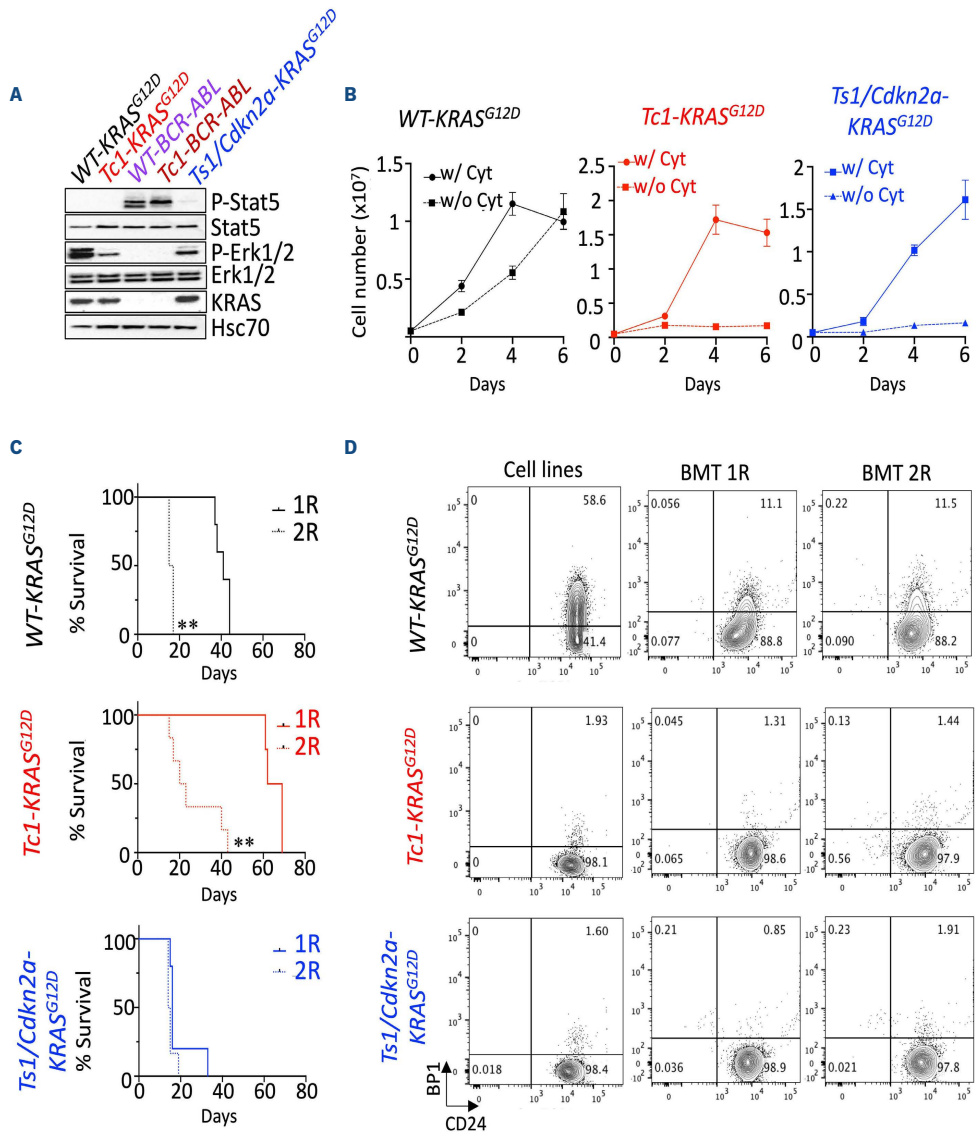


Figure 1. Establishment of novel Down syndrome acute lymphoblastic leukemia models for preclinical testing. (A) Constitutive phosphorylation of Stat5 and Erk1/2 in KRAS^{G12D} and BCR-ABL-expressing murine cells (starved for 6 hours). (B) Growth of murine wild-type (WT)-KRAS^{G12D}, Tc1-KRAS^{G12D} and Ts1/Cdkn2a-KRAS^{G12D} cells with or without cytokines (IL-7, Scf and Flt3-L, 10 ng/mL) over 6 days. (C) Kaplan-Meier analysis comparing survival of primary (1R) and secondary (2R) sub-lethally irradiated recipient mice engrafted with 1-2x10⁶ Tc1-KRAS^{G12D} (1R N=4, 2R N=6), WT-KRAS^{G12D} (1R N=5, 2R N=6) and Ts1Rh/Cdkn2a-KRAS^{G12D} (1R N=5, 2R N=6) cell lines; **P<0.01. (D) Phenotype of the murine cell lines assessing surface expression of BP1 and CD24 (phenotype of the WT-BCR-ABL and Tc1-BCR-ABL cell lines are in the *Online Supplementary Figure 1F*), and representative flow plots showing phenotype of mCherry-positive cell lines in primary and secondary recipients. w/: with; w/o: without. Cyt: cytokine.

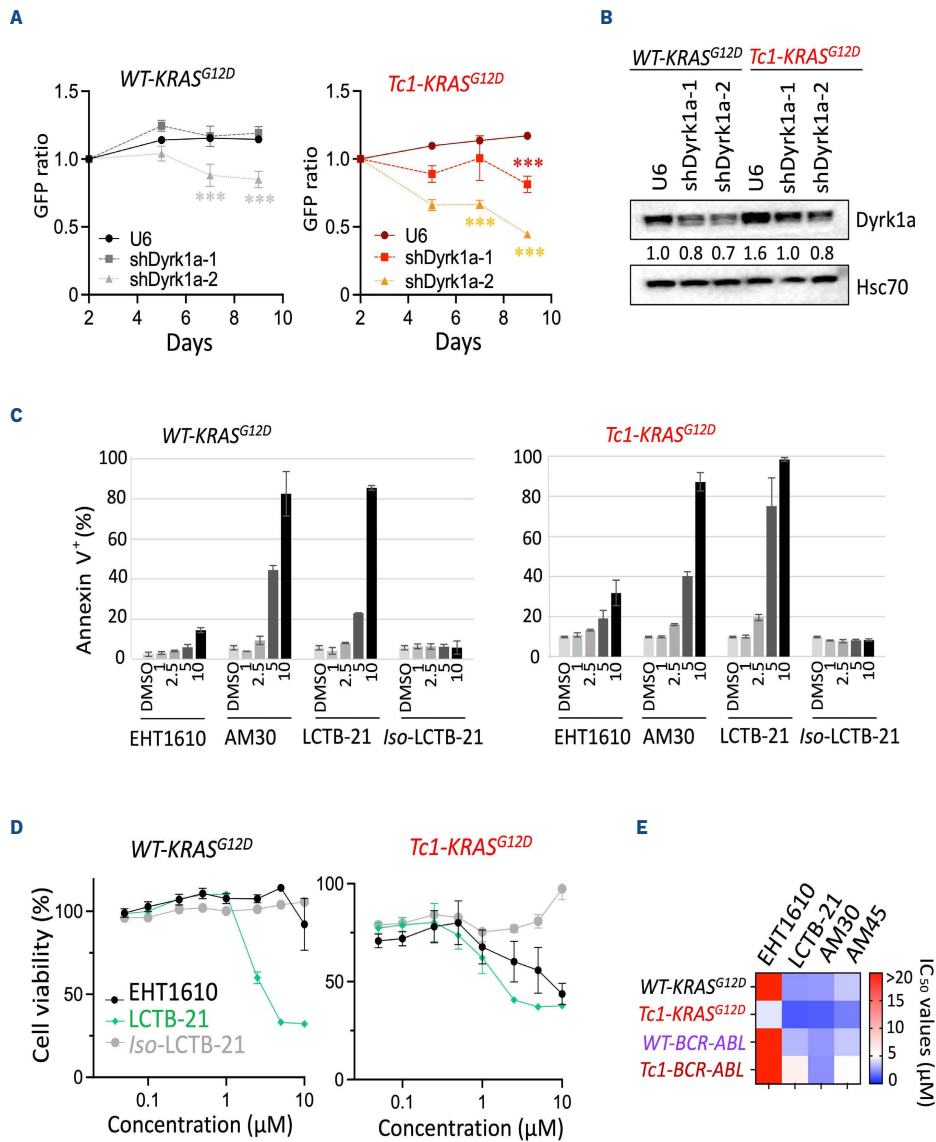
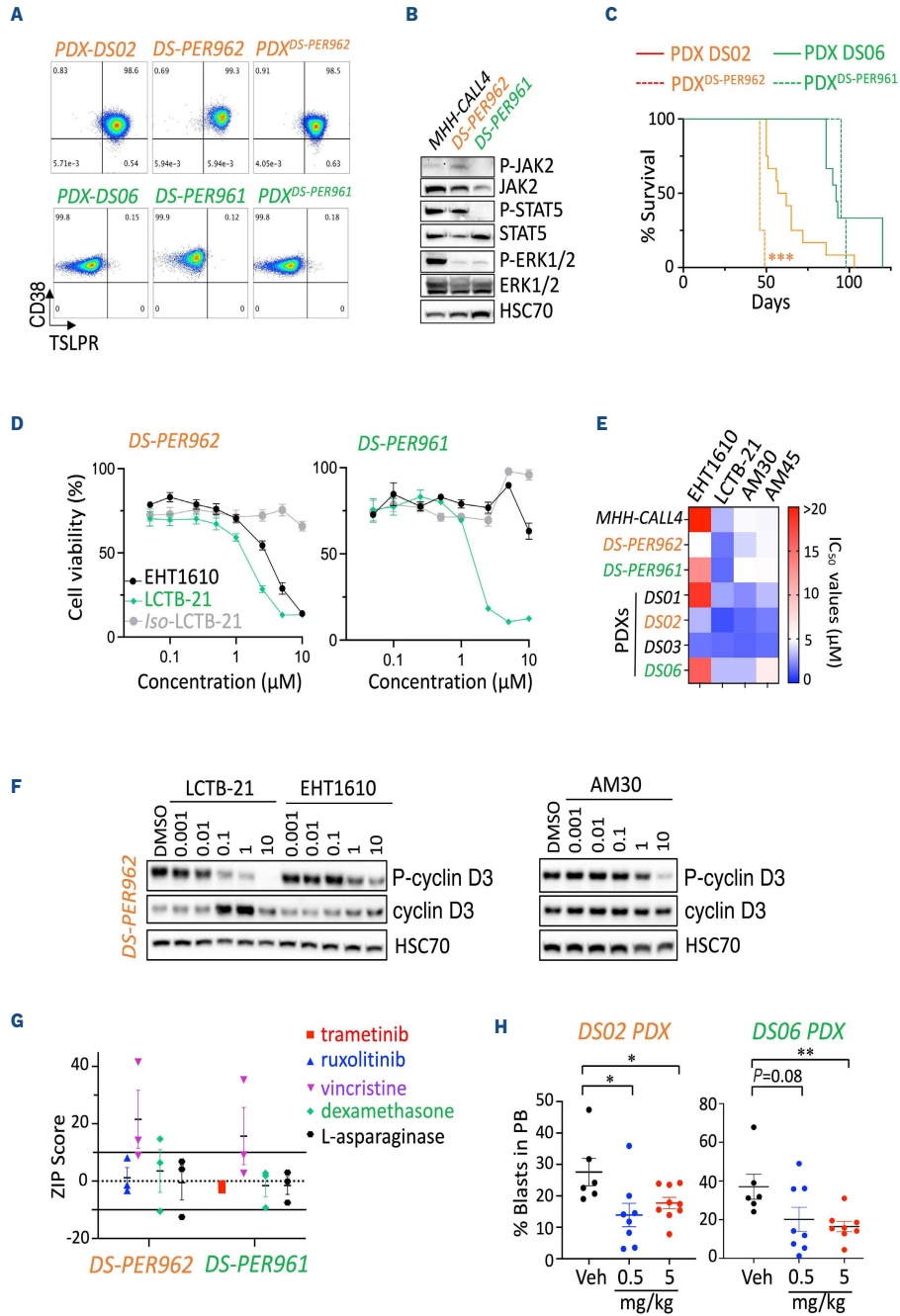


Figure 2. Genetic and pharmacological inhibition of DYRK1A decreases growth of Down syndrome acute lymphoblastic leukemia cells. (A) Ratio of wild-type (WT)-KRAS^{G12D} and Tc1-KRAS^{G12D} transduced with GFP-expressing Banshee vectors encoding two shDyrk1a compared to empty Banshee-U6 counterparts over 9 days (N=4 replicates); ***P<0.001. (B) Validation of Dyrk1a knock-down at the protein level 48 hours after transduction (GFP-sorted). Dyrk1a band intensities were quantified and normalized as a ratio of shDyrk1a-transduced to control U6-transduced WT-KRAS^{G12D} cells. (C) Cytotoxic effect of increasing doses (in μM) of the DYRK1A inhibitors EHT1610, AM30, Leucettinib-21 (LCTB-21) and its inactive isomer iso-Leucettinib-21 (Iso LCTB-21) at 48 hours in murine WT-KRAS^{G12D} and Tc1-KRAS^{G12D} cells assessed by flow cytometry (Annexin V staining). (D) Dose-response curves assessing efficacy of EHT1610, LCTB-21 and Iso LCTB-21 at 72 hours by alamarBlue cell viability assay in murine WT-KRAS^{G12D} and Tc1-KRAS^{G12D} cells. (E) Heatmap integrating relative half-maximal inhibitory concentration (IC_{50}) values obtained for the DYRK1A inhibitors tested in our murine cell lines.



Continued on following page.

LETTER TO THE EDITOR

Figure 3. Efficacy of DYRK1A inhibition in novel human Down syndrome acute lymphoblastic leukemia cell lines and patient-derived xenograft models. (A) Representative flow plots assessing CD38 and TSLPR expression of the human DS-PER962 and DS-PER961 Down syndrome acute lymphoblastic leukemia (DS-ALL) cell lines compared to their corresponding DS06 and DS02 patient-derived xenografts (PDX), and to NSG recipients engrafted with 1×10^6 DS-ALL cell lines (PDX^{NSG}). (B) Western blots assessing the constitutive phosphorylation of JAK2, STAT5 and ERK1/2 in DS-PER962 and DS-PER961 cell lines following a 6-hour starvation; the non-DS MHH-CALL4 (CRLF2-rearranged/JAK2 mutant) ALL cell line was used as control. (C) Kaplan-Meier curves comparing the survival of the DS-PER962 and DS-PER961 PDX (N=3-4) to their corresponding DS02 and DS06 PDX (N=9-12); *** $P < 0.001$. (D) Efficacy of EHT1610, Leucettinib-21 (LCTB-21) and its inactive isomer iso-Leucettinib-21 (iso LCTB-21) in the human DS-PER962 and DS-PER961 cell lines (72 hours). (E) Heatmap representing the relative half-maximal inhibitory concentration (IC_{50}) values obtained in the non-DS-ALL, DS-ALL human cell lines and DS-ALL cells freshly harvested from PDX models. (F) Western blot comparing the effect of EHT1610, LCTB-21 and AM30 on phospho-cyclin D3 and total cyclin D3 stability after 6 hours of treatment in the DS-PER962 cell line. (G) ZIP scores obtained from combining Leucettinib-21 (10 doses from 0.01 to 10 μ M) with trametinib (0.0001-20 μ M), ruxolitinib (0.0001-20 μ M), vincristine (0.0005-0.5 μ M), dexamethasone (0.0025-20 μ M) and L-asparaginase (0.1-20 μ M) in the human DS-ALL cell lines. ZIP scores < -10 =antagonism; -10 to 10 =additive; > 10 =synergy. (H) *In vivo* effect of Leucettinib-21 on leukemia burden in the peripheral blood (PB) of the DS02 and DS06 PDX models (oral gavage, 2 weeks and 4 weeks of treatment respectively); * $P < 0.05$, ** $P < 0.01$. Veh: vehicle.

(IC_{50}) values than its disomic counterpart WT-KRAS^{G12D} (Figure 2D, E; *Online Supplementary Figure S2A*).

In order to expand our observations, we next established two human DS-ALL cell lines: DS-PER961 and DS-PER962 from our previously reported DS06 (KRAS^{G12S}-positive) and DS02 (CRLF2-rearranged/JAK2^{682F}-positive) PDX.⁶ These unique models represent the first human cell lines for DS-ALL, with comprehensive characterization at the genomic, transcriptomic and phenotypic levels, confirming their resemblance to the PDX models from which they originated (Figure 3A; *Online Supplementary Figure S3A-E*). Western blot analyses confirmed phosphorylation of ERK1/2 and STAT5 downstream of KRAS^{G12S} and JAK2^{682F} mutants in DS-PER961 and DS-PER962 respectively (Figure 3B). Using NOD-SCID- γ c-/- (NSG) mice, we also showed that both DS-ALL cell lines engrafted into immunocompromised recipients with DS-PER962 cells being more aggressive than their PDX counterparts (Figure 3C). Using these human cells, we confirmed that Leucettinib-21, AM30 and AM45 were potent inhibitors in human DS-ALL cells and in MHH-CALL4 (a non-DS CRLF2-rearranged and JAK2 mutant ALL cell line known to be sensitive to DYRK1A inhibition) (Figure 3D, E; *Online Supplementary Figure S2B-D*).⁸ No significant effect was seen for AM28 nor for the inactive isomer of Leucettinib-21 (Figure 3D; *Online Supplementary Figure S2B, C*). Importantly, efficacy of these DYRK1A inhibitors was demonstrated in DS-ALL blasts freshly harvested from four DS-ALL PDX models (described in⁶), validating the suitability of our DS-ALL cells to assess efficacy of new therapies (Figure 3E). Compared to EHT1610 and AM30, Leucettinib-21 was the most potent compound in inhibiting phosphorylation of the known DYRK1A target cyclin D3 in a dose-dependent manner shown in DS-PER962 (Figure 3F), DS-PER961 and in murine cells (*Online Supplementary Figure S2E*), but had limited effect on FOXO1-phosphorylation (*Online Supplementary Figure S2F-I*). Next, we evaluated *in vitro* drug combinations of Leucettinib-21 with targeted and conventional therapies and identified synergy with vincristine and an additive effect with dexamethasone and L-asparaginase (Figure 3G; *Online Supplementary Figure S2J*). An additive effect between Leu-

cettinib-21 and the targeted therapies ruxolitinib (a JAK1/2 inhibitor) and trametinib (a MEK1/2 inhibitor) was also seen in DS-PER962 (CRLF2-positive/JAK2^{682F} mutant) and in the DS-PER961 (KRAS^{G12S}) cell lines, respectively (Figure 3G). Finally, we assessed the efficacy of Leucettinib-21 *in vivo* in the DS06 and DS02 PDX models and observed that *in vivo* treatment with Leucettinib-21 decreased leukemia burden but did not fully eradicate leukemia (Figure 3H). Together, this data demonstrates the suitability and clinical relevance of the novel murine and human models we have established and emphasizes the key role of DYRK1A in DS-ALL.

Compared to other children, higher sensitivity to treatment-related toxicity in children with DS-ALL remains a major clinical challenge. This has significantly limited the development of novel targeted therapies for this patient population, ultimately delaying translation into clinical trials. Recently, integration of immunotherapeutic approaches has offered promise in reducing toxicity. Indeed, Laetsch *et al.* reported comparable outcomes between DS- and non-DS children with relapsed/refractory B-ALL who received CD19-directed chimeric antigen receptor T-cell therapy, including similar rates of CD19-negative relapse,¹⁵ and an ongoing clinical trial is currently assessing whether blinatumomab can replace two blocks of consolidation chemotherapy for treatment of *de novo* DS-ALL (*clinicaltrial.gov. Identifier: NCT03911128*). As an alternative approach, identifying key vulnerabilities in DS-ALL blasts could provide the molecular basis for development of novel targeted therapies. While resources such as the recent in-depth characterization of the genetic landscape of DS-ALL can provide such insight,¹⁰ we have developed novel models of DS-ALL and shown that inhibiting dosage-sensitive mechanisms altered by trisomy 21 may also represent a new avenue to integrate agents with low toxicity and ultimately improve outcomes and quality of care for children with DS-ALL. We demonstrated that a reduction in DYRK1A expression is sufficient to decrease the growth of DS-ALL cell lines, confirmed the sensitivity of human and murine cells to DYRK1A inhibition and showed that the leading candidate, Leucettinib-21, potentiates the cytotoxic effect of other chemotherapeutic and targeted

LETTER TO THE EDITOR

agents and delayed leukemia expansion *in vivo*, with no detectable toxicity identified in the peripheral blood (*Online Supplementary Figure S2K*). Leucettinib-21 has recently completed regulatory preclinical safety studies and is primed for early phase clinical assessment. Strikingly, studies have demonstrated the preclinical impact of targeting DYRK1A activity in different subtypes of childhood leukemia,⁹ further emphasizing the potential benefit for investigating Leucettinib-21 or other new potent DYRK1A inhibitors in clinical trials for ALL.

Altogether, this study has established and comprehensively characterized the first DS-ALL cell lines, providing suitable and clinically relevant cellular models to identify new molecular weaknesses in DS-ALL and test the efficacy of novel targeted therapies (as exemplified here with DYRK1A inhibition), alone or in combination with standard of care, to ultimately develop new, less toxic treatments to improve the outcome for children with DS-ALL.

Authors

Shannon L. Carey-Smith,^{1,2*} Maryam H. Simad,^{3*} Kunjal Panchal,^{1,2} Carlos Aya-Bonilla,¹ Hannah Smolders,¹ Sang Lin,¹ Jesse D. Armitage,¹ Vivien T. Nguyen,¹ Kathryn Bentley,¹ Jette Ford,¹ Sajla Singh,¹ Joyce Oommen,¹ Anouchka P. Laurent,³ Thomas Mercher,³ John D. Crispino,⁴ Andrew P. Montgomery,⁵ Michael Kassiou,⁵ Thierry Besson,⁶ Emmanuel Deau,⁷ Laurent Meijer,⁷ Laurence C. Cheung,^{1,2,8} Rishi S. Kotecha^{1,2,9,10} and Sébastien Malinge^{12,10}

¹Telethon Kids Cancer Center, Telethon Kids Institute, Perth, Western Australia, Australia; ²Curtin Medical School, Curtin University, Perth, Western Australia, Australia; ³U1170 INSERM, Gustave Roussy, Villejuif, France; ⁴Department of Hematology, St Jude Children's Hospital, Memphis, TN, USA; ⁵School of Chemistry, University of Sydney, New South Wales, Australia; ⁶University Rouen Normandie, INSA Rouen Normandie, CNRS, COBRA UMR 6014, Rouen, France; ⁷Perha Pharmaceuticals, Perharidy Peninsula, Roscoff, France; ⁸Curtin Health Innovation Research Institute, Curtin University, Perth, Western Australia, Australia; ⁹Department of Clinical Hematology, Oncology, Blood and Marrow Transplantation, Perth Children's Hospital, Perth, Western Australia, Australia and ¹⁰University of Western Australia, Perth, Western Australia, Australia

*SLC-S and MHS contributed equally as first authors.

Correspondence:
S. MALINGE - sebastien.malinge@telethonkids.org.au

<https://doi.org/10.3324/haematol.2023.284271>

Received: September 13, 2023.

Accepted: February 19, 2024.

Early view: February 29, 2024.

©2024 Ferrata Storti Foundation

Published under a CC BY-NC license 

Disclosures

JDC is a member of the scientific advisory board for Alethiomics, a consultant for Cellarity, and receives research funding from Syndax. LM is a founder of Perha Pharmaceuticals. ED and LM are co-inventors in the Leucettinib patents. RSK discloses advisory board participation from Jazz Pharmaceuticals, Amgen and Link Healthcare. All other authors have no conflicts of interest to disclose.

Contributions

SLCS, MHS and SM conceived and designed the experiments. SLCS, MHS, KP, CAB, HS, SL, JDA, VTN, KB, JF, SS, JO and SM performed the experiments. APL, TM, JDC, TB, APM, MK, ED and LM provided reagents, materials and technical insight. SLCS, MHS, KP, CAB, LCC and RSK significantly contributed to analysis and interpretation of the results. SM supervised the project. SLCS and SM wrote the manuscript. All authors edited and approved the final version of the manuscript for submission.

Acknowledgments

We thank L. Munoz, T. Johns, G. Chua, P. Kumar, T. Lassmann, and staff members of the Bioresources facility at Telethon Kids Institute for their support in obtaining reagents, processing samples and housing/monitoring animals related to this study.

Funding

This research was supported by Australian Government Research Training Program (RTP) Scholarships (to SLCS and KP). CAB is supported by a Fellowship from the Jerome Lejeune and Sisley-d'Ornano Foundations. TB is supported by the University of Rouen Normandy, INSA Rouen Normandy, the Centre National de la Recherche Scientifique (CNRS), European Regional Development Fund (ERDF), Labex SynOrg (ANR-11-LABX-0029), Carnot Institute I2C, the XL-Chem Graduate School of Research (ANR-18-EURE-0020 XL CHEM), and by Region Normandie. APM is supported by a postdoctoral research fellowship from the University of Sydney's Drug Discovery Initiative. MK is a recipient of a National Health and Medical Research Council Principal Research Fellowship (APP1154692). LM is supported by grants from the Jerome Lejeune Foundation, l'Agence Nationale de la Recherche (ANR) (DYRK-DOWN), BpiFrance (i-Nov, vague 9), the European Union's Horizon 2020 research and innovation programme (Grant #848077) (GO-DS21), and the European Innovation Council (EIC) Accelerator Down-Autonomy project (190138295). SM is supported by a fellowship from the Cancer Council Western Australia (CCWA, Grant #877). This study was supported by project grants from the Child Cancer Research Foundation (RSK, LCC and SM), Cancer Council Western Australia (Grant #1068) and the Jerome Lejeune Foundation (Grant #1806).

Data-sharing statement

RNA-sequencing files are available via the Gene Expression Omnibus (GEO) database under the accession number GSE245056.

References

- Buitenkamp TD, Izraeli S, Zimmermann M, et al. Acute lymphoblastic leukemia in children with Down syndrome: a retrospective analysis from the Ponte di Legno study group. *Blood*. 2014;123(1):70-77.
- Ceppi F, Stephens D, den Hollander BS, et al. Clinical presentation and risk factors of serious infections in children with Down syndrome treated for acute lymphoblastic leukemia. *Pediatr Blood Cancer*. 2016;63(11):1949-1953.
- Rabin KR, Devidas M, Chen Z, et al. Outcomes in children, adolescents, and young adults with Down syndrome and ALL: a report from the Children's Oncology Group. *J Clin Oncol*. 2024;42(2):218-227.
- Meyr F, Escherich G, Mann G, et al. Outcomes of treatment for relapsed acute lymphoblastic leukaemia in children with Down syndrome. *Br J Haematol*. 2013;162(1):98-106.
- Rafei H, Kantarjian HM, Jabbour EJ. Targeted therapy paves the way for the cure of acute lymphoblastic leukaemia. *Br J Haematol*. 2020;188(2):207-223.
- Laurent AP, Siret A, Ignacimoutou C, et al. Constitutive activation of RAS/MAPK pathway cooperates with trisomy 21 and is therapeutically exploitable in Down syndrome B-cell leukemia. *Clin Cancer Res*. 2020;26(13):3307-3318.
- Lane AA, Chapuy B, Lin CY, et al. Triplication of a 21q22 region contributes to B cell transformation through HMGN1 overexpression and loss of histone H3 Lys27 trimethylation. *Nat Genet*. 2014;46(6):618-623.
- Bhansali RS, Rammohan M, Lee P, et al. DYRK1A regulates B cell acute lymphoblastic leukemia through phosphorylation of FOXO1 and STAT3. *J Clin Invest*. 2021;131(1):e135937.
- Page EC, Heatley SL, Eadie LN, et al. HMGN1 plays a significant role in CRLF2 driven Down Syndrome leukemia and provides a potential therapeutic target in this high-risk cohort. *Oncogene*. 2022;41(6):797-808.
- Li Z, Chang TC, Junco JJ, et al. Genomic landscape of Down syndrome-associated acute lymphoblastic leukemia. *Blood*. 2023;142(2):172-184.
- O'Doherty A, Ruf S, Mulligan C, et al. An aneuploid mouse strain carrying human chromosome 21 with Down syndrome phenotypes. *Science*. 2005;309(5743):2033-2037.
- Tahtouh T, Durieu E, Villiers B, et al. Structure-activity relationship in the Leucettine family of kinase inhibitors. *J Med Chem*. 2022;65(2):1396-1417.
- Lindberg MF, Deau E, Miegé F, et al. Chemical, biochemical, cellular, and physiological characterization of Leucettinib-21, a Down syndrome and Alzheimer's disease drug candidate. *J Med Chem*. 2023;66(23):15648-15670.
- Zhou Q, Phoa AF, Abbassi RH, et al. Structural optimization and pharmacological evaluation of inhibitors targeting dual-specificity tyrosine phosphorylation-regulated kinases (DYRK) and CDC-like kinases (CLK) in glioblastoma. *J Med Chem*. 2017;60(5):2052-2070.
- Laetsch TW, Maude SL, Balduzzi A, et al. Tisagenlecleucel in pediatric and young adult patients with Down syndrome-associated relapsed/refractory acute lymphoblastic leukemia. *Leukemia*. 2022;36(6):1508-1515.

Efficacy of DYRK1A inhibitors in novel models of Down syndrome acute lymphoblastic leukemia

Shannon L. Carey-Smith^{1,2,*}, Maryam H. Simad^{1*}, Kunjal Panchal^{1,2}, Carlos Aya-Bonilla¹, Hannah Smolders¹, Sang Lin¹, Jesse D. Armitage¹, Vivien T. Nguyen¹, Kathryn Bentley¹, Jette Ford¹, Sajla Singh¹, Joyce Oommen¹, Anouchka P. Laurent³, Thomas Mercher³, John D. Crispino⁴, Andrew P. Montgomery⁵, Michael Kassiou⁵, Thierry Besson⁶, Emmanuel Deau⁷, Laurent Meijer⁷, Laurence C. Cheung^{1,2,8}, Rishi S. Kotecha^{1,2,9,10} and Sébastien Malinge^{1,2,10}

¹Telethon Kids Cancer Centre, Telethon Kids Institute, Perth, WA, Australia

²Curtin Medical School, Curtin University, Perth, WA, Australia

³U1170 INSERM, Gustave Roussy, Villejuif, France

⁴Department of Hematology, St Jude Children`s Hospital, Memphis, TN, USA

⁵School of Chemistry, University of Sydney, NSW, Australia

⁶University Rouen Normandie, INSA Rouen Normandie, CNRS, COBRA UMR 6014, 76000 Rouen, France

⁷Perha Pharmaceuticals, Perharidy Peninsula, Roscoff, France

⁸Curtin Health Innovation Research Institute, Curtin University, Perth, WA, Australia

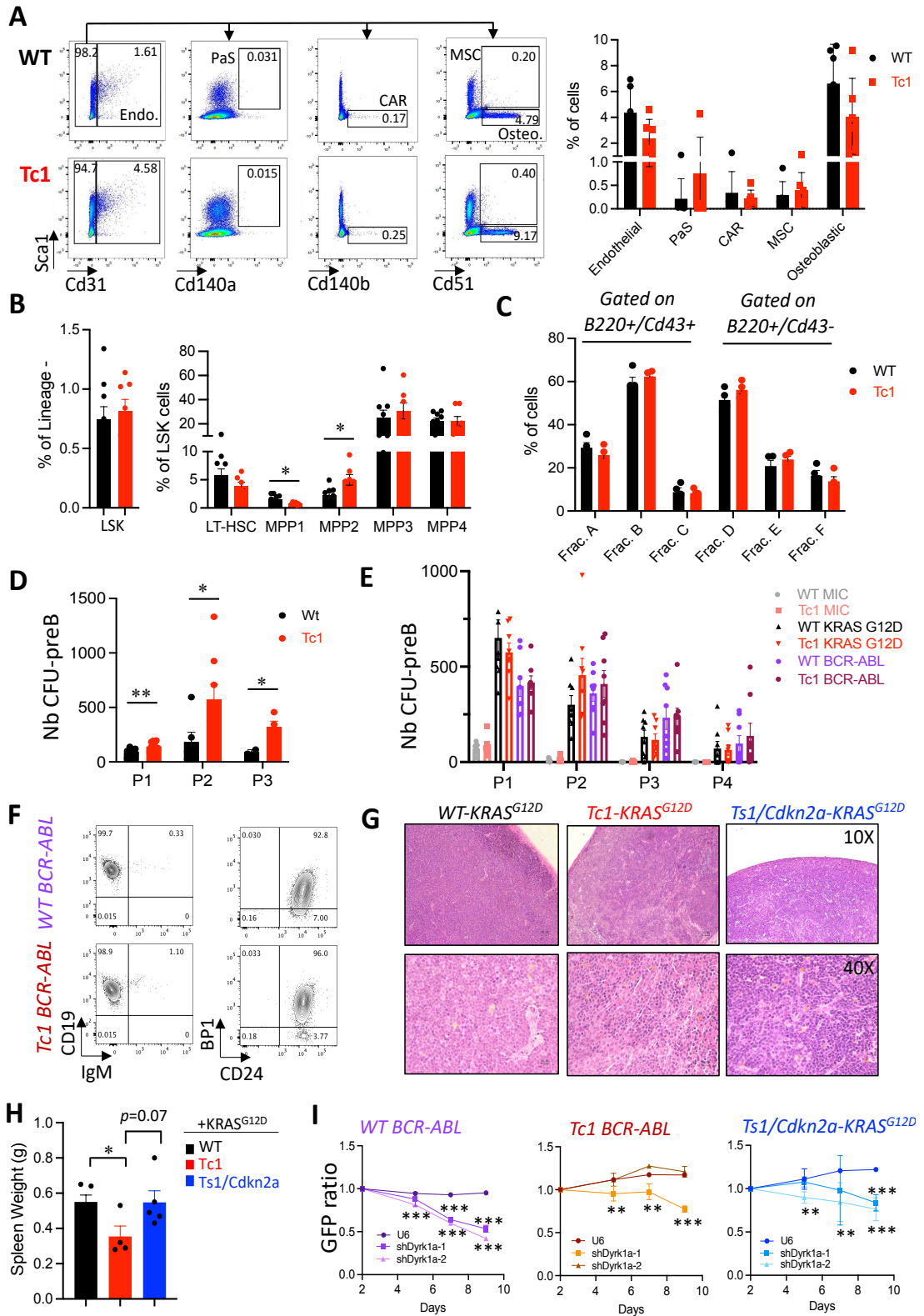
⁹Department of Clinical Haematology, Oncology, Blood and Marrow Transplantation, Perth Children`s Hospital, Perth, WA, Australia

¹⁰University of Western Australia, Perth, WA, Australia

*SLCS and MHS contributed equally to the study

Supplementary Figures and legends

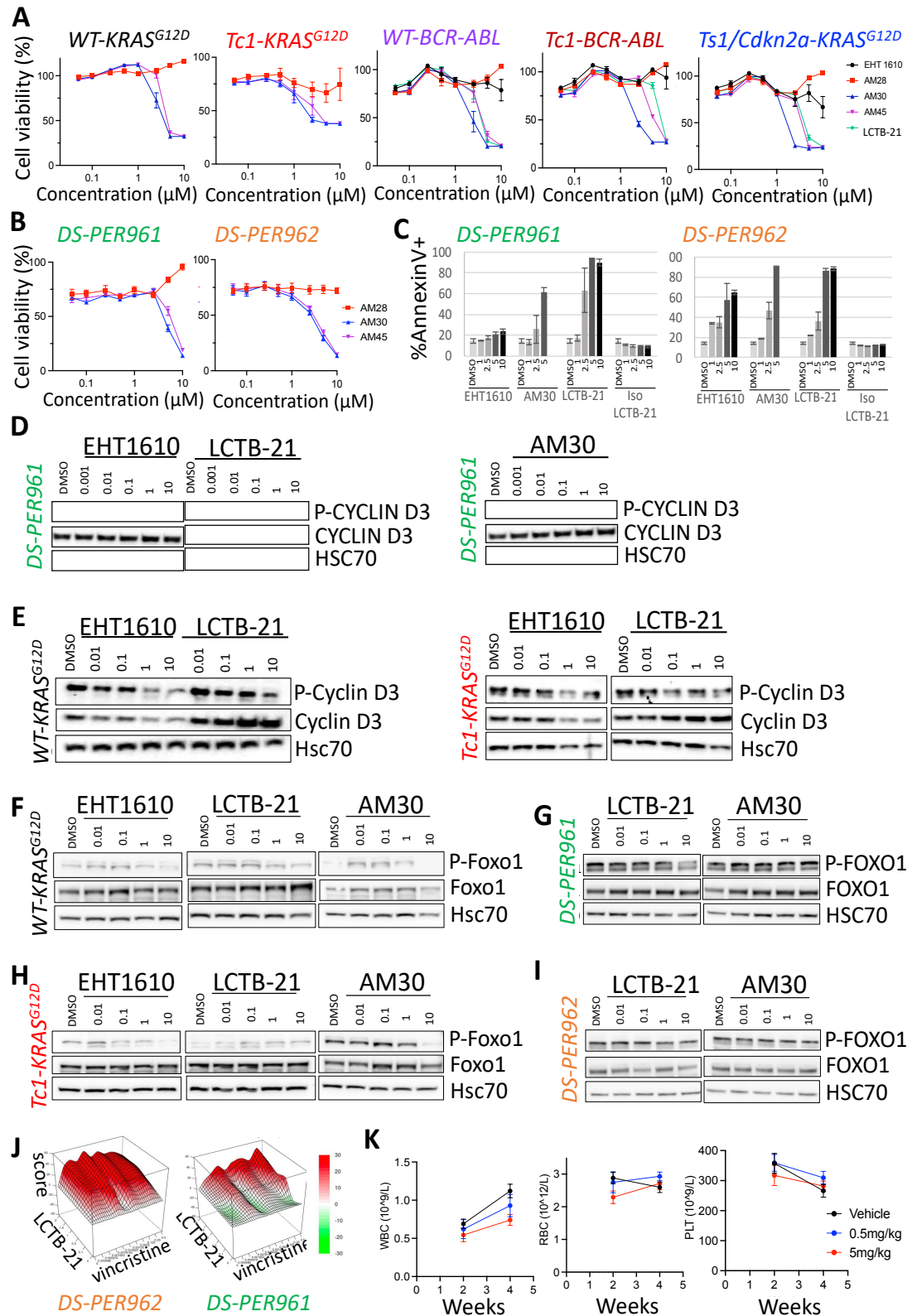
Supplementary Figure 1



Supplementary Figure 1: Establishment of murine DS-ALL cells.

A. Representative flow plots comparing the bone marrow stroma of 8-10 week old wild-type (WT) and trisomic (Tc1) mice, gated on CD45-Ter119- and depicting the percentage of endothelial cells (endo, CD31-positive), CD31-negative PaS (PDGFRa(Cd140a)+/Sca1+), Cxcl12-abundant reticular cells (CAR, PDGFRb(cd140b)+/Sca1-), mesenchymal stem cells (MSC, Sca1+/CD51+) and osteoblastic cells (osteo, Sca1-/CD51+). *Right panel*: box plot integrating all data (n=6). **B.** Bar graph displaying the percentage of the different hematopoietic stem cells and progenitors in 8-10 week old mice (n=7-9); * $p < 0.05$. LSK = Lineage-negative/Sca1+/Kit+, LT-HSC (Long-term hematopoietic stem cells, LSK+CD34-FLT3-CD150+CD48-), MPP1 (multipotent progenitor 1, LSK+CD34+FLT3-CD150+CD48-), MPP2 (LSK+CD34+FLT3-CD150+CD48+), MPP3 (LSK+CD34+FLT3-CD150-CD48+), MPP4 (LSK+CD34+FLT3+CD150-CD48+). **C.** Bar graph displaying the proportion of the hardy fraction in the bone marrow of WT and Tc1 mice (n=4); Fraction A (B220+CD43+CD24-BP1-), Fraction B (B220+CD43+CD24+BP1-), Fraction C (B220+CD43+CD24+BP1+), Fraction D (B220+CD43-IgM-IgD-), Fraction E (B220+CD43-IgM+IgD-) and Fraction F (B220+CD43-IgM+IgD+). **D.** Number of colony-forming unit (CFU)-preB colonies obtained from 8-10 week old WT and Tc1 donor bone marrow cells over 3 passages (n=8-9); * $p < 0.05$, ** $p < 0.01$. **E.** Number of CFU-preB colonies obtained from sorted mCherry-positive bone marrow progenitor cells transduced with KRAS^{G12D}, BCR-ABL retroviruses compared to empty vector retroviruses (MIC = MSCV-IRES-mCherry), over 4 passages (n=8). **F.** Phenotype of the WT-BCR-ABL and Tc1-BCR-ABL cell lines assessing surface expression of CD19, IgM, BP1 and CD24. **G.** Representative spleen sections from WT-KRAS^{G12D}, Tc1-KRAS^{G12D} and Ts1/cdkn2a-KRAS^{G12D} primary recipients, stained with hematoxylin and eosin (10X and 40X magnification). **H.** Average spleen weight at endpoint in WT-KRAS^{G12D} (n=5), Tc1-KRAS^{G12D} (n=4) and Ts1/Cdkn2a-KRAS^{G12D} (n=5) irradiated recipient mice; * $p < 0.05$. **I.** Ratio of GFP-expressing Banshee vectors encoding two shDyrk1a compared to empty Banshee-U6 counterparts over 9 days in the murine WT-BCR-ABL, Tc1-BCR-ABL and Ts1/cdkn2a-KRAS^{G12D} cells (n=4 replicates); ** $p < 0.01$, *** $p < 0.001$.

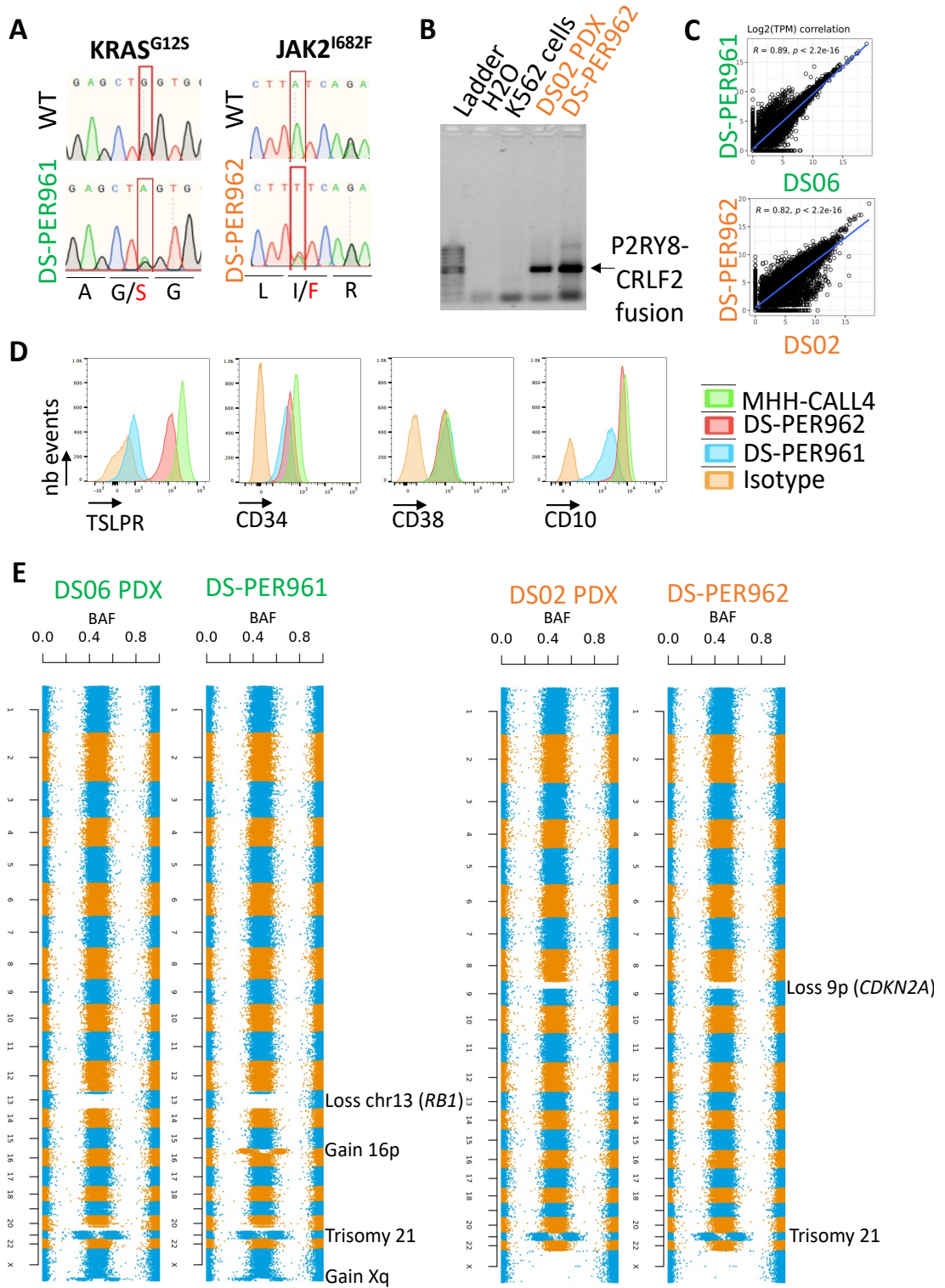
Supplementary Figure 2



Supplementary Figure 2: Preclinical testing of new DYRK1A inhibitors in non-DS and DS-ALL.

A. Dose-response curves for EHT1610, Leucettinib-21 (LCTB-21), AM28, AM30 and AM45 in murine cell lines. **B.** Dose-response curves for AM28, AM30 and AM45 in human DS-PER961 and DS-PER962 cell lines. **C.** Bar graphs showing the impact of increasing doses 1 μ M, 2.5 μ M, 5 μ M and 10 μ M of the DYRK1A inhibitors EHT1610, AM30, LCTB-21 and its inactive isomer iso-Leucettinib-21 (Iso LCTB-21) on cell viability of DS-PER961 and DS-PER962 at 48 hours assessed by flow cytometry (AnnexinV-positive cells). **D.** Western blots of phospho-Cyclin D3 performed from protein extracted from the DS-PER961 human cell line after a 6 hour treatment with increasing doses (in μ M) of the DYRK1A inhibitors EHT1610, Leucettinib-21 and AM30, compared to treatment with DMSO. **E.** Western blots of phospho-Cyclin D3 performed from protein extracted from WT-KRAS^{G12D} and Tc1-KRAS^{G12D} murine cells after a 6 hour treatment with increasing doses (in μ M) of the DYRK1A inhibitors EHT1610 and Leucettinib-21, compared to treatment with DMSO. **F-I.** Assessment of FOXO1 (Ser326) phosphorylation in response to DYRK1A inhibition (6 hour treatment) in **(F)** murine WT-KRAS^{G12D}, **(G)** human DS-PER961 (KRAS^{G12S}), **(H)** murine Tc1-KRAS^{G12D} and **(I)** human DS-PER962 (CRLF2-rearranged/JAK2^{682F}) cells. **J.** Representative plots showing synergy between LCTB-21 and vincristine in DS-PER962 and DS-PER961 cell lines. **K.** Blood count assessment showing WBC (white blood cell count), RBC (red blood cell count) and PLT (platelet counts) at week 2 and week 4 of treatment with 0.5 mg/kg and 5 mg/kg of Leucettinib-21 compared to vehicle in the DS06 patient-derived xenograft (n=3 per group and per timepoint).

Supplementary Figure 3



Supplementary Figure 3: Characterization of human DS-ALL cell lines.

A. Sanger sequencing of genomic DNA confirming the presence of the *KRAS*^{G12S} and *JAK2*^{T682F} mutations found in the DS-PER961 and DS-PER962 cell lines respectively. **B.** Validation of the P2RY8-CRLF2 fusion transcript in the DS02 patient-derived xenograft (PDX) and DS-PER962 cell line compared to K562 control cells (primer sequences are indicated in supplemental table 2). **C.** Spearman correlation of the transcriptional profiles obtained in the DS-PER961 and DS-PER962 cell lines (Y-axis) compared to the PDX model they originate from (X-axis). RNA sequencing files are available via the Gene Expression Omnibus (GEO) database under the accession number GSE245056. **D.** Representative flow plots comparing the Mean Fluorescence Intensity (MFI) for the surface markers TSLPR, CD34, CD38 and CD10 in the DS-PER961 (in blue) and DS-PER962 (in red) compared to MHH-CALL4 cells (in green); isotypes are represented in orange. **E.** Bi-allelic frequencies obtained from SNP arrays (HumanCytoSNP-12 BeadChip (HumanCytoSNP-12v2.1; Illumina) comparing DS-PER961 and DS-PER962 cell lines with the PDX they originate from, showing that the cell lines are relatively stable at the genomic level.

Chapter 3b: Therapeutically targeting the chromosome 21 gene *DYRK1A* additional data

Results:

Additional data from the study that was unpublished has been included in this chapter to give more insight into the research conducted on the DS-ALL models we developed. This chapter includes information on the characterisation of the Tc1 bone marrow microenvironment, the WT/Tc1 transduced CFU Pre-B cell assay (week 6), the WT/Tc1 cell line phenotypes, as well as the associated BMT assay, complementing the data in the publication “Efficacy of DYRK1A inhibitors in novel models of Down syndrome acute lymphoblastic leukemia”.

Time point analysis of WT and Tc1 microenvironment populations.

The bone marrow microenvironment was analysed in 6 weeks, 8-10 weeks, and 18-19 weeks old WT and Tc1 mice. This was to determine if the extra human chromosome present in the Tc1 mouse model had an impact on the presented non-haematopoietic stromal bone marrow microenvironment and examine if potential variation was age related (See Fig. 1, 2 below).

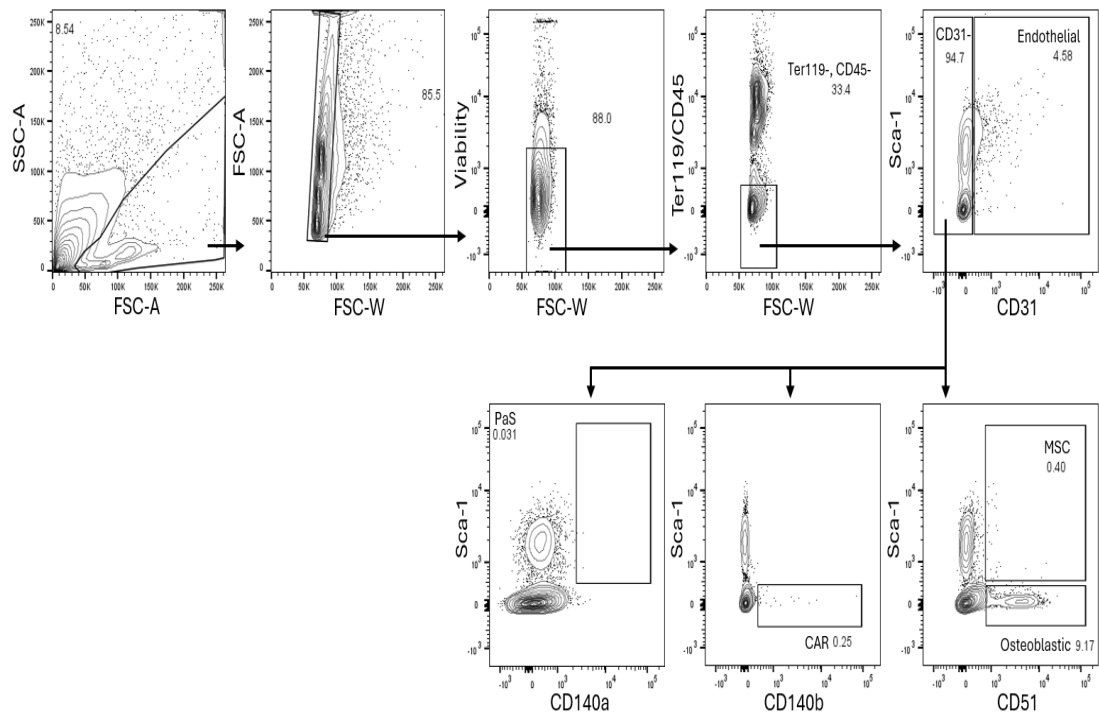


Figure 1. Flow cytometry gating strategy to assess bone marrow microenvironment cell populations. Gating strategy followed to identify Ter119-/CD45- cells including CD31+ endothelial cells, and the CD31- PaS cells (PDGFRa(CD140a)+/Sca-1+), CXCL12-abundant reticular cells (CAR, PDGFRb(CD140b)+/Sca-1-), mesenchymal stem cells (MSC, Sca-1+/CD51+) and osteoblastic cells (Sca-1-/CD51+). Ter119-/CD45- cells were gated upon total cell population (SSC-A/FSC-A), single cells (FSC-A/FSC-W) and live cell population (Horizon Fixable Viability Stain 700 negative) (63).

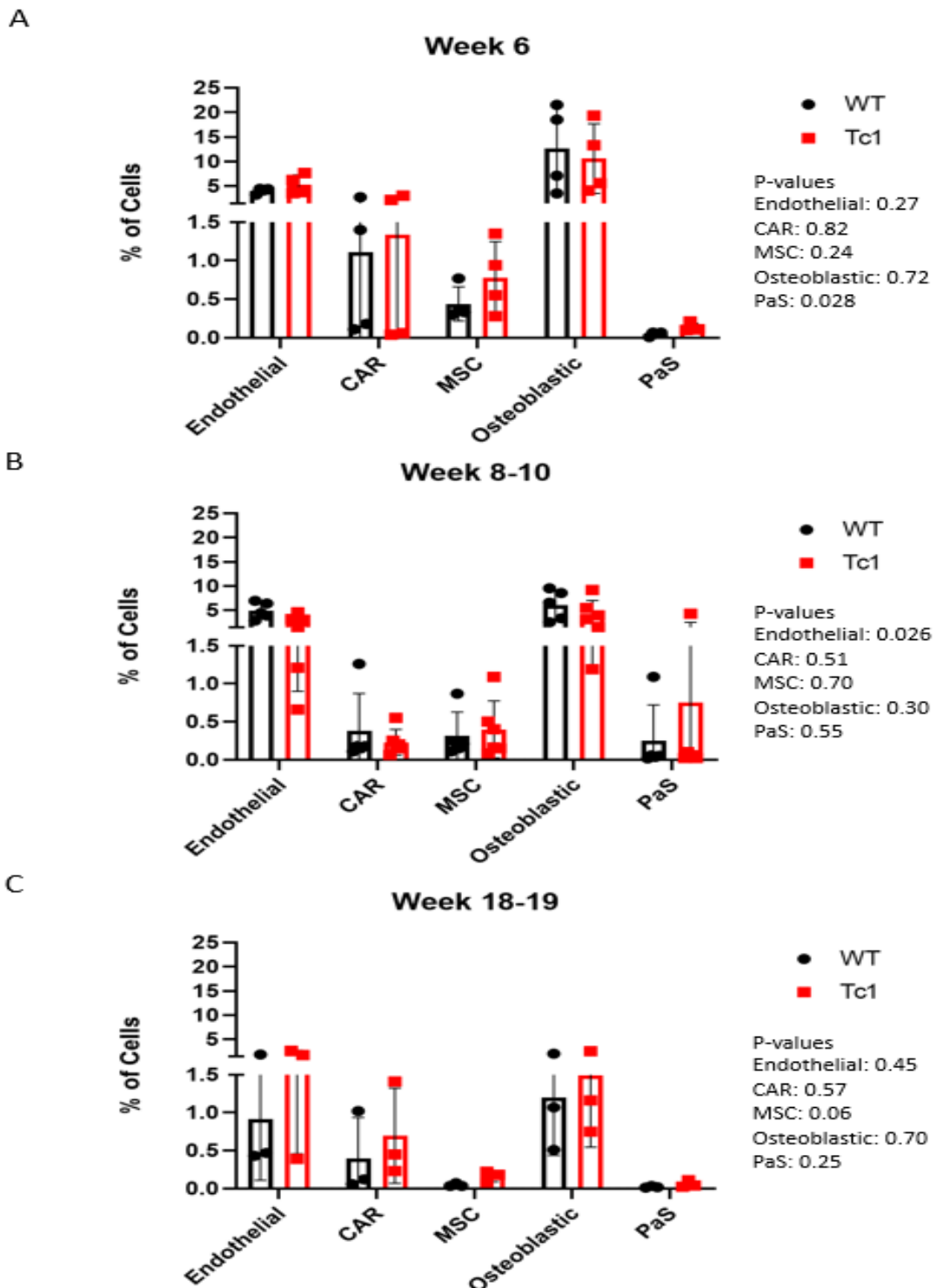


Figure 2. WT and Tc1 bone marrow microenvironment cell populations. (A) Characterisation of 6-week-old WT (n= 4) and Tc1 (n= 4) bone marrow microenvironment. (B) Characterisation of 8-10-week-old WT (n= 5) and Tc1 (n= 6) bone marrow microenvironment. (C) Characterisation of 18-19-week-old WT (n= 3) and Tc1 (n= 3) bone marrow microenvironment.

We analysed the MSC (Ter119-, CD45-, CD31-, Sca-1+, CD51+) populations based upon their role in assisting ALL development (66, 67), as well as assessing the endothelial (Ter119-, CD45-, CD31+), PaS (Ter119-, CD45-,

CD31-, CD140a+, Sca-1+) CAR (Ter119-, CD45-, CD31-, CD140b+, Sca-1-), and osteoblastic (Ter119-, CD45-, CD31-, Sca-1-, CD51+) cell populations, following the flow cytometry gating strategy in Figure 1 (63). Initially, femurs were collected and processed whereby bone marrow microenvironment cells were extracted, incubated with fluorochrome conjugated antibodies, and then assessed by flow cytometry. Upon analysis, statistical significance could only be determined for the difference between the WT and Tc1 PaS cell population at 6 weeks of age (P-value: 0.028, Fig. 2A) and the Endothelial cell population at 8-10 weeks of age (P-value: 0.026, Fig. 2B). Statistical significance could not be determined for any other cell population regardless of age. Since the difference between most of the cell populations were insignificant, including our population of interest (MSC), we decided to cease further analysis and conclude that the bone marrow microenvironment of the Tc1 mouse model is similar to the WT littermates, at the ages we tested.

Oncogenic cooperation in 6-week-old Tc1 mice.

CFU Pre-B cell assays were also performed on 6-week-old Tc1 and WT littermate bone marrow cells, after transduction with mCherry expressing MSCV containing the *KRAS*^{G12D} mutation (MSCV-*KRAS*^{G12D}), the *BCR-ABL1* fusion gene (MSCV-*BCR-ABL1*) or the empty vector control MIC (MSCV-IRES-mCherry). There was a trend of increased colony numbers observed at P2 in comparison to P1, as well as an increased replating capacity gained by some of the cells transduced with the *KRAS*^{G12D} mutation or the *BCR-ABL1* fusion gene compared to MIC transduced cells (Fig. 3).

Week 6 WT vs Tc1

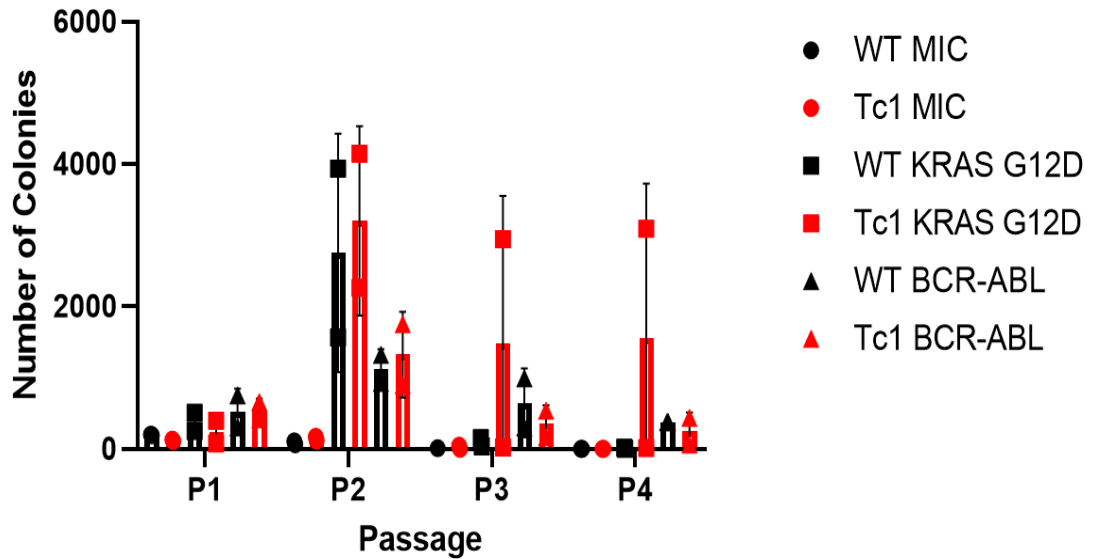


Figure 3. CFU Pre-B cell assay of 6-week-old WT/Tc1 transduced bone marrow cells. WT and Tc1 cells transduced with mCherry expressing MSCV-*KRAS*^{G12D}, MSCV-*BCR-ABL1* or empty vector control MIC (MSCV-IRES-mCherry) (n= 2). Colonies were counted and replated over 4 passages (P1-4).

Although transformation of B cell progenitors was not fully penetrant in this assay, we did observe transformation of some of the B cell progenitors due to the addition of the *KRAS*^{G12D} mutation or the *BCR-ABL1* fusion gene (Fig. 3). This cellular transformation was validated through the generation of the WT-*KRAS*^{G12D}, Tc1-*KRAS*^{G12D}, WT-*BCR-ABL* and Tc1-*BCR-ABL* cell lines. Additionally, we generated and genetically validated, several other WT and Tc1 *KRAS*^{G12D} or *BCR-ABL1* transformed cell line replicates from independent CFU Pre-B cell assays, which the laboratory will continue to validate in future experiments (n= 21 cell lines). Collectively, these observations indicate a capacity for transformation of WT and Tc1 B cell progenitors, like what was described in the Ts1Rhr mouse model (32) and previous B-ALL models (64) through the addition of the *KRAS*^{G12D} mutation or the *BCR-ABL1* fusion gene. Overall, there was no significant difference between the WT and Tc1 mice regarding oncogenic cooperation at 6-weeks of age, but a trend indicating increased proliferation capacity and self-renewal capacity was observed. This is in line with what we observed using 8-10-week-old donor bone marrow cells (see Chapter 3a).

Murine cell line model phenotype.

The WT-*KRAS*^{G12D}, Tc1-*KRAS*^{G12D}, WT-*BCR-ABL* and Tc1-*BCR-ABL* cell lines were also phenotypically validated by flow cytometry with antibody directed against B220, CD19, CD117 and IgM (Fig. 4). Interestingly, Tc1 cells were mostly B220 positive, with WT mostly B220 negative, however all cell lines were CD19 positive, CD117 and IgM negative. This data potentially indicating different stages in development between WT and Tc1 cells or consequences of the transformation process (clonal selection). The mixed B220/CD19 phenotype was mostly observed within the *BCR-ABL1* transduced cell lines. This warrants further investigation and continued phenotype analysis of the other established (genetically validated) *KRAS*^{G12D} and *BCR-ABL1* transformed cell lines will provide further insight on this observed phenotype. Overall, these cell lines are Pro/Pre-B cells based upon their cell surface phenotype, which confirms these cell lines accurately resemble the cells of interest regarding the investigation of DS-ALL.

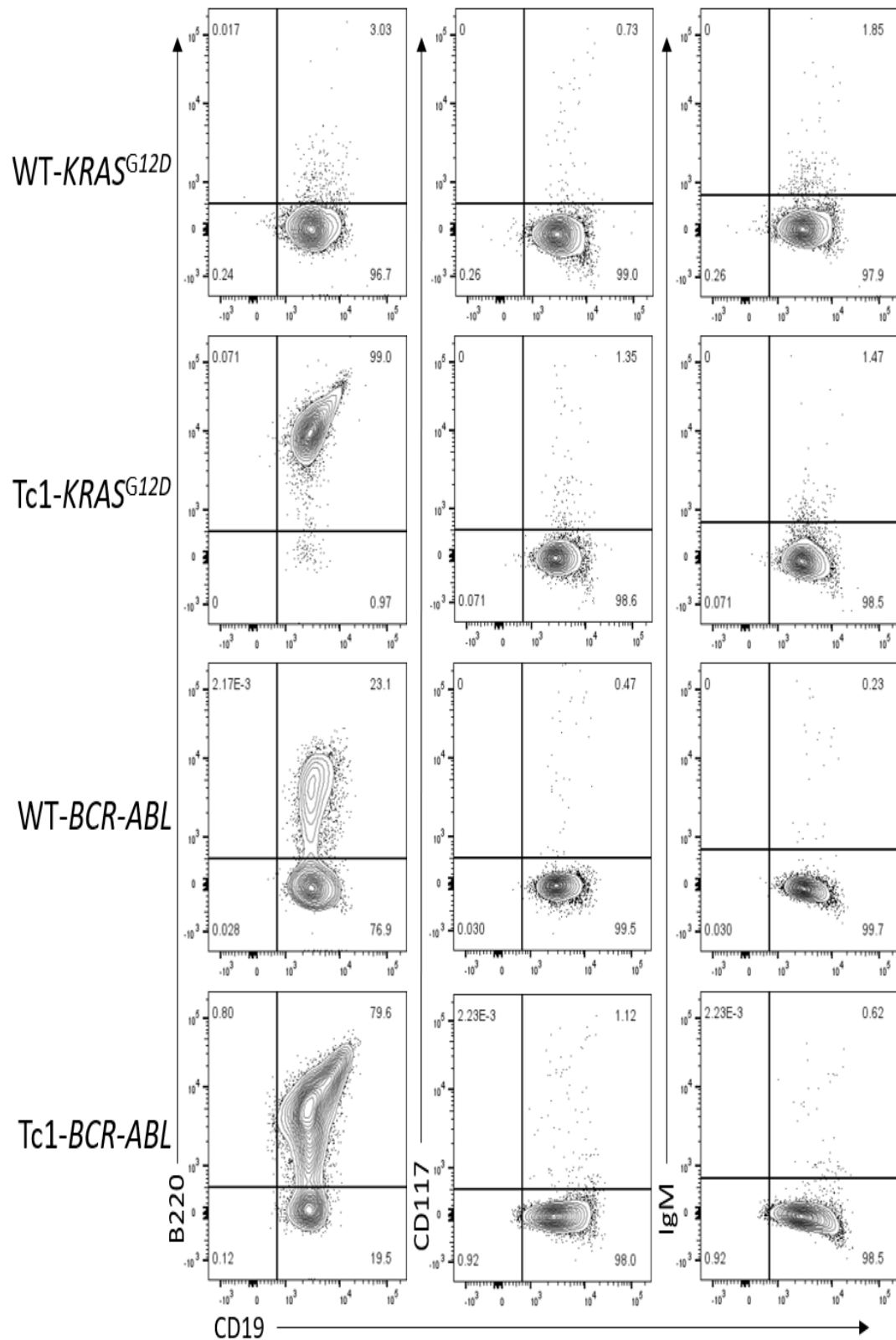


Figure 4. WT and Tc1 cell line phenotype. WT-KRAS^{G12D}, Tc1-KRAS^{G12D}, WT-BCR-ABL and Tc1-BCR-ABL cell line phenotype with B220, CD19, CD117 and IgM markers.

Phenotype analysis of the WT-KRAS^{G12D} and Tc1-KRAS^{G12D} bone marrow transplant.

Phenotype analysis was conducted on mCherry positive bone marrow and spleen samples collected from sub-lethally irradiated (550 Gy) primary C57BL/6J recipient mice that were injected with 2×10^6 WT-KRAS^{G12D} or Tc1-KRAS^{G12D} cells. This analysis was performed by following the representative flow cytometry gating strategy outlined in Figure 5A.

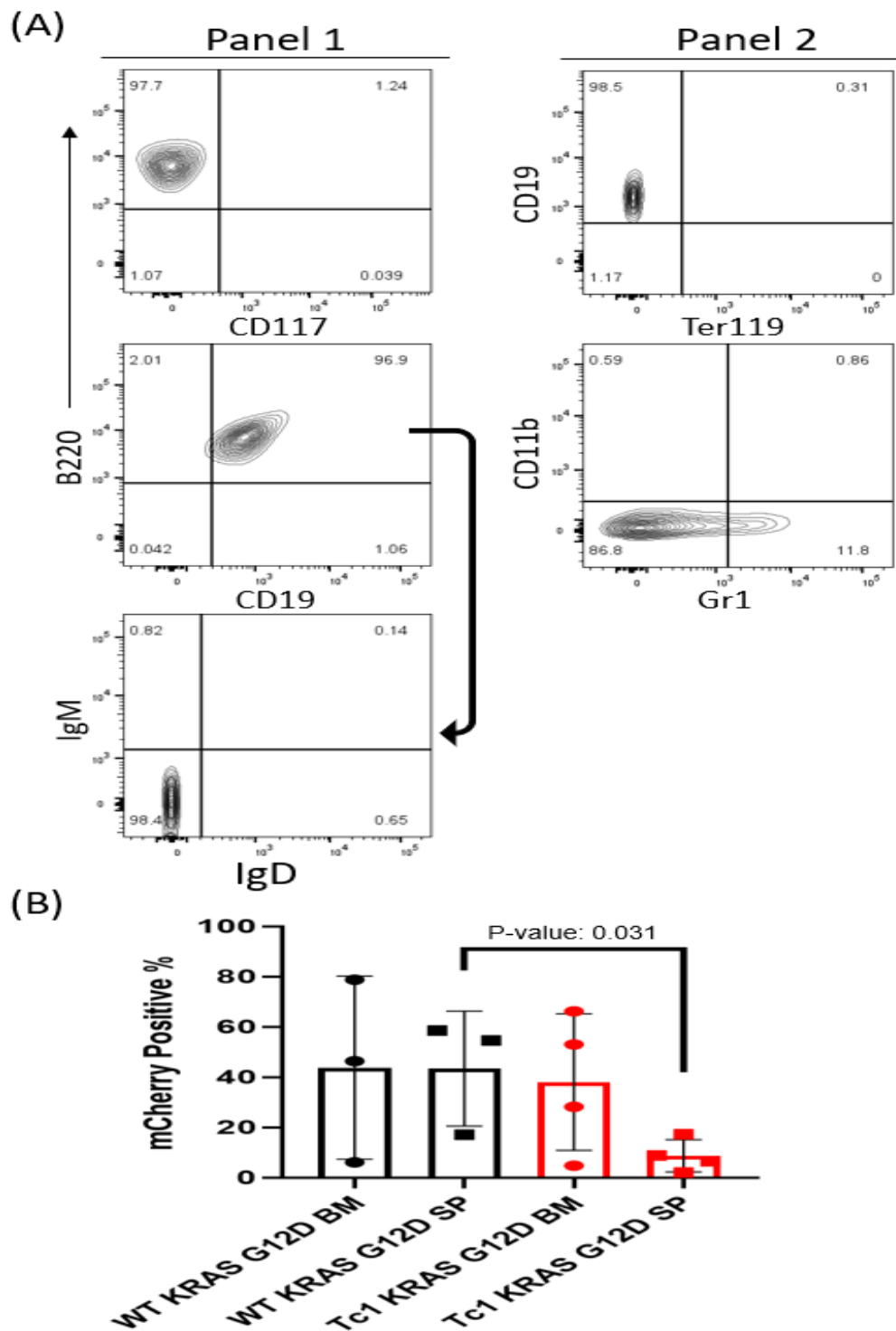


Figure 5. WT- $KRAS^{G12D}$ and Tc1- $KRAS^{G12D}$ bone marrow transplant sample representative phenotype strategy and mCherry positivity. (A) Representative flow cytometry gating strategy of BMT sample phenotype analysis with panel 1 and 2. (B) Flow cytometry analysis of mCherry expression in bone marrow (BM) and spleen (SP) samples collected from sub-lethally irradiated primary C57BL/6J recipient mice injected with 2×10^6 WT- $KRAS^{G12D}$ ($n = 3$) or Tc1- $KRAS^{G12D}$ ($n = 4$) cells.

Phenotype analysis revealed mCherry expression within bone marrow and spleen samples collected from the recipient mice transplanted with the WT-

KRAS^{G12D} or Tc1-*KRAS*^{G12D} cell lines (Fig. 5B). The mCherry expression was variable, which was likely due to the aggressiveness of the cell lines and the time to engraftment within the bone marrow and spleen. A significant difference could only be determined upon mCherry expression between WT-*KRAS*^{G12D} and Tc1-*KRAS*^{G12D} engrafted spleen (P-value: 0.031). Interestingly, we also observed a lower burden in the spleen of recipient animals engrafted with the Tc1-*KRAS*^{G12D} cells in the secondary BMT, confirming what we observed in the initial BMT (Chapter 3a). The reason for the lower burden is currently unknown. However, mCherry expression within bone marrow and spleen confirms successful engraftment of the WT-*KRAS*^{G12D} and Tc1-*KRAS*^{G12D} cell lines into recipient sub-lethally irradiated C57BL/6J mice.

Flow cytometry phenotype analysis of bone marrow and spleen samples collected from sub-lethally irradiated primary C57BL/6J recipient mice revealed mCherry positive samples had variable B cell marker expression, however, were mostly B220/CD19 positive with low CD117 and IgM positive expression (Fig. 6A). In comparison to the initial cell line phenotype, there was variable B220+/CD19- expression between both WT and Tc1-*KRAS*^{G12D} recipient replicates, with a significant difference between recipient WT-*KRAS*^{G12D} bone marrow and Tc1-*KRAS*^{G12D} spleen. Additionally, there was increased B220/CD19 positive expression observed in WT-*KRAS*^{G12D} recipient bone marrow and spleen, in comparison to the initial cell line phenotype. There was also significantly different expression of B220/CD19 positivity between WT bone marrow and Tc1 bone marrow/spleen samples, as well as between WT-*KRAS*^{G12D} spleen and Tc1-*KRAS*^{G12D} bone marrow (Fig. 6A). None to very low expression of IgD/IgM was observed in the B220/CD19 positive population. There was also very low expression of myeloid markers Gr1 and CD11b observed post-transplant, with no erythroid lineage marker Ter119 positive expression (Fig. 6B).

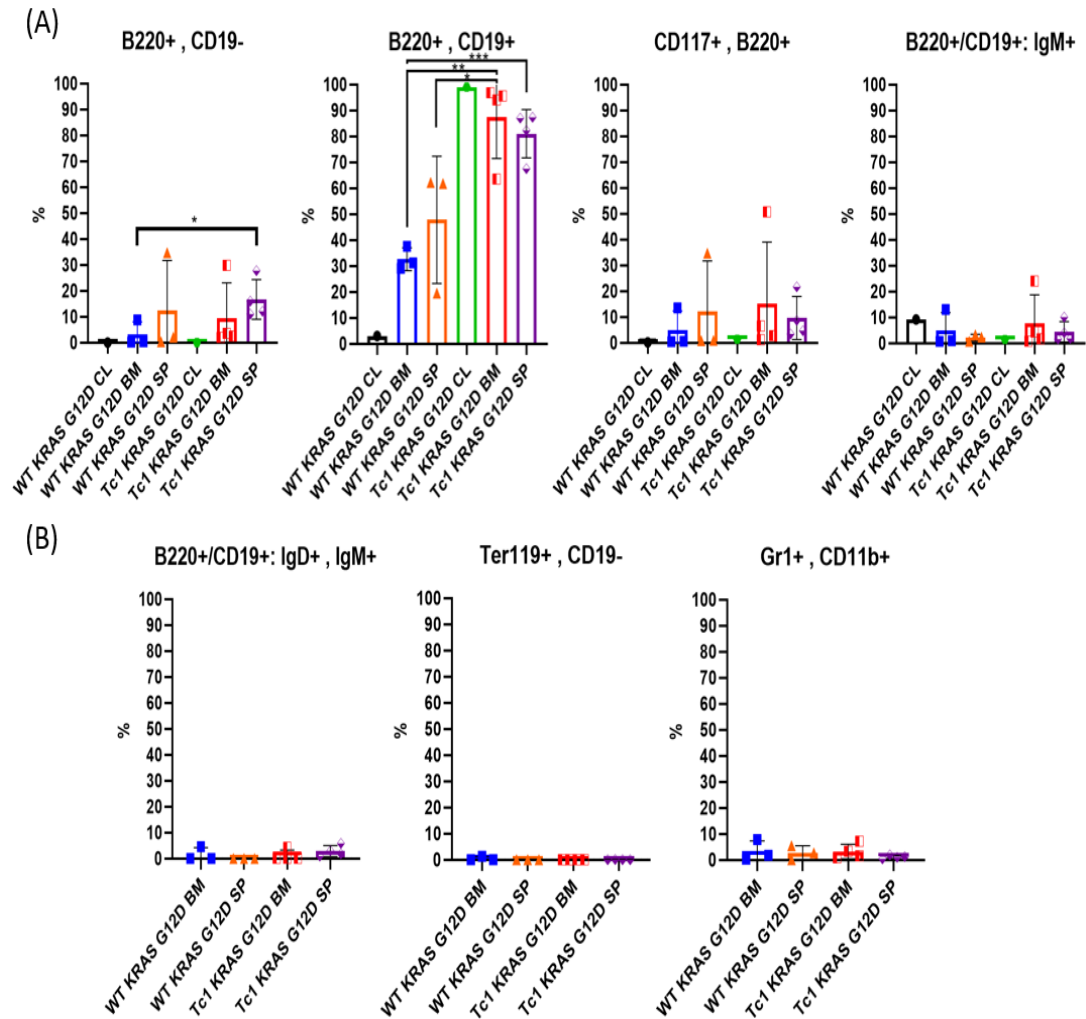


Figure 6. WT-*KRAS*^{G12D} and Tc1-*KRAS*^{G12D} bone marrow transplant phenotype. (A) Flow cytometry phenotype analysis of bone marrow (BM) and spleen (SP) samples from primary C57BL/6J recipient mice transplanted with WT-*KRAS*^{G12D} (n= 3) or Tc1-*KRAS*^{G12D} cell lines (n=4), compared to initial cell line (CL) phenotype. (B) Extended phenotype analysis of with IgD, Ter119, Gr1 and CD11b. (* P < 0.05, ** P < 0.01, *** P < 0.001).

The increase of B220/CD19 expression in recipient tissue samples collected from transplanted mice indicated clonal selection had occurred, suggesting a higher B220/CD19 expressing clone outcompeted other cells for engraftment. Future single cell analysis, as well as further investigation of the bone marrow microenvironment and haematopoietic stem cell compartment would likely provide insight into the phenotype shift upon engraftment. Overall, the WT-*KRAS*^{G12D} and Tc1-*KRAS*^{G12D} cell lines successfully engrafted into the recipient sub-lethally irradiated C57BL/6J mice, based upon positive mCherry expression and phenotype analysis, which confirmed the engrafted population were B cell progenitors. Therefore,

we were able to successfully recapitulate DS-ALL *in vitro* and *in vivo* with the generation of the WT-*KRAS*^{G12D} and Tc1-*KRAS*^{G12D} cell lines.

Discussion:

To improve the outcomes for DS children who develop leukaemia, new non-toxic and effective therapeutics are urgently required. Kinases, like DYRK1A, are commonly investigated and targeted in cancer due to the disruptive effects kinase inhibition has on cellular fitness and has been extensively studied in brain tumour Epidermal Growth Factor Receptor (*EGFR*) inhibition and used in chronic myelogenous leukaemia with imatinib treatment (68-70). DYRK1A inhibition is a topic of interest for many diseases, including Alzheimer's (71), Down syndrome neurological disorder (72) and leukaemia (29, 30). In leukaemia, DYRK1A has been targeted previously with EHT1610, harmine and INDY (30, 73). However, Leucettinib inhibitors, such as Leucettinib-21 (74, 75), pose a novel and potentially less toxic and effective therapeutic avenue. In our models of DS-ALL, DYRK1A was proven to be a therapeutically targetable kinase (genetically by shRNA strategy and pharmacologically using DYRK1A inhibitors).

In this chapter, we developed human (DS-PER961 and DS-PER962) and mouse DS-ALL cellular models and tested novel therapeutic agents directed against DYRK1A kinase function. Notably, we believe DS-PER961 and DS-PER962 are the first human DS-ALL cell lines developed for research, thus providing crucial models for further DS-ALL investigation. Additionally, the murine models we developed incorporated a trisomy of an almost entire human chromosome 21 with the *KRAS*^{G12D} or *BCR-ABL1* mutations, to create the WT-*KRAS*^{G12D}, Tc1-*KRAS*^{G12D}, WT-*BCR-ABL* and Tc1-*BCR-ABL* cell lines. We utilised the colony forming unit assay and methylcellulose to develop these models, whilst assessing oncogenic cooperation between the Tc1 extra ch21 and *KRAS*^{G12D}/*BCR-ABL1* mutations. Cell line development coincided with characterisation of the bone marrow microenvironment and haematopoietic stem cell populations of the Tc1 mouse model and WT littermates. We concluded the bone marrow microenvironment was similar to WT, with no impact on MSC populations regardless of age (from 6 to 19

weeks of age); whether there would be differences before 6 weeks or after 19 weeks is currently unknown. Nevertheless, this suggests that trisomy 21, at least in the Tc1 model, does not confer drastic differences to the bone marrow microenvironment. Analysis of the HSC and MPP compartment confirmed trisomy 21 perturbs haematopoiesis with MPP1 and MPP2 populations significantly affected, as in the Ts1Rhr model (unpublished data from our laboratory). These new murine cell line models were characterised to identify them as Pro/Pre-B cell progenitors with the WT-*KRAS*^{G12D} and Tc1-*KRAS*^{G12D} cell lines used to successfully re-create DS-ALL *in vivo*. Phenotype analysis confirmed the *in vivo* models maintained a similar phenotype to the initial cell line phenotype during BMT and recipient mouse bone marrow and spleen engraftment. Notably, there was variability in expression of B cell markers, indicating clonal selection occurred. Future work by the laboratory will investigate the clonal selection observed in these experiments to obtain a deeper understanding of how it occurred. Together, these results confirmed we developed a reproducible model of DS-ALL, as shown for the Ts1/Cdkn2a-*KRAS*^{G12D} model (Chapter 2), but with a larger trisomy 21 (Tc1) and that incorporated known and relevant genetic alterations (7, 27).

Since we successfully developed DS-ALL models, we next used these murine and human *in vitro* DS-ALL cell lines and PDX DS01, DS02, DS03 and DS06 models to test therapeutic inhibition of the DYRK1A kinase. This was conducted with the inhibitors AM28, AM30, AM45, EHT1610 and Leucettinib-21, alongside the inactive isomer of Leucettinib-21. Notably, specificity of these inhibitors has previously been determined against the DYRK1A kinase (74-79). Our results confirmed that DYRK1A is a therapeutic target in DS-ALL, coinciding with previous reports done in non-DS-ALL cellular models (30), and that DS-ALL cells are sensitive to DYRK1A inhibition. The Leucettinib-21 inhibitor proved to be the most potent inhibitor of DYRK1A in our models. Interestingly, our PDX models were more sensitive to Leucettinib-21 treatment, than inhibition of DYRK1A with EHT1610, which has previously been reported as an effective inhibitor with potential application in DS-ALL treatment (30). Notably, Leucettinib-21 is currently in

phase 1 clinical trial to assess safety and tolerability in DS and Alzheimer's patients, thus if approved could provide an effective adaptation to current DS leukaemia treatment protocols (LEUCETTA - NCT06206824). We highlighted that Leucettinib-21 synergised with vincristine, and had an additive effect with dexamethasone, L-asparaginase, and with targeted therapeutics ruxolitinib (JAK1/2 inhibitor) and trametinib (MEK1/2 inhibitor). Thus, proposing Leucettinib-21 as an ideal inhibitor that could be added to current treatment strategies. Future work by the laboratory is now including combination therapeutic strategies using Leucettinib-21 with standard of care treatment *in vivo*, to continue investigating the efficacy of Leucettinib-21. Additionally, the laboratory will also investigate *in vivo* toxicity with treatment of Leucettinib-21 alone and in combination with standard of care, utilising alanine and aspartate aminotransferase markers of liver toxicity, conducted via readily available kit assays. Notably, this work will provide further insight into the adaptability of Leucettinib-21 to current treatment strategies.

Overall, we were able to successfully characterise the microenvironment of the Tc1 mouse model, whilst generating novel murine DS-ALL models. Moreover, we also successfully generated clinically relevant human models of DS-ALL and demonstrated the effectiveness of targeting DYRK1A within both murine and human DS-ALL models. Thus, we demonstrated the applicability of Leucettinib-21 as a novel DS-ALL therapeutic. Moving forward, the new models we developed in this chapter will facilitate the identification of novel ch21 genes and the investigation of the mechanisms altered by trisomy 21 (within and outside the DSCR), ultimately leading to the discovery of new therapeutic vulnerabilities in DS-ALL.

Chapter 4: Targeting trisomy 21 in the human DS-ALL cell lines

Introduction:

As DS-ALL is predisposed by trisomy of ch21 (7, 20), and since trisomy 21 is known to cooperate with additional somatic mutations that lead to leukaemia development (32), we were interested to find novel ch21 genes implicated in DS-ALL, using gene editing technology. Previously, *HMGN1* (31) and *DYRK1A* (29, 30) have been identified as key ch21 genes involved in leukaemogenesis. Notably, *DYRK1A* has been successfully targeted therapeutically in our DS-ALL models (Chapter 3a) and by other laboratories (29, 30), to highlight the efficacy in targeting ch21 genes in DS-ALL. Therefore, since these ch21 genes significantly impact leukaemia development, we believe there may be more genes that contribute to DS-ALL progression, with their roles yet to be uncovered. In identifying novel genes involved in DS-ALL development and maintenance, new therapeutic vulnerabilities may be uncovered that can be used to improve clinical outcomes for children with DS-ALL.

Many gene editing technologies have been developed in the past to conduct experiments to understand gene function, including zinc finger nucleases (ZFN) (80), transcription activator-like effector nucleases (TALEN) (81) and CRISPR-Cas9 (38), with adaptations made to alter their functions for specific research purposes, including gene expression regulation. Of these, the Cas9 protein when bound to a locus specific sgRNA can recognise and bind to the genomic DNA of a cell and cleave both strands, resulting in a double stranded break (38). Notably, the Cas9 protein has been modified via point mutations in RuvC1 (D10A) and HNH (H840A) nuclease sites to make them catalytically inactive, so that it can bind to DNA without cleaving it, and is known as nuclease-dead Cas9 (dCas9) (38, 82). This modification has enabled further adaptations, such as the implementation of CRISPR interference (CRISPRi), leading to optimised fusion of the Krüppel-associated box (KRAB) repressor to dCas9 (dCas9-KRAB) that is used to selectively repress gene expression (82-84). Alternatively, CRISPR activating

(CRISPRa) constructs have also been developed, such as dCas9-VP64, dCas9-VPR and dCas9-p300, which are used for gene transcription activation (85). In the case of DS-ALL and trisomy 21, ch21 gene overexpression is the target for correction, thus CRISPR repression constructs would be suited for ch21 gene investigation. Inducibility of such constructs is also desirable as it can allow for controlled time point gene repression, as well as reversibility of function after initial activation of the system. Inducibility of the dCas9-KRAB fusion construct has been observed with doxycycline (84), whilst inducibility of Cas9 has also been achieved with the mutated estrogen receptor (ER) (86). Thus, we hypothesised that these techniques could be combined and applied to our DS-ALL research, through investigation of the ch21 genes responsible for DS-ALL development.

To investigate the role of ch21 genes in DS-ALL, we set out to use our human DS-ALL cell lines, DS-PER961 and DS-PER962, as models to screen for novel ch21 genes implicated in DS-ALL. To do so, we planned to use an inducible CRISPR gene repression tool I finished developing during my Honours project called ER-dCas9-KRAB. This CRISPR repression construct contains a dCas9 protein, that will target and bind to a specific gene via sgRNA binding (82) and is fused to a mutated 4-hydroxytamoxifen (4-OHT) inducible ER (86) and KRAB transcriptional repressor (83). We set out to integrate this construct within the human adeno-associated virus integration site 1 (AAVS1) safe harbour locus (allows integration and stable transgene expression without adverse cellular effects (87)), from which, our ER-dCas9-KRAB system would be constitutively expressed and sequestered in the cells cytoplasm (ER not induced). Thus, allowing us to test a variety of sgRNA directed to ch21 genes in an inducible manner. As such, the repression function of the construct can be used to target any gene in a controlled on/off method, via the presence or absence of 4-OHT (Fig. 1). Utilising this construct's ability to bind to a specific gene and repress its expression in an inducible manner, within the DS-ALL cell lines, would allow us to target overexpressed ch21 genes and assess the impact of correcting gene overexpression on leukaemogenesis.

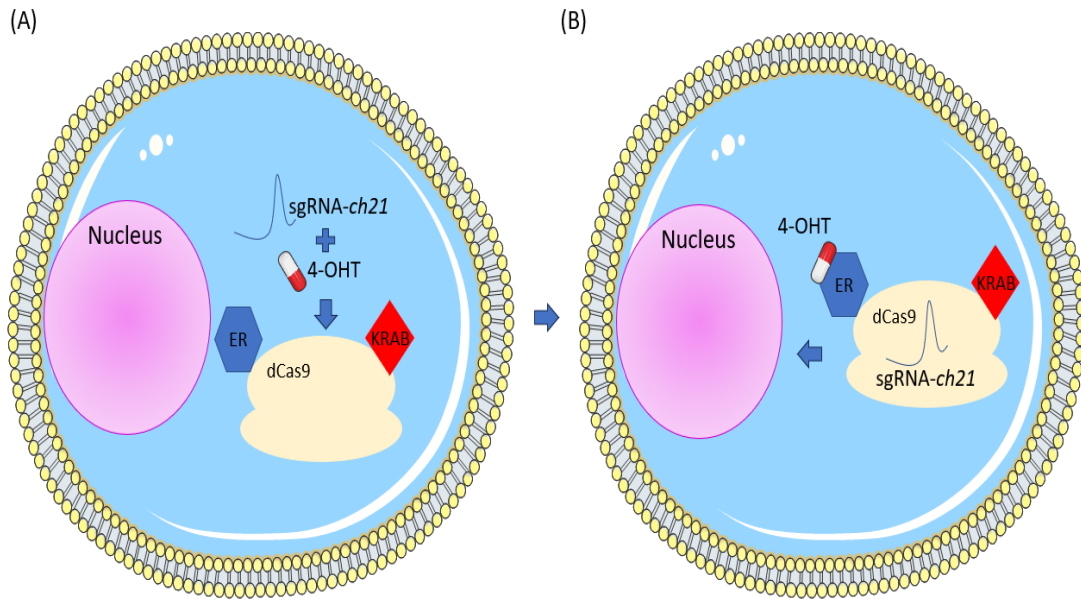


Figure 1. Inducible translocation of ER-dCas9-KRAB. (A) ER-dCas9-KRAB protein sequestered in the cell cytoplasm and exposed to delivery of sgRNA directed to ch21 genes (sgRNA-*ch21*), coinciding treatment with 4-OHT. (B) The ch21 directed sgRNA and dCas9 form a complex together and 4-OHT binds to the mutated ER, allowing translocation of the ER-dCas9-KRAB construct from the cytoplasm into the nucleus, allowing targeted ch21 gene repression. Created partly with Servier Medical Art (smart.servier.com).

Implementation of CRISPR technology requires a methodology that efficiently delivers the construct to the cells, and in our strategy, integrates it into the genome to allow constitutive expression of ER-dCas9-KRAB. Firstly, we needed to establish stable DS-ALL cell line clones, incorporating and expressing the ER-dCas9-KRAB construct. Then secondly, incorporate sgRNA directed to ch21 genes of interest in our modified DS-ALL cells, alongside 4-OHT treatment, and observe the impact of specific ch21 gene repression on DS-ALL. To implement this strategy and screen ch21 genes, we needed to initially optimise transfection/transduction protocols to deliver the ER-dCas9-KRAB construct to the cells. In parallel, we tested lentiviral transduction, lipofection and electroporation in our human DS-ALL cell lines. Overall, lipofection and transduction provided very low efficiencies, however we were able to successfully electroporate our DS-PER961 and DS-PER962 cell lines and assessed our ability to incorporate the ER-dCas9-KRAB construct into the DS-PER961 cell line.

Methods:

Cell culture:

The DS-PER961 and DS-PER962 DS-ALL cell lines were cultured in RPMI1640 media (Gibco) supplemented with 2 mM L-glutamine (Gibco), 50 μ M 2-mercaptoethanol (Sigma-Aldrich), penicillin (100 U/mL)-streptomycin (100 μ g/mL) (Thermo Fisher Scientific), 1% non-essential amino acids (MP Biomedicals), 1 mM sodium pyruvate (MP Biomedicals) and 20% of heat inactivated FCS (Cell Sera Australia). The DS-PER961 cell line was cultured with recombinant human IL-7 (10 ng/mL, PeproTech and STEMCELL Technologies), and DS-PER962 cells with recombinant human FLT3-ligand (10 ng/mL, PeproTech and STEMCELL Technologies). Cell line cultures were incubated at 37°C, with 5% CO₂ and 95% relative humidity (Heracell VIOS 160i incubator).

Plasmid constructs:

Plasmid constructs viewed with SnapGene Version 5.0.4.

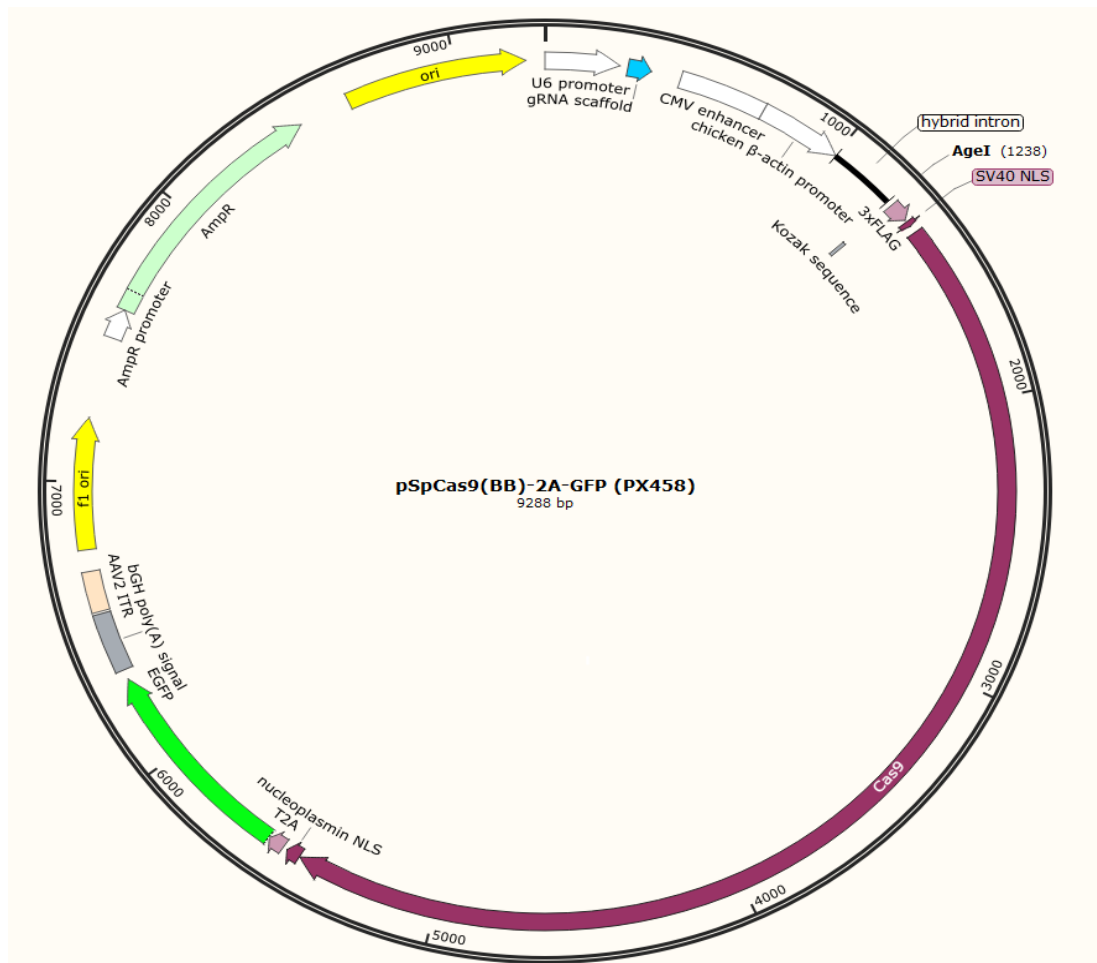


Figure 2. pSpCas9(BB)-2A-GFP (PX458) (Addgene). CRISPR-Cas9 construct containing green fluorescent protein (GFP) for determining transfection efficiency.



Figure 3. pSpCas9(BB)-2A-GFP-AAVS1_sgRNA-2 (PX458_sgRNA-2). Cas9 construct containing GFP and AAVS1_sgRNA-2 (Sequence: GTCACCAATCCTGTCCCTAG). This construct was generated, with functional validation via T7 endonuclease assay, during my Honours project; sgRNA-2 was the most efficient with the highest predicted specificity.

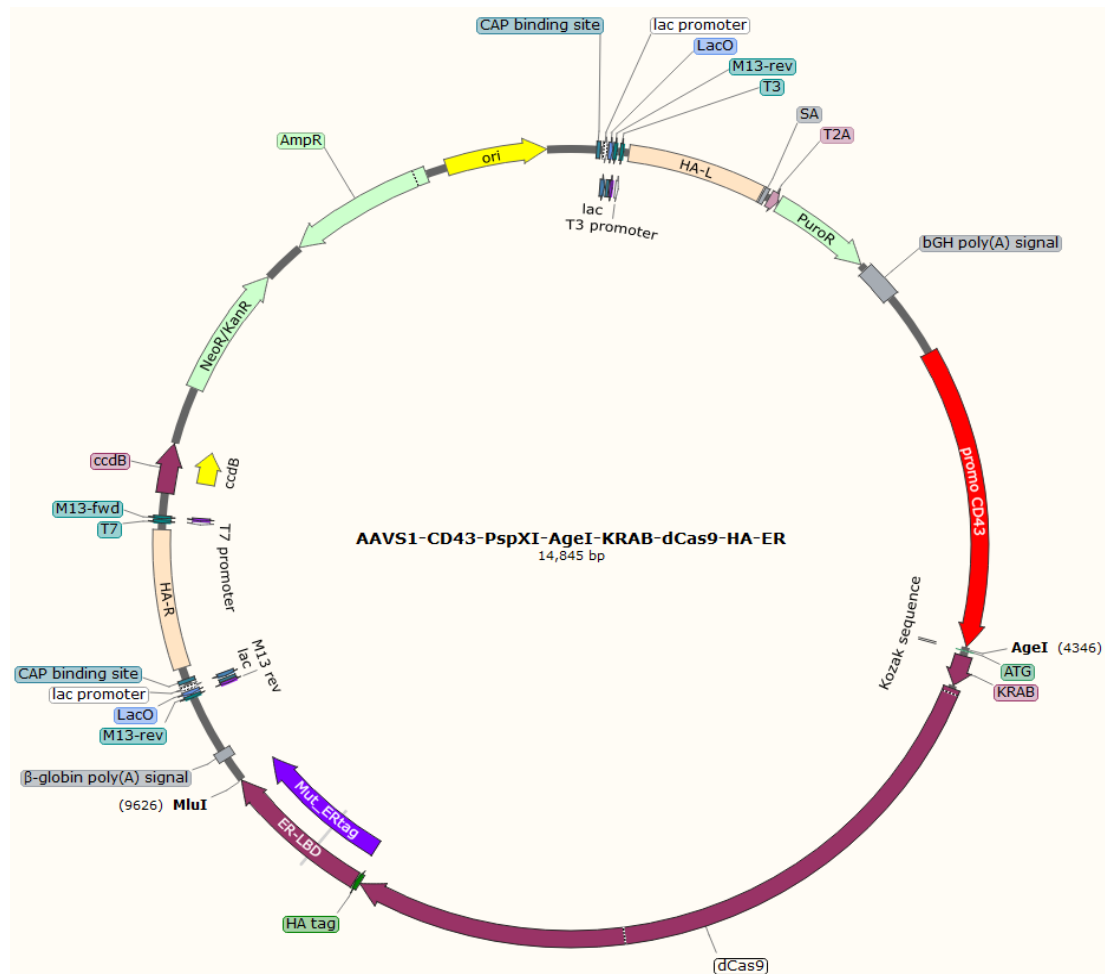


Figure 4. ER-dCas9-KRAB (AAVS1-CD43-PspXI-AgeI-KRAB-dCas9-HA-ER) construct. ER-dCas9-KRAB CRISPR repression construct containing AAVS1 locus directed left and right homology arms (HA-L/HA-R) to facilitate homology directed repair and Puromycin resistance gene (PuroR) for antibiotic selection.

Lentiviral transduction optimisation:

The DS-PER961 and DS-PER962 cell lines were transduced with lentiviral particles from the FUW-Luc-mCherry-puro vector, previously prepared by our laboratory (32), that expresses mCherry in successfully transduced cells. DS-PER961 and DS-PER962 cells were plated at 5×10^5 per 100 μL of culture media in a 96 well plate and transduced following the conditions in Table 1, including addition of 8 $\mu\text{g}/\text{mL}$ of hexadimethrine bromide (Polybrene - Pb) (Sigma-Aldrich) to attempt to increase transduction efficiency. Non-transduced (NT) cells did not have virus added, whilst only Pb was added to Pb controls (DS-PER961 Pb and DS-PER962 Pb). Cells were mixed inside the culture well and were incubated overnight at 37°C , with 5% CO_2 and 95% relative humidity. The following day, cells were harvested and washed with

2% FCS/PBS via centrifugation to remove lentiviral particles and were resuspended in fresh culture media to allow for normal culture conditions. Cells were incubated for 48 hours, 8 and 21 days, from which mCherry expression was assessed with flow cytometry at each time point, with Sytox Blue (Invitrogen) viability stain (1/4000 dilution in 2% FCS/PBS) to assess cell viability post transduction, using the BD LSRFortessa™ X-20 flow cytometer. All flow cytometry data generated was analysed with FlowJo software (Version 10.9.0, BD Biosciences).

Further lentiviral transduction optimisation was conducted by transducing the DS-PER962 cell line (5×10^5 in 100 μ L of culture media) with lentiviral particles and the addition of Pb (8 μ g/mL) and varying concentrations (5-10 μ g/mL) of protamine sulphate (PS) (Sigma-Aldrich) to assess if its addition would increase transduction efficiency, according to Table 2. Post transduction cells were incubated overnight at 37°C, with 5% CO₂ and 95% relative humidity. The following day, cells were harvested and washed via centrifugation to remove lentiviral particles and were resuspended in fresh culture media. Cells were then incubated for 48 hours, from which mCherry expression was then assessed by flow cytometry with Sytox Blue viability stain (1/4000 dilution in 2% FCS/PBS), using the BD LSRFortessa™ X-20 flow cytometer.

Condition	Volume of Virus (μL)	Polybrene (Pb 8 $\mu\text{g}/\text{mL}$)
DS-PER961 NT	-	-
DS-PER961 Pb	-	Yes
DS-PER961 1	1	No
DS-PER961 2	2	No
DS-PER961 5	5	No
DS-PER961 5 Pb	5	Yes
DS-PER962 NT	-	-
DS-PER962 Pb	-	Yes
DS-PER962 1	1	No
DS-PER962 2	2	No
DS-PER962 5	5	No
DS-PER962 5 Pb	5	Yes

Table 1. DS-PER961 and DS-PER962 lentiviral transduction parameters. Details the volume of virus delivered (μL) and if Pb (8 $\mu\text{g}/\text{mL}$) was added per condition (Yes/No). NT: non-transduced.

Condition	Volume of Virus (μL)	Polybrene (Pb 8 $\mu\text{g}/\text{mL}$)	Concentration of PS ($\mu\text{g}/\text{mL}$)
DS-PER962 NT	-	-	-
DS-PER962 Lenti Only	5	No	-
DS-PER962 Lenti Pb	5	Yes	-
DS-PER962 Lenti PS 5	5	No	5
DS-PER962 Lenti PS 8	5	No	8
DS-PER962 Lenti PS 10	5	No	10

Table 2. DS-PER962 lentiviral transduction optimisation parameters with PS. Details the volume of virus delivered (μL), if Pb (8 $\mu\text{g}/\text{mL}$) was added (Yes/No) and the concentration of PS added per condition. NT: non-transduced.

Lipofection of DS-PER962 with Lipofectamine Stem:

Firstly, a total of 1×10^6 to 2×10^6 DS-PER962 cells were seeded into a single well of a 24 well cell culture plate. Lipofection/plasmid complexes were delivered to the cells following standard preparation protocol according to the Thermo Fisher Scientific Lipofectamine Stem protocol, to mix and prepare transfection complexes consisting of Lipofectamine Stem (Thermo Fisher Scientific), Opti-MEM media (Thermo Fisher Scientific) and the PX458 plasmid (GFP reporter plasmid). Transfection efficiency was tested with multiple dilutions/cell number combinations as detailed in Table 3, which were based upon the providers recommended procedure. Post transfection, cells were incubated for 48 hours at 37°C , with 5% CO_2 and 95% relative humidity. Transfection efficiency was then determined based upon the expression level of GFP 48 hours post transfection by flow cytometry analysis, including Sytox Blue viability stain (1/4000 dilution in 2% FCS/PBS), using the BD LSRFortessa™ X-20 flow cytometer.

Condition	Cell Number	DNA Amount (μg)	Lipofectamine Stem (μL)
DS-PER962 1M NT	1×10^6	-	-
DS-PER962 1M $1 \mu\text{g}$	1×10^6	1	-
DS-PER962 1M $5 \mu\text{L}$	1×10^6	-	5
DS-PER962 1M 500ng + $1 \mu\text{L}$	1×10^6	0.5	1
DS-PER962 1M 500ng + $2 \mu\text{L}$	1×10^6	0.5	2
DS-PER962 1M 500ng + $5 \mu\text{L}$	1×10^6	0.5	5
DS-PER962 1M $1 \mu\text{g}$ + $1 \mu\text{L}$	1×10^6	1	1
DS-PER962 1M $1 \mu\text{g}$ + $2 \mu\text{L}$	1×10^6	1	2
DS-PER962 1M $1 \mu\text{g}$ + $5 \mu\text{L}$	1×10^6	1	5
DS-PER962 2M $1 \mu\text{g}$ + $1 \mu\text{L}$	2×10^6	1	1
DS-PER962 2M $1 \mu\text{g}$ + $2 \mu\text{L}$	2×10^6	1	2
DS-PER962 2M $1 \mu\text{g}$ + $5 \mu\text{L}$	2×10^6	1	5

Table 3. Lipofectamine Stem transfection conditions. Details the cell number used, amount of DNA (μg) and volume of Lipofectamine Stem (μL) reagent added per condition. NT: non-transfected.

Electroporation with the Neon Transfection System:

Electroporation of the PX458 plasmid DNA (GFP reporter plasmid) in the human DS-PER961 (within a 6 well plate) and DS-PER962 (within a 24 well plate) DS-ALL cell lines was conducted using the Neon Transfection System (Thermo Fisher Scientific, standard protocol). Electroporation was initially optimised by testing 29 pulse parameters (Table 4), whilst non-transfected (NT) controls were included for comparison and exposed to the same protocol without electroporation. Transfected cells were incubated for 48 hours at 37°C, with 5% CO₂ and 95% relative humidity post electroporation. Transfection efficiency was determined upon the expression level of GFP at 48 hours by flow cytometry analysis, including Sytox Blue viability stain (1/4000 dilution in 2% FCS/PBS), using the BD LSRFortessa™ X-20 flow cytometer.

Cell recovery and transfection efficiency was then further optimised through cell “pooling” experiments. Initially, 2x10⁵ DS-PER961 (within a 6 well plate) or DS-PER962 (within a 24 well plate) cells were electroporated using the Neon Transfection System (following standard protocol) with optimised pulse parameters, to transfect PX458 plasmid DNA, with cells pooled into one well post electroporation. For comparison, cells were pooled to a total cell number of 6x10⁵, 1.2x10⁶ and 2x10⁶ cells per well. Transfected and pooled cells were then incubated for 48 hours at 37°C, with 5% CO₂ and 95% relative humidity, from which GFP expression was assessed with flow cytometry.

Co-transfection with PX458 and pLuc-mCherry:

Co-transfection optimisation within the DS-PER961 and DS-PER962 cell lines with PX458 (GFP reporter plasmid - 9.2 kilobases) and pLuc-mCherry (mCherry reporter plasmid - 9.5 kilobases) was performed using the Neon Transfection System, following standard protocol, utilising the 100 µL Neon Transfection pipette tip variant that allows 2x10⁶ cells to be transfected per electroporation. Plasmid was prepared in transfection reagent with two plasmid dilutions tested: 1 µg total of PX458 and pLuc-mCherry in ratio (0.5 µg and 0.5 µg respectively) or 2 µg total of plasmid (1 µg of PX458 and 1 µg pLuc-mCherry) per 2x10⁵ transfected cells (2x10⁶ total cells transfected).

Post transfection, cells were incubated for 48 hours at 37°C, with 5% CO₂ and 95% relative humidity, from which they were washed, stained with Sytox Blue (1/4000 dilution in 2% FCS/PBS) and analysed for GFP/mCherry expression with flow cytometry using the BD FACSAria™ III Cell Sorter.

Co-transfection with pSpCas9(BB)-2A-GFP-AAVS1_sgRNA-2 and the ER-dCas9-KRAB construct:

Co-electroporation of the DS-PER961 cell line with plasmids pSpCas9(BB)-2A-GFP-AAVS1_sgRNA-2 and the ER-dCas9-KRAB construct using the Neon Transfection System with the 100 µL Neon Transfection pipette tip variant. A total of 44x10⁶ DS-PER961 cells were transfected with 1 µg of plasmid DNA dilution (0.385 µg of pSpCas9(BB)-2A-GFP-AAVS1_sgRNA-2 and 0.615 µg of the ER-dCas9-KRAB construct) per 2x10⁵ transfected cells. Post transfection, cells were incubated for 48 hours at 37°C, with 5% CO₂ and 95% relative humidity, from which they were washed, stained with Sytox Blue (1/4000 dilution in 2% FCS/PBS), and underwent FACS based upon GFP positivity using the BD FACSAria™ III Cell Sorter. Post cell sorting, the recovered cells were placed into liquid culture in fresh media at 37°C, with 5% CO₂ and 95% relative humidity.

Data analysis:

Data analysis was performed in GraphPad Prism (Version 8.4.3) and Microsoft Excel. All flow cytometry data was analysed with FlowJo Version 10.9.0.

Results:

Firstly, to integrate our ER-dCas9-KRAB construct into the genome of our human DS-PER961 and DS-PER962 cell lines, we needed to optimise a plasmid delivery protocol. In parallel, we assessed the efficacy of using lentiviral transduction, lipofection and electroporation on our human DS-ALL cell lines, to determine and optimise the most effective method of plasmid delivery.

Lentiviral transduction optimisation in the human DS-ALL cell lines.

We tested lentiviral transduction on the DS-PER961 and DS-PER962 cell lines utilising an mCherry expressing lentivirus construct, previously used by our laboratory (32). We assessed the effect on transduction efficiency through the addition of different amounts of lentivirus and addition of cationic polymer Pb at 8 µg/mL. Upon analysis of mCherry expression with flow cytometry 48 hours post transduction (Fig. 5), the DS-PER962 cell line had the highest efficiency with 5 µL of virus and addition of Pb, however very low transduction efficiency (<0.2%) was achieved across all conditions.

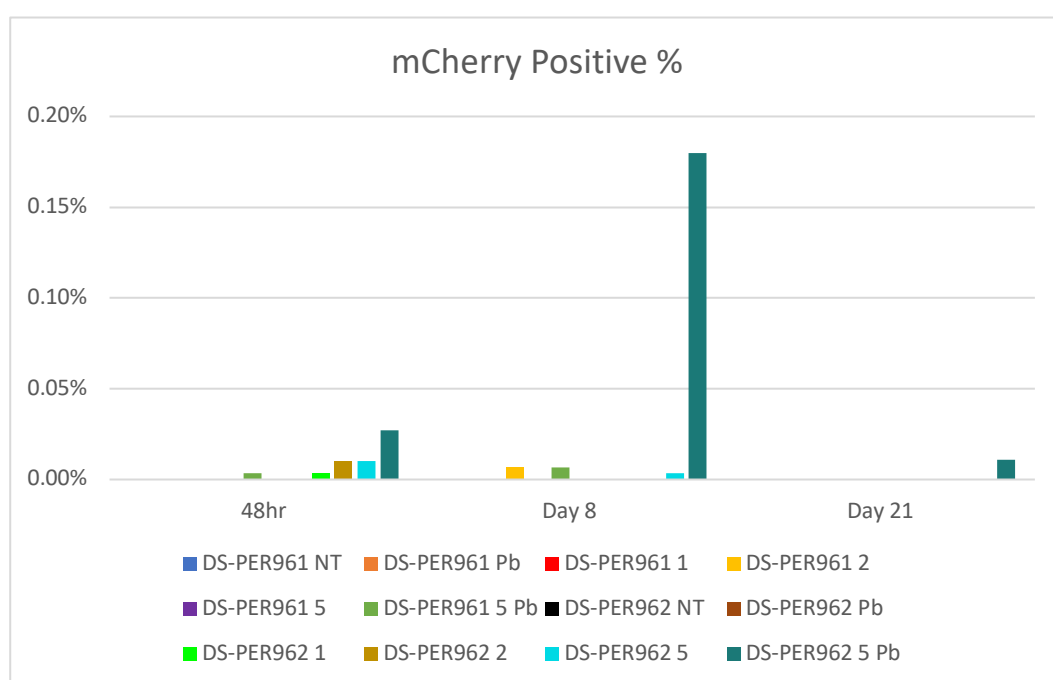


Figure 5. Lentiviral transduction of DS-PER961 and DS-PER962 cell lines. DS-PER961 and DS-PER962 mCherry expression 48 hours post lentiviral transduction with multiple virus volumes (1 µL (1), 2 µL (2) or 5 µL (5)) and the addition of Pb (8 µg/mL). NT: non-transduced.

To try to improve transduction efficiency, we tested the addition of the cationic polymer PS since it has been demonstrated as an effective alternative to Pb (88-90). This was performed in the DS-PER962 cell line alone, since it was the most efficiently transduced, comparing the addition of 5 µg/mL, 8 µg/mL or 10 µg/mL of PS, alongside 5 µL of lentivirus (Fig. 6).

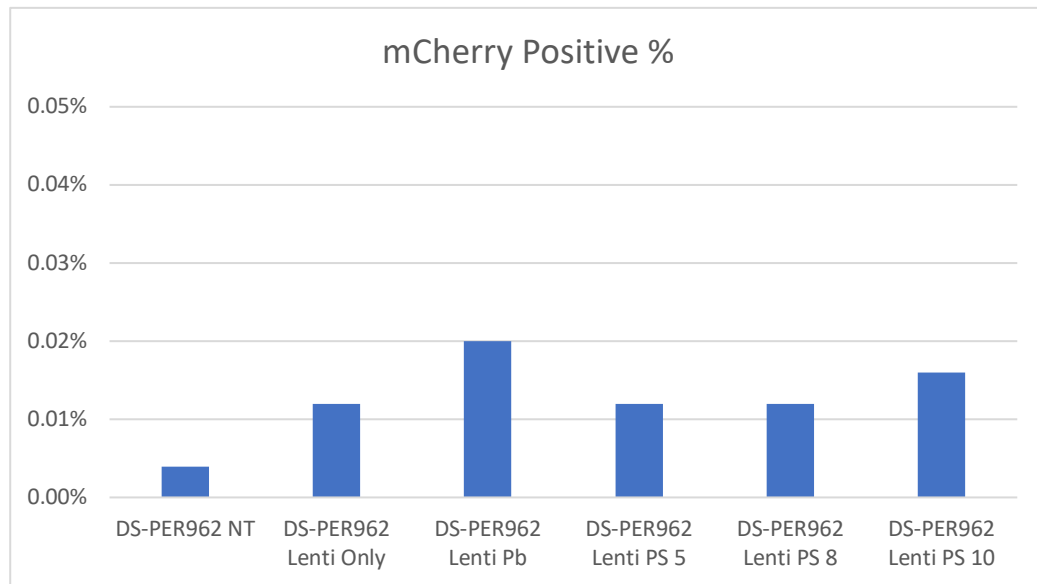


Figure 6. DS-PER962 lentiviral transduction optimisation test with PS. DS-PER962 lentiviral transduction optimisation with the addition of varying concentrations (5 $\mu\text{g}/\text{mL}$ (5), 8 $\mu\text{g}/\text{mL}$ (8) or 10 $\mu\text{g}/\text{mL}$ (10)) of PS with 5 μL of lentivirus (Lenti) in comparison to the addition of Pb. NT: non-transduced.

Addition of PS did not improve transduction efficiency, with the control 8 $\mu\text{g}/\text{mL}$ of Pb (DS-PER962 Lenti Pb) having the highest efficiency (0.02%) in comparison to all other conditions (Fig. 6). Overall, very low transduction efficiency was achieved in the DS-PER961 and DS-PER962 cell lines using lentiviral transduction (Fig. 5, 6). Therefore, we did not pursue further optimisation of any transduction methodology.

Lipofection optimisation in the human DS-ALL cell lines.

Lipofection efficiency was assessed in the DS-PER962 cell line with Lipofectamine Stem reagent, transfecting the PX458 plasmid (GFP reporter plasmid). Transfection efficiency was determined based upon GFP expression which was analysed by flow cytometry 48 hours post transfection (Fig. 7).

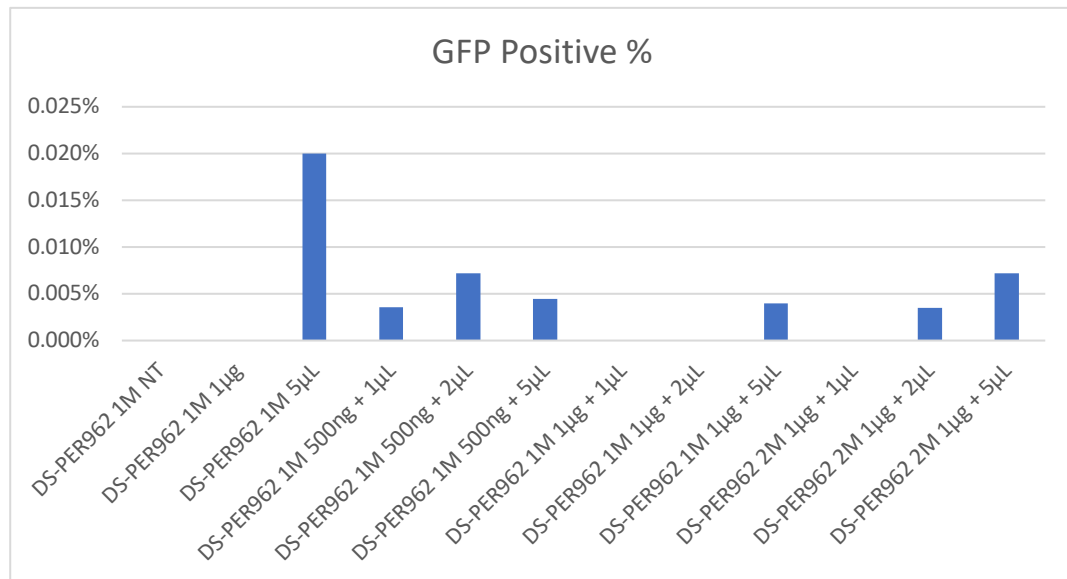


Figure 7. Transfection with Lipofectamine Stem in DS-PER962.

Lipofection optimisation with Lipofectamine Stem reagent, comparing transfection efficiency between two total cell amounts (1×10^6 (1M) or 2×10^6 (2M) cells), two amounts of PX458 plasmid DNA (500 ng or 1 µg) with multiple volumes of Lipofectamine Stem reagent (1, 2 or 5 µL). NT: non-transfected.

Upon analysis, a very low transfection efficiency (<0.01%) was achieved for all lipofection conditions including plasmid DNA, since the control without DNA added had the highest GFP expression (Fig. 7). Thus, highlighting the poor transfection potential this methodology provided. Overall, lipofection efficiencies with Lipofectamine Stem were lower than the lentiviral transduction efficiencies observed, therefore lipofection plasmid delivery methods were deemed unsuitable for delivering the ER-dCas9-KRAB construct into the human DS-ALL cell lines.

Electroporation optimisation in the human DS-ALL cell lines.

Coinciding lentiviral transduction and lipofection, we tested electroporation with the Neon Transfection System on the DS-PER961 and DS-PER962 cell lines, with multiple transfection parameters to optimise efficiency with the PX458 Cas9-GFP reporter plasmid (Table 4). Transfection efficiency was determined by GFP positive expression 48 hours post electroporation, which was detected via flow cytometry following the gating strategy outlined in Figure 8.

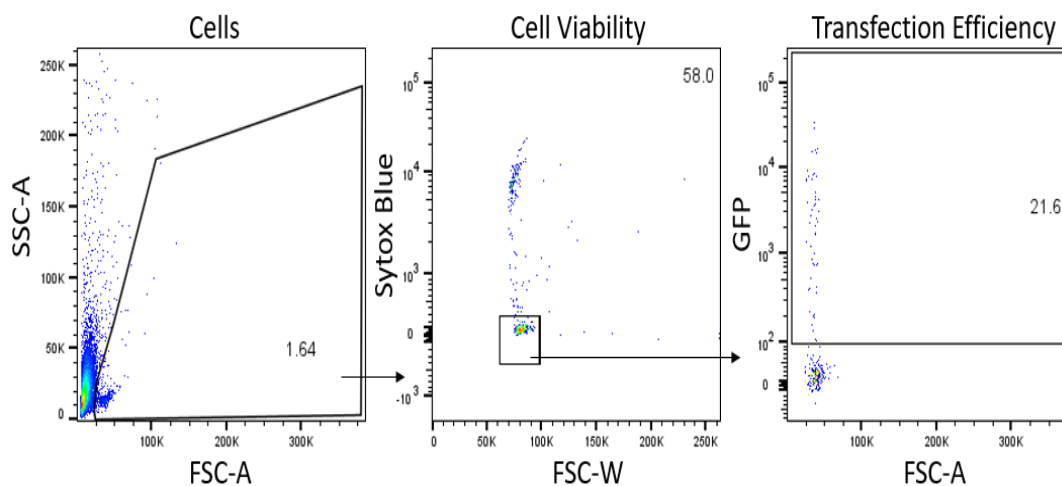


Figure 8. Flow cytometry gating strategy to determine GFP expression post electroporation. Cells were initially gated upon SSC-A and FSC-A, followed by cell viability with live single cells gated upon negative Sytox Blue expression and FSC-W. Transfection efficiency determined by gating GFP positive cells.

Cond	Cell Line	Pulse Voltage	Pulse Width	Pulse Number	Results			
					Cells	Cell Viability	Efficiency	Cell Number
1	DS-PER961	0	0	0	57.50%	76.60%	0.220%	193.8
2	DS-PER961	1800	20	1	4.58%	43.10%	19.000%	750.1
3	DS-PER961	1850	20	1	4.92%	42.50%	23.400%	978.6
4	DS-PER961	1900	20	1	3.29%	48.10%	10.000%	316.5
5	DS-PER961	1800	10	3	8.83%	66.90%	41.400%	4891.2
6	DS-PER961	1900	10	3	5.87%	55.00%	35.800%	2311.6
7	DS-PER962	0	0	0	74.80%	91.10%	0.000%	0.0
8	DS-PER962	1400	20	1	26.70%	63.20%	0.160%	54.0
9	DS-PER962	1500	20	1	14.20%	41.40%	1.100%	129.3
10	DS-PER962	1600	20	1	6.20%	26.20%	8.200%	266.4
11	DS-PER962	1800	20	1	2.60%	77.30%	7.170%	288.2
12	DS-PER962	1850	20	1	1.11%	66.70%	15.300%	226.6
13	DS-PER962	1900	20	1	1.01%	79.20%	0.000%	0.0
14	DS-PER962	1700	20	1	3.81%	17.40%	13.400%	177.7
15	DS-PER962	1100	30	1	63.00%	86.20%	0.000%	0.0
16	DS-PER962	1200	30	1	47.80%	76.50%	0.093%	68.0
17	DS-PER962	1300	30	1	29.40%	68.80%	0.150%	60.7
18	DS-PER962	1400	30	1	14.50%	46.30%	1.080%	145.0
19	DS-PER962	1000	40	1	73.00%	87.00%	0.010%	12.7
20	DS-PER962	1100	40	1	54.50%	79.80%	0.028%	24.4
21	DS-PER962	1200	40	1	36.70%	75.70%	0.110%	61.1
22	DS-PER962	1100	20	2	50.10%	76.40%	0.029%	22.2
23	DS-PER962	1200	20	2	52.10%	79.90%	0.045%	37.5
24	DS-PER962	1300	20	2	29.00%	64.80%	0.170%	63.9

Table 4 (continued).

25	DS-PER962	1400	20	2	13.00%	43.80%	1.440%	164.0
26	DS-PER962	850	30	2	73.60%	86.00%	0.003%	4.3
27	DS-PER962	950	30	2	71.40%	85.50%	0.020%	24.4
28	DS-PER962	1050	30	2	57.70%	80.50%	0.061%	56.7
29	DS-PER962	1150	30	2	33.80%	67.60%	0.170%	77.7
30	DS-PER962	1300	10	3	29.00%	62.10%	0.120%	43.2
31	DS-PER962	1400	10	3	53.20%	78.70%	0.083%	69.5
32	DS-PER962	1500	10	3	34.50%	70.60%	0.130%	63.3
33	DS-PER962	1600	10	3	18.60%	44.00%	0.500%	81.8
34	DS-PER962	1800	10	3	1.64%	58.00%	21.600%	410.9
35	DS-PER962	1900	10	3	1.80%	53.70%	10.400%	201.1

Table 4. DS-PER961 and DS-PER962 electroporation parameter optimisation. Optimisation of electroporation within the DS-PER961 and DS-PER962 cells (cell line), including the electroporation parameters used per condition (cond: 1-35, pulse voltage, pulse width and pulse number) and the corresponding flow cytometry results (cells, cell viability, transfection efficiency (efficiency), and calculated cell number).

Table 4, depicts the flow cytometry results post electroporation per the conditions tested including the total number of GFP positive cells, calculated on the electroporation of 2×10^5 cells total (cell number). Upon testing 29 different electroporation parameters, we identified the optimal electroporation parameters for DS-PER961 and DS-PER962 cells as 1800V, a pulse width of 10 and 3 pulses (Table 4: condition 5 and 34). Notably, cell viability was not the highest achieved overall with these parameters but was deemed the most efficient based upon the number of transfected cells recovered: 4891 (DS-PER961) and 410 (DS-PER962) (Table 4). These optimised electroporation parameters were used for all following electroporation experiments.

Even though these parameters provided the highest number of successfully transfected cells, we wanted to further optimise and maximise the return of GFP positive cells. To overcome the challenge of cell viability post electroporation, we sought to optimise the cell recovery by pooling transfected cells in the same cell culture well, to the final densities of 6×10^5 , 1.2×10^6 or 2×10^6 cells per well. After 48 hours of incubation, GFP expression was assessed with flow cytometry and the calculated return of GFP positive cells was determined (Table 5, Fig. 9).

Cell Line	Pool Number	Pulse Voltage	Pulse Width	Pulse Number	Results			
					Cells	Cell Viability	Efficiency	Cell Number
DS-PER961 NT	200K	0	0	0	90.50%	90.90%	0.00%	0.0
DS-PER961	600K	1800	10	3	8.35%	62.60%	73.40%	23020.1
DS-PER961	1.2M	1800	10	3	12.10%	59.80%	73.30%	63646.1
DS-PER961	2M	1800	10	3	9.47%	47.80%	71.40%	64640.7
DS-PER962 NT	200K	0	0	0	90.10%	98.00%	0.00%	0.0
DS-PER962	600K	1800	10	3	3.17%	57.00%	16.60%	1799.7
DS-PER962	1.2M	1800	10	3	6.64%	45.80%	17.20%	6276.9
DS-PER962	2M	1800	10	3	10.00%	12.70%	23.00%	5842.0

Table 5. DS-PER961 and DS-PER962 pooling transfection optimisation. Results table comparing the effect of pooling DS-PER961 and DS-PER962 cells to 6×10^5 (600K), 1.2×10^6 (1.2M), or 2×10^6 (2M) cells per well post electroporation. GFP positive cells (cell number) calculated based upon the number of transfected cells per condition. NT: non-transfected (200K - 2×10^5).

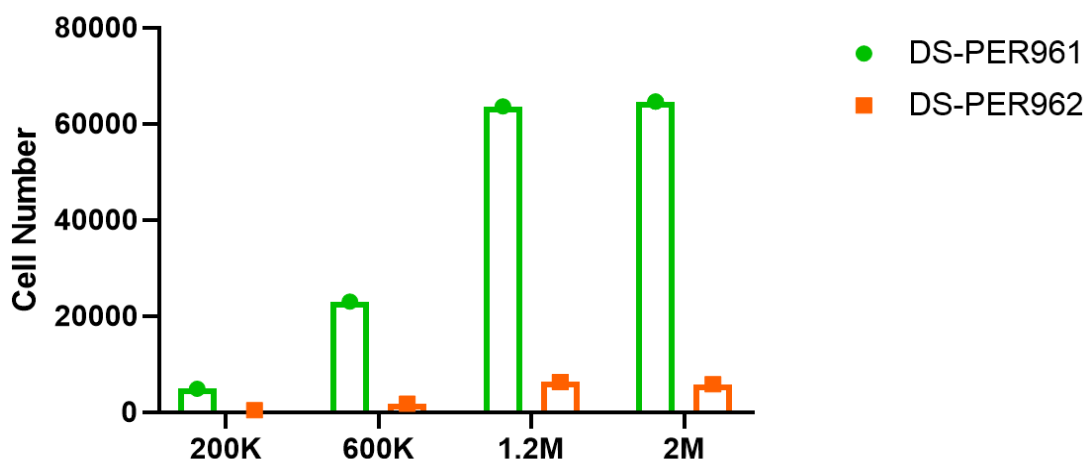


Figure 9. Total cell number of successfully transfected DS-PER961 and DS-PER962 cells from pooling transfection optimisation. Derived from Table 4, condition 5 and 34 cell number values (200K) and Table 5, cell number values.

Upon analysis with flow cytometry, it was revealed that pooling cells post electroporation for 48 hours increased the number of cells that were GFP positive (Table 5, Fig. 9). However, this was likely due to the higher number of cells transfected since cell viability for both DS-PER961 and DS-PER962

was not improved in comparison to Table 4, condition 5 (cell viability: 66.9%) and 34 (cell viability: 58%). Notably, transfection efficiency within the DS-PER961 cell line was improved upon cell pooling, indicating an improved cell uptake of plasmid DNA across all pooling conditions. Only a small increase in transfection efficiency was observed within the DS-PER962 cell line upon pooling to 2×10^6 cells (Table 4, 5). The greatest return of GFP positive cells came from pooling 2×10^6 DS-PER961 cells post transfection (Table 5: 64640 cells, Fig. 9). However, since transfection efficiency and cell viability of DS-PER961 and cell viability of DS-PER962 from pooling 2×10^6 cells was less than what was observed from pooling 1.2×10^6 cells, we determined pooling cells to 1.2×10^6 per well as the most optimal condition to improve overall efficiency of electroporation.

Overall, these results demonstrated that we could successfully transfect both the DS-PER961 and DS-PER962 human DS-ALL cell lines, using electroporation with the Neon Transfection System.

Co-transfection optimisation in DS-PER961 and DS-PER962.

Since it was proved possible to electroporate the DS-PER961 and DS-PER962 cell lines, we moved to the next stage of the project, where we attempted to optimise co-transfection of the DS-PER961 and DS-PER962 cell lines with two plasmids: PX458 and pLuc-mCherry. Transfection efficiency was determined by flow cytometry following the gating strategy outlined in Figure 10.

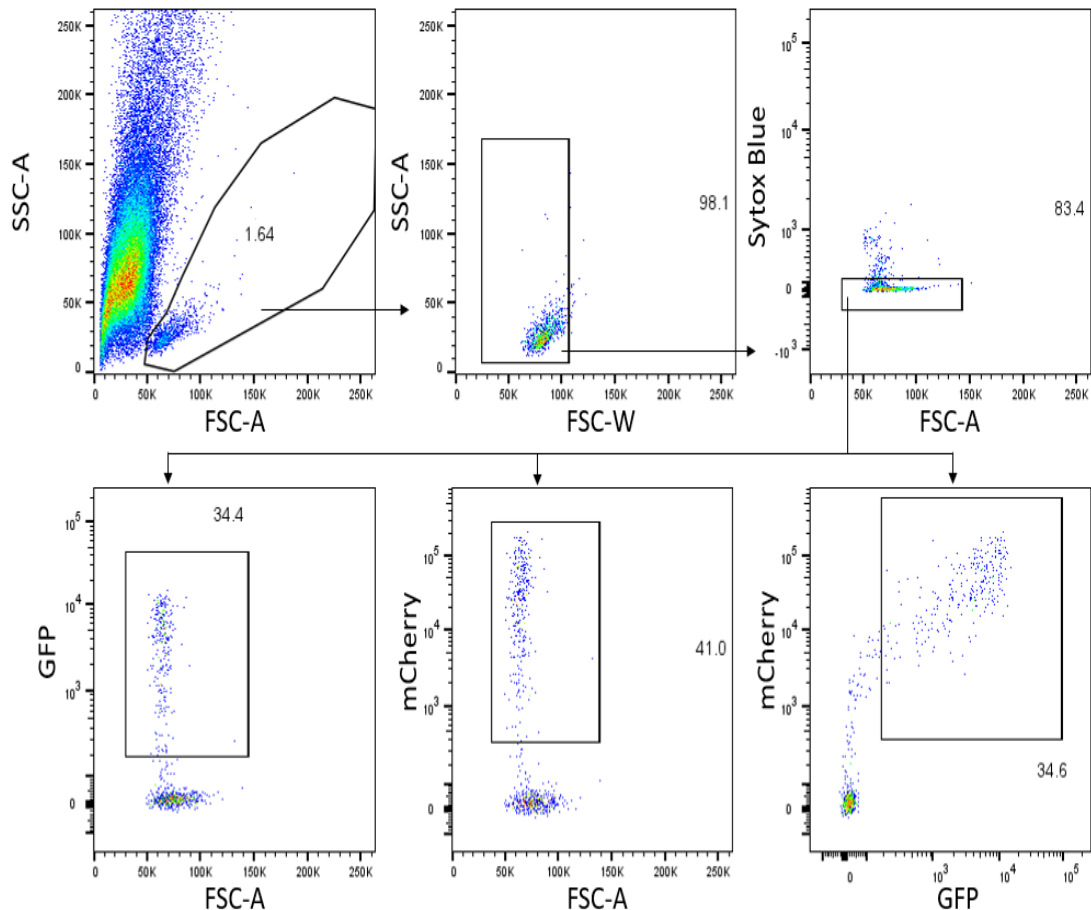


Figure 10. Flow cytometry gating strategy to determine efficiency of co-transfection in the DS-PER961 and DS-PER962 cell lines. Cells were gated upon SSC-A and FSC-A, single cells gated upon SSC-A and FSC-W, cell viability was determined with Sytox Blue negative expression, from which the GFP and mCherry expression was determined. Co-transfection efficiency was based upon mCherry/GFP co-expression.

In conducting co-transfection optimisation, DS-PER961 and DS-PER962 cells were transfected with two separate plasmid dilutions. The first being a 1 μg total plasmid dilution ratio between equal amounts of PX458 and pLuc-mCherry (GFP mCherry Ratio), and the second being a 2 μg total plasmid dilution consisting of 1 μg of each plasmid (GFP 1 μg mCherry 1 μg) (Table 6).

Controls	Results					
	Cells	Single Cells	Cell Viability	Transfection Efficiency GFP	Transfection Efficiency mCherry	
DS-PER961 GFP Only	7.61%	100%	74.40%	19.60%	0%	
DS-PER961 mCherry Only	3.41%	99.40%	100%	0%	34.30%	
Condition	Results					
	Cells	Single Cells	Cell Viability	Transfection Efficiency Co-T GFP	Transfection Efficiency Co-T mCherry	Transfection Efficiency Co-T GFP/mCherry
DS-PER961 GFP mCherry Ratio	4.14%	99.60%	87.40%	28.50%	46.90%	29.1%
DS-PER961 GFP 1 µg mCherry 1 µg	1.64%	98.10%	83.40%	34.40%	41%	34.6%
DS-PER962 GFP mCherry Ratio	0.40%	89.40%	61.90%	6.25%	8.48%	6.25%
DS-PER962 GFP 1 µg mCherry 1 µg	0.43%	91.40%	76.30%	0.67%	1%	0.67%

Table 6. Co-transfection of DS-PER961 and DS-PER962 with PX458 and pLuc-mCherry. Table of results for co-transfection of DS-PER961 and DS-PER962 cell lines with PX458 and pLuc-mCherry plasmids, testing two plasmid dilutions: GFP mCherry Ratio and GFP 1 µg mCherry 1 µg.

Both plasmid dilutions were able to be successfully transfected into the DS-PER961 and DS-PER962 cell lines, with the highest efficiency of co-transfection overall in the DS-PER961 cell line (GFP mCherry Ratio: 29.1% GFP/mCherry co-expression, GFP 1 µg mCherry 1 µg: 34.6% GFP/mCherry co-expression) (Table 6). Since DS-PER961 was the most efficient cell line to co-transfect, we decided to try and integrate the ER-dCas9-KRAB construct into the genome of this cell line only.

To achieve this, we sought to co-transfect the DS-PER961 cell line with PX458_sgRNA-2 and the ER-dCas9-KRAB plasmids, utilising the Neon Transfection System, with the optimised electroporation parameters and the strategy outlined in Figure 11.

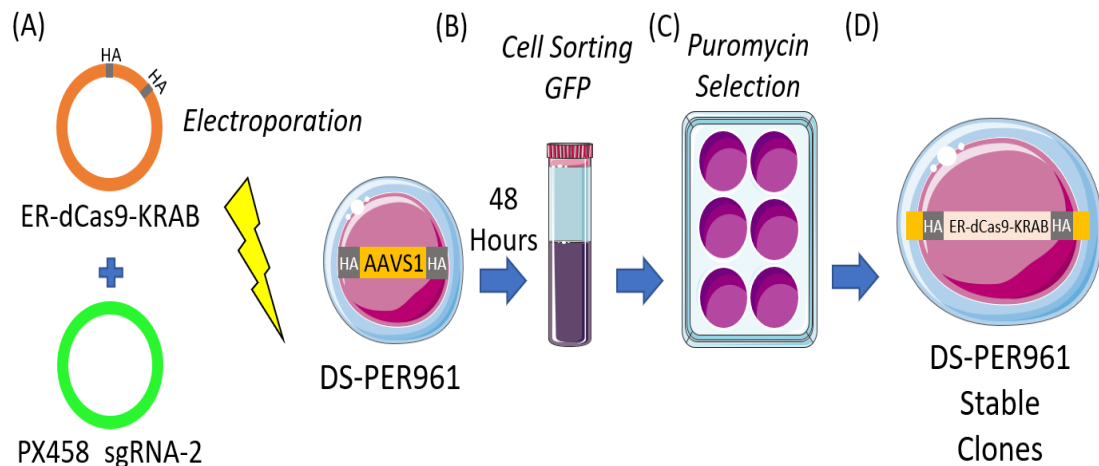


Figure 11. ER-dCas9-KRAB genome integration strategy. (A) Co-transfection strategy of the DS-PER961 cell line, utilising electroporation with the ER-dCas9-KRAB and PX458_sgRNA-2 plasmids. PX458_sgRNA-2 Cas9 protein will recognise, bind, and cleave the AAVS1 locus for integration of ER-dCas9-KRAB. DNA cleavage results in a double stranded break that then facilitates homology directed repair between the homology arms (HA) of the ER-dCas9-KRAB plasmid and the AAVS1 locus of DS-PER961. (B) 48 hours post electroporation; cells are sorted for GFP positive expression then dispensed into liquid culture. (C) Cells undergo puromycin selection (ER-dCas9-KRAB construct contains Puromycin resistance gene (Figure 4)) to obtain stable DS-PER961 clones constitutively expressing ER-dCas9-KRAB (D). Created partly with Servier Medical Art (smart.servier.com).

The PX458_sgRNA-2 construct was developed during my Honours degree, whereby sgRNA-2 directs the PX458 Cas9 protein to the AAVS1 safe harbour locus, from which it will bind and cleave the DNA resulting in a double stranded break. Opening the AAVS1 locus, via Cas9 mediated double stranded break, allows integration of the ER-dCas9-KRAB construct into the cells genome via homology directed repair. This is facilitated by the ER-dCas9-KRAB plasmid homology arms designed for the AAVS1 locus (Fig. 4, 11A). To detect successful transfection, the PX458-sgRNA-2 vector contains GFP, thus FACS is used to isolate GFP positively expressing DS-PER961 cells, that are placed back into liquid culture (Fig. 11B). Puromycin selection is then used to positively select for DS-PER961 clones that have successfully integrated the ER-dCas9-KRAB construct into their genome, as it contains a Puromycin resistance gene (Fig. 11C). Once stable clones are obtained (Fig. 11D), we would then be able to proceed with screening ch21 genes of interest.

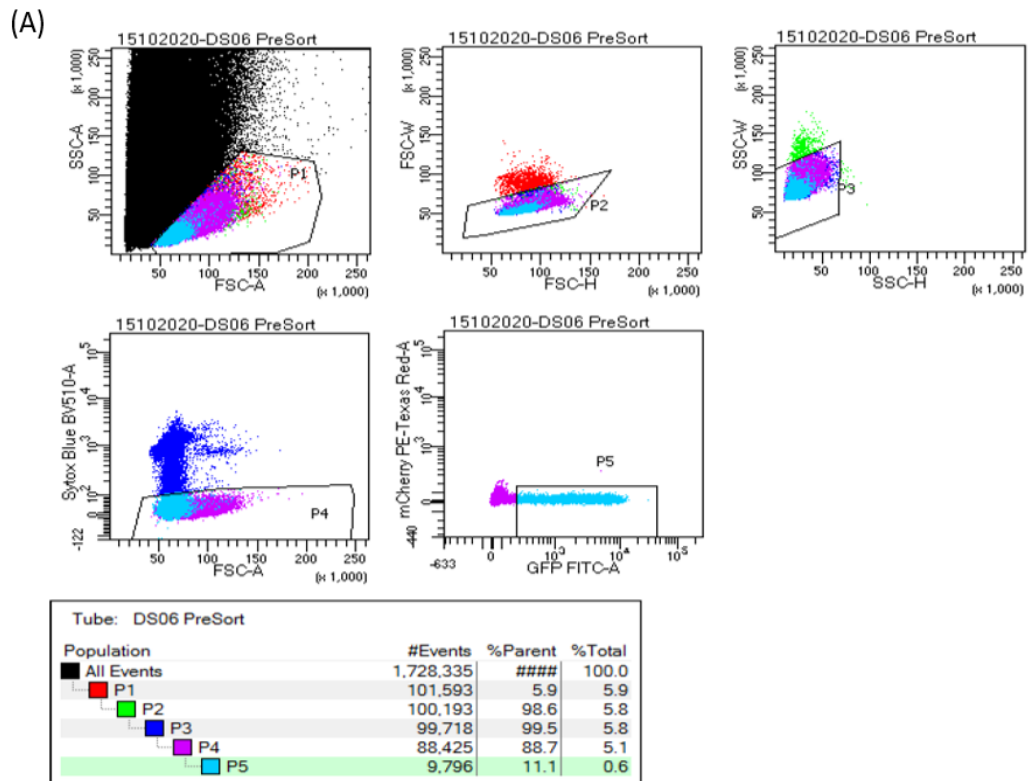


Figure 12. Incorporation of the ER-dCas9-KRAB construct into the DS-PER961 cell line. (A) Flow cytometry gating strategy for FACS to collect GFP positive DS-PER961 co-transfected cells with PX458-sgRNA_2 and ER-dCas9-KRAB plasmid. (B) Table depicting the electroporation pulse parameters (pulse voltage, pulse width and pulse number), gated populations including cells (SSC-A/FSC-A), singlets (single cells)-FSC (FSC-W/FSC-H), singlets-SSC (SSC-W/SSC-H), live cells (cell viability: Sytox Blue), transfection efficiency (mCherry/GFP) and cell number (calculated return from 44×10^6 transfected cells).

Upon co-transfection of 44×10^6 DS-PER961 cells and subsequent FACS with the BD FACSAria™ III Cell Sorter, 11.1% of live single cells were GFP positive, allowing for approximately 250756 cells to be collected and placed into liquid culture (Fig. 12). The co-transfected DS-PER961 cells collected did not proliferate in liquid culture and did not survive post cell sorting. One explanation may be that electroporation with our optimised parameters was too damaging to the cells, not allowing them to recover efficiently and continue expanding in culture. Further optimisation of co-transfection conditions may lead to an improvement in recovery; we did not pursue further

optimisation with electroporation since we agreed we could not genetically modify the DS-PER961 cell line with the techniques currently available.

Ultimately, we were only able to successfully use the Neon Transfection System to electroporate our DS-PER961 and DS-PER962 cell lines. Based upon our lentiviral transduction, Lipofectamine Stem and electroporation results (with both single plasmid and co-transfection), we concluded that we could not successfully integrate the ER-dCas9-KRAB repression system into our human DS-ALL cell line models.

Discussion:

Trisomy of ch21 in DS-ALL is the initiating alteration leading to leukaemia development, with studies highlighting its requirement for leukaemia maintenance and is a promising target in DS-ALL (7, 30). Understanding the impact of trisomy 21 and of the dosage sensitive genes implicated in leukaemia predisposition, maintenance and potential response to treatment is crucial for developing improved treatment strategies. To date, only the genes *HMGN1* (31) and *DYRK1A* (29, 30) have been confirmed as ch21 genes that impact leukaemogenesis in DS-ALL, however other ch21 gene involvement remains unknown. Therefore, we aimed to establish an inducible system to screen ch21 genes in our unique human DS-ALL cell line models, DS-PER961 and DS-PER962, to identify new candidate genes and determine their role in DS-ALL. Ultimately to highlight and understand any novel vulnerabilities and to assess if these could be targeted therapeutically.

In our strategy, we originally planned to incorporate the ER-dCas9-KRAB construct into the genome of the DS-PER961 and DS-PER962 cells, via homology directed repair at the AAVS1 safe harbour locus. From which, our ER-dCas9-KRAB system would be constitutively expressed, allowing us to test sgRNA directed to ch21 genes in an inducible manner. Upon specific gene binding through sgRNA and dCas9, the KRAB repressor can then inhibit expression of that gene, from which we can then observe the cellular outcome to determine its oncogenic potential in DS-ALL. Incorporating CRISPR technology into a cell line requires the use of a plasmid delivery method, of which there are many (91), that allows for appropriate CRISPR

function. We tested three methodologies including lentiviral transduction, lipofection and electroporation in both human DS-ALL cell lines.

Lentiviral transduction provided very low efficiency in both DS-PER961 and DS-PER962 cell lines overall (Fig. 5, 6). Notably, addition of Pb and PS made slight improvement to transduction efficiency, however, did not improve efficiency enough for this approach to be feasible. Therefore, we did not continue to optimise the transduction parameters any further, nor develop a lentiviral ER-dCas9-KRAB construct to suit this methodology. The lentiviral production used to test transduction efficiency in this project was also used by our collaborators in successful transduction experiments with high efficiency in non-B-ALL cell lines, therefore the resulting low transduction efficiency is likely due to our cell lines rather than the lentiviral transduction protocol. We currently do not know why our cell lines are not easily transduced; however low transduction efficiency in B cells has been previously demonstrated in the literature (92, 93), thus our transduction protocol warrants technical adaption in future experimentation, along with the potential use of new lentiviral constructs shown to more efficiently transduce human B-ALL cells (94).

We also attempted to utilise a stem cell specific lipofection reagent Lipofectamine Stem to transfect the DS-ALL cells. Lipofection works by enabling formation of positively charged lipid aggregates that merge with the phospholipid bilayer of the target cell, from which plasmid can transfer from the lipid aggregate into the cell (95). Since the Lipofectamine Stem reagent is specifically designed for transfection of human stem cells, we thought it would be ideal to test transfection efficiency in our DS-ALL cell lines. However, lipofection also provided extremely low efficiency in transfecting the PX458 plasmid into our DS-ALL cell line models (Fig. 7) and was not optimised further. The low transfection efficiency could have been due to the size of the plasmid, however transfecting a smaller reporter plasmid would not have accurately informed us if the ER-dCas9-KRAB construct would be transfecting. Additionally, poor lipofection efficiency has also previously been reported in B cells (93, 96-98), therefore our human cell lines are likely hard to transfect with lipofection.

We were able to achieve success in transfecting our DS-PER961 and DS-PER962 cell lines with electroporation, utilising the Neon transfection system, both with single plasmid delivery (PX458) (Table 4, 5) and co-transfection of the PX458 plasmid alongside the pLuc-mCherry plasmid (Table 6). Overall, the DS-PER961 cell line was the most efficient to co-transfect, thus only this cell line was co-transfected with the PX458-sgRNA_2 plasmid and ER-dCas9-KRAB construct (Fig. 12). The next step was to recover the successfully co-transfected cells via cell sorting for GFP positive expression, then placing these back into liquid culture, under normal growth conditions. Notably, successful integration of the construct would infer antibiotic resistance to puromycin, thus post recovery, cells with integrated ER-dCas9-KRAB could be positively selected for and cultured (Fig. 11).

Unfortunately, the DS-PER961 cell line did not successfully recover from the co-transfection/cell sorting procedures as we had intended, and therefore did not perform puromycin selection. We hypothesised this was due to several factors; electroporation was too damaging to the cells, the post cell sort recovery methodology was not optimal, and/or the DS-PER961 cell line is not genetically modifiable. Electroporation works by introducing an optimised electric charge to the cell membrane, which results in the formation of small hydrophilic pores that permeabilise the cell membrane, allowing the transfer of plasmid DNA into the cell (99). Transfected cells must then recover from the damage caused to the cell membrane post electroporation to survive and proliferate (99). Notably, including any potential cellular impact of the cell sorting process to obtain GFP positive co-transfected DS-PER961 cells. Coinciding these challenges, genetically modifying human B cell cancer cell lines for research has proved difficult in the past, thus is a common problem faced by researchers in the field that requires further investigation (93). Overall, we decided to cease optimisation of all delivery methods of the ER-dCas9-KRAB construct, agreeing that the models are not suitable for genetic modification with our current strategy and could not be used for screening purposes to identify ch21 genes implicated in DS-ALL.

Ultimately, testing other transfection methods, such as nucleofection, could be used to overcome the obstacle of introducing the ER-dCas9-KRAB

construct into the genome, without disrupting the cells stability in culture. Nucleofection has been shown to provide high transfection efficiency, fast transgene expression and improved viability/proliferation potential in cells post nucleofection (100-102). One method to perform nucleofection is with the Lonza 4D-Nucleofector system, which is now available to the laboratory. Notably, Lonza nucleofection systems have already been successfully used to introduce CRISPR systems into human primary T cells in regard to the development of chimeric antigen receptor T cells (CAR T cells) (103), as well as in human B cells, whereby the *CDKN2A* gene was successfully knocked-out (104). Alternatively, a different viral vector may have improved efficiency with less cellular toxicity within our DS-ALL models and warrants further investigation. Potential alternatives include the gibbon ape leukaemia virus (GaLV) or feline leukaemia virus (FeLV) viral envelope, which has demonstrated high efficiency of gene transfer in primary chronic lymphocytic leukaemia cells and germinal centre B cells (105, 106). Since success with these techniques have been achieved in primary human cells, it may have potential to improve the construct delivery efficiency, cell viability and cell recovery potential of the DS-PER961 and DS-PER962 cell lines post genetic modification.

Since both the DS-ALL cells are not easily recovered and brought back to normal growing conditions post modification, and since our recovery strategy was inefficient, perhaps more radical recovery alternatives are required. One method that may improve the recovery of the cells post genetic modification is to inject the transfected DS-PER961 and DS-PER962 cells back into a NSG mice, from which transfected DS-ALL cells could be engrafted to expand the cells *in vivo*, in a more adapted environment. For this assay, we have already established the conditions for injecting DS-PER961 and DS-PER962 (Chapter 3) into NSG mice. Here, GFP expression would be monitored by flow cytometry from peripheral blood, and upon euthanasia of symptomatic mice or upon significant GFP expression, human GFP positive cells will be extracted, cell sorted and then expanded in liquid culture. Once obtaining stable DS-ALL clones harbouring the ER-dCas9-KRAB repression construct, we would be able to deliver the ch21 specific sgRNA, treat cells

with 4-OHT and observe the impact of gene repression in DS-ALL as originally intended.

Overall, we were able to successfully electroporate the DS-PER961 and DS-PER962 cell lines but were unable to achieve the goal of targeting ch21 genes with the ER-dCas9-KRAB construct within these models. In future, applying the alternative strategies described above with further optimisation will need to be investigated, from which the ER-dCas9-KRAB repression system could be adapted to and incorporated within our DS-ALL models to identify novel ch21 genes of interest and identify therapeutically targetable vulnerabilities.

Chapter 5: Discussion and future directions

Leukaemia places a significant burden upon the Australian population, with lymphoid leukaemia accounting for 27% of cancer cases in children under the age of 14 (8). Significant advancement in treatment strategies has led to an improvement of survival for children diagnosed with ALL, reaching 92%, however ALL still accounts for 13% of “deaths” in children with cancer (8). This is due to certain subtypes of leukaemia that still suffer from inferior prognosis, such as children with DS-ALL (10, 40). Suboptimal treatment strategies and toxic therapeutics have resulted in children with DS-ALL suffering from a decreased overall survival rate in comparison to non-DS children, previously reported at 74% vs 89% respectively (40). More recently, it was reported in a cohort of DS-ALL patients aged 1-30, that improved treatment strategies has increased the DS-ALL overall survival to 86.8%, in comparison to non-DS-ALL at 93.6%, however, still highlighting that there is a need for improved therapeutics (50). Currently, treatment for DS-ALL patients involves a combination of multiple chemotherapeutic agents (40, 50), thus the addition of less toxic therapeutic agents that synergise with current chemotherapy strategies would improve efficacy and clinical outcomes.

Children with DS are characterised by a trisomy of ch21, which was first identified by genetic karyotyping in 1959 (1). Trisomy 21 results in an increase of gene dosage (3 copies) and expression, of which trisomy 21 mouse models have demonstrated to be between a 1.4-1.6 fold expression increase for the majority of triplicate genes (31, 107). Interestingly in the Ts1Rhr model, it was shown that not all of the triplicated genes reached expression above 1.4-1.6 fold over WT, such as Carbonyl reductase 1 (*Cbr1*), Potassium inwardly rectifying channel subfamily j member 15 (*Kcnj15*), and Integrin subunit beta 2-like (*Itgb2l*), suggesting the increase in expression is dependent upon the function of the gene (31), however these mechanisms still remain elusive. Notably, our novel models will likely contribute to gaining a deeper understanding of this phenomenon. The research that led to the development of trisomy 21 models focused on discovering the ch21 genes responsible for the clinical features of DS (35, 37, 108, 109), and the haematopoietic impact of trisomy 21 in ML-DS (21) and DS-ALL (31, 32).

These seminal studies ultimately led to the discovery of the functional impact of the DSCR in leukaemia, the minimalist region associated with the phenotypes observed in people with DS (108). Indeed, this DSCR has been associated with TAM in DS children hosting *GATA1* mutations and ML-DS development (21), as well as the identification of oncogenic cooperation between the DSCR and activation of the RAS/MAPK pathway (32). In DS leukaemia, the use of the Ts1Rhr mouse model and human PDX models has led to the identification of key ch21 genes, such as *HMGN1* in DS-ALL (31), and *DYRK1A* in both ML-DS (21) and DS-ALL (30). Notably, these genes are also impacted in non-DS leukaemia (30, 110).

HMGN1's role in DS-ALL was discovered through experiments on transformed Ts1Rhr B cell progenitors and in an *HMGN1* overexpression mouse model, identifying HMGN1 suppresses global H3K27me3 to promote B-ALL development (31). *HMGN1* overexpression has also been demonstrated to cooperate with the *P2RY8-CRLF2* rearrangement and subsequent overexpression, which together led to cytokine independent growth in murine stem cells (111). The *CRLF2* rearrangement with *P2RY8* (*P2RY8-CRLF2*), which results from deletion of Pseudoautosomal Region 1 (*PAR1*) (or overexpression via Immunoglobulin Heavy Locus (*IGH*)-*CRLF2* rearrangement) is commonly observed in DS-ALL (54% of cases) resulting in overexpression of *CRLF2* (27, 112, 113). *CRLF2* encodes a protein subunit of a heterodimeric complex with interleukin 7 receptor alpha, forming the thymic stromal lymphopoietin receptor (TSLPR), which is critical for B cell development (114-117). Interestingly, 50% of *CRLF2* rearranged DS-ALL cases contain *JAK2* alterations (27). *JAK2* encodes an intracellular signalling protein activated by binding to the TSLPR upon cytokine stimulation, leading to downstream activation of STAT transcription factors, which induces cell proliferation and survival (112, 118). It has been demonstrated that co-expression of *P2RY8-CRLF2* rearrangement and *JAK2* mutations constitutively activate the JAK-STAT pathway and provided cytokine independent growth of murine B cell progenitor BaF3 cells (112). Importantly, *in vitro* screening identified targeted inhibition of *JAK2* with fedratinib, alongside demethylase inhibition with GSK-J4, and showed promising results

within the *P2RY8-CRLF2* rearranged *HMGN1* overexpressed BaF3 cells, highlighting *HMGN1* as a therapeutic target (111). Additionally, *HMGN1* overexpression has been demonstrated to impair myeloid cell differentiation, providing a competitive advantage to haematopoietic stem and progenitor cells. It was also demonstrated to cooperate with the acute myeloid leukaemia (AML) oncogene fusion *AML-ETO9a* (also known as RUNX1-RUNX1T1 fusion transcript) *in vivo* leading to fatal leukaemia in transplant assays (110), highlighting the broad impact of *HMGN1* overexpression on haematopoietic malignancies which warrants further investigation. DYRK1A is a tyrosine kinase that can auto-phosphorylate and has activity across many substrates (119-121). DYRK1A regulates B and T cell development through cell cycle regulation, controlling the cells ability to enter quiescence from a proliferative state by phosphorylation of cyclin D3 and repression of *E2F* target genes (29). This research led to therapeutic testing in human DS-ALL PDX models using the historical DYRK1A inhibitor EHT1610 (30), identifying DYRK1A as a therapeutic target in DS-ALL and in other B-ALL types. This investigation also identified the role of DYRK1A on its substrates STAT3 and FOXO1. DYRK1A was shown to regulate B-ALL cell growth through phosphorylation of STAT3, whilst its phosphorylation of FOXO1 regulates DNA damage response. Due to these identified roles DYRK1A has within B cells, we sought to investigate the role of trisomy 21 in DS-ALL, whilst also testing the efficacy of novel DYRK1A inhibitors.

To this end, we initially focussed on the development of clinically relevant models of leukaemia, thus providing a platform for screening and assessing efficacy of novel inhibitors. We generated several murine and human models of DS-ALL, housing some of the most common and clinically relevant genomic alterations, including trisomy of ch21 (27.3% of paediatric B-ALL), deletion of the tumour suppressor *Cdkn2a* (*CDKN2A* alterations - 15-24% of DS-ALL), activation of the RAS/MAPK pathway with the *KRAS*^{G12D} mutation (*KRAS* alterations - 13-21% of DS-ALL) and activation of the JAK/STAT pathway with the *JAK2*^{I682F} mutation (*JAK2* alterations - 22-31% of DS-ALL) with *CRLF2* rearrangement (54% of DS-ALL) (7, 27, 41, 42). To achieve this within the murine setting, we firstly developed the Ts1Rhr/Mb1-Cre/*Cdkn2a*^{fl/fl}

mouse model, from which we identified that homozygous deletion of *Cdkn2a* in conjunction with trisomy of the DSCR was insufficient to lead to DS-ALL *in vivo*. However, since activation of the RAS/MAPK pathway and trisomy of the DSCR oncogenically cooperate (32), we adapted this approach to the Ts1Rhr/Mb1-Cre/*Cdkn2a*^{fl/fl} and WT/Tc1 mouse model bone marrow cells. This was accomplished via transduction with MSCV harbouring the *KRAS*^{G12D} mutation to generate the Ts1/Cdkn2a-*KRAS*^{G12D}, WT-*KRAS*^{G12D} and Tc1-*KRAS*^{G12D} cell lines. In doing so, validating that trisomy 21 cooperates with activation of the RAS/MAPK pathway, aligning with previous investigation (32), and that activation of additional pathways are required in *CDKN2A* deleted DS-ALL. The Ts1/Cdkn2a-*KRAS*^{G12D}, WT-*KRAS*^{G12D} and Tc1-*KRAS*^{G12D} cell lines successfully engrafted the bone marrow and spleen of sub-lethally irradiated recipient C57BL/6J mice upon BMT, allowing us to re-create DS-ALL *in vivo*.

Ultimately, using our strategy to develop DS-ALL models, we were able to investigate the genetic interplay between two distinct trisomy's of ch21, containing both murine (Ts1Rhr) and human (Tc1) genes, with additional somatic mutations. Notably, we were unable to generate a murine model incorporating a *CRLF2* rearrangement, however, it is a future goal of the laboratory since it is so prevalent in DS-ALL and will likely benefit the investigation of therapeutically targeting *HMGN1* within *CRLF2* rearranged DS-ALL. Additionally, we characterised the bone marrow microenvironment and haematopoietic stem and progenitor cell compartment, revealing the Tc1 mouse model is similar to WT, and confirmed trisomy 21 perturbs haematopoiesis, aligning with previous reports (122-124), with trisomy 21 affecting the MPP1 and MPP2 populations. Thus, highlighting the impact of trisomy 21 on haematopoiesis within the Tc1 model.

Moreover, in the human setting, development of the first human DS-ALL cell lines, DS-PER961 (*KRAS*^{G12S}) and DS-PER962 (*P2RY8-CRLF2/JAK2*^{682F}), allowed for efficacy validation of the inhibitors tested in clinically relevant human models. These cell lines were established in liquid culture from PDX models previously published by our laboratory (32). Overall, both human models provided us with two genetically distinct mechanisms of DS-ALL

development for investigation, thus our therapeutic investigation would be relatable to a large proportion of DS-ALL cases.

Since we established the models of DS-ALL, we next assessed the efficacy of novel DYRK1A kinase inhibitors: AM28, AM30, AM45, EHT1610, Iso Leucettinib-21 and Leucettinib-21. Our investigation on the impact of these inhibitors indicated that both non-trisomic and trisomy 21 models were sensitive to DYRK1A inhibition, as previously demonstrated with EHT1610 (30). Interestingly when comparing the *KRAS*^{G12D} transformed murine cell lines, we observed that indeed the Tc1 cells were more sensitive to inhibition of DYRK1A. This finding will need to be further validated in additional murine models that harbour DS-ALL specific mutations, considering *BCR-ABL1* fusion is rarely seen in DS-ALL (0.3% (27)). Overall inhibition of DYRK1A with Leucettinib-21 in these models proved to be our most potent kinase inhibitor. Inhibition of DYRK1A by Leucettinib-21 resulted in decreased cell growth and survival, with a dose dependent decrease of phosphorylation of cyclin D3 and FOXO1, the downstream substrates of the DYRK1A kinase (29, 30), confirming successful inhibition of DYRK1A. In comparison however, the decrease in phosphorylation was less impactful on FOXO1 and thus has prompted further investigation of the downstream targets of DYRK1A. Notably, the phosphorylation of FOXO1 by DYRK1A and its impact on cell cycle was initially discovered in a non-DS murine background and in disomic murine primary pre-B cells, with its impact on leukaemia being validated in B-ALL models through inhibition assays (30). Thus, the DYRK1A phosphorylation pattern and impact on cell cycle may slightly differ in a context of trisomy 21 and warrants further investigation. Kinase inhibitors for DYRK1A, or other ch21 genes, are currently not utilised in the treatment of DS-ALL. Therefore, we also tested Leucettinib-21 in combination with chemotherapeutic agents such as vincristine, dexamethasone, L-asparaginase, and targeted therapeutics ruxolitinib and trametinib. Importantly, we discovered that Leucettinib-21 synergises with vincristine *in vitro*, highlighting the potential for integrating DYRK1A inhibition to current treatment strategies, with future work focussing on the *in vivo* effects. Notably as mentioned in Chapter 3, Leucettinib-21 is currently in clinical trial

(LEUCETTA - NCT06206824), thus if approved, could be considered to be integrated into treatment protocols to improve outcomes for children with DS that develop DS-ALL.

Coinciding this research, our laboratory is currently investigating the downstream phosphorylation patterns and substrates effected by DYRK1A inhibition, investigating both known and unknown substrates (120, 121). This is being conducted with DYRK1A inhibited WT-*KRAS*^{G12D} and Tc1-*KRAS*^{G12D} cell lines treated with Leucettinib-21 and analysed with phosphoproteomics and RNA sequencing (RNA-seq). Thus, we will be able to analyse the differences between DYRK1A inhibition in both WT and trisomy 21 backgrounds. This work will aid in identifying novel substrates of DYRK1A and highlight mechanistically how DYRK1A inhibition decreases cell growth/survival in DS-ALL, beyond what is currently known. Therefore, allowing us to therapeutically test novel targets solely and in combination with DYRK1A inhibition. Ultimately, our results confirmed previous findings that DYRK1A is a therapeutic target in DS-ALL (30), whilst comparing efficacy of multiple DYRK1A inhibitors, identifying Leucettinib-21 as a potential therapeutic agent that could be applied to the clinic.

Recently, a new *de novo* model of DS-ALL was developed by Junco *et al.*, incorporating a murine trisomy of ch21 through the Dp(16)1Yey mouse model, which develops a fully penetrant B cell leukaemia upon CD19-Cre mediated introduction of *Kras*^{G12D} and *Pax5* heterozygosity (58). They generated ALL *in vivo* and established cell lines from these animal models to be used to screen for novel DS-ALL therapeutics. From which, the nicotinamide phosphoribosyltransferase (NAMPT) inhibitor FK866 was identified and validated in DS-ALL PDX, highlighting it significantly reduced leukaemic burden in a preclinical setting. In comparison to our DS-ALL models, the Dp(16)1Yey mouse model contains a larger trisomy of ch21 orthologues (approximately 113-115 genes (58, 125)) than the Ts1Rhr model (33 genes (44)), but less than the Tc1 mouse model chromosome with 269 human genes (37). The only genetic alteration shared between the models is *KRAS*^{G12D}; note that we overexpressed it while they used a *Kras*^{G12D} transgene. Junco *et al.*, crossed Dp(16)1Yey/*Kras*^{G12D} models with

conditional knock-out of *Pax5* (instead of the *Cdkn2a* deletion we used), which resulted in B-ALL development. As mentioned above, we did not achieve *de novo* leukaemia development in our transgenic Ts1Rhr/Mb1-Cre/*Cdkn2a*^{fl/fl} model *in vivo* (only combining two genetic alterations), but rather established derived cell lines ectopically overexpressing *KRAS*^{G12D} to then inject and re-create *in vivo* leukaemia in sub-lethally irradiated recipients. Addition of *Pax5* heterozygosity, or endogenous expression of the *KRAS*^{G12D} mutation in our Ts1Rhr/Mb1-Cre/*Cdkn2a*^{fl/fl} mouse model would likely add to the oncogenic potential of the model, thus is worth investigating in future experiments. Notably, our strategy resulted in faster development of *in vivo* DS-ALL from both Ts1/*Cdkn2a*-*KRAS*^{G12D} and Tc1-*KRAS*^{G12D} transplanted models (<70, compared to >100 days), which favours effective therapeutic investigation. Since Junco *et al.*, demonstrated *in vivo* efficacy of FK866, it would be interesting to assess its efficacy in our DS-ALL models, as well as testing Dyrk1a inhibition in their models to continue to validate these therapeutics in different DS-ALL subtypes.

As presented in Chapter 4, we initially aimed to identify other novel ch21 genes implicated in DS-ALL, utilising the DS-PER961 and DS-PER962 cell lines. Our strategy to identify ch21 genes implicated in DS-ALL development was to screen these human models with an inducible CRISPR repression system, ER-dCas9-KRAB. Theoretically, integration of this construct into the genome of the human cell lines, in combination with specific ch21 gene sgRNA, would result in repression of the target gene. We initially attempted to optimise lipofection and lentiviral transduction protocols that would integrate our construct, however achieved low transfection/transduction efficiency. Thus, we proposed that co-transfection via electroporation of the ER-dCas9-KRAB construct with an additional CRISPR-Cas9 construct containing sgRNA directed to the AAVS1 safe harbour locus would facilitate integration of the ER-dCas9-KRAB construct into the genome. We proved we were able to successfully electroporate the human models of DS-ALL but were unable to recover successfully co-transfected clones with the ER-dCas9-KRAB construct and the additional CRISPR-Cas9 vector. Ultimately, we concluded that our human models of DS-ALL could not be genetically

modified, which aligns with other laboratories findings, in that modifying human B-ALL cell lines is extremely challenging (93).

Moving forward, the laboratory can now apply the co-transfection strategy to our newly established murine Tc1-*KRAS*^{G12D} cell line. Since the Tc1-*KRAS*^{G12D} cell line harbours an additional trisomy of human ch21 (269 genes) (37), we can adapt our current strategy to this model. Adaption of this strategy to murine cell lines would initially involve development of sgRNA directed toward another integration site, such as the *Rosa26* safe harbour locus (126), that would facilitate integration of ER-dCas9-KRAB into the Tc1-*KRAS*^{G12D} cell line genome, as well as plasmid delivery optimisation to murine cells. Since only the extra copy of ch21 consists of human genes, we can selectively target the human chromosome with human gene specific sgRNA, the same we would have used for the human DS-ALL cell lines. Alternatively, we could also design a CRISPR-Cas9 knock-out strategy to individually target the human ch21 genes with human specific sgRNA and observe any potential impact gene loss could confer. Notably, the Tc1-*KRAS*^{G12D} cell line has already undergone genetic modification in its establishment and demonstrated its ability to be further transduced (shRNA inhibition of *DYRK1A* in Chapter 3a), thus we hypothesise it will be able to be further genetically modified. Therefore, we could actively target any human gene located on the Tc1 models extra ch21, utilising our laboratory's RNA-seq investigation on treated WT-*KRAS*^{G12D} and Tc1-*KRAS*^{G12D} cells and the publicly available DS-ALL RNA-seq data (27) of differentially expressed genes to identify novel targets for repression. Ultimately, identifying novel ch21 genes implicated in DS-ALL will allow us to further test novel therapeutics in our models to attempt to improve clinical outcomes for children with DS-ALL.

In completing this project, we endeavoured to reduce the impact of limitations on our research as much as possible, however we acknowledge the presence of remaining limitations that now lead to further investigation. The major limitation of this project was the sample size of the Ts1Rhr/Mb1-*Cre/Cdkn2a*^{fl/fl} mouse model cohort and controls, which was severely impacted by the COVID-19 pandemic and the difficulty in generating desired

genotypes from our breeding strategy. Additionally, we acknowledge there is a large number of genetic mutations that need to cooperate to lead to DS-ALL *in vivo* (31). This is hardly feasible using transgenic models as combining more than 3 transgenes is challenging and would require a significant number of animals (ethical limitations). Nevertheless, our laboratory will continue to find alternatives to increase the number of models available that represent other genetic subtypes of DS-ALL. Notably, our study identified novel inhibitors of the ch21 kinase DYRK1A, which warrants further investigation. We only tested the efficacy of Leucettinib-21 in two human DS-ALL models available in the laboratory, which is still limiting. Therapeutic testing of Leucettinib-21 in other genetic subtypes of DS-ALL, as well as in other subtypes of childhood B-ALL that harbour gain of chromosome 21, not represented in this study, will require further investigation, and provide key results regarding potential toxicity/safety in preclinical settings.

Throughout this project, we have significantly contributed to the DS leukaemia research space by developing relevant murine (n= 5) and human (n= 2) preclinical models of DS-ALL, as well as testing efficacy of novel therapeutic kinase inhibitors, highlighting Leucettinib-21 as the most potent inhibitor of DYRK1A within our models. The generation of these new DS-ALL models has formed the basis of future experimental design within our laboratory and abroad, as our new DS-ALL models allow for a multitude of investigations of how trisomy 21 impacts leukaemogenesis (Fig. 1).

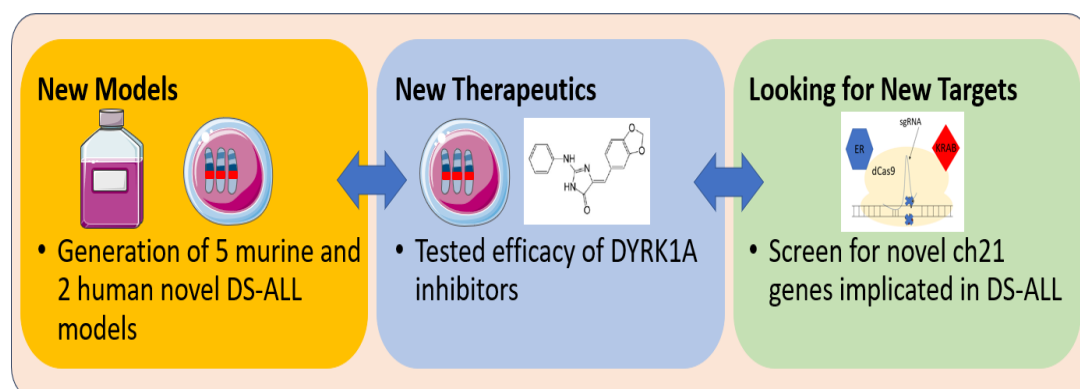


Figure 1. Project outcomes, integration, and future investigation. Created partly with Servier Medical Art (smart.servier.com).

These include using our newly established models to identify the novel downstream targets of DYRK1A with phosphoproteomics, identifying novel

ch21 genes implicated in DS-ALL with RNA-seq and CRISPR approaches, and integrating these aims to find and test novel therapies to improve outcomes for DS-ALL patients. Since the only other ch21 gene known to be implicated in DS-ALL is *HMGN1*, our models provide the perfect setting for further mechanistic investigation and therapeutic targeting of this gene. Notably, any novel findings from targeting *HMGN1* within our models will likely benefit AML research, due to its impact on this malignancy (110). Moreover, gain of ch21 is one of the most common chromosomal abnormalities found in haematological malignancies (7). Thus, our models can be used for mechanistic and therapeutic investigation that will benefit all trisomy 21 malignancies, including non-DS leukaemia, to improve outcomes for all children with trisomy 21 leukaemia. To conclude, this project has made significant advancement to DS-ALL research, providing numerous DS-ALL models, as well as insight into the mechanisms and treatment of DS-ALL.

Chapter 6: References

1. Lejeune J, Turpin, R. and Gautier, M. Mongolism First Example of Human Autosomal Aberration. *Annals of Genetics*. 1959;1:41-9.
2. Hanahan D, Weinberg Robert A. Hallmarks of Cancer: The Next Generation. *Cell*. 2011;144(5):646-74.
3. Conrad DF, Pinto D, Redon R, Feuk L, Gokcumen O, Zhang Y, et al. Origins and functional impact of copy number variation in the human genome. *Nature*. 2010;464(7289):704-12.
4. Steele CD, Abbasi A, Islam SMA, Bowes AL, Khandekar A, Haase K, et al. Signatures of copy number alterations in human cancer. *Nature*. 2022;606(7916):984-91.
5. Shao X, Lv N, Liao J, Long J, Xue R, Ai N, et al. Copy number variation is highly correlated with differential gene expression: a pan-cancer study. *BMC Medical Genetics*. 2019;20(1):175.
6. Harbers L, Agostini F, Nicos M, Poddighe D, Bienko M, Crosetto N. Somatic Copy Number Alterations in Human Cancers: An Analysis of Publicly Available Data From The Cancer Genome Atlas. *Frontiers in Oncology*. 2021;11.
7. Laurent AP, Kotecha RS, Malinge S. Gain of Chromosome 21 in Hematological Malignancies: Lessons from studying Leukemia in Children with Down Syndrome. *Leukemia*. 2020.
8. Health Alo, Welfare. Australia's children. Canberra: AIHW; 2022.
9. Kroll M, Kaupat-Bleckmann K, Mörickel A, Altenl J, Schewel DM, Stanullal M, et al. Methotrexate-associated toxicity in children with Down syndrome and acute lymphoblastic leukemia during consolidation therapy with high dose methotrexate according to ALL-BFM treatment regimen. *Haematologica*. 2020;105(4):1013-20.
10. Schmidt MP, Colita A, Ivanov AV, Coriu D, Miron IC. Outcomes of patients with Down syndrome and acute leukemia: A retrospective observational study. *Medicine (Baltimore)*. 2021;100(40):e27459.
11. Malinge S, Izraeli S, Crispino JD. Insights into the Manifestations, Outcomes, and Mechanisms of Leukemogenesis in Down Syndrome. *Blood*. 2009;113(12):2619-28.
12. Jagannathan-Bogdan M, Zon LI. Hematopoiesis. *Development (Cambridge, England)*. 2013;140(12):2463-7.
13. Yamashita M, Dellorusso PV, Olson OC, Passegué E. Dysregulated Haematopoietic Stem Cell Behaviour in Myeloid Leukaemogenesis. *Nat Rev Cancer*. 2020;20(7):365-82.
14. Doulatov S, Notta F, Laurenti E, Dick John E. Hematopoiesis: A Human Perspective. *Cell Stem Cell*. 2012;10(2):120-36.
15. Jennifer JT, Stuart HO. DNMT3A Silences Hematopoietic Stem Cell Self-Renewal. *Nature Genetics*. 2011;44(1):13.
16. Liu T, Kong W-x, Tang X-y, Xu M, Wang Q-h, Zhang B, et al. The Transcription Factor Zfp90 Regulates the Self-Renewal and Differentiation of Hematopoietic Stem Cells. *Cell Death & Disease*. 2018;9(6):677.
17. Adolfsson J, Borge OJ, Bryder D, Theilgaard-Mönch K, Åstrand-Grundström I, Sitnicka E, et al. Upregulation of Flt3 Expression within the Bone Marrow Lin⁻Sca1⁺c-kit⁺ Stem Cell Compartment Is Accompanied by Loss of Self-Renewal Capacity. *Immunity*. 2001;15(4):659-69.

18. Aoyama K, Oritani K, Yokota T, Ishikawa J, Nishiura T, Miyake K, et al. Stromal Cell CD9 Regulates Differentiation of Hematopoietic Stem/Progenitor Cells. *Blood*. 1999;93(8):2586-94.
19. Riether C, Schürch CM, Ochsenbein AF. Regulation of hematopoietic and leukemic stem cells by the immune system. *Cell Death & Differentiation*. 2015;22(2):187-98.
20. Hasle H, Clemmensen IH, Mikkelsen M. Risks of Leukaemia and Solid Tumours in Individuals with Down's Syndrome. *The Lancet*. 2000;355(9199):165-9.
21. Malinge S, Bliss-Moreau M, Kirsammer G, Diebold L, Chlon T, Gurbuxani S, et al. Increased Dosage of the Chromosome 21 Ortholog DYRK1A Promotes Megakaryoblastic Leukemia in a Murine Model of Down Syndrome. *The Journal of Clinical Investigation*. 2012;122(3):948-62.
22. Antonarakis SE, Skotko BG, Ruffi MS, Strydom A, Pape SE, Bianchi DW, et al. Down syndrome. *Nat Rev Dis Primers*. 2020;6(1):9.
23. Zipursky A, Brown E, Christensen H, Sutherland R, Doyle J. Leukemia and/or Myeloproliferative Syndrome in Neonates with Down Syndrome. *Seminars in Perinatology*. 1997;21(1):97-101.
24. Kenichi Y, Tsutomu T, Yusuke O, Rika K, Yuichi S, Aiko S-O, et al. The Landscape of Somatic Mutations in Down Syndrome–related Myeloid Disorders. *Nature Genetics*. 2013;45(11):1293.
25. Fisher JB, McNulty M, Burke MJ, Crispino JD, Rao S. Cohesin Mutations in Myeloid Malignancies. *Trends Cancer*. 2017;3(4):282-93.
26. Bhatnagar N, Nizery L, Tunstall O, Vyas P, Roberts I. Transient Abnormal Myelopoiesis and AML in Down Syndrome: an Update. *Curr Hematol Malig Rep*. 2016;11(5):333-41.
27. Li Z, Chang T-C, Junco JJ, Devidas M, Li Y, Yang W, et al. Genomic landscape of Down syndrome–associated acute lymphoblastic leukemia. *Blood*. 2023;142(2):172-84.
28. Baruchel A, Bourquin J-P, Crispino J, Cuartero S, Hasle H, Hitzler J, et al. Down syndrome and leukemia: from basic mechanisms to clinical advances. *Haematologica (Roma)*. 2023;108(10):2570-81.
29. Thompson BJ, Bhansali R, Diebold L, Cook DE, Stolzenburg L, Casagrande A-S, et al. DYRK1A Controls the Transition from Proliferation to Quiescence During Lymphoid Development by Destabilizing Cyclin D3. *The Journal of Experimental Medicine*. 2015;212(6):953-70.
30. Bhansali RS, Rammohan M, Lee P, Laurent AP, Wen Q, Suraneni P, et al. DYRK1A regulates B cell acute lymphoblastic leukemia through phosphorylation of FOXO1 and STAT3. *The Journal of clinical investigation*. 2021;131(1):e135937.
31. Lane AA, Chapuy B, Lin CY, Tivey T, Li H, Townsend EC, et al. Triplication of a 21q22 Region Contributes to B Cell Transformation through HMGN1 Overexpression and Loss of Histone H3 Lys27 Trimethylation. *Nature Genetics*. 2014;46(6):618-23.
32. Laurent AP, Siret A, Ignacimoutou C, Panchal K, Diop M, boyba, et al. Constitutive Activation of RAS/MAPK Pathway Cooperates with Trisomy 21 and is Therapeutically Exploitable in Down Syndrome B-cell Leukemia. *Clinical Cancer Research*. 2020;26(13):3307-18.

33. Parekh C, Crooks GM. Critical Differences in Hematopoiesis and Lymphoid Development between Humans and Mice. *The Journal of Clinical Immunology*. 2013;33(4):711-5.
34. Korbelt JO, Tirosh-Wagner T, Urban AE, Chen X-N, Kasowski M, Dai L, et al. The Genetic Architecture of Down Syndrome Phenotypes Revealed by High-Resolution Analysis of Human Segmental Trisomies. *Proceedings of the National Academy of Sciences of the United States of America*. 2009;106(29):12031-6.
35. Olson LE, Roper RJ, Sengstaken CL, Peterson EA, Aquino V, Galdzicki Z, et al. Trisomy for the Down Syndrome 'Critical Region' is Necessary but not Sufficient for Brain Phenotypes of Trisomic Mice. *Human Molecular Genetics*. 2007;16(7):774-82.
36. Pelleri MC, Cicchini E, Locatelli C, Vitale L, Caracausi M, Piovesan A, et al. Systematic Reanalysis of Partial Trisomy 21 Cases With or Without Down Syndrome Suggests a Small Region on 21q22.13 as Critical to the Phenotype. *Human Molecular Genetics*. 2016;25(12):2525-38.
37. O'Doherty A, Ruf S, Mulligan C, Hildreth V, Errington ML, Cooke S, et al. An Aneuploid Mouse Strain Carrying Human Chromosome 21 with Down Syndrome Phenotypes. *Science (New York, NY)*. 2005;309(5743):2033-7.
38. Jinek M, Chylinski K, Fonfara I, Hauer M, Doudna JA, Charpentier E. A Programmable Dual-RNA-Guided DNA Endonuclease in Adaptive Bacterial Immunity. *Science (New York, NY)*. 2012;337(6096):816.
39. He C, Han S, Chang Y, Wu M, Zhao Y, Chen C, et al. CRISPR screen in cancer: status quo and future perspectives. *Am J Cancer Res*. 2021;11(4):1031-50.
40. Buitenkamp TD, Izraeli S, Zimmermann M, Forestier E, Heerema NA, van den Heuvel-Eibrink MM, et al. Acute lymphoblastic leukemia in children with Down syndrome: a retrospective analysis from the Ponte di Legno study group. *Blood*. 2014;123(1):70-7.
41. Nikolaev SI, Garieri M, Santoni F, Falconnet E, Ribaux P, Guipponi M, et al. Frequent Cases of RAS-Mutated Down Syndrome Acute Lymphoblastic Leukaemia Lack JAK2 Mutations. *Nature Communications*. 2014;5:4654-.
42. Schwartzman O, Savino AM, Gombert M, Palmi C, Cario G, Schrappe M, et al. Suppressors and Activators of JAK-STAT Signaling at Diagnosis and Relapse of Acute Lymphoblastic Leukemia in Down Syndrome. *Proceedings of the National Academy of Sciences of the United States of America*. 2017;114(20):E4030-E9.
43. Sewastianik T, Jiang M, Sukhdeo K, Patel SS, Roberts K, Kang Y, et al. Constitutive Ras Signaling and Ink4a/Arf Inactivation Cooperate During the Development of B-ALL in Mice. *Blood advances*. 2017;1(25):2361-74.
44. Olson LE, Richtsmeier JT, Leszl J, Reeves RH. A Chromosome 21 Critical Region does not cause Specific Down Syndrome Phenotypes. *Science (New York, NY)*. 2004;306(5696):687.
45. Hobeika E, Thiemann S, Storch B, Jumaa H, Nielsen PJ, Pelanda R, et al. Testing gene function early in the B cell lineage in mb1-cre mice. *Proc Natl Acad Sci U S A*. 2006;103(37):13789-94.
46. Krimpenfort P, Quon KC, Mooi WJ, Loonstra A, Berns A. Loss of p16Ink4a confers susceptibility to metastatic melanoma in mice. *Nature*. 2001;413(6851):83-6.

47. Kim H, Kim M, Im SK, Fang S. Mouse Cre-LoxP system: general principles to determine tissue-specific roles of target genes. *Lab Anim Res.* 2018;34(4):147-59.
48. Sherr CJ. The INK4a/ARF network in tumour suppression. *Nature Reviews Molecular Cell Biology.* 2001;2(10):731-7.
49. Sherr CJ. Ink4-Arf locus in cancer and aging. *Wiley Interdiscip Rev Dev Biol.* 2012;1(5):731-41.
50. Rabin KR, Devidas M, Chen Z, Ji L, Kairalla J, Hitzler JK, et al. Outcomes in Children, Adolescents, and Young Adults With Down Syndrome and ALL: A Report From the Children's Oncology Group. *Journal of Clinical Oncology.* 2024;42(2):218-27.
51. Rafei H, Kantarjian HM, Jabbour EJ. Targeted therapy paves the way for the cure of acute lymphoblastic leukaemia. *British journal of haematology.* 2020;188(2):207-23.
52. Gialesaki S, Bräuer-Hartmann D, Issa H, Bhayadia R, Alejo-Valle O, Verboon L, et al. RUNX1 isoform disequilibrium promotes the development of trisomy 21-associated myeloid leukemia. *Blood.* 2023;141(10):1105-18.
53. Maude SL, Tasian SK, Vincent T, Hall JW, Sheen C, Roberts KG, et al. Targeting JAK1/2 and mTOR in murine xenograft models of Ph-like acute lymphoblastic leukemia. *Blood.* 2012;120(17):3510-8.
54. Qin H, Cho M, Haso W, Zhang L, Tasian SK, Oo HZ, et al. Eradication of B-ALL using chimeric antigen receptor-expressing T cells targeting the TSLPR oncoprotein. *Blood.* 2015;126(5):629-39.
55. Wagenblast E, Araújo J, Gan OI, Cutting SK, Murison A, Krivdova G, et al. Mapping the cellular origin and early evolution of leukemia in Down syndrome. *Science.* 2021;373(6551):eabf6202.
56. Feng J, Guo Y, Yang W, Zou Y, Zhang L, Chen Y, et al. Childhood Acute B-Lineage Lymphoblastic Leukemia With CDKN2A/B Deletion Is a Distinct Entity With Adverse Genetic Features and Poor Clinical Outcomes. *Frontiers in Oncology.* 2022;12.
57. Sulong S, Moorman AV, Irving JAE, Strefford JC, Konn ZJ, Case MC, et al. A comprehensive analysis of the CDKN2A gene in childhood acute lymphoblastic leukemia reveals genomic deletion, copy number neutral loss of heterozygosity, and association with specific cytogenetic subgroups. *Blood.* 2009;113(1):100-7.
58. Junco JJ, Rashid R, Terrell M, Alozie M, Rochette M, Zorman B, et al. A Novel Transgenic Mouse Model of Down Syndrome Acute Lymphoblastic Leukemia Identifies Targetable Vulnerabilities. *Blood.* 2023;142(Supplement 1):2981-.
59. Xavier AC, Taub JW. Acute leukemia in children with Down syndrome. *Haematologica.* 2010;95(7):1043-5.
60. Buitenkamp TD, Mathôt RA, de Haas V, Pieters R, Zwaan CM. Methotrexate-induced side effects are not due to differences in pharmacokinetics in children with Down syndrome and acute lymphoblastic leukemia. *Haematologica.* 2010;95(7):1106-13.
61. Hardy RR, Carmack CE, Shinton SA, Kemp JD, Hayakawa K. Resolution and characterization of pro-B and pre-pro-B cell stages in normal mouse bone marrow. *J Exp Med.* 1991;173(5):1213-25.
62. Cabezas-Wallscheid N, Klimmeck D, Hansson J, Lipka Daniel b, Reyes A, Wang Q, et al. Identification of Regulatory Networks in HSCs and

- Their Immediate Progeny via Integrated Proteome, Transcriptome, and DNA Methylome Analysis. *Cell Stem Cell*. 2014;15(4):507-22.
63. Hughes AM, Kuek V, Oommen J, Chua G-A, van Loenhout M, Malinge S, et al. Characterization of mesenchymal stem cells in pre-B acute lymphoblastic leukemia. *Frontiers in cell and developmental biology*. 2023;11:1005494-.
64. Cheung LC, Tickner J, Hughes AM, Skut P, Howlett M, Foley B, et al. New therapeutic opportunities from dissecting the pre-B leukemia bone marrow microenvironment. *Leukemia*. 2018;32(11):2326-38.
65. Ianevski A, Giri AK, Aittokallio T. SynergyFinder 3.0: an interactive analysis and consensus interpretation of multi-drug synergies across multiple samples. *Nucleic Acids Res*. 2022;50(W1):W739-w43.
66. Hughes AM, Kuek V, Kotecha RS, Cheung LC. The Bone Marrow Microenvironment in B-Cell Development and Malignancy. *Cancers (Basel)*. 2022;14(9).
67. Fallati A, Di Marzo N, D'Amico G, Dander E. Mesenchymal Stromal Cells (MSCs): An Ally of B-Cell Acute Lymphoblastic Leukemia (B-ALL) Cells in Disease Maintenance and Progression within the Bone Marrow Hematopoietic Niche. *Cancers (Basel)*. 2022;14(14).
68. Riegel K, Vijayarangakannan P, Kechagioglou P, Bogucka K, Rajalingam K. Recent advances in targeting protein kinases and pseudokinases in cancer biology. *Frontiers in Cell and Developmental Biology*. 2022;10.
69. Roskoski R. A historical overview of protein kinases and their targeted small molecule inhibitors. *Pharmacological Research*. 2015;100:1-23.
70. Shah R, Lester JF. Tyrosine Kinase Inhibitors for the Treatment of EGFR Mutation-Positive Non-Small-Cell Lung Cancer: A Clash of the Generations. *Clinical lung cancer*. 2020;21(3):e216-e28.
71. Coutadeur S, Benyamine H, Delalonde L, de Oliveira C, Leblond B, Foucourt A, et al. A novel DYRK1A (Dual specificity tyrosine phosphorylation-regulated kinase 1A) inhibitor for the treatment of Alzheimer's disease: effect on Tau and amyloid pathologies in vitro. *Journal of Neurochemistry*. 2015;133(3):440-51.
72. Stensen W, Rothweiler U, Engh RA, Stasko MR, Bederman I, Costa ACS, et al. Novel DYRK1A Inhibitor Rescues Learning and Memory Deficits in a Mouse Model of Down Syndrome. *Pharmaceuticals (Basel)*. 2021;14(11).
73. Ayyadevara VSSA, Wertheim G, Chukinas J, Loftus JP, Lee SJ, Kumar A, et al. Pharmacologic Inhibition of DYRK1A Results in Hyperactivation and Hyperphosphorylation of MYC and ERK Rendering KMT2A-R ALL Cells Sensitive to BCL2 Inhibition. *Blood*. 2022;140(Supplement 1):3486-8.
74. Tahtouh T, Durieu E, Villiers B, Bruyère C, Nguyen TL, Fant X, et al. Structure-Activity Relationship in the Leucettine Family of Kinase Inhibitors. *Journal of medicinal chemistry*. 2022;65(2):1396-417.
75. Lindberg MF, Deau E, Arfwedson J, George N, George P, Alfonso P, et al. Comparative Efficacy and Selectivity of Pharmacological Inhibitors of DYRK and CLK Protein Kinases. *Journal of medicinal chemistry*. 2023;66(6):4106-30.
76. Zhou Q, Phoa AF, Abbassi RH, Hoque M, Reekie TA, Font JS, et al. Structural Optimization and Pharmacological Evaluation of Inhibitors

- Targeting Dual-Specificity Tyrosine Phosphorylation-Regulated Kinases (DYRK) and CDC-like kinases (CLK) in Glioblastoma. *Journal of medicinal chemistry*. 2017;60(5):2052-70.
77. Chaikuad A, Diharce J, Schröder M, Foucourt A, Leblond B, Casagrande A-S, et al. An Unusual Binding Model of the Methyl 9-Anilinothiazolo[5,4-f]quinazoline-2-carbimidates (EHT 1610 and EHT 5372) Confers High Selectivity for Dual-Specificity Tyrosine Phosphorylation-Regulated Kinases. *Journal of medicinal chemistry*. 2016;59(22):10315-21.
78. Deau E, Lindberg MF, Miege F, Roche D, George N, George P, et al. Leucettinibs, a Class of DYRK/CLK Kinase Inhibitors Inspired by the Marine Sponge Natural Product Leucettamine B. *Journal of medicinal chemistry*. 2023;66(15):10694-714.
79. Lindberg MF, Deau E, Miege F, Greverie M, Roche D, George N, et al. Chemical, Biochemical, Cellular, and Physiological Characterization of Leucettinib-21, a Down Syndrome and Alzheimer's Disease Drug Candidate. *Journal of medicinal chemistry*. 2023;66(23):15648-70.
80. Smith J, Bibikova M, Whitby FG, Reddy AR, Chandrasegaran S, Carroll D. Requirements for Double-Strand Cleavage by Chimeric Restriction Enzymes with Zinc Finger DNA-Recognition Domains. *Nucleic acids research*. 2000;28(17):3361.
81. Christian M, Cermak T, Doyle EL, Schmidt C, Feng Z, Hummel A, et al. Targeting DNA Double-Strand Breaks with TAL Effector Nucleases. *Genetics*. 2010;186(2):757.
82. Qi LS, Larson MH, Gilbert LA, Doudna JA, Weissman JS, Arkin AP, et al. Repurposing CRISPR as an RNA-Guided Platform for Sequence-Specific Control of Gene Expression. *Cell*. 2013;152(5):1173-83.
83. Gilbert Luke a, Larson Matthew h, Morsut L, Liu Z, Brar Gloria a, Torres Sandra e, et al. CRISPR-Mediated Modular RNA-Guided Regulation of Transcription in Eukaryotes. *Cell*. 2013;154(2):442-51.
84. Gilbert Luke a, Horlbeck Max a, Adamson B, Villalta Jacqueline e, Chen Y, Whitehead Evan h, et al. Genome-Scale CRISPR-Mediated Control of Gene Repression and Activation. *Cell*. 2014;159(3):647-61.
85. Cai R, Lv R, Shi Xe, Yang G, Jin J. CRISPR/dCas9 Tools: Epigenetic Mechanism and Application in Gene Transcriptional Regulation. *International Journal of Molecular Sciences*. 2023;24(19):14865.
86. Zhao C, Zhao Y, Zhang J, Lu J, Chen L, Zhang Y, et al. HIT-Cas9: A CRISPR/Cas9 Genome-Editing Device under Tight and Effective Drug Control. *Molecular Therapy Nucleic Acids*. 2018;13:208-19.
87. Hayashi H, Kubo Y, Izumida M, Matsuyama T. Efficient viral delivery of Cas9 into human safe harbor. *Sci Rep*. 2020;10(1):21474.
88. Cornetta K, Anderson WF. Protamine sulfate as an effective alternative to polybrene in retroviral-mediated gene-transfer: implications for human gene therapy. *Journal of Virological Methods*. 1989;23(2):187-94.
89. Lin P, Lin Y, Lennon DP, Correa D, Schluchter M, Caplan AI. Efficient lentiviral transduction of human mesenchymal stem cells that preserves proliferation and differentiation capabilities. *Stem Cells Transl Med*. 2012;1(12):886-97.
90. Balak JRA, de Graaf N, Zaldumbide A, Rabelink TJ, Hoeben RC, de Koning EJP, et al. Highly efficient ex vivo lentiviral transduction of primary human pancreatic exocrine cells. *Scientific Reports*. 2019;9(1):15870.

91. Yang W, Yan J, Zhuang P, Ding T, Chen Y, Zhang Y, et al. Progress of delivery methods for CRISPR-Cas9. *Expert opinion on drug delivery*. 2022;19(8):913-26.
92. Serafini M, Naldini L, Introna M. Molecular evidence of inefficient transduction of proliferating human B lymphocytes by VSV-pseudotyped HIV-1-derived lentivectors. *Virology*. 2004;325(2):413-24.
93. Edelstein J, Fritz M, Lai SK. Challenges and opportunities in gene editing of B cells. *Biochemical Pharmacology*. 2022;206:115285.
94. Levy C, Fusil F, Amirache F, Costa C, Girard-Gagnepain A, Negre D, et al. Baboon envelope pseudotyped lentiviral vectors efficiently transduce human B cells and allow active factor IX B cell secretion in vivo in NOD/SCID γ c $^{-/-}$ mice. *Journal of thrombosis and haemostasis*. 2016;14(12):2478-92.
95. Chong ZX, Yeap SK, Ho WY. Transfection types, methods and strategies: a technical review. *PeerJ*. 2021;9:e11165.
96. Moghimi B, Zolotukhin I, Sack BK, Herzog RW, Cao O. High Efficiency Ex Vivo Gene Transfer to Primary Murine B Cells Using Plasmid or Viral Vectors. *J Genet Syndr Gene Ther*. 2011;2(103).
97. Buttgereit P, Weineck S, Röpke G, Märten A, Brand K, Heinicke T, et al. Efficient gene transfer into lymphoma cells using adenoviral vectors combined with lipofection. *Cancer Gene Therapy*. 2000;7(8):1145-55.
98. Mascarenhas L, Stripecke R, Case SS, Xu D, Weinberg KI, Kohn DB. Gene Delivery to Human B-Precursor Acute Lymphoblastic Leukemia Cells. *Blood*. 1998;92(10):3537-45.
99. Shi J, Ma Y, Zhu J, Chen Y, Sun Y, Yao Y, et al. A Review on Electroporation-Based Intracellular Delivery. *Molecules*. 2018;23(11).
100. Zanin MP, Hellström M, Shepherd RK, Harvey AR, Gillespie LN. Development of a cell-based treatment for long-term neurotrophin expression and spiral ganglion neuron survival. *Neuroscience*. 2014;277:690-9.
101. Jacobsen F, Mertens-Rill J, Beller J, Hirsch T, Daigeler A, Langer S, et al. Nucleofection: A New Method for Cutaneous Gene Transfer? *Journal of Biomedicine and Biotechnology*. 2006;2006:026060.
102. Skrzyszowska M, Samiec M, Słomski R, Lipiński D, Mały E. Development of porcine transgenic nuclear-transferred embryos derived from fibroblast cells transfected by the novel technique of nucleofection or standard lipofection. *Theriogenology*. 2008;70(2):248-59.
103. Hu B, Zou Y, Zhang L, Tang J, Niedermann G, Firat E, et al. Nucleofection with Plasmid DNA for CRISPR/Cas9-Mediated Inactivation of Programmed Cell Death Protein 1 in CD133-Specific CAR T Cells. *Human Gene Therapy*. 2018;30(4):446-58.
104. Akidil E, Albanese M, Buschle A, Ruhle A, Pich D, Keppler OT, et al. Highly efficient CRISPR-Cas9-mediated gene knockout in primary human B cells for functional genetic studies of Epstein-Barr virus infection. *PLOS Pathogens*. 2021;17(4):e1009117.
105. Caesar R, Di Re M, Krupka JA, Gao J, Lara-Chica M, Dias JML, et al. Genetic modification of primary human B cells to model high-grade lymphoma. *Nature Communications*. 2019;10(1):4543.
106. Mangolini M, Maiques-Diaz A, Charalampopoulou S, Gerhard-Hartmann E, Bloehdorn J, Moore A, et al. Viral transduction of primary

- human lymphoma B cells reveals mechanisms of NOTCH-mediated immune escape. *Nature Communications*. 2022;13(1).
107. Yamakawa K. Towards the understanding of Down syndrome using mouse models. *Congenital anomalies*. 2012;52(2):67-71.
108. Belichenko NP, Belichenko PV, Kleschevnikov AM, Salehi A, Reeves RH, Mobley WC. The "Down syndrome critical region" is Sufficient in the Mouse Model to Confer Behavioral, Neurophysiological, and Synaptic Phenotypes Characteristic of Down Syndrome. *The Journal of Neuroscience*. 2009;29(18):5938-48.
109. Sago H, Carlson EJ, Smith DJ, Kilbridge J, Rubin EM, Mobley WC, et al. Ts1Cje, a Partial Trisomy 16 Mouse Model for Down Syndrome, Exhibits Learning and Behavioral Abnormalities. *Proceedings of the National Academy of Sciences of the United States of America*. 1998;95(11):6256-61.
110. Cabal-Hierro L, van Galen P, Prado MA, Higby KJ, Togami K, Mowery CT, et al. Chromatin accessibility promotes hematopoietic and leukemia stem cell activity. *Nature Communications*. 2020;11(1):1406.
111. Page EC, Heatley SL, Eadie LN, McClure BJ, de Bock CE, Omari S, et al. HMGN1 plays a significant role in CRLF2 driven Down Syndrome leukemia and provides a potential therapeutic target in this high-risk cohort. *Oncogene*. 2022;41(6):797-808.
112. Mullighan CG, Collins-Underwood JR, Phillips LAA, Loudin MG, Liu W, Zhang J, et al. Rearrangement of CRLF2 in B-Progenitor- and Down Syndrome-Associated Acute Lymphoblastic Leukemia. *Nature Genetics*. 2009;41(11):1243-6.
113. Harvey RC, Mullighan CG, Chen IM, Wharton W, Mikhail FM, Carroll AJ, et al. Rearrangement of CRLF2 is Associated with Mutation of JAK Kinases, Alteration of IKZF1, Hispanic/Latino Ethnicity, and a Poor Outcome in Pediatric B-progenitor Acute Lymphoblastic Leukemia. *Blood*. 2010;115(26):5312-21.
114. Levin SD, Koelling RM, Friend SL, Isaksen DE, Ziegler SF, Perlmutter RM, et al. Thymic Stromal Lymphopoietin: A Cytokine That Promotes the Development of IgM+ B Cells In Vitro and Signals Via a Novel Mechanism. *The Journal of Immunology*. 1999;162(2):677.
115. Park LS, Martin U, Garka K, Gliniak B, Di Santo JP, Muller W, et al. Cloning of the murine thymic stromal lymphopoietin (TSLP) receptor: Formation of a functional heteromeric complex requires interleukin 7 receptor. *J Exp Med*. 2000;192(5):659-70.
116. Pandey A, Ozaki K, Baumann H, Levin SD, Puel A, Farr AG, et al. Cloning of a receptor subunit required for signaling by thymic stromal lymphopoietin. *Nature Immunology*. 2000;1(1):59-64.
117. Scheeren FA, van Lent AU, Nagasawa M, Weijer K, Spits H, Legrand N, et al. Thymic stromal lymphopoietin induces early human B-cell proliferation and differentiation. *European Journal of Immunology*. 2010;40(4):955-65.
118. Rochman Y, Kashyap M, Robinson GW, Sakamoto K, Gomez-Rodriguez J, Wagner KU, et al. Thymic stromal lymphopoietin-mediated STAT5 phosphorylation via kinases JAK1 and JAK2 reveals a key difference from IL-7-induced signaling. *Proc Natl Acad Sci U S A*. 2010;107(45):19455-60.

119. Soundararajan M, Roos AK, Savitsky P, Filippakopoulos P, Kettenbach AN, Olsen JV, et al. Structures of Down syndrome kinases, DYRKs, reveal mechanisms of kinase activation and substrate recognition. *Structure*. 2013;21(6):986-96.
120. Deboever E, Fistrovich A, Hulme C, Dunckley T. The Omnipresence of DYRK1A in Human Diseases. *International Journal of Molecular Sciences*. 2022;23(16):9355.
121. Rammohan M, Harris E, Bhansali RS, Zhao E, Li LS, Crispino JD. The chromosome 21 kinase DYRK1A: emerging roles in cancer biology and potential as a therapeutic target. *Oncogene*. 2022;41(14):2003-11.
122. De Vita S, Canzonetta C, Mulligan C, Delom F, Groet J, Baldo C, et al. Trisomic dose of several chromosome 21 genes perturbs haematopoietic stem and progenitor cell differentiation in Down's syndrome. *Oncogene*. 2010;29(46):6102-14.
123. Roy A, Cowan G, Mead AJ, Filippi S, Bohn G, Chaidos A, et al. Perturbation of fetal liver hematopoietic stem and progenitor cell development by trisomy 21. *Proc Natl Acad Sci U S A*. 2012;109(43):17579-84.
124. Chou ST, Byrska-Bishop M, Tober JM, Yao Y, Vandorn D, Opalinska JB, et al. Trisomy 21-associated defects in human primitive hematopoiesis revealed through induced pluripotent stem cells. *Proc Natl Acad Sci U S A*. 2012;109(43):17573-8.
125. Li Z, Yu T, Morishima M, Pao A, LaDuca J, Conroy J, et al. Duplication of the entire 22.9 Mb human chromosome 21 syntenic region on mouse chromosome 16 causes cardiovascular and gastrointestinal abnormalities. *Human Molecular Genetics*. 2007;16(11):1359-66.
126. Chu VT, Weber T, Graf R, Sommermann T, Petsch K, Sack U, et al. Efficient generation of Rosa26 knock-in mice using CRISPR/Cas9 in C57BL/6 zygotes. *BMC Biotechnology*. 2016;16(1):4.

Every reasonable effort has been made to acknowledge the owners of copyright material. I would be pleased to hear from any copyright owner who has been omitted or incorrectly acknowledged.